Shaping and conditioning of high percolating alginate-polyethylenimine membranes for the design of sorbents and supported catalysts

Yayuan Mo

THÈSE POUR OBTENIR LE GRADE DE DOCTEUR DE L'UNIVERSITÉ DE MONTPELLIER

En Génie des Procédés

École doctorale GAIA - Biodiversité, Agriculture, Alimentation, Environnement, Terre, Eau

Unité de recherche C2MA - Centre des Matériaux des Mines d'Alès

Shaping and conditioning of high percolating alginate-polyethylenimine membranes for the design of sorbents and supported catalysts

Présentée par Yayuan MO

Le 7 Octobre 2020

Sous la direction de Catherine FAUR

Devant le jury composé de

Jacques DESBRIERES, Professeur émérite, Université de Pau et des Pays de l'Adour	Rapporteur
Stéphanie DEGOUTIN, Maître de conférences HDR, Université de Lille	Rapporteure
Bénédicte PRELOT, Directrice de recherche CNRS, Université de Montpellier	Présidente du jury
Enrique RODRIGUEZ-CASTELLON, Professeur, Université de Malaga	Examinateur
Eric GUIBAL, Maître de recherche, IMT Mines Alès	Co-encadrant de thèse
Catherine FAUR, Professeur, Université de Montpellier	Directrice de thèse
Nathalie TANCHOUX, Maître de conférences, Université de Montpellier	Invitée

UNIVERSITÉ DE MONTPELLIER

Acknowledgements

Three years of doctoral study has been a truly life-changing experience for me and this thesis would not been achievable without the support, encouragement and guidance which I received from many people.

Firstly, I would like to extend my heartfelt gratitude to my mentors, Dr. Eric Guibal and Prof. Catherine Faur, whose patient guidance, valuable suggestions and constant encouragement make me complete this thesis. I am not your best student, but you two are my most respected teachers. I would like to thank Prof. Catherine Faur again for your kind help in my registration every year in Montpellier and gives me much help and advice during the whole process of my writing. Thanks Dr. Eric Guibal again for your enthusiasm, patience, insightful comments, helpful information, practical advice and unceasing ideas that have helped me tremendously at all times in my research and writing of this thesis; your conscientious academic spirit and modest, open-minded personality inspire me both in academic study and daily life.

I also would like to thank Mr. Thierry Vincent and Mrs. Corinne Vincent. Thanks Mr. Thierry Vincent for his providing innovative ideas and suggestions on the implementation of the experiment and he always can finding the chemicals and devices needed for me. Thanks Mrs. Corinne Vincent for her kind help in my daily life when I have trouble with language problems. I am so happy to have you as friends in ALES.

I would like to thank the members of my thesis committee: Dr. Antoine Collignan, Dr. Nathalie Tanchoux and Dr. Rodolphe Sonnier, for their insightful comments and the hard question which incented me to widen my research from various perspectives.

I also would like to express my sincere gratitude to Dr. Stéphanie Degoutin (Université Lille), Prof. Jacques Desbrieres (Université de Pau et des Pays de l'Adour), Dr. Bénédicte Prelot (Université de Montpellier), and Prof. Enrique Rodríguez-Castellón (Université de Malaga) for your willingness to be my jury members and for your suggestions not only help me improve my thesis, but also have great value for my future research.

I am indebted to Mr. Jean-claude Raux for his technical help with SEM-EDX analysis and Mr. Mohammed F. Hamza (Nuclear Materials Authority, Egypt) for his technical support for XPS analyses. I would also like to say a heartfelt thank you to the colleagues of my group and all of my friends (Dr. Shengye Wang, Mr. Lionel Sabourin, Ms. Pamela-Viridiana Sierra-trejo, Ms. Yue Zhang, Mr. Ahmed Masoud, Mr. Islam Alhindawy and so on) for their support and assistant.

In addition, I am grateful to the China Scholarship Council (CSC, Grant N° 201708450080) for providing scholarship. This financial support has enabled me to complete my PhD studies successfully.

My thanks also go to the authors whose books and articles have given me inspiration in the writing of this paper.

Last but not least, I would like to express my special thanks to my family for their always believing in me and encouraging me to become a better person in life.

Résumé étendu

1. Introduction

Le développement industriel pour satisfaire une demande croissante des consommateurs exerce une pression importante sur la ressource en matières premières et induit des impacts significatifs sur l'environnement et par voie de conséquence sur la biosphère. La question des métaux lourds, des métaux précieux ou stratégiques illustre parfaitement cette dualité de contraintes: préserver l'environnement pour éviter que les effets accumulatifs dans la chaine alimentaire ne conduisent à une toxicité critique pour le biotope et la santé humaine, et produire des matières premières stratégiques (rareté, contraintes géostratégiques, etc.) à partir de ressources secondaires (déchets, minerais infra-marginaux) afin de satisfaire une demande croissante (développement de produits high-tech).

De nombreux secteurs industriels mettent en œuvre des procédés hydrométallurgiques qui génèrent des flux aqueux contenant des métaux lourds, toxiques (traitement de surface, industrie minière, etc.). Il n'est donc pas rare de rencontrer dans leurs eaux de process et leurs rejets des concentrations relativement élevées en ions métalliques tels que: Pb(II), Cu(II), Cr(VI), As(V) et Hg(II). Certains de ces métaux présentent des toxicités critiques qui ont conduit les organisations internationales à fixer des concentrations limites très basses dans les eaux de boisson et même à fixer des valeurs limites très contraignantes dans les rejets industriels. Une large palette de procédés a été développée pour faire face à la nécessité d'éliminer les ions métalliques de ces rejets, ou de les récupérer sélectivement pour les valoriser. Des procédés tels la réduction chimique, la précipitation, l'électrocoagulation, l'extraction par solvant, les membranes séparatives ou les techniques d'adsorption (supports adsorbants par échange d'ion, ou chélation) sont fréquemment appliqués pour traiter des effluents métallifères et valoriser des métaux stratégiques [1]. Les conditions opératoires (notamment la concentration des métaux ainsi que les flux à traiter) et la valeur des contaminants vont orienter le choix des procédés à mettre en œuvre. Ainsi la précipitation est rarement sélective; elle produit des boues métallifères, toxiques et complexes, difficile à valoriser. Par ailleurs, les rendements de précipitation ne suffisent pas toujours pour atteindre les valeurs limites requises. Les procédés d'extraction par solvant sont préférentiellement utilisés pour des métaux à valeur ajoutée importante et dans la gestion de flux plus réduits. Le coût de ces extractants et les pertes dans les cycles d'extraction et de stripping constituent des contraintes non négligeables. Les techniques membranaires sont relativement coûteuses en termes énergétiques et s'accommodent mal de la complexité des effluents (notamment par la présence de colloïdes et de matières en suspension qui induisent un colmatage membranaire). Les procédés d'adsorption, mettant en œuvre des bioadsorbants, des résines échangeuses d'ions, des résines chélatantes ou des résines imprégnées, sont plus particulièrement adaptés au traitement d'effluents et de solutions faiblement concentrés [2]. La solution consiste souvent dans la combinaison de différents procédés; cette modularité des procédés peut associer notamment technique de précipitation éliminant une partie des métaux toxiques et une étape d'adsorption (plus sélective et permettant de concentrer certains métaux toxiques et/ou valorisables).

Parmi les adsorbants, outre les polymères synthétiques utilisés dans les résines commerciales, les charbons actifs, ou les zéolites, un important effort a été mené au cours des dernières décennies sur le développement de bioadsorbants mettant en œuvre des sous-produits agricoles (cellulose, lignine, etc.), ou des pêcheries (et plus généralement de l'industrie de la mer : alginate, chitine/chitosane) [3]. Au sein de l'Ecole des Mines d'Alès (aujourd'hui IMT – Mines Alès) de nombreux travaux ont été menés, au cours des 3 dernières décennies, sur la fonctionnalisation et la mise en forme de biopolymères (chitosane et alginate) et sur leur application dans le domaine du traitement des eaux (notamment métallifères) [4, 5]. En jouant sur les "différents états de la matière", il a été possible notamment de développer des procédés de coagulation-floculation, d'ultrafiltration assistée par complexation (UFAC) pour la forme liquide (mise en solution des biopolymères) mais aussi des hydrogels conditionnés sous formes de billes, de membranes, de fibres, de fibres creuses et plus récemment sous forme de mousses et éponges. Ces mises en forme, combinées avec la possibilité d'incorporer et/ou immobiliser des solides (échangeurs ioniques) ou des liquides (extractants, liquides ioniques), mais aussi de fonctionnaliser chimiquement (greffage de groupements fonctionnels) ont ainsi permis de créer une bibliothèque très diversifiée de matériaux adsorbants. C'est dans ce contexte que s'est inscrit le présent projet de recherche, avec un objectif centré sur la mise en forme de membranes à haut pouvoir de percolation associant un biopolymère (l'alginate) et un polymère synthétique (la polyéthyleneimine) en vue de deux applications: l'adsorption d'une série d'ions métalliques et l'utilisation de membranes chargées en métaux catalytiques pour la réalisation de catalyseurs hétérogènes.

L'alginate est un polymère extrait commercialement des algues brunes, biocompatible et biodégradable portant de nombreuses fonctions carboxyliques (acides mannuronique et guluronique) et de groupes hydroxyles [6]. Il s'agit donc d'un matériau très hydrophile qui a été largement utilisé pour ses propriétés de gélification dans l'industrie agro-alimentaire, la pharmacie et la cosmétique. Cette gélification est basée sur l'interaction entre les groupements carboxyliques et les cations, essentiellement divalents (en particulier Ca(II), même s'il est possible de gélifier en présence de cations trivalents, mais également en milieu acide), par le mécanisme qualifié de manière très imagé, de boîte à œufs. Ces fonctions carboxyliques ont naturellement des propriétés de complexation et d'échange d'ions, en fonction du pH, et notamment de leur état d'ionisation (les pK_a de l'acide mannuronique et de l'acide guluronique valent respectivement: 3,38 et 3,65 [7]). La structure chimique de l'alginate n'est toutefois pas favorable à l'adsorption d'anions métalliques (chromate, palladium en milieu HCl). Pour élargir le champ d'application de matériaux adsorbants basés sur l'alginate, il est alors nécessaire d'incorporer (greffage, immobilisation) d'autres polymères, échangeurs d'ions etc. Dans ce travail, cet objectif a été atteint en réalisant une "association" entre l'alginate et la polyethyleneimine (PEI), un polymère synthétique (ramifié dans cette étude) portant à la fois des fonctions amine primaire, secondaire et tertiaire (pK_a: 4,5, 6,7, 11,6, respectivement [8]).

La réalisation de mousses et éponges d'alginate à forte macroporosité a été largement décrite dans la littérature. Cependant ces techniques nécessitent généralement la mise en œuvre de

séchages complexes et énergivores (lyophilisation, aérogels par séchage dans des conditions de CO_2 supercritique) afin de préserver, autant que possible, les propriétés structurales et texturales de l'hydrogel [9, 10]. C'est en rupture avec ces procédés conventionnels et avec l'objectif de faciliter la structuration des mousses (membranes) à haut pouvoir de percolation sans mettre en œuvre de processus complexe de séchage, qu'une nouvelle méthode de fabrication a été développée. Elle consiste à faire directement réagir l'alginate et la PEI, dans des conditions de pH contrôlées, afin de structurer l'hydrogel par interaction ionique. Dans une seconde étape la membrane est réticulée dans une solution de glutaraldéhyde (GA). L'interaction des fonctions carboxyliques de l'alginate avec les groupes amines de la PEI et la réticulation de fonctions aminées résiduelles par le glutaraldéhyde conduisent à une structuration "forte" de l'hydrogel (double réseau d'interactions: (a) alginate/PEI, PEI/GA) qui peut ensuite être séché à l'air libre sans perdre sa macroporosité (en minimisant l'effondrement du réseau poreux de l'hydrogel). Cette macroporosité a pour objet de faciliter l'utilisation de l'adsorbant dans un mode de drainage naturel (percolation simple, éventuellement sans l'assistance d'une pompe). Le matériau composite est caractérisé par la présence de groupements carboxyliques (acides) et de fonctions aminées (basiques) qui ouvrent le champ pour la fixation d'un large spectre d'ions métalliques (cationiques et anioniques).

Ce matériau a été développé et utilisé pour deux types d'applications : (a) l'adsorption d'ions métalliques (cationiques et anioniques), et (b) l'hydrogénation de composés nitrophénoliques par catalyse hétérogène. Ces deux thèmes sont illustrés par les publications composant ce mémoire de thèse.

Cette thèse s'inscrit dans la continuité de la thèse de doctorat présentée devant l'Université de Montpellier, en 2019, par Shengye Wang, intitulée « algal and alginate based beads and foams as sorbents for metal sorption and catalyst supports for 3-nitrophenol hydrogenation».

2. Principaux résultats et discussions

2.1. Principales caractéristiques des membranes

L'interaction des carboxylates de l'alginate avec les fonctions aminées protonées de la PEI (la solution de PEI est ajustée à pH 6.5 avant d'être mélangée à la solution d'alginate) conduit à la formation d'un premier réseau polymérique (structuration de la masse floconneuse). A l'issue de cette étape, qui peut prendre près de 24 h, l'hydrogel s'est contracté en gardant la forme globale de l'hydrogel coulé dans son moule. Dans la deuxième étape du processus, la réticulation de fonctions aminées résiduelles par le glutaraldéhyde renforce la structuration et la stabilité mécanique du matériau.

Cette stabilité mécanique a été mise en évidence par évaluation de la perte de masse après avoir soumis la membrane à une agitation forte (i.e., 150 tours/min) pendant 24 h. A l'issue de cette agitation, la perte de masse n'excède pas 6-14 % (en fonction des paramètres de fabrication). Prenant en compte que le mode d'utilisation de la mousse consiste à l'immobiliser dans une colonne (ou un module de filtration, type Swinnex, Millipore), les contraintes mécaniques sont limitées à la percolation de la solution ; ce sont donc des conditions d'agitation bien moins

agressives que celles utilisées dans le test. Ce résultat est confirmé par un test réalisé en mode dynamique: la membrane immobilisée dans une colonne est alimentée pendant 3 jours avec une solution aqueuse; la perte de masse est inférieure à 3%. La structuration assurée à la membrane par le processus de fabrication permet d'obtenir une mousse ouverte particulièrement stable (au moins pour le mode d'application préconisé).

Les propriétés de percolation simple ont été évaluées en disposant la membrane dans une colonne et en imposant une hauteur constante de colonne d'eau (correspondant à une pression de 0,006 bar). Le flux d'eau correspondant au mode de drainage simple correspond à une plage de valeurs comprise entre 13 et 34 mL cm^{-2} min^{-1} (soit une vitesse superficielle de 7,8 à 20,4 m h^{-1}). Comparée aux valeurs rapportées par d'autres membranes, ces valeurs sont très nettement supérieures ; cela confirme l'intérêt de ces matériaux pour l'application envisagée en percolation (naturelle) réactive.

Ces propriétés de percolation sont clairement corrélées à la macroporosité confirmée par l'observation en microscopie électronique à balayage (MEB), qui met en évidence un réseau très ouvert.

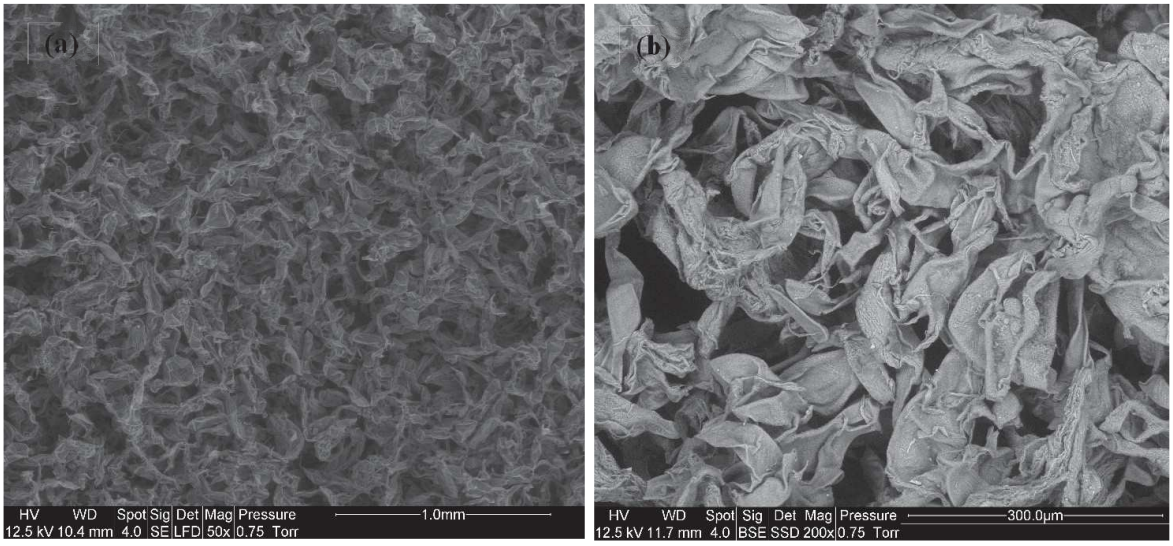

Fig. 1 Image MEB de la membrane dans différents magnifiques (a) 50 × et (b) 200 ×.

L'analyse par spectroscopie infrarouge permet de confirmer la réticulation de la PEI par le glutaraldéhyde. En effet la formation de bases de Schiff est attestée par l'apparition de deux pics à 1596 cm^{-1} et 1317 cm^{-1} qui correspondent d'une part à la superposition des bandes caractéristiques des liaisons C=N et de N-H, et d'autre part à la liaison C-N. L'apparition de cette bande confirme l'incorporation de la PEI dans le composite; ces nouvelles fonctions apportées à l'alginate permettront d'étendre le champs d'application du composite à la fixation d'anions en milieu acide (cf. travaux ultérieurs sur les anions métalliques: Cr(VI), Se(VI) et chloropalladate, par exemple. La coexistence de groupements carboxyliques, de fonctions hydroxyles offre la possibilité d'adsorber d'autres ions métalliques de type cations (Cu(II), Hg(II), etc.).

Par ailleurs, le pH de Point de Charge Nulle (pH_{PCN}) de la membrane est compris dans l'intervalle [5,7; 6,3]; pour des pH inférieurs à 5,7, la surface protonnée de l'adsorbant devrait ainsi permettre la sorption d'anions par attraction électrostatique.
Ces quelques caractérisations confirment que le procédé de fabrication permet de préparer des membranes stables, réactives avec d'excellentes performances de percolation, capables de répondre aux objectifs initialement fixés.

2.2. Adsorption des ions chromates [11]

Cette étude a été menée sur des membranes ayant été préparées suivant le procédé décrit ci-dessus en utilisant une teneur en PEI de 3 % en poids. Les membranes sont immobilisées dans un porte filtre et alimentées par une pompe avec recirculation de la solution (simulation d'un réacteur parfaitement agité). Les essais d'adsorption réalisés entre pH 0.5 et pH 6 ont permis de mettre en évidence un pH optimal de 2. Il convient de noter qu'en milieu acide et en présence de matière organique, le Cr(VI) est assez facilement réduit en Cr(III); cette propriété complique l'interprétation des mécanismes effectifs de fixation mais aussi l'évaluation des performances d'adsorption. L'analyse du Cr(VI) par la méthode colorimétrique à la diphénylcarbazide permet de distinguer la concentration effective des deux formes (chrome total, TCr) en analysant les échantillons par ICP-AES (spectrométrie d'émission atomique à plasma à couplage inductif). La comparaison des profils de concentrations résiduelles Cr(VI) et du TCr permet de distinguer les contributions respectives des deux espèces: en fait le phénomène de réduction détectable à pH inférieur à 2, s'exprime essentiellement à pH 0.5. La fixation du Cr(VI) a été testée à deux débits (15 et 30 mL min^{-1}, vitesse superficielle V_s =1,83-3,66 m h^{-1}) (Fig. 2a), une légère différence est observée entre les deux profils cinétiques qui présentent tous les deux une forte décroissance initiale de la concentration (dans la première heure de contact, représentant environ 41-48 % de la fixation totale), suivie d'une phase de transfert plus lente (pour atteindre un abattement de 58 à 66 % de la fixation totale, entre 1 h et 6 h de contact); enfin une phase finale assez longue (jusqu'à 78 h) où s'exprime la résistance à la diffusion intraparticulaire. Les profils (tant du Cr(VI) que du TCr) sont correctement modélisés par l'équation cinétique de pseudo-second ordre (PSORE).

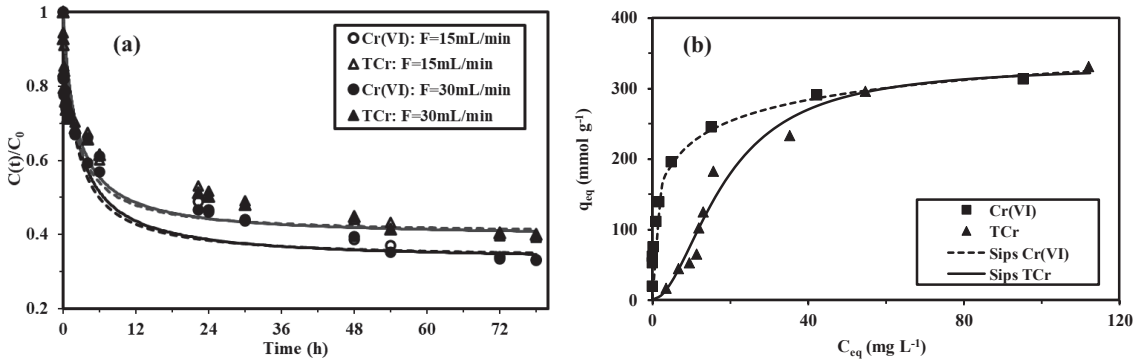

Fig. 2 Cinétiques de fixation (Cr(VI) et TCr) (a) et isothermes d'adsorption (b) à pH 2 (Cinétiques : C_0 = 200 mg Cr L^{-1}; concentration en sorbant = 0,2 g L^{-1}; V= 1000 mL ;

pH: 2; température = 20 ± 1 °C. Isothermes : concentration en sorbant = 0,6 g L^{-1}; V= 50 mL ; durée = 78 h; débit = 15 mL min^{-1}; température = 20 ± 1 °C).

Les isothermes d'adsorption sont représentées sur la Fig. 2b: la pente initiale est corrélée à la forte affinité de la membrane pour l'ion métallique. Cette courbe est également caractérisée par un plateau de saturation atteint pour une concentration résiduelle de 50 mg Cr(VI) L^{-1}. Ce plateau de saturation correspond à la saturation de la monocouche à la surface de l'adsorbent et confirme que l'adsorption des ions chromates sur la membrane peut être décrite par l'isotherme de Langmuir. Il convient de noter que les capacités maximales d'adsorption atteignent 314 mg Cr g^{-1} et 331 mg TCr g^{-1}. La courbe représentative de l'isotherme du TCr se distingue de celle du Cr(VI) par une allure sigmoïdale, modélisée préférentiellement par l'équation de Sips. Ces valeurs sont particulièrement élevées par rapport aux données disponibles dans la littérature. Un inconvénient majeur reste lié à la difficulté de désorber les ions chromates adsorbés sur la membrane (le rendement de désorption n'atteint pas 50 %), rendant le recyclage de l'adsorbant progressivement moins performant. C'est probablement lié à un phénomène de réduction du Cr(VI) en Cr(III) (associée à une dégradation du matériau par oxydation de certains groupements fonctionnels) qui limite la régénération du support.

Les membranes PEI/alginate ont été testées pour finir sur un effluent de galvanoplastie reconstitué, contenant différents ions compétiteurs. La présence de ces ions compétiteurs ne semble pas affecter les performances d'adsorption (comparée à une solution synthétique ne contenant que les ions chromates). La présence d'ions nitrate ou chlorure n'a qu'un effet négligeable sur la fixation du chrome, contrairement aux ions sulfates (divalents).

2.3. Adsorption des ions sélénates [12]

Dans la continuité du travail réalisé sur les anions chromates, de nouveaux essais ont été réalisés sur des membranes composites PEI/alginate (avec une teneur en PEI portée à 4 %) pour augmenter la stabilité et la réactivité du matériau. Les ions sélénates se caractérisent par une moindre propension à être réduits en milieu acide (comparativement aux ion Cr(VI)). L'affinité maximale de l'adsorbant pour les anions sélénates est également obtenue à pH 2 par interaction avec les groupements aminés protonés à la surface de l'adsorbant.

Les cinétiques de fixation ne sont pas significativement affectées par le flux de solution circulant au travers des membranes pour des valeurs de (ou supérieures à) 15 mL min^{-1} (V_s=1,83 m h^{-1}); pour des valeurs inférieures (i.e., 5 mL min^{-1} ; V_s=0,61 m h^{-1}) (Fig. 3a). Il est vraisemblablement nécessaire d'imposer une vitesse de passage suffisante pour forcer le passage de la solution dans des pores moins accessibles ou de plus grande tortuosité (lié à l'hétérogénéité du réseau poreux). Une autre différence fondamentale avec le cas des ions chromates porte sur le temps de contact nécessaire pour atteindre l'équilibre : 2 h pour Se(VI) contre plusieurs jours pour Cr(VI). Les cinétiques de fixation sont décrites par le modèle de l'équation cinétique de pseudo premier ordre (PFORE, même si le PSORE permet une meilleure approche de la capacité de fixation à l'équilibre).

Les isothermes d'adsorption sont présentées sur la Fig. 3b: la meilleure corrélation mathématique est obtenue avec le modèle de Sips (à 3 paramètres ajustables) mais l'équation de Langmuir (plus mécanistique) permet une bonne simulation de la courbe expérimentale. La capacité maximale de fixation approche 80 mg Se g^{-1}, cette valeur dépasse les capacités de fixation rapportée pour la majorité des bioadsorbants mais se révèle inférieure à celles de certaines résines synthétiques. Contrairement au cas du chromate, la désorption du Se(VI) est quasi complète en utilisant des solutions de soude (0.01 M). La Fig. 4 montre que la désorption varie entre 90 et 98 % au cours des 4 cycles d'utilisation alors que la capacité de fixation reste stable (autour de 63-66 mg Se g^{-1}, dans les conditions expérimentales choisies).

Cette différence est probablement liée à la différence des contributions de réduction pour Cr (VI) et Se (VI). Même si l'analyse XPS met en évidence des phénomènes de réduction partielle dans le cas des ions sélénates, il semblerait que ces phénomènes présentent une acuité plus marquée pour la fixation des ions chromates soit directement par "l'empoisonnement" de la surface de l'adsorbant soit par dégradation (oxydation) des groupes réactifs (ou des éléments de structure du matériau).

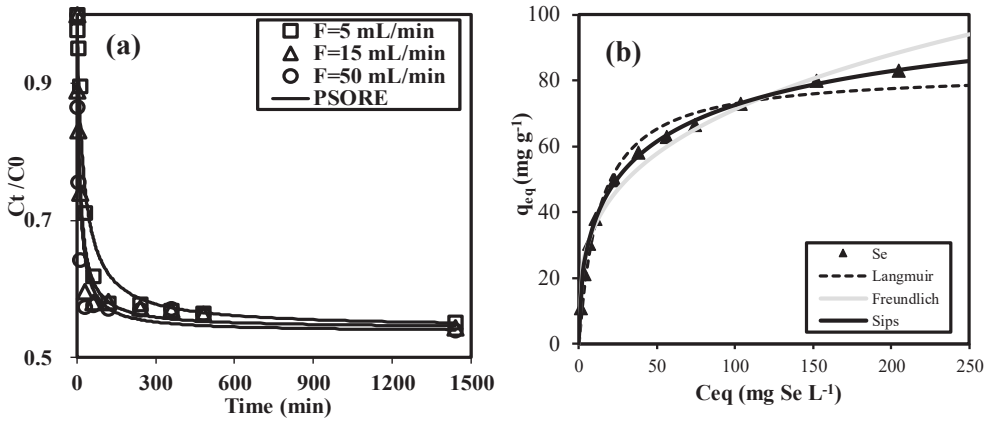

Fig. 3 Cinétiques de fixation (a) et isothermes d'adsorption (b) pour la fixation de Se(VI) sur les membranes PEI/Alginate à pH 2 (Cinétiques : C_0 = 50 mg Se L^{-1}; concentration en sorbant = 0,4 g L^{-1}; V= 500 mL ; pH: 2; température = 20 ± 1 °C. Isothermes : concentration en sorbant = 0,8 g L^{-1}; V= 50 mL ; durée = 24 h; débit = 15 mL min^{-1}; température = 20 ± 1 °C).

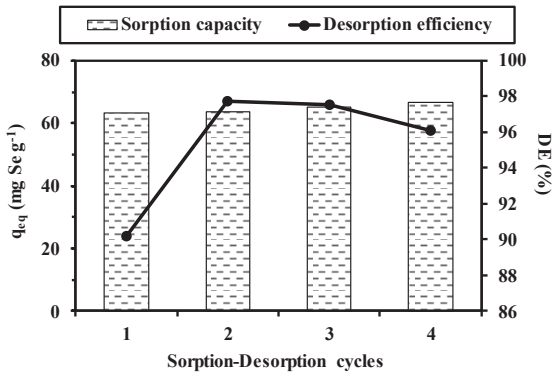

Fig. 4 Cycles de sorption – désorption du Se(VI) (Sorption : C_0 = 100 mg Se L^{-1}; concentration en sorbant = 0,8 g L^{-1}; pH: 2; débit = 15 mL min^{-1}; température = 20 ± 1

°C. Désorption : agent de désorption : 0,01 M NaOH; V= 50 mL ; durée = 30 min; débit = 15 mL min^{-1}; température = 20 ± 1 °C).

2.4. Adsorption de cations métalliques (Hg(II) and Cu(II))

Afin d'étudier l'applicabilité de notre matériau bioadsorbant vis-à-vis des métaux lourds, l'adsorption de deux cations (Hg(II) et Cu(II)) a été testée sur des membranes PEI/Alginate (contenant 4 % de PEI). Les études ont été menées en solutions simple et binaire afin d'examiner la sélectivité de l'adsorbant vis-à-vis de ces deux ions métalliques, qui ont été sélectionnés pour leurs comportements différents en milieu aqueux (vis-à-vis notamment de la formation de complexes avec les ions chlorure). Une attention particulière est portée également à l'effet du pH sur l'adsorption de ces deux métaux lourds (Fig. 5). Cette figure démontre clairement, pour une gamme de pH de 1 à 4, l'effet limité du pH sur la fixation du mercure, et la capacité de l'adsorbant de fixer l'ion métallique même en milieu très acide.

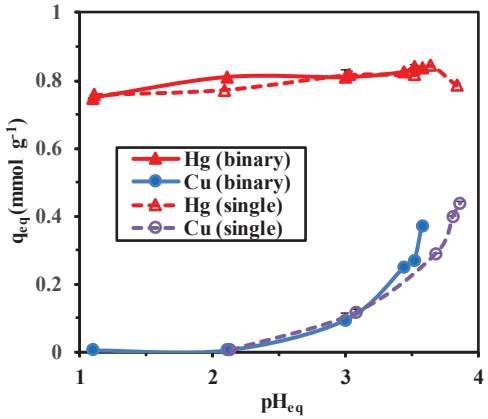

Fig. 5 Effet du pH sur l'adsorption de Hg(II) et Cu(II) sur les membranes de PEI/Alginate en solutions mono-composé et bi-composés. (pH initial = 1-7 (ajusté par HCl et NaOH) ; concentration metal = 0.5 mmol L^{-1} pour Cu(II) ou Hg(II) en solution monocomposé and 1.0 mmol L^{-1} du mélange équimolaire [Hg(II):Pb(II)=1:1]; concentration du sorbant = 0.5 g L^{-1}; temps de contact = 3 j ; température, T= 20± 1 °C).

A pH acide, en milieu HCl, le Hg forme des complexes chloroanioniques ($HgCl_4^{2-}$) pouvant être fixés sur les sites protonés de la PEI. La protonation du support sur une large plage de pH, en accord avec le pH_{PCN} du sorbant inférieur à 5,7, permet de stabiliser cette fixation sur la plage de pH 1-4. Le comportement du cuivre est complètement différent : ne formant pas de complexe chloroanionique, à pH acide (1-2,1) l'adsorption des cations Cu(II) reste négligeable car la protonation tant des fonctions aminées que des groupements carboxyliques limite l'adsorption du cation. Au-delà de pH 2,2, l'adsorption du cuivre augmente progressivement, en lien avec la diminution de la protonation des groupements réactionnels (fonctions aminées et formation de groupes carboxylates). Il convient de noter que l'adsorbant peut ainsi séparer sélectivement le cuivre du mercure entre pH 1 et 2 (en milieu HCl).

Les isothermes d'adsorption du mercure et du cuivre sont comparées à pH 5 pour différentes compositions de solutions: en solution mono-composé comme référence, ainsi que dans des

conditions d'équimolarité et de large excès (4:1) de l'un des ions métalliques vis-à-vis de l'autre (Fig. 6). La Fig. 6a montre que l'adsorption du mercure n'est pas affectée par la présence de cuivre (même en large excès). La capacité maximale de fixation atteint 1,39 mmol Hg g^{-1} (i.e., 279 mg Hg g^{-1}). L'isotherme approche le profil type de Langmuir, bien que le plateau de saturation ne soit pas observé sur cette plage de concentrations; l'isotherme de Sips permet une meilleure simulation du profil expérimental. Le comportement du cuivre est complètement différent: la capacité maximale de fixation obtenue dans des solutions mono-composé n'excède pas 0,56 mmol Cu g^{-1}, (i.e., 35,6 mg Cu g^{-1}). Il apparaît clairement sur la Fig. 6b que la présence de mercure réduit drastiquement la fixation du cuivre : cela s'exprime par une diminution de la pente initiale (corrélée à l'affinité de l'adsorbant pour le métal) et de la capacité d'adsorption à saturation de l'adsorbant. Comme expliqué précédemment, les ions mercure (complexés sous forme chloro-anioniques) se fixent préférentiellement sur les groupements fonctionnels protonés de l'adsorbant tout en limitant l'accès des ions Cu(II). Bien que les deux métaux s'adsorbent potentiellement sur différents groupes fonctionnels (étude de l'effet du pH), certains sites fixant le cuivre sont également saturés par le mercure en solutions bi-métalliques. Plus la quantité de mercure est élevée par rapport à celle de cuivre (rapport molaire Hg-Cu = 4:1), plus la sorption de cuivre est abaissée.

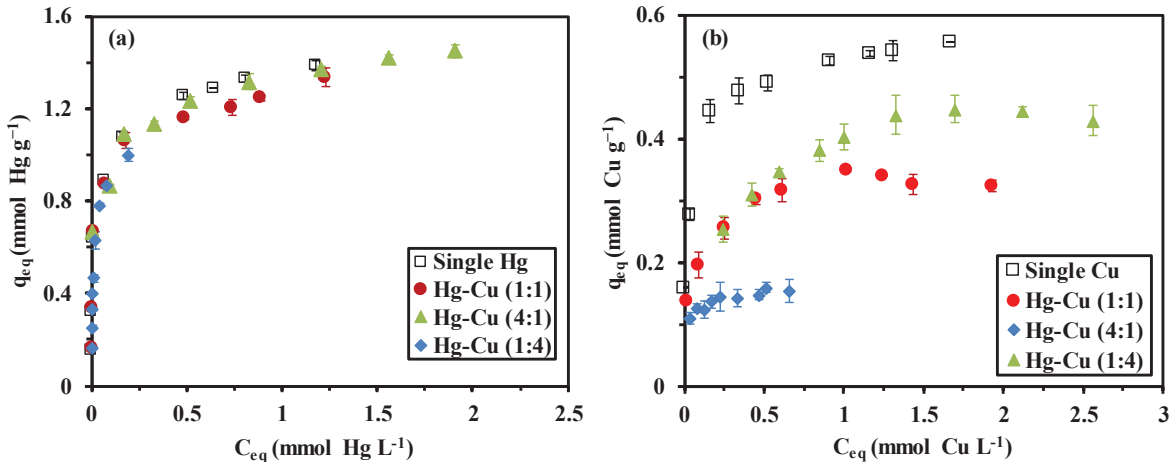

Fig. 6 Isothermes d'adsorption de Hg(II) et Cu(II) pour différentes conditions opératoires: solutions mono-composé, solution équimolaire, excès molaire (Hg(II)/Cu(II) = 4/1 et 1/4). (concentration en sorbant = 0,6 g L^{-1} ; pH initial = 5; temps de contact = 78 h; T = 20± 1 °C; concentration en Hg(II) ou Cu(II) = 0,1-2 mmol L^{-1} en solution monocomposé ou équimolaire Hg-Cu(1:1); 0,1-2,8 mmol L^{-1} en excès molaire de l'un des deux cations, Hg-Cu(4:1) et Hg-Cu(1:4) où Hg-Cu: rapport molaire de Hg(II) et Cu(II)).

L'équation de Sips (étendue à l'adsorption en solutions multi-composés) a été utilisée pour modéliser l'adsorption simultanée du Cu(II) et du Hg(II) (Fig. 7). Le modèle permet une bonne simulation des profils expérimentaux: le coefficient de détermination (R^2) atteint 0,97. Cette représentation en 3D illustre les différences de comportement pour l'adsorption du mercure en présence de cuivre: la surface est régulière avec un profil en plateau (type Langmuir) variant peu en fonction de la concentration en cuivre; au contraire, le mercure réduit drastiquement

l'accumulation du cuivre. Cette figure confirme la préférence de l'adsorbant pour le mercure qui forme des espèces anioniques (en milieu HCl) directement adsorbées sur les groupes aminés protonés de la membrane composite (les formes Hg^{2+} peuvent être également fixées par chélation sur les fonctions amines primaires libres), alors que la fixation du cuivre libre (Cu^{2+}) s'opère par chélation sur les fonctions aminées libres et les carboxylates (en milieu moins acide, à savoir pH >2,5).

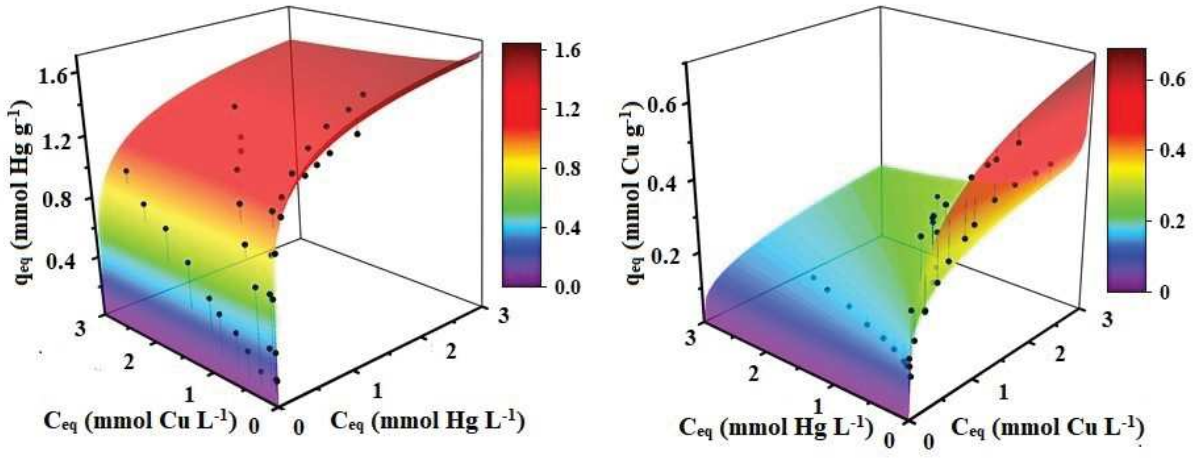

Fig. 7 Représentation en 3D de la "surface" d'adsorption du mercure (gauche) et du cuivre (droite) simulée par le modèle de Sips en mode multiéléments (adsorption compétitive): points expérimentaux et surfaces de simulation.

2.5. Comparaison de l'adsorption des ions sélénates et des ions cuivre pour différents niveaux de réticulation (adsorbant : PEI/GA) – Effet des conditions de stockage [13]

La comparaison des performances de fixation du cuivre et du mercure à la section précédente a permis d'illustrer l'effet de la spéciation des ions métalliques (formation favorable d'espèces chloro-anioniques de mercure) sur les mécanismes de fixation. La réticulation des fonctions aminées de la PEI par le glutaraldéhyde se traduit par la formation de liaisons imines qui diminue la quantité de fonctions amine primaires libres susceptibles de chélater des cations métalliques. Il est donc apparu pertinent d'évaluer l'effet du taux de réticulation (au travers de la quantité de GA mise en œuvre) sur la fixation de deux types d'ions métalliques par un adsorbant constitué de PEI réticulé par le GA et conditionné en poudre de granulométrie inférieure à 0,2 mm : un anion métallique (sélénates, Se(VI)) et un cation métallique (Cu(II)). Dans cette étude, des adsorbants ont ainsi été préparés avec 10 g, 16 g, 20 g, et 30 g de GA. Ils sont dénommés PEI-GA1, PEI-GA2, PEI-GA3 et PEI-GA4 et possèdent des taux de réticulation respectifs de 48,0 ± 3,8%, 56,7 ± 3,1%, 62,5 ± 1,9% et 72,0 ± 0,8%.

Par ailleurs, cette partie de l'étude a permis d'évaluer la stabilité de l'adsorbant et de préconiser des conditions de stockage appropriées pour éviter une baisse de son affinité pour les ions métalliques.

La Fig. 8 compare les cinétiques de fixation du Se(VI) et du Cu(II) pour différents niveaux de réticulation, et pour deux modes de stockage (flacon scellé et flacon ouvert, correspondant notamment à une éventuelle sorption de CO_2 atmosphérique).

Dans le cas des ions sélénates (Se(VI)), il convient de noter les niveaux très élevés des capacités d'adsorption enregistrées compris, à l'équilibre des cinétiques de fixation, entre 4 et 5 mmol Se g^{-1}. Bien que ces capacités n'aient pas été obtenues dans des conditions de saturation (plateau de l'isotherme), elles démontrent que cet adsorbent atteint les capacités les plus élevées parmi les résines testées pour la fixation du Se(VI) [12]. L'adsorption des anions métalliques Se(VI) n'est pratiquement pas modifiée par le taux de réticulation, à l'exception remarquable du taux de réticulation le plus élevé (72%) pour lequel une baisse de 0,6-0,7 mmol Se g^{-1} est observée. En effet, l'adsorption des ions sélénates par échange ionique/attraction électrostatique n'est que marginalement influencée par la réticulation, car ce sont les fonctions aminées protonées qui opèrent l'adsorption des anions métalliques. Un stockage de l'adsorbant en flacon scellé est suffisant pour maintenir, au moins pendant 20 jours, les performances de fixation. Au contraire, dans le cas d'un stockage en flacon ouvert, la capacité de fixation est légèrement diminuée (par moins de 0,1 mmol Se g^{-1}).

Dans le cas de Cu(II), l'augmentation du taux de greffage réduit drastiquement et progressivement les capacités de fixation de 1,3 mmol Cu g^{-1} à 0,57 mmol Cu g^{-1} pour le taux de réticulation le plus élevé. Le greffage réduit la densité de sites aminés libres susceptibles de complexer le cuivre libre. Toujours pour le cuivre, le stockage en flacon fermé induit une faible diminution de la capacité de fixation (moins de 0,1 mmol Cu g^{-1}); cette diminution est nettement plus marquée lorsque l'adsorbant est stocké en flacon ouvert (pouvant atteindre jusqu'à 0,3 mmol Cu g^{-1}, soit une baisse de 25 %).

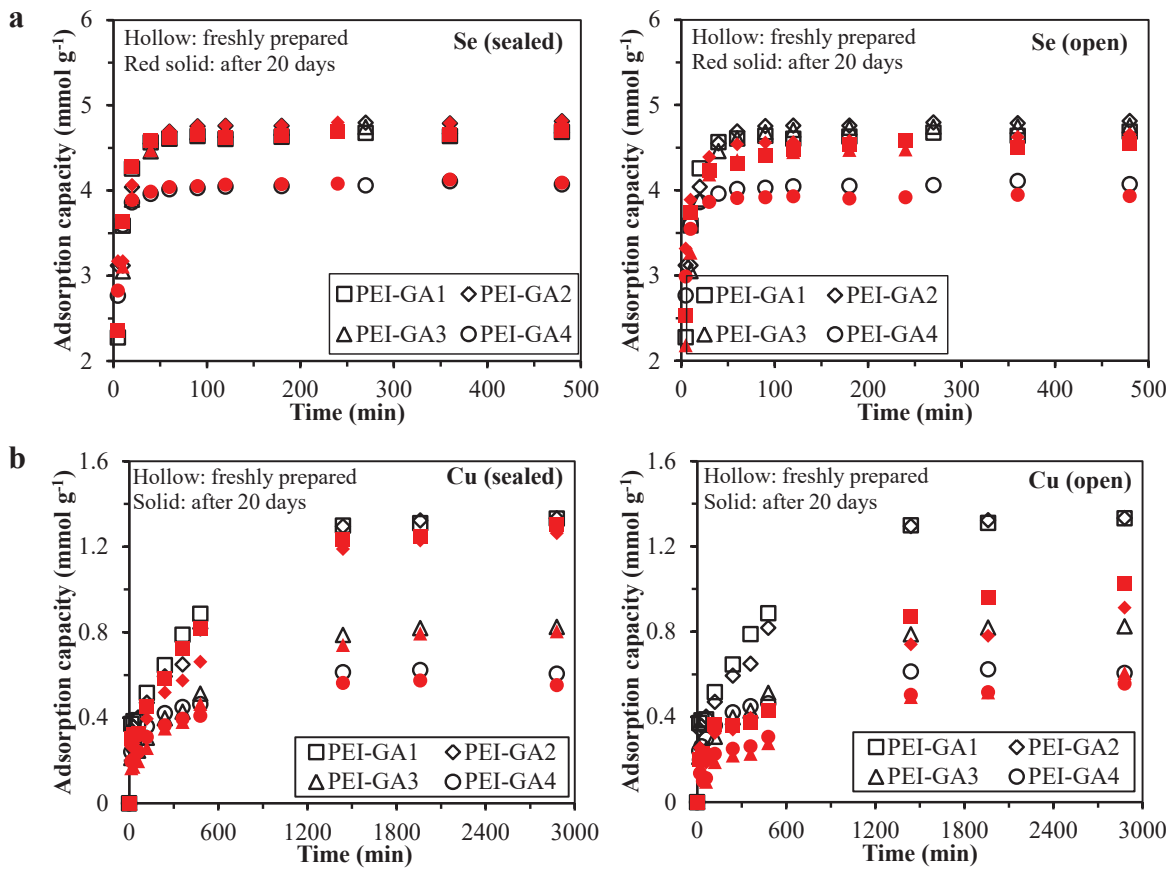

Fig. 8 Effet des conditions de stockage et des niveaux de réticulation de la PEI sur les cinétiques de fixation de Se(VI) (a) et Cu(II) (b) (V = 0,5 L; T ambiante (19-25 °C); masse adsorbant = 100 mg pour Se(VI) et 200 mg pour Cu(II); C_0 = 0,5 mmol L^{-1} pour Se(VI) et 1 mmol L^{-1} pour Cu(II); pH_0 = 2 pour Se(VI) et 3 pour Cu(II)). Note: freshly prepared adsorbents were the materials stored in sealed condition within 5 days.

L'effet des conditions de stockage a été expliqué par l'adsorption de CO_2 atmosphérique à la surface de l'adsorbant (au niveau des fonctions amines) suivie de la formation de carbamate. Cette modification chimique au niveau des groupes réactifs aminés se traduit par une diminution de l'activité chélatante des fonctions aminées (effet plus marqué pour le cuivre vis-à-vis du sélénium).

L'influence du taux de réticulation de la PEI sur les propriétés d'adsorption sélective a été également testée en solution binaires contenant deux cations divalents (Pb(II) et Cu(II)) ou deux anions (sélénate et arséniate) à trois valeurs différentes de pH (Fig. 9). A pH 2, l'adsorbant (PEI/GA) est sélectif pour Se(VI) vis-à-vis de As(V): les capacités de fixation à l'équilibre pour Se(VI) atteignent 3,8-4,6 mmol Se g^{-1}; elles n'excèdent pas 0,1 mmol As g^{-1}. Quand le pH augmente, l'adsorption de l'arsenic As(V) augmente progressivement, jusqu'à 0,2-0,4 mmol As g^{-1}, alors que celle de Se(VI) tend à légèrement diminuer (3,6-4,1 mmol Se g^{-1}). Le taux de réticulation a un effet relativement limité sur les performances de fixation: les deux anions métalliques se fixent sur des sites protonés à la surface de l'adsorbent.

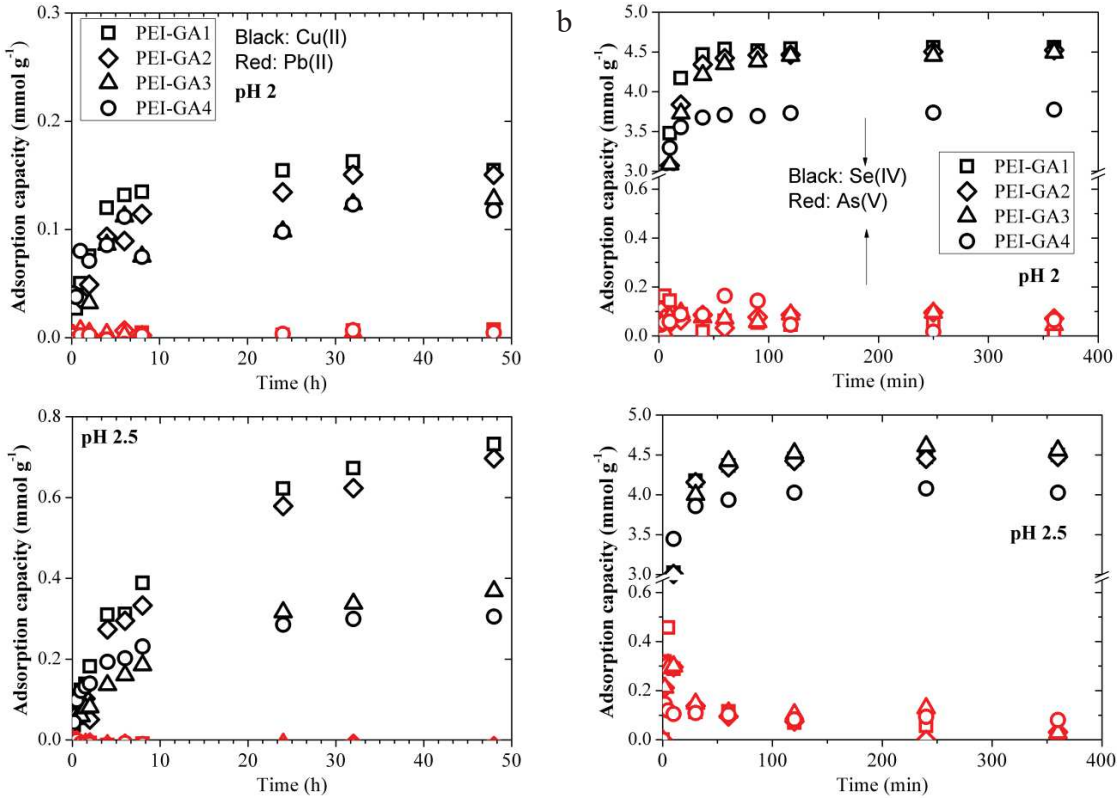

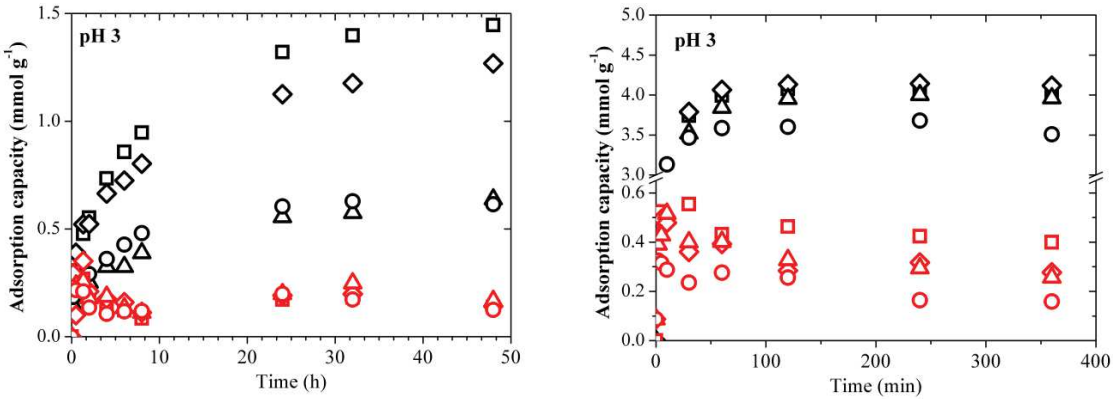

Fig. 9 Comparaison des cinétiques de fixation en solutions binaires Cu(II)/Pb(II) et Se(VI)/As(V) à différentes valeurs de pH = 2; 2,5; 3 (V = 0,5 L ; T ambiante ; masse adsorbant = 100 mg; C_0 = 0,5 mmol L^{-1} pour Se(VI) et As(V) et 1 mmol L^{-1} pour Cu(II) et Pb(II)).

La sélectivité de l'adsorbant pour Se(VI) (vs. As(V)) peut s'expliquer par des différences dans leurs profils de spéciation: espèces anioniques pour Se(VI) facilement adsorbées par attraction électrostatique sur les fonctions aminées protonées en milieu acide, alors que pour As(V) les espèces prédominantes en milieu très acides sont neutres. L'augmentation du pH favorise la formation d'espèces anioniques, adsorbables sur les sites aminés protonés: les ions arséniate entrent en compétition avec les ions sélénates (même si la capacité de fixation du sélénium ne diminue que légèrement).

Dans le cas de la paire Pb(II)/Cu(II), la capacité de fixation augmente avec le pH pour le cuivre (de 0,12 à 0,15 mmol Cu g^{-1} à pH 2 à 0,55-1,45 mmol Cu g^{-1} à pH 3). L'adsorption du plomb reste négligeable à pH 2 et 2.5 mais augmente légèrement à 0.2 mmol Pb g^{-1} à pH 3. L'adsorbant présente une sélectivité pour le cuivre par rapport au plomb. Cette différence a été associée au mode de chélation (square-planar pour Cu(II) *vs.* octahedral pour Pb(II)). C'est également corrélé aux différences observées dans les constantes de complexation des deux ions métalliques avec les amines (par exemple, log $K(Cu/NH_3)$ = 4,12 > log $K(Pb/NH_3)$ = 1,6).

2.6. Hydrogénation du 3-nitrophénol sur des nanoparticules de palladium immobilisé sur membrane PEI/Alginate [14]

L'intérêt de la fixation d'ions métalliques sur des supports adsorbants n'est pas limité aux seules applications environnementales et de valorisation des métaux; en effet ces interactions peuvent être mises à profit pour synthétiser par exemple des catalyseurs supportés. L'hydrogénation hétérogène de composés nitrophénolés (NP) par des nanoparticules de palladium représente un exemple emblématique et très simple d'application dans ce domaine [15]. Le concept est basé sur une première phase d'immobilisation du Pd(II) par adsorption des ions métalliques ($PdCl_4^{2-}$ en milieu HCl) par recirculation de la solution au travers de la membrane. Des capacités maximales d'adsorption proches de 224 mg Pd g^{-1} ont été ainsi obtenues. La deuxième phase consiste à provoquer la réduction (souvent partielle) du palladium immobilisé sur l'adsorbant

au moyen d'un agent réducteur. Cette opération est réalisée au moyen d'une solution alcaline d'hydrate d'hydrazine ($N_2H_4 \cdot H_2O$), des analyses XPS ayant montré que le rendement de réduction était proche de 44%. Le catalyseur obtenu peut ensuite être utilisé en colonne (en mode recirculation, équivalent au réacteur parfaitement agité) pour l'hydrogénation du 3-NP en présence de formiate de sodium. Les différents travaux réalisés au sein de l'IMT-Mines Alès, notamment sur des supports de type chitosane, ont mis en évidence l'impact de la concentration en Pd sur la taille des nanoparticules immobilisées sur le support et par voie de conséquence sur leurs propriétés catalytiques. C'est sur ce paramètre que les premiers essais ont été menés. Les membranes PEI/Alginate (pour un poids sec de 255 ± 10 mg) ont été chargées en Pd avec des solutions (volume, 1 L) de différentes concentrations (i.e., 11, 16, 21, 28 et 52 mg L^{-1}). Afin d'obtenir une membrane homogène en terme de distribution du palladium, le flux de circulation de la solution a été maintenu à une valeur de 30 mL min^{-1}. Ainsi, le palladium ne s'accumule pas préférentiellement sur la face d'alimentation de la membrane mais dans la totalité de son volume. Les taux élevés de rétention du palladium (respectivement : 100, 99,8, 98,5, 97,1 et 71 %) confirment l'affinité des membranes pour le palladium (par interaction entre les anions chloro-palladate et les groupements aminés protonés). Les capacités d'adsorption correspondantes atteignent: 43,8, 67,7, 84,0, 110,4 et 154,5 mg g^{-1}, respectivement.

La Fig. 10 compare les profils cinétiques d'hydrogénation du 3-NP pour différentes valeurs de la charge en Pd (a) et pour différents flux de solution métallifère (b). Un test mené en contrôle sur une membrane vierge (sans Pd) montre une diminution négligeable de la concentration relative du 3-NP dans la solution: l'adsorption du substrat sur la membrane est négligeable. Aux plus faibles charges (i.e., 11 et 16 mg) les niveaux d'abattement sont négligeables: ils correspondent à un abattement de la concentration en 3-NP de quelques pourcents. Il faut atteindre une teneur limite proche de 21 mg (pour une membrane d'environ 255 mg) pour qu'une activité catalytique significative s'exprime. Il est important de remarquer qu'au-delà de cette quantité critique un ajout supplémentaire de palladium (i.e., 27 et 37 mg) n'améliore que marginalement le profil d'hydrogénation. L'observation en MET montre une dispersion homogène du palladium à la surface des feuillets de la membrane, avec des tailles de particules nanométriques de 4,5 à 10,5 nm (distribution centrée autour de 7,61 ± 1,93 nm).

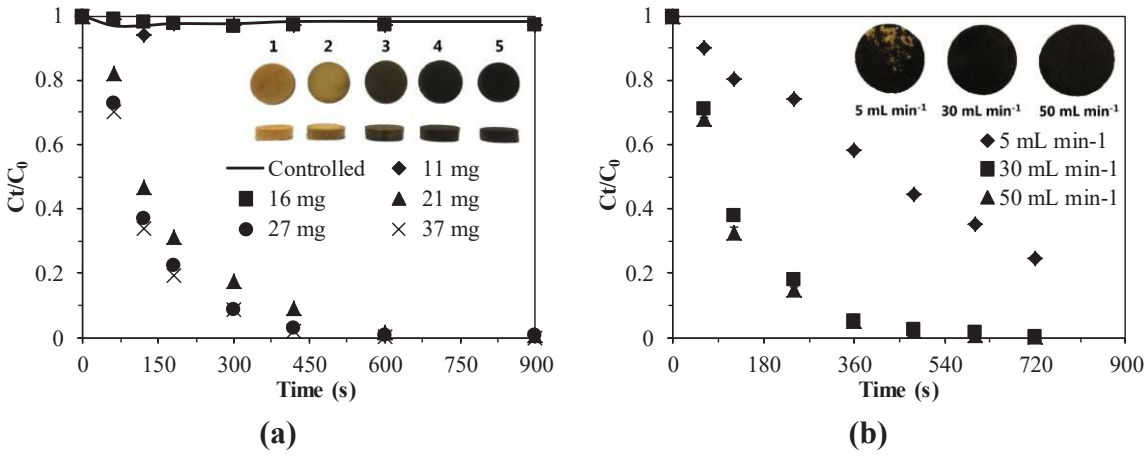

(a) (b)

Fig. 10 Effet sur la cinétique d'hydrogénation hétérogène du 3-NP par la membrane Pd/PEI/Alginate de la charge en Pd (mg/membrane) (a) (procédé de sorption du Pd(II): masse de membrane = 255±10 mg; débit = 30 mL min^{-1} ; concentration d'alimentation C_0 (Pd(II)), 10-50 mg L^{-1}. Etape d'hydrogénation du 3-NP : concentration d'alimentation C_0 (3-NP) = 50 mg L^{-1}; V = 0,1 L; pH (non-contrôllé), 2,86 ; débit = 50 mL min^{-1}; concentration d'acide formique $C_{(HCOOH)}$, 0.2%) ; du flux d'alimentation en solution métallifère (étape de synthèse du catalyseur) (b) procédé de sorption du Pd(II): masse de membrane = 255±10 mg ; concentration d'alimentation C_0 (Pd(II)) = 28 mg L^{-1}. Etape d'hydrogénation du 3-NP: concentration d'alimentation C_0 (3-NP) = 50 mg L^{-1}; quantité de Pd = 27 mg; V = 0,1 L; pH (non-contrôllé), 2,86 ; débit = 50 mL min^{-1}; $C_{(HCOOH)}$, 0.2%)).

La Fig. 10b illustre la nécessité d'imposer un flux minimum au travers de la membrane pour assurer une distribution homogène de la solution dans la totalité de la membrane et donc une répartition homogène du Palladium dans tout le volume du catalyseur. Ainsi un débit de 5 mL min^{-1} induit probablement une accumulation préférentielle du Pd sur la face d'entrée de la membrane au détriment du reste du volume de la membrane: le Pd forme potentiellement des agrégats sur cette face alors que le reste du catalyseur présentera une densité insuffisante en NPs de palladium. Cette hypothèse est confirmée par les photographies (insérées dans la Fig. 10b) représentant la face arrière des membranes. Alors que pour les débits d'imprégnation élevés, la face arrière apparaît homogène (coloration brun foncé/noir), dans le cas du débit réduit, des zones présentent une coloration proche de celle de la membrane non-imprégnée de Pd. Cet effet peut s'exprimer à travers une hétérogénéité de dispersion du Pd ou d'hétérogénéité de réduction du Pd. Cela se manifeste sur le profil d'hydrogénation par une moindre réactivité et une cinétique défavorable. Au contraire, pour les membranes chargées en Pd avec des flux plus importants (i.e., 30 et 50 mL min^{-1}), la distribution homogène de la même quantité de Pd dans la totalité du volume de la membrane, tout en évitant la formation d'agrégats, permet d'optimiser le profil cinétique et donc d'améliorer le TOF de la réaction (taux de conversion rapporté à la masse de métal catalytique). Un bon compromis pour la préparation de ces membranes en tant que supports catalytiques consiste donc à imposer un flux de 50 mL min^{-1} pour la fixation du palladium (et sa réduction).

Sur la base de ces conclusions, les membranes optimisées ont été testées pour différentes conditions opératoires. Les profils cinétiques ont été modélisés avec succès en utilisant l'équation cinétique de pseudo-premier ordre. La stabilité du catalyseur a été testée en comparant les performances catalytiques pour 30 cycles successifs: une diminution progressive de l'efficacité est observée à partir du $20^{ème}$ cycle. Pour finir, des essais ont été réalisés sur des membranes utilisées en mode dynamique (percolation sans recirculation, à plus faible débit d'alimentation). Une baisse progressive de l'efficacité de conversion est observée due à un empoisonnement du catalyseur. Il convient toutefois de noter qu'une phase de lavage simple (avec de l'eau déminéralisée) permet de restaurer l'efficacité catalytique. Ces différents résultats démontrent l'intérêt de ces membranes à haut pouvoir de percolation comme supports

de métaux catalytiques pour la catalyse hétérogène (l'hydrogénation hétérogène étant prise comme exemple simple de réaction catalytique).

3. Conclusions

Un procédé original de fabrication de membranes à haut pouvoir de percolation a été mis au point et optimisé. Cette méthode simple permet, par mélange dans des conditions contrôlées de deux solutions d'alginate et de polyethyleneimine, d'obtenir un hydrogel structuré dont la stabilité est améliorée par réticulation (des fonctions aminées de la PEI par le glutaraldéhyde). Cette double interaction (PEI/Alginate, PEI/GA) permet d'obtenir après séchage à l'air libre (donc peu énergivore et sans moyen sophistiqué contrairement aux procédés conventionnels) de produire des membranes "hyper" macroporeuses autorisant la percolation par drainage simple de solutions.

La coexistence de deux types de groupements fonctionnels (carboxylates et amines) offre de nombreuses possibilités d'interaction avec les ions métalliques en jouant tant sur des propriétés de chélation (carboxylates, amines libres) que des propriétés d'échange ionique/attraction électrostatique (amines protonés) en fonction de la typologie du métal, de sa spéciation et du pH de la solution. Ces différentes possibilités ont été illustrées par une série d'expérimentations portant sur des ions métalliques tels que: Hg(II), Cu(II), Pb(II), Se(VI), Cr(VI), As(V). Ces différentes études ont permis d'illustrer: (a) l'affinité particulière des membranes pour les anions métalliques (préférentiellement aux cations) en raison notamment de la plus grande disponibilité des fonctions aminées protonées, (b) la criticité du taux de réticulation, en particulier pour les interactions mettant en œuvre des mécanismes de chélation (essais réalisés sur un adsorbant spécifique: PEI/GA en poudre). Sur ce même adsorbant, un phénomène inattendu a été mis en évidence: la fixation de CO_2 sur les fonctions aminées conduit à la formation de carbamates et diminue les performances d'adsorption pour certains métaux (notamment ceux impliquant une adsorption par chélation). Cela conduit à préconiser un stockage en flacon scellé des adsorbants PEI/GA pour éviter cette contamination et ses effets associés.

L'affinité de ces membranes PEI/Alginate pour les anions métalliques a été mise à profit pour synthétiser des catalyseurs hétérogènes portant des nanoparticules de palladium à partir d'une séquence: adsorption du palladium (par échange d'ions/attraction électrostatique de $PdCl_4^{2-}$ en milieu HCl), suivie d'une réduction par l'hydrate d'hydrazine. Les résultats obtenus montrent que plutôt que de privilégier une forte concentration en palladium, il est préférable de réaliser une distribution homogène du métal à concentration intermédiaire (de l'ordre de 8 % en masse) afin d'éviter la formation d'agglomérats de moindre efficacité catalytique. Le catalyseur est régénérable par rinçage à l'eau, pour la réaction simple sélectionnée dans cette étude (hydrogénation du 3-nitrophénol par le formiate de sodium).

Ces matériaux ouvrent de nouvelles perspectives tant par leur mode de synthèse (peu énergivore), que par leurs propriétés de percolation (incluant une application en drainage par écoulement naturel) ou que la versatilité offerte par les groupements fonctionnels présents

(groupes carboxyliques et fonctions aminées). Ils ouvrent également des perspectives en vue de fonctionnaliser ces membranes par greffage de fonctions spécifiques en vue d'améliorer leur sélectivité ou réactivité (thèse en cours), par analogie avec les travaux réalisés sur des adsorbants innovants à base d'algues et PEI (APEI) [16-18].

Références

[1] F. Fu, Q. Wang, Removal of heavy metal ions from wastewaters: a review, Journal of environmental management, 92 (2011) 407-418.
[2] M. Bilal, J.A. Shah, T. Ashfaq, S.M.H. Gardazi, A.A. Tahir, A. Pervez, H. Haroon, Q. Mahmood, Waste biomass adsorbents for copper removal from industrial wastewater—a review, Journal of hazardous materials, 263 (2013) 322-333.
[3] E. Cochrane, S. Lu, S. Gibb, I. Villaescusa, A comparison of low-cost biosorbents and commercial sorbents for the removal of copper from aqueous media, Journal of hazardous materials, 137 (2006) 198-206.
[4] E. Guibal, Interactions of metal ions with chitosan-based sorbents: a review, Separation and purification technology, 38 (2004) 43-74.
[5] C. Jouannin, C. Vincent, I. Dez, A.-C. Gaumont, T. Vincent, E. Guibal, Study of alginate-supported ionic liquid and Pd catalysts, Nanomaterials, 2 (2012) 31-53.
[6] Y. Huang, H. Wu, T. Shao, X. Zhao, H. Peng, Y. Gong, H. Wan, Enhanced copper adsorption by DTPA-chitosan/alginate composite beads: mechanism and application in simulated electroplating wastewater, Chemical Engineering Journal, 339 (2018) 322-333.
[7] A. Haug, Dissociation of alginic acid, Acta Chemica Scandinavia, 15 (1961) 950-952.
[8] K.D. Demadis, M. Paspalaki, J. Theodorou, Controlled release of bis(phosphonate) pharmaceuticals from cationic biodegradable polymeric matrices, Industrial & Engineering Chemistry Research, 50 (2011) 5873-5876.
[9] T. Andersen, J.E. Melvik, O. Gåserød, E. Alsberg, B.E. Christensen, Ionically gelled alginate foams: physical properties controlled by type, amount and source of gelling ions, Carbohydrate polymers, 99 (2014) 249-256.
[10] M. Robitzer, A. Tourrette, R. Horga, R. Valentin, M. Boissière, J.-M. Devoisselle, F. Di Renzo, F. Quignard, Nitrogen sorption as a tool for the characterisation of polysaccharide aerogels, Carbohydrate polymers, 85 (2011) 44-53.
[11] Y. Mo, S. Wang, T. Vincent, J. Desbrieres, C. Faur, E. Guibal, New highly-percolating alginate-PEI membranes for efficient recovery of chromium from aqueous solutions, Carbohydrate Polymers, 225 (2019).
[12] Y. Mo, T. Vincent, C. Faur, E. Guibal, Se(VI) sorption from aqueous solution using alginate/polyethylenimine membranes: Sorption performance and mechanism, International Journal of Biological Macromolecules, 147 (2020) 832-843.
[13] S. Wang, K. Xiao, Y. Mo, B. Yang, T. Vincent, C. Faur, E. Guibal, Selenium(VI) and copper(II) adsorption using polyethyleneimine-based resins: Effect of glutaraldehyde crosslinking and storage condition, Journal of Hazardous Materials, 386 (2020).
[14] S. Wang, Y. Mo, T. Vincent, J.-C. Roux, E. Rodriguez-Castellon, C. Faur, E. Guibal, Palladium nanoparticles supported on amine-functionalized alginate foams for hydrogenation of 3-nitrophenol, Journal of Materials Science, 55 (2020) 2032-2051.
[15] S. Wang, T. Vincent, C. Faur, E. Rodriguez-Castellon, E. Guibal, A new method for incorporating polyethyleneimine (PEI) in algal beads: High stability as sorbent for palladium recovery and supported catalyst for nitrophenol hydrogenation, Materials Chemistry and Physics, 221 (2019) 144-155.
[16] M.F. Hamza, A.E. Mubark, Y. Wei, T. Vincent, E. Guibal, Quaternization of composite algal/PEI beads for enhanced uranium sorption – Application to ore acidic leachate, Gels (Basel, Switzerland), in press (2020).
[17] M.F. Hamza, Y. Wei, E. Guibal, Quaternization of algal/PEI beads (a new sorbent): characterization and application to scandium recovery from aqueous solutions, Chemical Engineering Journal, in press, DOI: 10.1016/j.cej.2019.123210 (2020).

[18] Y. Wei, K.A.M. Salih, S. Lu, M.F. Hamza, T. Fujita, T. Vincent, E. Guibal, Amidoxime functionalization of algal/polyethyleneimine beads for the sorption of Sr(II) from aqueous solutions, Molecules, 24 (2019) Art. N° 3893.

Table of contents

List of figures

List of tables

List of abbreviations

AB	Alginate beads
A-PEI	Alginate polyethylenimine
AP	Attapulgite
CS	Competitive Sips model
DI	Demineralized
EDTA	Ethylenediaminetetraacetic acid
EDX	Energy dispersive X-ray diffraction analysis
EPA	Environmental Protection Agency
FTIR	Fourier-transform infrared
G	α-l-(1,4)-guluronic
GA	Glutaraldehyde
GO	Graphene oxide
ICP-AES	Inductively coupled plasma atomic emission spectrometer
ILs	Ionic liquids
M	β-d- (1,4)-mannuronic
MB	Methylene blue
MO	Methyl orange
MS	Melamine sponge
NA	Nitroaniline
NP	Nitrophenol
NP	Nanoparticle
PEI	Polyethyleneimine
PFORE	The pseudo-first order rate equation
PGM	Platinum group metal
pH_{PZC}	The points of zero charge
PSORE	The pseudo-second order rate equation
SA	Sodium alginate
SEM	Scanning electron microscopy
SF	Separation factor
TEM	Transmission electron microscope
TOF	Turnover frequency
WHO	World Health Organization
XPS	X-ray photoelectron spectroscopy
3D	Three-dimensional

List of publications

Including 4 edited publications and one in preparation as follows:

1. **Yayuan Mo**, Shengye Wang, Thierry Vincent, Jacques Desbrieres, Catherine Faur, and Eric Guibal. New highly-percolating alginate-PEI membranes for efficient recovery of chromium from aqueous solutions. Carbohydrate Polymers, volume 225, 115177 (2019).
2. **Yayuan Mo**, Thierry Vincent, Catherine Faur, and Eric Guibal. Se(VI) sorption from aqueous solution using alginate/polyethylenimine membranes: Sorption performance and mechanism. International Journal of Biological Macromolecules, volume 147, 832-843(2020).
3. Shengye Wang, **Yayuan Mo**, Thierry Vincent, Catherine Faur, Jean-Claude Roux, Enrique Rodríguez-Castellón, Catherine Faur, and Eric Guibal. Palladium nanoparticles supported on amine-functionalized alginate foams for hydrogenation of 3-nitrophenol. Journal of Materials Science, volume 55, 2032–2051(2020).
4. Shengye Wang, Ke Xiao, **Yayuan Mo**, Bo Yang, Thierry Vincent, Catherine Faur, and Eric Guibal. Selenium(VI) and copper(II) adsorption using polyethyleneimine-based resins: Effect of glutaraldehyde crosslinking and storage condition. Journal of Hazardous Materials, volume 386, 121637(2020).
5. **Yayuan Mo**, Thierry Vincent, Catherine Faur, and Eric Guibal. Investigation of Hg(II) and Cu(II) sorption in single and binary systems by alginate/polyethylenimine membranes. In preparation.

Chapter 1 Introduction

The water pollution and scarcity problems are increasing day by day due to the rapid development of industrialization and the growth of population. According to the World Health Organization (WHO) [1], current trends in water use indicate that by 2025, half of the world's population will be living in water-stressed areas. Wastewater treatment and reuse play key roles in solving this problem. Meanwhile, the recovery of some valuable substances such as heavy metals, precious or strategic metals from wastewater becomes an attractive research direction.

It is well known that heavy metals, such as Pb(II), Cu(II), Cr(VI), As(V) and Hg(II) discharged from some industrial processes (electroplating, smelting, and mining), have toxic effects on organisms and accumulate in biota which can result in various undesirable consequences. Hence, the metal ions contained in wastewater must be eliminated and recovered for preserving the environment to avoid hazardous effects to the biotope and human health and producing materials first strategic (scarcity, geostrategic constraints, etc.) from secondary resources (waste, infra-marginal minerals) in order to meet growing demand (development of high-tech products). Commonly used technologies, including chemical reduction, precipitation, coagulation, solvent extraction, ion exchange, membrane separation and sorption etc. have been applied to remove and recover the contaminants from water [2-4]. The sorption process has been viewed as simple, eco-friendly, efficient and low-cost technique with more selective and allowing certain toxic and / or recoverable metals to be concentrated. Various sorbents such as natural minerals [5], agricultural waste [6] and biopolymers [7] have been investigated for the treatment of different kinds of effluents. However, low stability and mechanical properties, difficulty in solid-liquid separation after treatment, and unsuitability for column operation become restrictions in their practical application. Thus, finding new economical and effective materials for wastewater treatment is becoming an urging challenge.

Recently, biopolymers such as cellulose, gelatin, starch, chitosan and alginate received a great deal of attention due to their special mechanical, chemical, and electrochemical properties in the synthesis of novel materials [8, 9]. Among the numerous biopolymers, alginate is a hydrophilicity and biocompatible polymer with abundant free carboxyl and hydroxyl groups, which makes it an excellent gel-forming candidate to obtain multi-functional materials for effluence purification. For example, the affinity of carboxylic groups (existed in alginate) for cations facilitates it to synthesize beads [10], gels [11], fibers [12], foams [13], etc. for the removal of dye and metal ions. Meanwhile, alginate can be combined with cross-linkers such

as polyethylenimine (PEI) which allows to introduce new functional groups for improving the mechanical strength and sorption capacity of materials [14].

On the other side, moving the utilization of biopolymer-based materials toward as a source of catalyst has been shown to be a promising way recently. Wang et al. [15] successfully loaded palladium nanoparticles into algal beads by adsorption and reduction and used it as a supported catalyst for nitrophenol hydrogenation. Hammouda et al. [16] immobilized iron in alginate beads and found that indole can be effectively treated by the heterogeneous electro-Fenton process using Fe alginate beads as catalyst. An ionic liquid and a transition metal were supported on alginate matrix to form the porous monolith catalyst which was efficiently used for the hydrogenation of 4-nitroaniline, reported by Jouannin et al. [17]. In summary, using alginate as a basis material to prepare economical and effective adsorbents and catalysts for water purification has great potential.

1.1. Alginate overview

1.1.1. Sources of alginate

Alginate is a linear anionic polysaccharide richly existed in marine algae and bacteria: structurally, it forms by linear block copolymerization of β-d-mannuronic (M) acid and α-l-guluronic (G) acid; commercially, it is mainly extracted from brown seaweeds including *Laminaria*, *Sargassum*, *Macrocystis*, *Turbinaria*, *Padina* and *Ascophyllum* species [18]. Since alginic acid was first reported by the British chemist E.C.C. Stanford in 1881, various forms of alginate salts such as sodium, calcium and potassium have continuous appeared and been used in food, textile, biomedical, pharmaceutical and chemical industries [19]. Commercial alginates are naturally present in the cell wall of brown seaweeds, and the general procedures of obtaining alginates mainly involve three major stages: pre-extraction, neutralization, and precipitation (presented in Figure 1-1) [20]. Initially, the pre-extraction process is soaking the milled algal tissue in 0.1-0.2 M mineral acid (e.g., HCl or H_2SO_4) to remove the counter ions by proton exchange and convert the alginate salts into free alginic acids. The next step is converting the insoluble alginic acid using an alkali solution (e.g., NaOH or Na_2CO_3) though neutralization to soluble sodium alginate. Finally, the sodium alginate powder is obtained from the extraction solution by precipitation with hydrochloric acid, calcium chloride, or alcohol before drying and milling. Sodium alginate, as the first by-product of algae processing, has become the main form of alginate used in the industry, especially for wastewater treatment.

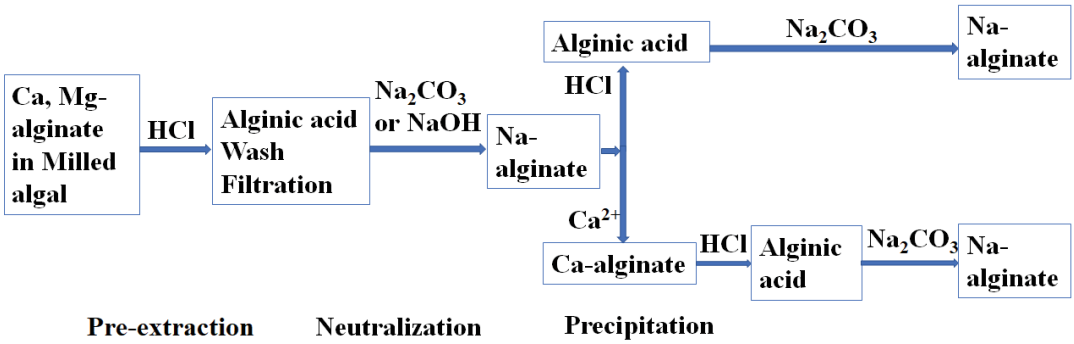

Figure 1-1 Generalized extraction process of sodium alginate.

1.1.2. Properties

As a natural biopolymer, alginate has several valuable and unparalleled properties that enabled it to be widely used in the wastewater treatment industry as a basic material for the formation of different forms products such as hydrogels, beads, fibrous, foams and membranes. The unique properties of alginates, which are important to the particular field, include: (i) Alginate is non-toxic, abundant, renewable, biocompatible, and biodegradable and has a relatively low cost, which make it become an ideal candidate for the synthesis of new materials; (ii) Alginate has the ability to form gels in the presence of multivalent cations (e.g. Ca(II), Zn(II) and Ba(II)) by the ionotropic gelation method, making them popular for material encapsulation; (iii) Alginate is an anionic polymer which can achieve covalent cross-linking by reacting with covalent cross-linker (e.g. epichlorohydrin, PEI and glutaraldehyde (GA)) for improving the physical and mechanical properties of the gel; and (iv) Alginate has a number of free hydroxyl and carboxyl groups distributed along the backbone, which may be used for metal cations binding (e.g. through interactions between cations and carboxylate groups at pH above the pKa values of the M and G acids: 3.38 and 3.65) and chemical modifications (including sulfation, amidation, and graft copolymerization) [21-23].

However, the unique properties of alginate may be influenced by the composition, sequential structure, and molecular size of the polymer [24]. It is noteworthy that alginate with a backbone of β-D- (1,4)-mannuronic (M) and α-L-(1,4)-guluronic (G) acid residues can arranged in various proportions and sequential arrangements of GG, MG, and MM blocks (Figure 1-2) [25, 26]. The M units exhibit linear and flexible construction due to the connection of β-(1,4) linkages, while the G units are stiff structures of buckled shape linked via α-(1,4) linkages, which introduce steric hindrance around the carboxyl group [27]. For these reasons the composition and content of M and G units distributed along the alginate backbone can affect

the physicochemical properties of alginate such as mechanical property, gel-forming property and the variable affinity of alginates for heavy metals [28]. Qin [29] tested the gel-forming abilities of a number of different types of alginate fibers and the results showed that alginates with high G content tend to form strong and firm gels, whereas those rich in M content results in the formation of weak and soft gels. Smidsrød and Haug [30] studied the affinity of divalent metals on different types of alginates and revealed that alginates with the G content show a stronger affinity for divalent cations such as Pb(II), Cu(II), Ca(II), etc. Hence, alginate with a high content of G-residues possible has far more industrial significance in the wastewater treatment field.

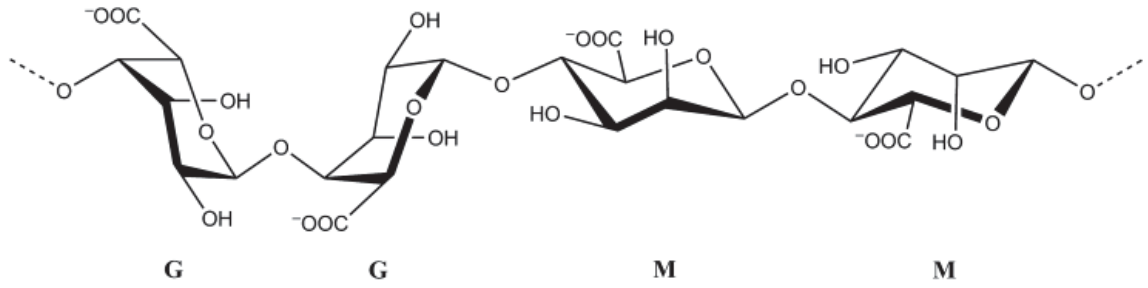

Figure 1-2 Chemical structures of G blocks, M blocks, and alternating blocks in alginate.

1.2. Alginate-based material

Due to its special properties, alginate is widely used in wastewater treatment. At first, the biomass containing alginate (such as, algae-based biomass and their derivatives) was directly used as the adsorbent. However, some organic compounds of raw algae biomass are readily leached during the sorption process; this may cause, in turn, a secondary pollution. Moreover, another problem to be addressed after treatment is the solid-liquid separation of biomass, when used under powder-form. Therefore, there is still a need for developing alternative conditionings of algal-based materials having enhanced sorption properties and facilitated operating process. Considering that the extracted alginate has strong cationic cross-linking ability and excellent gelation property, it is directly used to synthesize alginate-based composites for environmental remediation.

1.2.1. Synthesis of alginate-based material

The physicochemical properties of alginate-based material, such as mechanical strength, stability and functional ability, are closely related to their synthetic techniques. For overcoming

the high solubility and low mechanical strength of alginate, crosslinking methods that occur through ionic or covalent interaction to form stable intra- or inter-molecular attractive forces are widely used in alginates to prepare materials with desired functions [31]. Here, we focus on two common crosslinking methods: ionic crosslinking and covalent crosslinking.

Ionic crosslinking is the most common approach used to form alginate-based material. It states on the generation of three-dimensional networks mainly by the interaction between alginate chains and multivalent cations (i.e., Ca^{2+}). It is noteworthy that the interaction is mainly occurring on G blocks of alginate: especially Ca^{2+} combines with two facing helical stretches of G blocks to form "egg-box" structure; this means alginate with a higher G contents yield can obtain stronger gel networks and materials [32, 33]. Meanwhile, this also means that the affinity of alginate towards cations is higher when the amount of G blocks is increased. According to previous studies [34, 35], the binding ability of alginate to some cations mostly follows the order: $Mn^{2+} < Ni^{2+} < Ca^{2+} < Sr^{2+} < Ba^{2+} < Cu^{2+} < Pb^{2+} <$ trivalent cations. Among them, Calcium (Ca) has been the most frequently used cation to ionically cross-link alginate due to its economy, abundance, easily access and nontoxicity attractions. The typical way is mixing sodium alginate and calcium chloride ($CaCl_2$) to obtain gels. However, the high diffusion rate of Ca^{2+} ions in $CaCl_2$ solution leads to a fast gelation rate, which may affect the uniformity and mechanical properties of gels [36]. Thus, gelation rate is an essential factor in controlling gels formation. To widen the gelling time and delay the gelation process, temperature of gelation could be adjusted or solubility of calcium salts could be lowered through replacing $CaCl_2$ by insoluble calcium salt, like $CaCO_3$ [37]. However, the Ca alginate gels or materials obtained by these methods have a critical drawback: these gels are unstable in the presence of chelators such as citrate, phosphate, lactate or ethylenediaminetetraacetic acid (EDTA) due to ion exchange [38]. Furthermore, other divalent or trivalent cationic gels (obtained by ionic crosslinking) face the same limited stability: these multivalent cations exchange with monovalent cations like K(I), involving the rupture of three-dimensional networks and the dissolution of gels [39]. This limits the flexibility and practical application of ionically crosslinked alginate materials.

Another covalent crosslinking method, has been used in the synthesis of alginate-based material, as a very effective strategy for overcoming the limited stability of ionic gelation. In these crosslinked alginates, the polymer chains which contain carboxyl (-COOH) or hydroxyl (-OH) groups are interlinking with covalent bonds of a crosslinker to form stronger linkages and more stable three-dimensional networks. Epichlorohydrin is a well-known agent for covalent crosslinking of alginates, and the covalent alginate networks can be formed by reacting the -OH groups with an epoxide of epichlorohydrin though a ring-opening polymerization process

under basic conditions [40]. Figure 1-3 shows the reaction mechanism of alginate crosslinking with epichlorohydrin. The reaction can take place at 25 °C and the obtained polymer needs to be thoroughly washed with distilled water finally. These polymers are very stable and can remain intact under many extreme conditions, such as a wide pH range of 1-13, temperature up to 100 °C and high ionic strength of 0.5 M NaCl [41, 42].

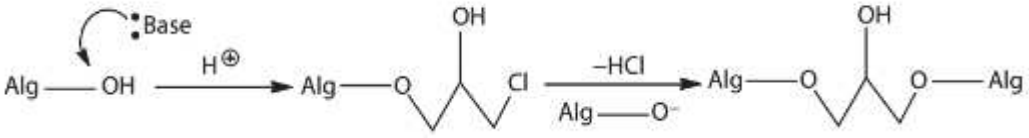

Figure 1-3 Mechanism for alginate crosslinking using epichlorohydrin.

Alginate chains can also be covalently crosslinked by reacting the -OH groups with dialdehyde groups such as glutaraldehyde though acetalization process under acid conditions, as shown in Figure 1-4 . Kim et al. [43] prepared alginate superabsorbent filament fibers using glutaraldehyde as a crosslinking agent in the presence of HCl solution. These filaments maintained the integrity of the fiber structure which also showed the high saline solution and synthetic urine absorbencies than alginates crosslinked with divalent cations. This may be because ionic crosslinking produces tightly packed junction points which are not favorable for liquid entrance, while covalent crosslinking using glutaraldehyde has linkers of adjustable lengths that can be used to create crosslink junctions allowing more liquid to be absorbed [44]. It is noteworthy that an increase in the glutaraldehyde concentration leads to a decrease in saline absorbency. Lu et al. [45] reported the use of a glutaraldehyde crosslinked alginate beads for the removal of dye and heavy metals. These beads showed high sorption capacities of methylene blue (572 mg g^{-1}) and Fe^{3+} ions (136 mg g^{-1}) and controllable swelling behavior which can meet specific applications.

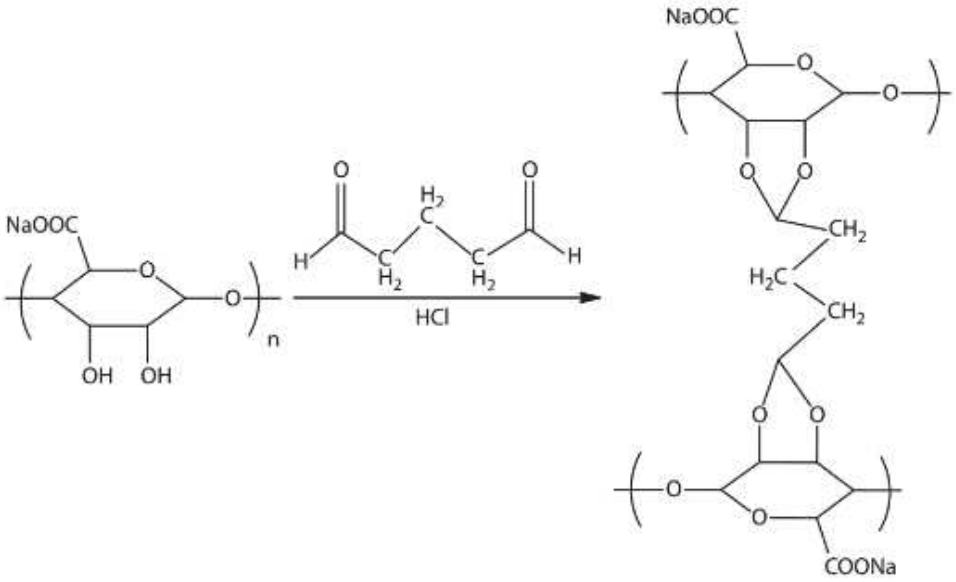

Figure 1-4 Mechanism for alginate crosslinking using glutaraldehyde.

In addition, other covalent crosslinkers like adipic dihydrazide, methyl ester L-lysine and N,N-(3-dimethylaminopropyl)-N-ethyl carbodiimide (EDC) have also been used to synthetic alginate polymers via condensation reactions [46, 47]. It is noteworthy that since pure crosslinking materials may have several limitations in providing biomaterials with the desired properties, other functional materials with required properties can be loaded during the preparation process. For instance, the introduction of graphene oxide into porous alginate fibers can enhance the mechanical property of the material [48]. The gel ability and inherent biocompatibility of alginates make crosslinking alginate materials particularly attractive for numerous applications in diverse areas. Continue to develop potential modification ways of alginate is open to trial.

1.2.2. Interaction of metal ions with alginate-based material

Studying the interaction mechanism of metal ions and sorbent materials is interesting for a better use of alginate materials as sorbents or catalysts for wastewater treatment. As mentioned above, raw alginate is able to bind metal cations easily because of the presence of hydroxyl and carboxyl groups. However, the alginate-based materials which were obtained by crosslinking or reaction with other functional materials, will present other functional groups (e.g. amine and sulfate groups) and a more complex structure, which may disturb interactions with metal ions. Functional groups of materials play a dominant role in the metal binding and can capture metal ions through two main interaction mechanisms: complexation (or chelation) and electrostatic

attraction (or ion exchange); it is possible to predict the interactions as a function of the acidity and composition of the solution since their values can influence the protonation of binding sites (or functional groups), the charged state of the material and the speciation of metal ions [49]. Generally, in the case of materials with uncharged functional groups, the metal ions binding is mainly due to complexation reactions leading to new chemical bonds formation between the material surface and the metals; whereas for the materials with charged functional groups, the interaction with metal ions is more likely ion exchange through the electrostatic attraction between the material surface and the metals [50].

The commonly functional groups present in the alginate-based material include carboxylic, amine, hydroxyl, sulfate, and phosphate groups. Among them, carboxylic groups are the most abundant functional groups in alginate and their interaction with metal ions may depend on the solution pH and the conjugate acid dissociation constant (pK_a) of the selected group: when the solution pH is higher than the pK_a, the carboxylic group is deprotonated and converted into carboxylate anions ($COOH \rightarrow COO^- + H^+$) and exhibit a negative charge which can be used to electrostatically adsorb positively charged cations; conversely when the solution pH is lower than the pK_a, the carboxylic group is protonated and uncharged which can lead to the formation of coordination bonds [51, 52]. Hu et al. [53] investigated the effect of solution pH on Pb(II) sorption using carboxylated cellulose nanocrystal/sodium alginate hydrogel beads and found an increase in Pb(II) uptake over the pH range of 2 to 4 followed by a plateau between pH values 4 to 6. They explained that this is because the carboxylic groups were converted into carboxylate anions which are beneficial to the Pb(II) ions binding though electrostatic attraction. Indeed, since the pK_a of carboxylic groups in alginate are 3.38 for mannuronic and 3.65 for guluronic acid [54], an increase of the solution pH above 4 can led to a completely deprotonation of carboxylic groups; this is favorable for the binding of metallic cations though electrostatic interaction. Similarly, other acidic groups such as phosphonic or sulfonic groups also can show their negatively charged and uncharged state according their own pK_a and the solution pH. In contrast, amine group is a classic example which exhibits a positive charge in their protonated form (in acidic solutions) and becomes uncharged when it is deprotonated (generally in neutral pH solutions): this means the amine group can not only interact with metallic anions through electrostatic attraction but also chelate metallic cations by complexation. Amine groups have been linked to the alginate-based materials due to their excellent uptake performance on metal ions [55, 56]. Several studies have shown that the binding of metal anions on amine group in alginate-based materials occurred through

electrostatic attraction [57]. Yan et al. [58] analyzed the Cr(VI) binding mechanism on the obtained core-shell/bead-like alginate@PEI sorbents though the studies of metal uptake performance and the characterization of FTIR and XPS. They concluded that the main interaction between metals and sorbents was due to the amino groups protonated to an ammonium form (NH^{3+}) under acidic condition, leading to a positive-negative charge bridge for electrostatic binding of Cr(VI) anions. It is noteworthy that the chloro-anionic species of Au, Pt and Pd also can be electrostatic captured by protonated amino groups; this is beneficial for the recovery of precious metals [59, 60]. On the other side, the amine group also can interact with cationic species by complexation. Zhang et al. [61] indicated that Cu(II) ions can be absorbed due to the strong chelating interaction between Cu(II) and amino groups on the adsorbent at pH 5.5. Shun et al. [62] also pointed out that the complexation of amino group with Cu(II) play a role in the metal binding at pH 6 using functionalized PEI/sodium alginate porous membrane.

In addition, it is worth mention that during the interaction between metals and materials, the porosity of the material may influence the performance of metal ions binding: this phenomenon is obviously highlighted by comparison between porous structure and non-porous structure of materials. To confirm this point, a research group prepared porous alginate aerogel beads and non-porous xerogel analogues though different drying methods (supercritical CO_2 versus air drying) and used them for the sorption of Cu(II) and Cd(II) [63]. The results showed that the porous structure of alginate aerogels greatly enhances the metal uptake ability and decreases equilibrium time of the material compared to non-porous xerogels: for porous aerogels, the maximum sorption capacities are 126.8 mg g^{-1} for Cu(II) and 244.5 mg g^{-1} for Cd(II) and 99% removal of both metal ions were achieved in around 950 min; while for non-porous xerogels, the maximum sorption capacities are 89.6 mg g^{-1} for Cu(II) and 198.4 mg g^{-1} for Cd(II) and 99% removal of both metal ions were achieved in 1550-1750 min. Other studies also pointed out that metals sorption performance, especially sorption rate, can be limited by the low porosity of material, which slows down the diffusion of the adsorbate in the adsorbent [64, 65].

1.2.3. Shaping of alginate-based material

Alginate-based materials can be readily formulated into various forms in the presence of suitable methods and meanwhile, the different shaping forms of the materials have an influence on the application of water treatment. The following mainly lists the commonly shaping forms of alginate-based materials including beads, fibers, sponges, foams, and membranes.

(1) Beads

Many works have been performed with alginate-based materials shaped as beads (i.e. gel- and solid-beads), since they are easy to produce and shape through ionic or covalent crosslinking, compare to some other forms such as fibers and membranes [66-68]. Basically, alginate beads are fabricated by adding the alginate mixture dropwise to a crosslinking solution with constant stirring under mild conditions; these beads also can be applied for encapsulation of other functional materials. As mentioned in the introduction of ionic crosslinking, alginate solution can quickly form hydrogels in the presence of divalent cations such as Ca^{2+}, which has become the simplest pathway to obtain alginate beads. Fiol et al. [69] prepared calcium gel beads loaded with grape stalks wastes by the crosslinking reaction between sodium alginate with 0.1 M $CaCl_2$ solution and applied them for chromium (VI) removal from aqueous solution. Results showed that these gel beads have a great sorption ability: the maximum uptake can up to 86.42 mmol of Cr(VI) L^{-1} of wet gel beads volume. However, the alginate gel beads were semi-transparent, which always exhibit poor mechanical properties and need to be stored in aqueous media; these drawbacks limited their large-scale applications. For example, Lagoa and Rodrigues [65] studied kinetic analysis of metal uptake by gel alginate beads and dry/solid alginate beads (obtained though oven-drying part of gel beads). They pointed out that gel bead with higher porosity adsorbed metal ions faster than the solid ones, while solid beads showed a higher sorption capacity and mechanical stability. These may be because the oven-drying process of the gel beads will shrink their structure and form a more compact and stiffer material, slowing the diffusion rate of metal ions inside the bead. Here, the low porosity becomes a limitation of solid beads for their application in water treatment. Some methods for improving the porosity of the beads have been studied. Kim et al. [70] compared the structures of alginate beads obtained by different drying methods including air drying, oven drying, vacuum drying and freeze drying and discovered that freeze drying keep higher porosity while other drying methods cause a collapsed pore structure of the bead. Chen et al. [71] prepared modified alginate beads by mixing graphene oxide (GO) and alginate solution followed by crosslinking with $CaCO_3$ and then freeze-dried. Results showed that the modified alginate beads have higher porosities and mechanical properties than pure alginate beads. They also concluded that the adsorption abilities of modified beads are much higher than those of pure alginate beads: their sorption capacities for Cu(II) and Pb(II) increased from 50.6 mg g^{-1} and 144.4 mg g^{-1} to 81.5 and 204.4 mg g^{-1}, respectively.

Covalent crosslinked alginate beads have also been widely studied by introducing new functional groups and structures to improve the material stability and sorption capacity. Gotoh

et al. [72] fabricated covalent crosslinked alginate beads by modifying Ca alginate beads with cyanogen bromide and 1,6-diaminohexane for Cu(II) and Mn(II) removal: this made the beads durable under alkaline conditions. Rocher et al. [73] covalently crosslinked Ca-alginate magnetic beads with epichlorohydrin and obtained higher porosity and stability beads for dyes removal. It has been concluded that the use of epichlorohydrin accelerates the adsorption process and that adsorption capacities are 0.02 mmol g^{-1} for negatively charged methyl orange and 0.7 mmol g^{-1} for positively charged methylene blue.

The materials in the form of beads are commonly performed in lab scale of batch experiments or fixed-bed column system, while at large scale continuous systems they may cause the head loss and column clogging, limiting their applications.

(2) Fibers

Alginate-based materials in the form of fibers have a high specific surface area and porosity, leading to fast adsorption abilities during removal of contaminates from aqueous solution [74]. The fibers conditioning will be more suitable in column systems because of an easier hydrodynamic transfer in column coupled with a fully recycling possibility by complete contact with the fibers. The alginate fibers shape has been studied for the adsorption of metal ions, dyes and antibiotics from wastewater. Electroplating and wet-spinning technology are two common methods for producing alginate fibers. Wu et al. [75] described a procedure for the preparation of graphene oxide (GO) doped alginate fibers by wet spinning: a homogeneous mixture of GO and alginate is injected into a coagulation bath containing 5 wt% $CaCl_2$ through a 0.75 mm diameter needle and then the as-prepared fibers are collected on a rotating collector outside the bath, washed with deionized water and air-dried. These fibers were used to remove antibiotic ciprofloxacin from aqueous solution and the removal efficiency can be 80%. Konwar et al. [76] adopted the same wet spinning technique to prepare magnetic alginate-Fe_3O_4 fibers and find that these fibers can play an efficient role in the successful adsorption of antibiotic. Thermogravimetric analysis and tensile strength measurements also proved that the obtained fibers have a high thermal stability and mechanical strength. In addition, Sui et al. [77] investigated the adsorption behavior of methylene blue (MB) and methyl orange (MO) dyes by alginate carbon nanotube fibers which were fabricated though the wet spinning method. The isotherm analyses showed that the fibers have a high affinity to cationic dye MB: the maximum adsorption of MB reached 606 mg g^{-1}.

Electrospinning is another facility and controllable fabrication technique to produce alginate fibers. Pan et al. [78] used this method to prepare an enhanced strength-toughness alginate composite

fiber. A homogeneously electrospinning solution was prepared by mixing alginate with GO, polyethylene oxide, Triton X-100™ and dimethyl sulfoxide followed by magnetically stirring for 6 h. Perfect fibers were performed in the following electrospinning condition: a 10 mL plastic syringe capped with a stainless steel needle (21 gauge), a spinneret to a rectangular aluminum foil was used as a static collector distance of 16 cm, a polymer-flow-rate of 1.5 mL h^{-1} and an applied voltage of 16 kV. The obtained fibers were uniformly distributed with a diameter of 400 nm and could be used to remove Pb(II) and Cu(II) ions from water. The results showed that the maximum adsorption capacity for Pb(II) and Cu(II) reached 386.5 and 102.4 mg g^{-1}. They also found that the fibers exhibited high porosity and mechanical properties which can be used repeatedly with minimal loss in application.

(3) Membranes/sponges /foams

Three-dimensional (3D) porous alginate scaffolds like membranes, sponges and foams have been synthesized and extensively applied in tissue engineering and biomedical application. They recently received attentions in the field of wastewater treatment since they are readily to manage and reuse compared with beads and fibers, especially at large scale continuous systems. Several studies have reported on the synthesized methods and the application of elaborating membranes, sponges and foams. Guo et al. [79] prepared alginate membrane for the removal of dye brilliant blue (BB) from aqueous solutions by the procedure of re-dissolving the as-prepared carbon nanotubes composite nanofibers and crosslinking with $CaCl_2$ solution. The obtained membrane exhibited a higher mechanical property, hydrophilic property and dye removal ability compared with most other materials: the tensile strength, water flux and BB dye rejection rate of the membrane are 2.59 MPa, 32.95 L m^{-2} h^{-1} and 98.20%, respectively. Feng et al. [13] fabricated alginate melamine sponge by alginate soaking and then hardening method for Cu(II) adsorption. They firstly immersed commercial melamine sponge (MS) into the sodium alginate solution overnight; after lyophilization, the sponge was put into the $CaCl_2$ solution for 6 h to crosslink followed by washing and oven-drying. The whole synthesis process, which is simple and economical, enhances the mechanical property of the sponge. In addition, the as-prepared alginate sponge presents high heavy metal adsorption performance and good recycling ability: the maximum adsorption uptake is 90 mg g^{-1} for Cu(II) and 162 mg g^{-1} for Cd(II) and can achieve at least five sorption-desorption cycles. Wang et al. [80] directly used alginate suspensions, either pure or mixed with attapulgite, to produce floatable and porous alginate-based foams though freeze-drying and post cross-linking method. The addition of attapulgite (AP) was favorable to enhance the material mechanical property. The AP foams are readily recyclable and applied for the adsorption of heavy metals. Results showed that the

maximum uptake of Cu(II) and Cd(II) by foams reach to 119 mg g^{-1} and 160 mg g^{-1}, respectively, and don't show any significant decrease after five successive adsorption-desorption cycles, illustrating the good reusability of the foams. However, in the chemical stability test, the weight loss of AP foams reached to 23 % after immersing in a strong acid solution (0.2 mol L^{-1} HCl) for 6 days, which may be caused by the ion exchange between Ca(II) (existed in the foam) with H^+ ions. This phenomenon will limit the use of the AP foam in industrial wastewater treatment.

On the other side, Chen et al. [81] synthesized humic acid-immobilized sodium alginate porous membrane though covalent crosslinking with glutaraldehyde (GA) and used it for the removal of Cu(II) ions from aqueous solutions. The results show that the maximum adsorption capacity of Cu(II) is 63.1 mg g^{-1} at pH 6 and adsorption equilibrium can be arrived within 60 min. They also used the same method to produce a new membrane by introducing hydroxyl ethyl cellulose and applied them to remove Cd(II) ions [82]. Here the maximum uptake of the obtained membrane reached to 148.9 mg g^{-1} for Cd(II) and have no significant losses after five adsorption-desorption cycles.

1.3. Applications of alginate-based materials

Alginate-based materials have been fabricated and applied in pharmaceutical science, chemical industries and environmental engineering. This section focuses on the application of alginate-based materials in water treatment as adsorbents or catalysts for both inorganic and organic contaminants, such as heavy metals, dyes and nitroaromatic compounds.

1.3.1. Alginate-based materials as adsorbents for water treatment

The application of alginate-based materials as adsorbents in the removal or recovery of heavy metals, precious or strategic metals from wastewater have been reported in the literature. As mentioned above, different species of metals have a crucial impact on sorption performance and uptake mechanism. Thus, the sorption properties of alginate-based materials on different metal types, cations and anions are discussed below and their sorption capacities are briefly summarized in Table 1-1 (for cations) and Table 1-2 (for anions).

(1) Metallic cations

Commonly metallic cations include Pb(II), Cu(II), Cd(II), Zn(II), Ni(II) which are mainly presented in positive or neutral form in aqueous solutions, depending on the solution pH and metal concentration. Due to the precipitation of cations as pH increases, most sorption studies are conducted at pH below 6; the optimum pH range for metallic cations binding on the alginate-based materials is achieved at higher pH conditions (i.e. pH 4–6) since lower pH contains more

H^+ ions which will cause stronger competition with metallic cations. Chen et al. [83] studied the sorption behaviors of Ca–alginate beads for Cu(II) removal from aqueous solution under different experimental conditions such as pH values (from 1.5 to 6), ionic strength (0.005, 0.05, and 0.5 M of sodium perchlorate), and metal concentration. The Cu(II) binding on Ca–alginate beads was found to be stronger and faster with increasing pH, decreasing ionic strength and initial concentration. More specifically, a sharp increase of Cu(II) removal efficiency was observed at pH ranging from 1.5 to 3.5 and followed a slight increase from 3.5 to 6. Chiew et al. [84] investigated the Pb(II) uptake mechanism of the Halloysite/alginate nanocomposite beads using various methods including equilibrium, kinetics, diffusion studies, FTIR, zeta potential, and compression tests and found that both the ion exchange interaction between Pb(II) and Ca(II) ions and complexation interaction of Pb(II) ions on carboxylate groups presented in alginate are significantly involved in Pb(II) removal. They also reported that the Hal/alginate nanocomposite beads show a higher uptake capacity for Pb(II) (1.56 mmol g^{-1}) than the free Hal nanotubes (0.41 mmol g^{-1}) without alginate. This may be due to the introduction of carboxylate groups (existed in alginate) which show higher affinity to Pb(II) ions compare to the silanol groups of the Hal nanotubes. In addition, Arica et al. [85] in the study of Cd(II) sorption by the plain alginate beads and both entrapped live and dead cells of *T. versicolor* into alginate beads suggested that the metal binding mechanism is due to the deprotonation of carboxyl groups (in both alginate and the cells) which can attract positively charged Cd(II) ions when carrying negative charges.

Understanding the adsorption properties of materials for different metallic cations is beneficial for selective targeting of certain metals. A study has been carried out to compare the recovery ability of various cations including Pb(II), Cu(II), Cd(II), Co(II), Zn(II), Ni(II) from aqueous solutions through Ca-alginate gels [86]. Results showed that the ion-exchange between the cations and Ca(II) ions was observed in the sorption process and the metal sorption capacities of the alginate gels can be ranked according the series: Pb>Cu>Cd>Ni>Zn>Co. Similar results were reported by Papageorgiou et al. [87] in the study of Pb(II), Cu(II) and Cd(II) sorption using calcium alginate beads. They also pointed out the metals sorption capacities followed the rank Pb (1.79 mmol g^{-1}) >Cu (1.38 mmol g^{-1}) > Cd (1.16 mmol g^{-1}), which was commonly controlled by the Pearson acid-base theory based on the principle: hard acids prefer to bind with hard bases (high electronegativity) whereas soft acids with soft bases (low electronegativity) [88]. In this case, the interactions of cations binding on sorbents is mainly due to the deprotonation of carboxyl groups present in the alginate; thus, the “hard” carboxyl base has a preference for Pb(II) and Cu(II) (intermediate acids) over Cd(II) (soft acid) ions.

Moreover, investigating the competitive sorption in multicomponent systems is important. Caroline et al. [89] studied the single, binary and ternary systems of Cu(II), Cd(II) and Zn(II) sorption using three kinds of sorbents (alginate, PEI/alginate and PEI-CS_2/ alginate). They found that regardless of the type of sorbents, the adsorbing metals ability followed the sequence Cu(II) > Cd(II) > Zn(II) which was in agreement with the point: higher electronegativity (Cu (1.90) > Cd (1.69) > Zn (1.65)) and smaller hydrated radius (Cu (4.19 Å) < Cd (4.26 Å) < Zn (4.30 Å)) of metal ions lead to higher metal binding ability. Simultaneously, in multicomponent solution, the presence of Cu(II) can greatly reduce the affinity of the sorbents for Zn(II) and Cd(II), which is beneficial for the recovery of Cu(II) from multicomponent systems.

(2) Metallic anions

Alginates have been shown to effectively bind cations due to the presence of numerous carboxyl and hydroxyl groups that exhibit negative charges under certain conditions, while their use for the binding of anions (such as oxyanions Cr(VI), As(V), and Se(VI)) has been limited. Linking some positively charged ions or functional groups on alginate materials are favorable to enhance the affinity between negatively charged alginate materials and anionic contaminants. Min et al. [90] reported that the As(V) sorption capacity can greatly increase after Ca alginate beads were further treated with Fe(III) ions: the As(V) sorption capacities are 0.013 mg g^{-1} for wet Ca bead versus 1.57 mg g^{-1} for wet Ca–Fe alginate beads at an As(V) initial concentration of 5 mg L^{-1}. However, it must be noticed that the leaching of Fe ions in acidic medium will lead to a significant impact on the stability of bead and become a limitation. Zhang et al. [91] introduced positively charged amines group by encapsulated triethylenetetramine-chitosan into alginate beads and found that the introduction of functional materials not only improved the affinity between alginate beads with chromium anions, but also enhanced the mechanical strength of materials. The Cr(VI) removal was studied in the pH range of 2–10 and results showed that the optimal Cr(VI) removal was observed at pH 3 and the maximum sorption capacity of modified beads (291.3 mg g^{-1}) was much higher than that of alginate beads (26.1 mg g^{-1}), because of the strongly electrostatic interaction between positively charged amine group of modified beads and the mainly existing species ($HCrO_4^-$) of chromium ions. Indeed, many different metal species may coexist in the solution (such as Cr(VI) exists as $Cr_2O_7^{2-}$, $HCrO_4^-$, CrO_4^{2-} and $HCr_2O_7^-$ in aqueous solution) and it is important to understand the distribution of ionic species, which depends on both the solution pH and metal concentration since the two parameters can influence the charge and the size of metal ions that predominate in the solution. Many studies pointed out that the sorption of Cr(VI) were sensitive to solution pH and in most cases the optimal anions binding on alginate-based materials was achieved at

lower pH such as in the pH range 2–4 [92, 93]. For instance, Karthik and Meenakshi [57] studied the Cr(VI) removal by alginate-polyaniline nanofibers in the range of pH 2–10 and found the optimal pH was 2 to reach the maximum sorption capacity of nanofibers for Cr(VI) ion of 73.34 mg g^{-1}. Vu et al. [94] investigated the sorption behaviors of Cr(VI) and As(V) from aqueous solutions using magnetite GO alginate beads. Results showed that as the initial pH increased from 3 to 10, the sorption capacities of both metals decreased, with the optimal pH values being obtained at pH 3 (where Cr(VI) exists as $HCrO_4^-$, and As(VI) exists as $H_2AsO_4^-$ in aqueous solution). It is noteworthy that the formation of neutral species (e.g. H_2CrO_4 or H_3AsO_4) and the competitor effect of counter anions contribute to decrease sorption properties when the pH is too low [95].

Apart from oxyanions, several metals such as Hg(II), Pt(IV) and Pd(II) forms chloro-anionic complexes in the presence of chloride ions. The speciation of these metal ions depends on both solution pH and chloride concentration which are thus significant to know the interaction between sorbents and sorbates for obtaining the best efficiency in sorption process. Cataldo et al. [96] studied the Pd(II) sorption by calcium alginate gel beads under different solution pH and chloride concentrations and pointed out that in acidic medium the deprotonation of carboxylate groups present in alginate, bearing negative charge, preferentially bind the positively charged species of Pd(II) including Pd^{2+}, $PdCl^+$, $Pd(OH)^+$, while the protonated amino groups with positive charge have a marked preference for the chloro-anionic species of Pd(II) such as $PdCl_3^-$ and $PdCl_4^{2-}$, $PdCl_3(OH)^{2-}$. Wang et al. [59] also reported the presence of protonated amine groups (introduced by adding PEI) drastically improved the sorption capacities of alginate for chloro-anionic metal species of Pd(II) and Pt(IV). They found that the alginate composite sorbent have a marked preference for Pd(II) over Pt(IV): the maximum uptake capacities are 1.28 mmol Pd g^{-1} and 0.59 mmol Pt g^{-1} at pH 2.5. They concluded that this may be in relation with metal speciation and steric hindrance: the speciation of Pd(II) is more sensitive to chloride concentration and readily to form chloro-anionic species compared to Pt(IV); moreover, Pd(II) forms with chloride ions (i.e. tetrachloropalladate species) in the square D4d configuration while Pt(IV) forms with chloride ions (i.e. hexachloroplatinate species) is characterized by an octahedral electronic configuration (with 4 unpaired electrons that require accommodating other ligands or water molecules) which shows a greater difficulty to spatial arrangement in the frame of the biopolymer/biomass matrix (and composite sorbent). It is noteworthy that the presence of chloride ions causes these metals to form chloride anion complexes, which is beneficial to the positive charge electrostatic adsorption of the adsorbent; however, the excess of chloride ions might lead to a competition effect which in turn limited

uptake ability. Guibal et al. [97] investigated the Hg(II) uptake performance using Cyphos IL 101 immobilized into a gelatin and alginate capsules from HCl medium and presented that the sorption capacity of Hg(II) decreased with an increase of chloride concentration from 0.1 M ($HgCl_4^{2-}$ represents about 46% of total Hg(II) species, remaining species are 31% for $HgCl_2$ and 23% for $HgCl_3^-$) to 1 M ($HgCl_4^{2-}$ represents about 95% of total Hg(II) species, remaining species is $HgCl_3^-$): this indicated that there is no direct correlation between uptake efficiency with the predominance species of Hg(II). They also observed the same phenomenon in the study of Pd(II) sorption [98].

In addition, understanding the desorption of metal ions is the foundation of sorbent materials recycling and reusability. In general, the selected elute for desorption is mainly dependent on the type of adsorbed ions: the metallic cations can be easily desorbed by the highly acidic solutions such as HCl and H_2SO_4 in most cases, while for the anions, alkaline solutions such as NaOH and $NaHCO_3$ are required to eliminate the adsorbed ions from the loaded material [99]. Moreover, some strongly metal chelating agents like EDTA which have a strong affinity to a certain targeted metal and form a stable complex also can be used to desorb the bound metals from the material.

Table 1-1 Sorption performance of alginate-based materials for removal of some metal cations from aqueous solution.

Sorbent	Sorbate: sorption capacity (mmol g^{-1})					pH	Ref.
	Pb(II)	Cu(II)	Cd(II)	Ni(II)	Zn(II)		
Calcium alginate beads	1.81	1.40	1.16	-	-	4.5	[87]
Scenedesmus quadricauda immobilized in alginate beads	-	1.15	-	0.46	0.93	5	[100]
Alginate hydrogel beads	1.1	0.48	-	0.13	-	4-6	[51]
Alginate-gel beads	1.80	1.78	1.53	-	-	4.5	[101]
Chlamydomonas reinhardtii immobilized in alginate beads	1.49	-	0.71	-	-	6	[102]
Chitosan–alginate beads	-	0.33	-	-	-	4.5	[55]
Chitosan coated calcium alginate beads	-	-	-	3.78	-	5	[103]
Activated carbon-containing alginate bead	1.61	2.25	0.78	-	0.63	5	[104]

Sorbent	Sorbate: sorption capacity (mmol g^{-1})					pH	Ref.
	Pb(II)	Cu(II)	Cd(II)	Ni(II)	Zn(II)		
Nano-sized graphite carbon immobilized alginate beads	-	-	-	0.19	-	5	[105]
Ethylenediamine-modified calcium alginate aerogel	1.06	1.38	-	-	-	4.5	[106]
alginate beads	2.88	3.04	2.32	-	-	4.5 for	[107]
Urea-grafting alginate beads	4.75	4.74	3.82	-	-	Pb; 5.5	
Biuret -grafting alginate beads	4.82	4.63	3.99	-	-	for Cd and Cu	
Alginate/graphene oxide composite aerogel beads	1.78	1.54	1.63	-	-	4	[108]
Alginate/magadiite/Di-(2-ethylhexyl) phosphoric acid beads	0.95	-	-	0.75	-	4	[109]
PEI/alginate beads	-	1.55	1.32	-	0.99	4	[89]
PEI/carbon disulfide/alginate beads	-	1.13	0.97	-	0.64	4	[89]
Polyaniline nanofibers modified alginate beads	1.21	1.07	-	-	-	5	[110]
Alginate composite fibers	1.86	1.61	-	-	-	4	[78]
Alginate/polyurethane composite foams	0.02	-	0.01	-	-	4	[111]
Sulfhydryl-modified sodium alginate films	2.01	-	-	-	-	5	[112]
Sodium alginate-melamine sponge	-	1.42	-	-	-	-	[13]
Alginate-based attapulgite foams	-	1.87	1.42	-	-	4.7 for Cu; 6.4 for Cd	[113]
Glutaraldehyde/humic acid /alginate membrane	-	0.99	-	-	-	6	[81]
Glutaraldehyde/humic acid /alginate and hydroxyl ethyl cellulose membrane	-	-	1.32	-	-	6	[82]

Table 1-2 Sorption performance of alginate-based materials for removal of some metal anions from aqueous solution.

Sorbent	Sorbate: sorption capacity (mmol g^{-1})					pH	Ref.
	Cr(VI)	As(V)	Hg(II)[a]	Pd(II)[a]	Pt(IV)[a]		
Ca-alginate beads	0.46-0.50	-	-	0.38-1.19	0.088	2-3	[14, 59, 91, 96]
Grape stalks wastes encapsulated in alginate beads	1.66	-	-	-	-	3	[69]
Bacterial consortia immobilized in alginate beads	12.63	-	-	-	-	3	[95]
Zr anchored alginate/gelatin biocomposite	0.49	-	-	-	-	2	[114]
Sodium alginate-based magnetic carbonaceous biosorbents	1.66	-	-	-	-	2	[93]
Nanoscale zerovalent iron/biochar/Ca-alginate composite	1.66	-	-	-	-	4	[115]
Triethylenetetramine-chitosan/alginate beads	5.60	-	-	-	-	3	[91]
Core-shell/bead-like alginate@PEI	8.30	-	-	-	-	2	[14]
Sodium alginate-polyaniline nanofibers	1.41	-	-	-	-	2	[57]
Nano-akaganeite encapsulated alginate beads	-	0.34	-	-	-	7	[116]
Zirconium oxide immobilized alginate beads	-	0.38	-	-	-	5	[117]
Hydrous iron oxide-alginate beads	-	0.73	-	-	-	2	[118]
Cyphos IL101 immobilized in gelatin and alginate capsule	-	-	0.75	-	-	1 M HCl	[97]
Bacillus cereus cells immobilized in alginate	-	-	0.52	-	-	7	[119]

Sorbent	Sorbate: sorption capacity (mmol g^{-1})					pH	Ref.
	Cr(VI)	As(V)	Hg(II)[a]	Pd(II)[a]	Pt(IV)[a]		
Ionic liquid [A336][MTBA] entrapped PVA-alginate gel beads			0.25	-	-	5.8	[120]
Bentonite-alginate composite	-	-	0.62	-	-	6	[121]
Morin incorporated dry alginate beads	-	-	0.91	-	-	6.5	[122]
Chitosan-alginate nanoparticles	-	-	1.08	-	-	5	[123]
Clay/alginate composite beads	-	-	-	1.6	-	3	[124]
PEI/alginate-based alga (*Laminara digitata*) beads	-	-	-	0.85	-	1	[125]
Ion-imprinted epicholorohydrin/thiourea modified alginate beads	-	-	-	0.97	-	3	[126]
Poly(styrenesulfonic acid)-impregnated alginate capsule	-	-	-	2.74	0.05	4.3	[127]
Cyphos IL-101-immobilized gelatin and alginate capsules	-	-	-	1.3	-	1 M HCl	[98]
Cyphos IL101 encapsulated into alginate beads	-	-	-	-	0.91	1 M HCl	[128]

a: Hg(II), Pd(II) and Pt(IV) in the forms of chloro-anionic species.

1.3.2. Alginate-based materials as catalysts for water treatment

Considering the difficult post-treatment of homogeneous catalysts after the reaction, the heterogeneous catalysts with fixing catalytic species on supported materials are more popular in industrial application since they favor the recovery and reuse. Alginate materials have recently been used to support catalytic species (especially transition metals) as heterogeneous catalysts for water treatment due to their interesting affinities for catalytic metals (such as Fe) and stability in most organic solvents [129, 130]. The freely conditioned structure of the alginate hydrogels and the allowed accessibility of the active functions are also essential for becoming catalytic support materials. Here we special focus on the transition metal species supported on alginate materials to become catalysts and discuss their applications in water treatment.

(1) Fenton and Fenton-like metals

Iron is a cheap, low-toxic transition metal which is the most extensive use as a Fenton catalyst to remove organic contaminants from aqueous solution. Iron alginate catalysts can be obtained by a very simple immobilization process by the reaction of Fe cations with carboxyl groups of alginates though the formation of "egg-box". Dong et al. [131] directly drop homogeneous alginate solution into the $FeCl_3$ solution to produce beads and use them to Fenton degrade azo dyes from aqueous solution. The study proves that the obtained beads catalysts exhibit a great degradation efficiency for the azo dyes in a wide range of pH (from 3 to 8), while the structure of the catalyst is unstable and easily worn down in the reusing process. The introduction of some other functional specials may enhance the stability of the material. Hammouda et al. [16] synthesized Fe alginate beads (Fe-ABs) by a wet impregnation technique though adding alginate mixture dropwise into a hardening solution composed of $CaCl_2$ and $FeSO_4$. The as-prepared Fe-ABs catalysts are used to catalytic remove a malodorous compound indole. The complete indole removal was observed within 60 min at an initial pH of 2. They also find the Fe-ABs catalysts exhibit good stabilities and reusability: after at least four recycles, there is no iron leaching and obvious decrease in catalytic activity. Iglesias et al. [132] use the same method to prepare Fe alginate catalysts for the electro-Fenton oxidation of pesticide imidacloprid. They find that the reaction has a good degradation efficiency for imidacloprid in a wide pH range of 2-7 and produce better results under acidic conditions: imidacloprid can be completely degraded in 120 min at pH 2. The continuous electro-Fenton process presented no operational problems and the bead shapes and degradation efficiencies of catalysts still can be kept. Here, another challenge we need to focus is to avoid the large leaching of alginate-supported catalytic metals which will cause secondary pollution. Quadrado and Fajardo [133] produce Fe alginate films by a first preparation of alginate/glycerol films through the solvent-casting technique, followed by crosslinking with Fe(II) or Fe(III) ions. The obtained Fe(II) or Fe(III) alginate films both present great catalytic activities for the azo methyl orange dyes, and the Fe ions leaching are low, 0.28 mg (1.5%) and 0.023 mg (0.4%). The immobilization of Fe(III) ions on the alginate proved to be more stable than Fe(II) ions in this reaction.

This ionic crosslink method for preparation of Fenton catalysts has been extended to various transition metals such as Cu [134], Mn [135], Ni [136] and Co [137]. Liquid-phase catalytic hydroxylation of phenol was performed using metal crosslinked alginate catalyst with hydrogen peroxide as an oxidant.

(2) Precious metals

Precious metals (such as Ag, Au and Pd) catalysts, including nanoparticles, have been prepared using alginate as the support. The common method for the preparation of precious metal catalyst is to immobilize metal ions on the alginate structure followed by a reduction step. The containing carboxyl and hydroxyl groups in alginate play key roles as a reductant and a stabilizer in this process. Lou et al. [138] described a procedure to obtain Ag-GO-alginate catalyst: disperse $AgNO_3$ in alginate (SA) solution first and then add the mixture to GO suspension; Ag(I) ions anchored on GO sheets were reduced to triangular Ag nanoparticles after the hydrothermal treatment. The as-prepared Ag-GO-alginate catalyst presents a highlighted catalytic activity in the oxidation of hydroquinone: the conversion efficiency reached to 99% within 2 h which is 12 times higher than that of Ag-GO catalyst without alginate. Saha et al. [139] report another method to obtain Ag and Au alginate nanoparticles for catalytic 4-nitrophenol reduction. In this study, Ca-alginate beads are prepared firstly and then Ag(I) and Au(III) ions are immobilized on the materials by immersing obtained beads in the desired metal solutions, followed by a photochemical technique using UV irradiation in order to accelerate the reduction of Ag(I) and Au(III) ions to nanoparticles. The characterizing analysis demonstrates that the obtained nanoparticles are mostly spherical and the size ranges are lower than10 nm. Most importantly, both Ag and Au catalysts allowed reaching an almost complete reduction for 4-nitrophenol within a short time in the presence of reductant sodium borohydride ($NaBH_4$): the yield was 99% at 8 min for Ag catalysts while the yield was 92% at 50 min for Au catalysts. This proves the catalytic reduction of alginate-based Ag catalyst was much faster than that of the Au catalyst.

In addition, the possibility to support Pd particles on alginate material for the formation of catalyst has also been addressed. Primo et al. [140] prepare Pd/alginate nanoparticles catalyst by the immobilization of Pd(II) ions on alginate through the electrostatic interactions to obtain beads, followed by the reduction of Pd(II) by the process of dehydratation with ethanol. The distributions of the nanoparticles in the beads are homogeneous and the catalyst materials are confirmed to have high activities in the Suzuki carbon−carbon coupling reactions. Remarkably, a strategy has been used for the immobilization of ionic liquids (ILs) onto the metal alginate catalysts, because of the high affinity between most ILs and catalytic metal ions. Jouannin et al. [17] prepared highly porous monolith supporting Cyphos IL-101 and Pd nanoparticles (alginate/IL/Pd-HPM) and used them for the hydrogenation of 4-nitroaniline (4-NA) in a fixed-bed column with single-pass mode and recycling mode. The as-prepared alginate/IL/Pd-HPM demonstrate an enhanced performance for the hydrogenation of 4-NA in the presence of

formate (as the hydrogen donor): the complete conversion of 4-NA is observed in less than 15 min using the alginate/IL/Pd-HPM, while the conversion yield was lower than 44% after continuously running for 60 min using alginate HPM (without IL or Pd). They also find that the alginate/IL/Pd-HPM can keep higher catalytic activity for 68 h (the conversion yield above 95%) in the single-pass running mode.

1.4. Objectives of the thesis

As demonstrated by the state of art, alginate has been confirmed to be a very promising biopolymer for the fabrication of adsorbents and catalysts and its interesting properties including strong affinity for metal ions, easily further functionalization ability and freely adjustable formability, allowing for continuously exploring new pathways in the aspects of material synthesis. Theoretically, the chemical structure of the alginate is not favorable for the adsorption of metal anions (chromate, palladium in HCl medium). To widen the field of application of adsorbent materials based on alginate, it is necessary to incorporate other functional polymers. In addition, high porosity is significant to materials design, but the techniques described in the literature for production of high macroporosity alginate membranes generally require the use of complex and energy-consuming dryers (e.g. lyophilization and supercritical CO_2 conditions). It is thus a need to facilitate the structuring of membranes with high percolation power without implementing a complex drying process. Meanwhile, the application of the alginate-based materials in various aqueous contaminations removals remaining open to trial. The challenges still existing in industrial applications include the improvement of the stability of alginate-based materials for recycling and reusability and the achievement of continuous applications. Thus, the objective of the present thesis is to develop alginate membranes with high efficiency, percolation, stability and reusability using a facile and economical way. The applications of prepared materials as adsorbents and catalysts in water treatment will also be investigated.

1.5. Outline of the thesis

The thesis is organized into six chapters structured as shown in Figure 1-5.

The first chapter (Chapter 1), as a state of art, has reviewed the background of alginate and the synthesis method of alginate-based materials and has briefly described the interaction mechanisms between metal ions and alginate-based materials. It has summarized the common shaping forms of the alginate-based materials and their application in water treatment as adsorbents or catalysts. The objectives and outlines of the thesis were also given at the end of this chapter.

Chapter 2 focuses on the preparation of highly-percolating alginate membranes by the interaction of PEI and alginate followed by crosslinking using GA solution. This double interaction allows the "strong structuring" of the hydrogel which makes it possible to dry the membrane in the open air without collapsing the porous structure. The properties of the membrane are characterized and the sorption performances of the membrane in the removal of chromate and selenite ions are evaluated in this section.

Chapter 3 provides the results of Hg(II) and Cu(II) sorption in single and binary systems using alginate/PEI membranes. These two metal ions are characterized by different behaviors in terms of speciation and by a great stability in terms of redox stability (under the selected experimental conditions none of these two metal ions undergoes reduction, contrary to Cr (VI) and Se (VI)). FTIR and SEM-EDX are used to characterize the materials and study the mechanisms of the metal ions binding. A special attention is paid to the modeling of the adsorption isotherms (in single and binary solutions). The selectivity property of the membrane is analyzed by plotting the three-dimensional surfaces of the adsorption isotherms.

In order to clarify and confirm the effect of the crosslinking of PEI and GA on the fixation of metal ions and their interaction mechanisms (chelation and attraction electrostatic), an additional study was conducted on polyethyleneimine crosslinked with GA solution (packaged in powder form). In Chapter 4, the effect of different levels of GA crosslinking and storage conditions on the adsorption properties of PEI-GA resins for Se(VI) (selenate anions) and Cu(II) (cations) are investigated.

Chapter 5 deals with alginate/PEI membranes as supported material for catalytic metals in comparison to the reference materials by evaluating their catalytic performance, recycling and reusable.

A conclusion states on the main achievements which have been obtained in this research work and introduces the next steps for future recommendations on the use of alginate-based membranes in wastewater treatment.

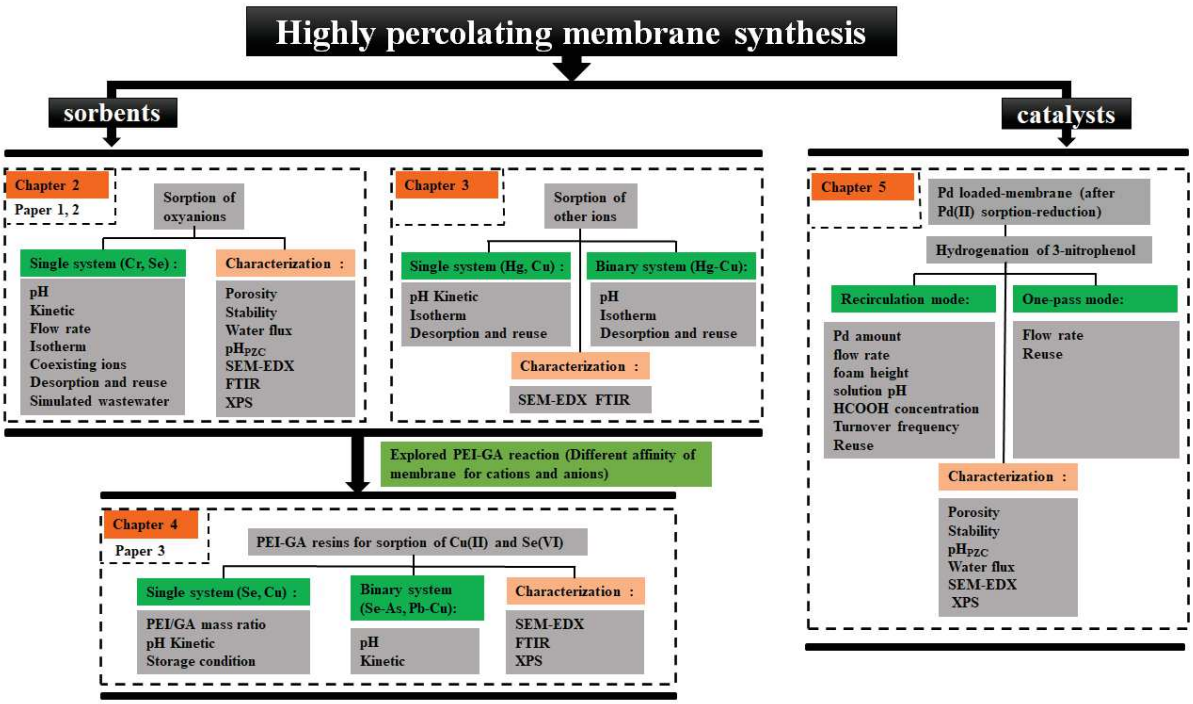

Figure 1-5 The structure of this PhD thesis

1.6. References

[1] W.H. Organization, Drinking-water, in, 2019.
[2] W. Peng, H. Li, Y. Liu, S. Song, A review on heavy metal ions adsorption from water by graphene oxide and its composites, Journal of Molecular Liquids, 230 (2017) 496-504.
[3] A. Smara, R. Delimi, C. Poinsignon, J. Sandeaux, Electroextraction of heavy metals from diluted solutions by a process combining ion-exchange resins and membranes, Separation and purification technology, 44 (2005) 271-277.
[4] D. Adekeye, O. Popoola, S. Asaolu, A. Adebawore, O. Aremu, K. Olabode, Adsorption and Conventional Technologies for Environmental Remediation and Decontamination of Heavy Metals: An Overview, International Journal of Research and Review, 6 (2019) 505-516.
[5] E. Katsou, S. Malamis, K.J. Haralambous, M. Loizidou, Use of ultrafiltration membranes and aluminosilicate minerals for nickel removal from industrial wastewater, Journal of Membrane Science, 360 (2010) 234-249.
[6] T.A.H. Nguyen, H.H. Ngo, W.S. Guo, J. Zhang, T.V. Nguyen, Applicability of agricultural waste and by-products for adsorptive removal of heavy metals from wastewater, Bioresource Technology, 148 (2013) 574-585.
[7] M. Badawi, N. Negm, M.A. Kana, H. Hefni, M.A. Moneem, Adsorption of aluminum and lead from wastewater by chitosan-tannic acid modified biopolymers: isotherms, kinetics, thermodynamics and process mechanism, International Journal of Biological Macromolecules, 99 (2017) 465-476.
[8] S. Kalia, L. Averous, Biopolymers: biomedical and environmental applications, John Wiley & Sons, 2011.
[9] X. Wang, K. Yang, S. Tao, B. Xing, Sorption of aromatic organic contaminants by biopolymers: Effects of pH, copper(II) complexation, and cellulose coating, Environmental science & technology, 41 (2007) 185-191.
[10] N. Pippa, T. Sentoukas, S. Pispas, C. Demetzos, A. Papalois, N. Bouropoulos, pH-responsive polymeric nanoassemblies encapsulated into alginate beads: morphological characterization and swelling studies, Journal of Polymer Research, 25 (2018) 117.
[11] P. Kanmani, J. Aravind, M. Kamaraj, P. Sureshbabu, S. Karthikeyan, Environmental applications of chitosan and cellulosic biopolymers: A comprehensive outlook, Bioresource Technology, 242 (2017) 295-303.
[12] Y. Li, F. Liu, B. Xia, Q. Du, Y. Xia, Removal of copper from aqueous solution by carbon nanotube/calcium alginate composites, Journal of Hazardous Materials, 177 (2010) 876-880.
[13] Y. Feng, Y. Wang, Y. Wang, X.-F. Zhang, J. Yao, In-situ gelation of sodium alginate supported on melamine sponge for efficient removal of copper ions, Journal of colloid and interface science, 512 (2018) 7-13.
[14] Y. Yan, Q. An, Z. Xiao, W. Zheng, S. Zhai, Flexible core-shell/bead-like alginate@PEI with exceptional adsorption capacity, recycling performance toward batch and column sorption of Cr(VI), Chemical Engineering Journal, 313 (2017) 475-486.
[15] S. Wang, T. Vincent, C. Faur, E. Rodríguez-Castellón, E. Guibal, A new method for incorporating polyethyleneimine (PEI) in algal beads: High stability as sorbent for palladium

recovery and supported catalyst for nitrophenol hydrogenation, Materials Chemistry and Physics, 221 (2019) 144-155.
[16] S.B. Hammouda, F. Fourcade, A. Assadi, I. Soutrel, N. adhoum, A. Amrane, L. Monser, Effective heterogeneous electro-Fenton process for the degradation of a malodorous compound, indole, using iron loaded alginate beads as a reusable catalyst, Applied Catalysis B: Environmental, 182 (2015) 47-58.
[17] C. Jouannin, I. Dez, A.-C. Gaumont, J.-M. Taulemesse, T. Vincent, E. Guibal, Palladium supported on alginate/ionic liquid highly porous monoliths: Application to 4-nitroaniline hydrogenation, Applied Catalysis B: Environmental, 103 (2011) 444-452.
[18] M. Zubia, C. Payri, E. Deslandes, Alginate, mannitol, phenolic compounds and biological activities of two range-extending brown algae, *Sargassum mangarevense* and *Turbinaria ornata* (Phaeophyta: Fucales), from Tahiti (French Polynesia), Journal of Applied Phycology, 20 (2008) 1033-1043.
[19] Y. Qin, Alginate fibres: an overview of the production processes and applications in wound management, Polymer international, 57 (2008) 171-180.
[20] K.I. Draget, Alginates, in: Handbook of hydrocolloids, Elsevier, 2009, pp. 807-828.
[21] A.M. Holban, Nanoarchitectonics for Smart Delivery and Drug Targeting, 2016.
[22] K.I. Draget, C. Taylor, Chemical, physical and biological properties of alginates and their biomedical implications, Food Hydrocolloids, 25 (2011) 251-256.
[23] Y. Cao, X. Shen, Y. Chen, J. Guo, Q. Chen, X. Jiang, pH-induced self-assembly and capsules of sodium alginate, Biomacromolecules, 6 (2005) 2189-2196.
[24] W.R. Gombotz, S.F. Wee, Protein release from alginate matrices, Advanced Drug Delivery Reviews, 31 (1998) 267-285.
[25] A. Pettignano, A. Duarte-Rodrigues, F. Quignard, N. Tanchoux, Alginate and Carrageenan Based Aerogels: Processing and Morphology, in: Biobased Aerogels, 2018, pp. 54-66.
[26] A.C. Hodsdon, J.R. Mitchell, M.C. Davies, C.D. Melia, Structure and behaviour in hydrophilic matrix sustained release dosage forms: 3. The influence of pH on the sustained-release performance and internal gel structure of sodium alginate matrices, Journal of Controlled Release, 33 (1995) 143-152.
[27] J.S. Yang, Y.-J. Xie, W. He, Research progress on chemical modification of alginate: A review, Carbohydrate Polymers, 84 (2011) 33-39.
[28] N. Sari-Chmayssem, S. Taha, H. Mawlawi, J.-P. Guégan, J. Jeftić, T. Benvegnu, Extracted and depolymerized alginates from brown algae *Sargassum vulgare* of Lebanese origin: chemical, rheological, and antioxidant properties, Journal of Applied Phycology, 28 (2016) 1915-1929.
[29] Y. Qin, Gel swelling properties of alginate fibers, Journal of Applied Polymer Science, 91 (2004) 1641-1645.
[30] O. Smidsrød, A. Haug, B. Larsen, S. Gronowitz, The Effect of Divalent Metals on the Properties of Alginate Solutions. I. Calcium Ions, Acta Chemica Scandinavica, 19 (1965) 329-340.

[31] F.I.P. Shanura, K. Daekyung, N. Jae-Woon, J. You-Jin, Advances in functionalizing fucoidans and alginates (bio)polymers by structural modifications: a review, Chemical Engineering Journal, (2018).
[32] M.J. Costa, A.M. Marques, L.M. Pastrana, J.A. Teixeira, S.M. Sillankorva, M.A. Cerqueira, Physicochemical properties of alginate-based films: effect of ionic crosslinking and mannuronic and guluronic acid ratio, Food Hydrocolloids, 81 (2018) 442-448.
[33] L. Zhang, T. Liu, N. Chen, Y. Jia, R. Cai, W. Theis, X. Yang, Y. Xia, D. Yang, X. Yao, Scalable and controllable synthesis of atomic metal electrocatalysts assisted by an egg-box in alginate, Journal of Materials Chemistry A, 6 (2018) 18417-18425.
[34] B. Larsson, H. Tjälve, Studies on the melanin-affinity of metal ions, Acta Physiologica Scandinavica, 104 (1978) 479-484.
[35] A. Haug, O. Smidsrød, The effect of divalent metals on the properties of alginate solutions, Acta chem. scand, 19 (1965) 341-351.
[36] Y. Zhao, M.T. Carvajal, Y.-Y. Won, M.T. Harris, Preparation of Calcium Alginate Microgel Beads in an Electrodispersion Reactor Using an Internal Source of Calcium Carbonate Nanoparticles, Langmuir, 23 (2007) 12489-12496.
[37] J.P. Paques, E.V.D. Linden, C.J.M.V. Rijn, L.M.C. Sagis, Preparation methods of alginate nanoparticles, Adv Colloid Interface Sci, 209 (2014) 163-171.
[38] S.H. Ching, N. Bansal, B. Bhandari, Alginate gel particles–A review of production techniques and physical properties, Critical reviews in food science and nutrition, 57 (2017) 1133-1152.
[39] L. Agüero, D. Zaldivar-Silva, L. Peña, M.L. Dias, Alginate microparticles as oral colon drug delivery device: A review, Carbohydrate polymers, 168 (2017) 32-43.
[40] X. Chen, D. Wang, W. Wang, Y. Su, C. Gao, A novel composite nanofiltration (NF) membrane prepared from sodium alginate/polysulfone by epichlorohydrin cross-linking, Desalination and Water Treatment, 30 (2011) 146-153.
[41] V. Dave, K. Tak, C. Gupta, K. Verma, S. Sharma, Alginates in Pharmaceutical and Biomedical Application: A Critique, Alginates: Applications in the Biomedical and Food Industries, (2019) 95.
[42] B.H. Rehm, M.F. Moradali, Alginates and their biomedical applications, Springer, 2018.
[43] Y.J. Kim, K.J. Yoon, S.W. Ko, Preparation and properties of alginate superabsorbent filament fibers crosslinked with glutaraldehyde, Journal of Applied Polymer Science, 78 (2000) 1797-1804.
[44] S.N. Pawar, K.J. Edgar, Alginate derivatization: A review of chemistry, properties and applications, Biomaterials, 33 (2012) 3279-3305.
[45] T. Lu, T. Xiang, X.-L. Huang, C. Li, W.-F. Zhao, Q. Zhang, C.-S. Zhao, Post-crosslinking towards stimuli-responsive sodium alginate beads for the removal of dye and heavy metals, Carbohydrate polymers, 133 (2015) 587-595.
[46] V.S. Ghorpade, Preparation of hydrogels based on natural polymers via chemical reaction and cross-Linking, in: Hydrogels Based on Natural Polymers, Elsevier, 2020, pp. 91-118.

[47] K.Y. Lee, J.A. Rowley, P. Eiselt, E.M. Moy, K.H. Bouhadir, D.J. Mooney, Controlling mechanical and swelling properties of alginate hydrogels independently by cross-linker type and cross-linking density, Macromolecules, 33 (2000) 4291-4294.
[48] Y. He, N. Zhang, Q. Gong, H. Qiu, W. Wang, Y. Liu, J. Gao, Alginate/graphene oxide fibers with enhanced mechanical strength prepared by wet spinning, Carbohydrate Polymers, 88 (2012) 1100-1108.
[49] T.A. Davis, B. Volesky, A. Mucci, A review of the biochemistry of heavy metal biosorption by brown algae, Water research, 37 (2003) 4311-4330.
[50] B.L. Rivas, E. Pereira, A. Maureira, Functional water-soluble polymers: polymer–metal ion removal and biocide properties, Polymer international, 58 (2009) 1093-1114.
[51] B. An, H. Lee, S. Lee, S.-H. Lee, J.-W. Choi, Determining the selectivity of divalent metal cations for the carboxyl group of alginate hydrogel beads during competitive sorption, Journal of hazardous materials, 298 (2015) 11-18.
[52] S. Schiewer, Modelling complexation and electrostatic attraction in heavy metal biosorption by *Sargassum* biomass, Journal of Applied Phycology, 11 (1999) 79-87.
[53] Z.-H. Hu, A.M. Omer, X.k. Ouyang, D. Yu, Fabrication of carboxylated cellulose nanocrystal/sodium alginate hydrogel beads for adsorption of Pb(II) from aqueous solution, International Journal of Biological Macromolecules, 108 (2018) 149-157.
[54] A.B. Hegge, T. Andersen, J.E. Melvik, E. Bruzell, S. Kristensen, H.H. Tonnesen, Formulation and bacterial phototoxicity of curcumin loaded alginate foams for wound treatment applications: Studies on curcumin and curcuminoides XLII, Journal of Pharmaceutical Sciences, 100 (2011) 174-185.
[55] W.W. Ngah, S. Fatinathan, Adsorption of Cu(II) ions in aqueous solution using chitosan beads, chitosan–GLA beads and chitosan–alginate beads, Chemical Engineering Journal, 143 (2008) 62-72.
[56] S. Deng, Y.P. Ting, Polyethylenimine-modified fungal biomass as a high-capacity biosorbent for Cr(VI) anions: sorption capacity and uptake mechanisms, Environmental science & technology, 39 (2005) 8490-8496.
[57] R. Karthik, S. Meenakshi, Removal of Cr(VI) ions by adsorption onto sodium alginate-polyaniline nanofibers, International Journal of Biological Macromolecules, 72 (2015) 711-717.
[58] Y. Yan, Q. An, Z. Xiao, W. Zheng, S. Zhai, Flexible core-shell/bead-like alginate@ PEI with exceptional adsorption capacity, recycling performance toward batch and column sorption of Cr(VI), Chemical Engineering Journal, 313 (2017) 475-486.
[59] S. Wang, T. Vincent, J.-C. Roux, C. Faur, E. Guibal, Pd(II) and Pt(IV) sorption using alginate and algal-based beads, Chemical Engineering Journal, 313 (2017) 567-579.
[60] J.K. Bediako, S. Lin, A.K. Sarkar, Y. Zhao, J.-W. Choi, M.-H. Song, W. Wei, D.H.K. Reddy, C.-W. Cho, Y.-S. Yun, Benignly-fabricated crosslinked polyethylenimine/calcium-alginate fibers as high-performance adsorbents for effective recovery of gold, Journal of cleaner production, 252 (2020) 119389.
[61] Z. Zhang, H. Liu, L. Wu, H. Lan, J. Qu, Preparation of amino-Fe(III) functionalized mesoporous silica for synergistic adsorption of tetracycline and copper, Chemosphere, 138 (2015) 625-632.

[62] X. Sun, J.H. Chen, Z. Su, Y. Huang, X. Dong, Highly effective removal of Cu(II) by a novel 3-aminopropyltriethoxysilane functionalized polyethyleneimine/sodium alginate porous membrane adsorbent, Chemical Engineering Journal, 290 (2016) 1-11.
[63] E.G. Deze, S.K. Papageorgiou, E.P. Favvas, F.K. Katsaros, Porous alginate aerogel beads for effective and rapid heavy metal sorption from aqueous solutions: Effect of porosity in Cu^{2+} and Cd^{2+} ion sorption, Chemical Engineering Journal, 209 (2012) 537-546.
[64] E. Guibal, M. Jansson-Charrier, I. Saucedo, P.L. Cloirec, Enhancement of metal ion sorption performances of chitosan: effect of the structure on the diffusion properties, Langmuir, 11 (1995) 591-598.
[65] R. Lagoa, J.R. Rodrigues, Kinetic analysis of metal uptake by dry and gel alginate particles, Biochemical Engineering Journal, 46 (2009) 320-326.
[66] A. Esposito, A. Reverberi, Copper adsorption on calcium alginate beads: equilibrium pH-related models, Hydrometallurgy, 65 (2002) 43-57.
[67] A. Bée, D. Talbot, S. Abramson, V. Dupuis, Magnetic alginate beads for Pb(II) ions removal from wastewater, Journal of colloid and interface science, 362 (2011) 486-492.
[68] M. Jain, V. Garg, K. Kadirvelu, Cadmium (II) sorption and desorption in a fixed bed column using sunflower waste carbon calcium–alginate beads, Bioresource technology, 129 (2013) 242-248.
[69] N. Fiol, J. Poch, I. Villaescusa, Chromium (VI) uptake by grape stalks wastes encapsulated in calcium alginate beads: equilibrium and kinetics studies, Chemical Speciation & Bioavailability, 16 (2004) 25-33.
[70] T.Y. Kim, H.J. Jin, S.S. Park, S.J. Kim, S.Y. Cho, Adsorption equilibrium of copper ion and phenol by powdered activated carbon, alginate bead and alginate-activated carbon bead, Journal of Industrial and Engineering Chemistry, 14 (2008) 714-719.
[71] K. Chen, Y. Ling, C. Cao, X. Li, X. Chen, X. Wang, Chitosan derivatives/reduced graphene oxide/alginate beads for small-molecule drug delivery, Materials Science and Engineering: C, 69 (2016) 1222-1228.
[72] Gotoh, T., Matsushima, K., Kikuchi, K., I., Adsorption of Cu and Mn on covalently cross-linked alginate gel beads.
[73] V. Rocher, A. Bee, J.-M. Siaugue, V. Cabuil, Dye removal from aqueous solution by magnetic alginate beads crosslinked with epichlorohydrin, Journal of Hazardous Materials, 178 (2010) 434-439.
[74] C. Guo, Q. Kong, J. Gao, J. Quan, Y. Xia, Removal Of methylene blue dye from simulated wastewater by alginic acid fiber as adsorbent: Equilibrium, kinetic, and thermodynamic studies, Canadian Journal of Chemical Engineering, 89 (2011) 1545-1553.
[75] S. Wu, X. Zhao, Y. Li, C. Zhao, Q. Du, J. Sun, Y. Wang, X. Peng, Y. Xia, Z. Wang, Adsorption of ciprofloxacin onto biocomposite fibers of graphene oxide/calcium alginate, Chemical Engineering Journal, 230 (2013) 389-395.
[76] A. Konwar, A. Gogoi, D. Chowdhury, Magnetic alginate–Fe_3O_4 hydrogel fiber capable of ciprofloxacin hydrochloride adsorption/separation in aqueous solution, RSC Advances, 5 (2015) 81573-81582.

[77] K. Sui, Y. Li, R. Liu, Y. Zhang, X. Zhao, H. Liang, Y. Xia, Biocomposite fiber of calcium alginate/multi-walled carbon nanotubes with enhanced adsorption properties for ionic dyes, Carbohydrate polymers, 90 (2012) 399-406.
[78] L. Pan, Z. Wang, X. Zhao, H. He, Efficient removal of lead and copper ions from water by enhanced strength-toughness alginate composite fibers, International Journal of Biological Macromolecules, 134 (2019) 223-229.
[79] J. Guo, Q. Zhang, Z. Cai, K. Zhao, Preparation and dye filtration property of electrospun polyhydroxybutyrate-calcium alginate/carbon nanotubes composite nanofibrous filtration membrane, Separation & Purification Technology, 161 (2016) 69-79.
[80] Y. Wang, Y. Feng, X.F. Zhang, X. Zhang, J. Jiang, J. Yao, Alginate-based attapulgite foams as efficient and recyclable adsorbents for the removal of heavy metals, Journal of Colloid & Interface Science, 514 (2017) 190-198.
[81] J.H. Chen, Q.L. Liu, S.R. Hu, J.C. Ni, Y.S. He, Adsorption mechanism of Cu(II) ions from aqueous solution by glutaraldehyde crosslinked humic acid-immobilized sodium alginate porous membrane adsorbent, Chemical Engineering Journal, 173 (2011) 511-519.
[82] J.H. Chen, J.C. Ni, Q.L. Liu, S.X. Li, Adsorption behavior of Cd(II) ions on humic acid-immobilized sodium alginate and hydroxyl ethyl cellulose blending porous composite membrane adsorbent, Desalination, 285 (2012) 54-61.
[83] J. Chen, F. Tendeyong, S. Yiacoumi, Equilibrium and kinetic studies of copper ion uptake by calcium alginate, Environmental science & technology, 31 (1997) 1433-1439.
[84] C.S.C. Chiew, H.K. Yeoh, P. Pasbakhsh, K. Krishnaiah, P.E. Poh, B.T. Tey, E.S. Chan, Halloysite/alginate nanocomposite beads: kinetics, equilibrium and mechanism for lead adsorption, Applied Clay Science, 119 (2016) 301-310.
[85] M.Y. Arıca, Y. Kacar, Ö. Genç, Entrapment of white-rot fungus *Trametes versicolor* in Ca-alginate beads: preparation and biosorption kinetic analysis for cadmium removal from an aqueous solution, Bioresource technology, 80 (2001) 121-129.
[86] Y. Jodra, F. Mijangos, Ion exchange selectivities of calcium alginate gels for heavy metals, Water Science and Technology, 43 (2001) 237-244.
[87] S.K. Papageorgiou, F.K. Katsaros, E.P. Kouvelos, J.W. Nolan, H. Le Deit, N.K. Kanellopoulos, Heavy metal sorption by calcium alginate beads from *Laminaria digitata*, Journal of hazardous materials, 137 (2006) 1765-1772.
[88] R.G. Pearson, Hard and soft acids and bases, Journal of the American Chemical society, 85 (1963) 3533-3539.
[89] C. Bertagnolli, A. Grishin, T. Vincent, E. Guibal, Recovering heavy metal ions from complex solutions using polyethylenimine derivatives encapsulated in alginate matrix, Industrial & Engineering Chemistry Research, 55 (2016) 2461-2470.
[90] J.H. Min, J.G. Hering, Arsenate sorption by Fe(III)-doped alginate gels, Water research, 32 (1998) 1544-1552.
[91] W. Zhang, H. Wang, X. Hu, H. Feng, W. Xiong, W. Guo, J. Zhou, A. Mosa, Y. Peng, Multicavity triethylenetetramine-chitosan/alginate composite beads for enhanced Cr(VI) removal, Journal of cleaner production, 231 (2019) 733-745.

[92] X. Lv, G. Jiang, X. Xue, D. Wu, T. Sheng, C. Sun, X. Xu, Fe^0-Fe_3O_4 nanocomposites embedded polyvinyl alcohol/sodium alginate beads for chromium (VI) removal, Journal of hazardous materials, 262 (2013) 748-758.
[93] Z. Lei, S. Zhai, J. Lv, Y. Fan, Q. An, Z. Xiao, Sodium alginate-based magnetic carbonaceous biosorbents for highly efficient Cr(VI) removal from water, RSC Advances, 5 (2015) 77932-77941.
[94] H.C. Vu, A.D. Dwivedi, T.T. Le, S.-H. Seo, E.-J. Kim, Y.-S. Chang, Magnetite graphene oxide encapsulated in alginate beads for enhanced adsorption of Cr(VI) and As(V) from aqueous solutions: role of crosslinking metal cations in pH control, Chemical Engineering Journal, 307 (2017) 220-229.
[95] J. Samuel, M. Pulimi, M.L. Paul, A. Maurya, N. Chandrasekaran, A. Mukherjee, Batch and continuous flow studies of adsorptive removal of Cr(VI) by adapted bacterial consortia immobilized in alginate beads, Bioresource technology, 128 (2013) 423-430.
[96] S. Cataldo, A. Gianguzza, A. Pettignano, Sorption of Pd(II) ion by calcium alginate gel beads at different chloride concentrations and pH. A kinetic and equilibrium study, Arabian Journal of Chemistry, 9 (2016) 656-667.
[97] E. Guibal, K.C. Gavilan, P. Bunio, T. Vincent, A. Trochimczuk, Cyphos IL 101 (tetradecyl (trihexyl) phosphonium chloride) immobilized in biopolymer capsules for Hg(II) recovery from HCl solutions, Separation Science and Technology, 43 (2008) 2406-2433.
[98] T. Vincent, A. Parodi, E. Guibal, Immobilization of Cyphos IL-101 in biopolymer capsules for the synthesis of Pd sorbents, Reactive and Functional Polymers, 68 (2008) 1159-1169.
[99] S. Mishra, Adsorption–desorption of heavy metal ions, Current Science, (2014) 601-612.
[100] G. Bayramoğlu, M.Y. Arıca, Construction a hybrid biosorbent using *Scenedesmus quadricauda* and Ca-alginate for biosorption of Cu(II), Zn(II) and Ni(II): kinetics and equilibrium studies, Bioresource technology, 100 (2009) 186-193.
[101] F. Wang, X. Lu, X.-y. Li, Selective removals of heavy metals (Pb^{2+}, Cu^{2+}, and Cd^{2+}) from wastewater by gelation with alginate for effective metal recovery, Journal of hazardous materials, 308 (2016) 75-83.
[102] G. Bayramoğlu, I. Tuzun, G. Celik, M. Yilmaz, M.Y. Arica, Biosorption of mercury (II), cadmium (II) and lead (II) ions from aqueous system by microalgae *Chlamydomonas reinhardtii* immobilized in alginate beads, International Journal of Mineral Processing, 81 (2006) 35-43.
[103] Y. Vijaya, S.R. Popuri, V.M. Boddu, A. Krishnaiah, Modified chitosan and calcium alginate biopolymer sorbents for removal of nickel (II) through adsorption, Carbohydrate polymers, 72 (2008) 261-271.
[104] H.G. Park, T.W. Kim, M.Y. Chae, I.-K. Yoo, Activated carbon-containing alginate adsorbent for the simultaneous removal of heavy metals and toxic organics, Process Biochemistry, 42 (2007) 1371-1377.
[105] W. Jung, B.-H. Jeon, D.-W. Cho, H.-S. Roh, Y. Cho, S.-J. Kim, D.S. Lee, Sorptive removal of heavy metals with nano-sized carbon immobilized alginate beads, Journal of Industrial and Engineering Chemistry, 26 (2015) 364-369.

[106] Y. Huang, Z. Wang, Preparation of composite aerogels based on sodium alginate, and its application in removal of Pb^{2+} and Cu^{2+} from water, International Journal of Biological Macromolecules, 107 (2018) 741-747.
[107] A. Benettayeb, E. Guibal, A. Morsli, R. Kessas, Chemical modification of alginate for enhanced sorption of Cd(II), Cu(II) and Pb(II), Chemical Engineering Journal, 316 (2017) 704-714.
[108] L. Pan, Z. Wang, Q. Yang, R. Huang, Efficient removal of lead, copper and cadmium ions from water by a porous calcium alginate/graphene oxide composite aerogel, Nanomaterials, 8 (2018) 957.
[109] K. Attar, H. Demey, D. Bouazza, A.M. Sastre, Sorption and desorption studies of Pb(II) and Ni(II) from aqueous solutions by a new composite based on alginate and magadiite materials, Polymers, 11 (2019) 340.
[110] N. Jiang, Y. Xu, Y. Dai, W. Luo, L. Dai, Polyaniline nanofibers assembled on alginate microsphere for Cu^{2+} and Pb^{2+} uptake, Journal of hazardous materials, 215 (2012) 17-24.
[111] H. Sone, B. Fugetsu, S. Tanaka, Selective elimination of lead (II) ions by alginate/polyurethane composite foams, Journal of hazardous materials, 162 (2009) 423-429.
[112] Q. Gao, X. Wang, H. Wang, D. Liang, J. Zhang, J. Li, Sulfhydryl-modified sodium alginate film for lead-ion adsorption, Materials Letters, 254 (2019) 149-153.
[113] Y. Wang, Y. Feng, X.-F. Zhang, X. Zhang, J. Jiang, J. Yao, Alginate-based attapulgite foams as efficient and recyclable adsorbents for the removal of heavy metals, Journal of colloid and interface science, 514 (2018) 190-198.
[114] V. Gopalakannan, N. Viswanathan, One pot synthesis of metal ion anchored alginate–gelatin binary biocomposite for efficient Cr(VI) removal, International Journal of Biological Macromolecules, 83 (2016) 450-459.
[115] Z. Wan, D.-W. Cho, D.C. Tsang, M. Li, T. Sun, F. Verpoort, Concurrent adsorption and micro-electrolysis of Cr(VI) by nanoscale zerovalent iron/biochar/Ca-alginate composite, Environmental Pollution, 247 (2019) 410-420.
[116] K. Cho, B.Y. Shin, H.K. Park, B.G. Cha, J. Kim, Size-controlled synthesis of uniform akaganeite nanorods and their encapsulation in alginate microbeads for arsenic removal, RSC Advances, 4 (2014) 21777-21781.
[117] O.-H. Kwon, J.-O. Kim, D.-W. Cho, R. Kumar, S.H. Baek, M.B. Kurade, B.-H. Jeon, Adsorption of As(III), As(V) and Cu(II) on zirconium oxide immobilized alginate beads in aqueous phase, Chemosphere, 160 (2016) 126-133.
[118] A. Sigdel, J. Park, H. Kwak, P.-K. Park, Arsenic removal from aqueous solutions by adsorption onto hydrous iron oxide-impregnated alginate beads, Journal of Industrial and Engineering Chemistry, 35 (2016) 277-286.
[119] A. Sinha, K.K. Pant, S.K. Khare, Studies on mercury bioremediation by alginate immobilized mercury tolerant *Bacillus cereus* cells, International Biodeterioration & Biodegradation, 71 (2012) 1-8.
[120] Y. Zhang, D. Kogelnig, C. Morgenbesser, A. Stojanovic, F. Jirsa, I. Lichtscheidl-Schultz, R. Krachler, Y. Li, B.K. Keppler, Preparation and characterization of immobilized

[A336][MTBA] in PVA–alginate gel beads as novel solid-phase extractants for an efficient recovery of Hg(II) from aqueous solutions, Journal of hazardous materials, 196 (2011) 201-209.
[121] L. Sellaoui, F.E. Soetaredjo, S. Ismadji, Y. Benguerba, G.L. Dotto, A. Bonilla-Petriciolet, A.E. Rodrigues, A.B. Lamine, A. Erto, Equilibrium study of single and binary adsorption of lead and mercury on bentonite-alginate composite: experiments and application of two theoretical approaches, Journal of Molecular Liquids, 253 (2018) 160-168.
[122] K. Sarkar, Z. Ansari, K. Sen, Detoxification of Hg(II) from aqueous and enzyme media: pristine vs. tailored calcium alginate hydrogels, International Journal of Biological Macromolecules, 91 (2016) 165-173.
[123] R. Dubey, J. Bajpai, A. Bajpai, Chitosan-alginate nanoparticles (CANPs) as potential nanosorbent for removal of Hg(II) ions, Environmental Nanotechnology, Monitoring & Management, 6 (2016) 32-44.
[124] S. Cataldo, N. Muratore, S. Orecchio, A. Pettignano, Enhancement of adsorption ability of calcium alginate gel beads towards Pd(II) ion. A kinetic and equilibrium study on hybrid Laponite and Montmorillonite–alginate gel beads, Applied Clay Science, 118 (2015) 162-170.
[125] S. Wang, T. Vincent, C. Faur, E. Guibal, A comparison of palladium sorption using polyethylenimine impregnated alginate-based and carrageenan-based algal beads, Applied Sciences, 8 (2018) 264.
[126] X. Gao, C. Guo, J. Hao, Z. Zhao, H. Long, M. Li, Selective adsorption of Pd(II) by ion-imprinted porous alginate beads: Experimental and density functional theory study, International Journal of Biological Macromolecules, (2020).
[127] W. Wei, S. Lin, D.H.K. Reddy, J.K. Bediako, Y.-S. Yun, Poly (styrenesulfonic acid)-impregnated alginate capsule for the selective sorption of Pd(II) from a Pt(IV)-Pd(II) binary solution, Journal of hazardous materials, 318 (2016) 79-89.
[128] T. Vincent, A. Parodi, E. Guibal, Pt recovery using Cyphos IL-101 immobilized in biopolymer capsules, Separation and purification technology, 62 (2008) 470-479.
[129] H. Niu, Z. Meng, Y. Cai, Fast defluorination and removal of norfloxacin by alginate/Fe@ Fe_3O_4 core/shell structured nanoparticles, Journal of hazardous materials, 227 (2012) 195-203.
[130] E. Rosales, O. Iglesias, M. Pazos, M. Sanromán, Decolourisation of dyes under electro-Fenton process using Fe alginate gel beads, Journal of hazardous materials, 213 (2012) 369-377.
[131] Y. Dong, W. Dong, Y. Cao, Z. Han, Z. Ding, Preparation and catalytic activity of Fe alginate gel beads for oxidative degradation of azo dyes under visible light irradiation, Catalysis Today, 175 (2011) 346-355.
[132] O. Iglesias, J. Gómez, M. Pazos, M.Á. Sanromán, Electro-Fenton oxidation of imidacloprid by Fe alginate gel beads, Applied Catalysis B: Environmental, 144 (2014) 416-424.
[133] R.F. Quadrado, A.R. Fajardo, Fast decolorization of azo methyl orange via heterogeneous Fenton and Fenton-like reactions using alginate-Fe^{2+}/Fe^{3+} films as catalysts, Carbohydrate polymers, 177 (2017) 443-450.

[134] F. Shi, Y. Chen, L. Sun, L. Zhang, J. Hu, Hydroxylation of phenol catalyzed by different forms of Cu-alginate with hydrogen peroxide as an oxidant, Catalysis Communications, 25 (2012) 102-105.
[135] M.Á. Fernández de Dios, E. Rosales, M. Fernández-Fernández, M. Pazos, M.Á. Sanromán, Degradation of organic pollutants by heterogeneous electro-Fenton process using Mn-alginate composite, Journal of Chemical Technology & Biotechnology, 90 (2015) 1439-1447.
[136] X. Qiao, L. Niu, H. Zhang, X. Wen, Y. Cao, G. Bai, Controllable fabrication of a novel porous Ni-alginate hybrid material for hydrogenation, Applied Catalysis B Environmental, 218 (2017) S0926337317306392.
[137] T. Zhan, S. Lu, X. Liu, H. Teng, W. Hou, Alginate derived Co_3O_4/Co nanoparticles decorated in N-doped porous carbon as an efficient bifunctional catalyst for oxygen evolution and reduction reactions, Electrochimica Acta, 265 (2018) 681-689.
[138] X. Lou, P. Hui, S. Zhu, C. Zhu, Z. Chen, Synthesis of silver nanoprisms on reduced graphene oxide for high-performance catalyst, Catalysis Communications, 69 (2015) 43-47.
[139] S. Saha, A. Pal, S. Kundu, S. Basu, T. Pal, Photochemical Green Synthesis of Calcium-Alginate-Stabilized Ag and Au Nanoparticles and Their Catalytic Application to 4-Nitrophenol Reduction, Langmuir the Acs Journal of Surfaces & Colloids, 26 (2010) 2885-2893.
[140] A. Primo, M. Liebel, F.O. Quignard, Palladium Coordination Biopolymer: A Versatile Access to Highly Porous Dispersed Catalyst for Suzuki Reaction, Chemistry of Materials, 21 (2009) 621-627.

Chapter 2 New highly-percolating alginate-PEI membranes for efficient recovery of chromium and selenium ions from aqueous solutions

2.1. Introduction Générale

La nécessité de développer des procédés de traitement des effluents métallifères avec un double objectif de récupération de métaux valorisables et d'élimination de métaux toxiques, associée à la tendance actuelle à intégrer des matériaux biosourcés renouvelables en remplacement de matières premières pétrosourcées, est à l'origine du développement de nouveaux composites associant l'alginate (ou la biomasse algale) et la polyethylèneimine (PEI). Une première génération de matériaux a été élaborée sous forme de billes composites. Récemment des matériaux de type membranaire (mousses à porosité ouverte, éponges) à base de biopolymères ont été élaborés pour envisager des processus de traitement en continu d'effluents liquides par percolation (ou drainage naturel). Ces procédés nécessitent souvent des procédés complexes et énergivores pour maintenir une porosité suffisante facilitant le transfert de solutions aqueuses. Le procédé développé dans ce travail marque une rupture par rapport à ces technologies conventionnelles, en mettant à profit d'une part l'interaction entre les groupes carboxylates de l'alginate et les fonctions aminées de la PEI et d'autre part la réticulation de la PEI par du glutaraldéhyde. Cette double interaction permet la "structuration forte" de l'hydrogel qui permet de procéder au séchage de la mousse (membrane) à l'air libre sans effondrement de la structure poreuse. Ces interactions ont été caractérisées par spectroscopie infrarouge à transformée de Fourier. La texture de surface "hyper" macroporeuse a été caractérisée, et le haut pouvoir de percolation a été étudié en écoulement gravitaire (sans pompe, colonne d'eau réduite imposant une pression statique de 0.006 bar) pour des débits de drainage de quelques dizaines de valeurs comprise entre 13 et 34 mL cm^{-2} min^{-1} (correspondant à des vitesses superficielles de 7,8 à 20,4 m h^{-1}).

La présence de groupements fonctionnels variés (carboxylates libres et fonctions aminées) confère au matériau : (a) des propriétés de complexation des cations par les groupes carboxylates et les fonctions aminées libres à des pH neutres ou d'acidité modérée (pH supérieur à 3-4), (b) ainsi que des propriétés d'échange ionique et d'attraction électrostatique des anions métalliques (en milieu acide). C'est précisément cette interaction de type électrostatique qui est étudiée dans ce chapitre à travers l'évaluation des propriétés adsorbantes de membranes PEI/Alginate vis-à-vis des ions chromates et sélénates. Ces deux types de contaminants se caractérisent par des comportements différents : les ions chromates sont

facilement réduits en Cr(III)) en milieu acide en présence de composés organiques alors que les ions sélénates sont plus stables. Une attention particulière est donc portée, lors de l'étude sur les ions chromates, à analyser systématiquement le Cr(VI) (par colorimétrie à la diphenylcarbazide) et le chrome total (TCr, par ICP-AES). L'effet du pH est étudié, en lien avec les caractéristiques de charge des membranes (protonation des fonctions aminées) et la spéciation des ions métalliques (anions). L'étude des cinétiques en mode statique (recirculation d'un volume fini de la solution au travers de la membrane) est menée en faisant varier le débit de la solution. Les isothermes d'adsorption sont également acquises à pH 2 vis-à-vis des deux éléments métalliques, sans et avec la présence d'anions compétiteurs (chlorure, nitrate et sulfate).

Enfin, les propriétés et la stabilité des matériaux adsorbants sont évaluées sur plusieurs cycles d'adsorption et de désorption.

Ce chapitre a fait l'objet de deux articles scientifiques publiés :

1. **Yayuan Mo**, Shengye Wang, Thierry Vincent, Jacques Desbrieres, Catherine Faur, and Eric Guibal. New highly-percolating alginate-PEI membranes for efficient recovery of chromium from aqueous solutions. Carbohydrate Polymers, volume 225, 115177 (2019).
2. **Yayuan Mo**, Thierry Vincent, Catherine Faur, and Eric Guibal. Se(VI) sorption from aqueous solution using alginate/polyethylenimine membranes: Sorption performance and mechanism. International Journal of Biological Macromolecules, volume 147, 832-843(2020).

2.2. Introduction

Cr(VI) and Se(VI) are two types of oxyanion contaminants that characterized in different behaviors. With the growing demand for chromium-based products and equipments, many industrial processes, such as electroplating, textile dyeing, petroleum refineries, leather tanning, wood preservation, and nuclear power plant, generate large amounts of chromium-contaminated wastewater. In aqueous solutions, Cr mainly occurs under the most stable forms of trivalent Cr(III) cations (e.g., $Cr_2(OH)_2^{4+}$ and $Cr(OH)_2^{+}$) and hexavalent Cr(VI) anions (e.g., $HCrO_4^{-}$, $Cr_2O_7^{2-}$ and CrO_4^{2-}) [1, 2]. Cr(III) is an essential nutrient, at low concentrations, that plays an important role in the proper functioning of living organisms, while Cr(VI) is a highly toxic pollutant because of its teratogenicity, mutagenicity and carcinogenicity to living organisms even at ppb levels [3, 4]. Therefore, removal of Cr(VI) from wastewater is very essential for protecting natural environment and human health.

Selenium (Se) is a rare non-metallic chemical element with a double beneficial and harmful character to living organisms: at low concentration, it is an essential nutrient (important role in

the proper functioning of the human immune system); while at certain concentration little above homeostatic level, it is a huge threat because of specific toxicity and bio-accumulation [5]. To minimize the possible risks associated with Se, the World Health Organization (WHO) has set a maximum Se concentration in drinking water of 40 μg L^{-1}, while in the European Union (EU) regulations Se concentration should not exceed 10 μg L^{-1} [6, 7]. Therefore, Se removal from surface waters, ground waters or wastewaters (derived from mining, coal-fired power plants, petrochemical, refineries and agricultural drain) requires a proper treatment in order to achieve the purification and re-use of natural water resources. Another interest for Se removal from water streams consists of the sustainable recovery and re-use of the element to face future Se scarcity [8]. Selenium may occurs under five forms in geochemical environments: selenide (Se(-II)), elemental Se (Se^0), selenite (Se(IV)), selenate (Se(VI)) and organic Se. However, Se(IV) and Se(VI) are the predominant species in aqueous systems [9]. Although both Se(IV) and Se(VI) could bioaccumulate in organisms and be harmful to health, Se(VI) is found to be higher toxic; existing as SeO_4^{2-}, $HSeO_4^{2-}$, H_2SeO_{4aq}. In addition, it is more difficult to remove due to its more stable species in aqueous solutions, compared with Se(IV) [10-12]. The concentration and speciation of Se in wastewater are affected by environmental factors such as pH and redox conditions [13].

Several technologies, including chemical reduction, coagulation, membrane separation, ion exchange and adsorption have been proposed to remove Se and Cr from aqueous solution [14-17]. The selection of the appropriate method is based on criteria such as the concentration of the metal ion, the pH of the solution, its complexity and the produced flow rates. Among these methods, sorption is a simple, efficient and low-cost technique and various sorbents such as abundant materials (e.g. activated carbon) [18], agricultural waste [19] and natural minerals [20] have been investigated for the treatment of low-concentration effluents or as a polishing treatment. However, these sorbents may face several drawbacks including low stability and mechanical properties, difficulty in solid-liquid separation after treatment, generation of secondary pollution or cost-efficiency questions. To solve these problems, biosorbents have retained particular attention, including biopolymer matrixes such as chitosan or alginate [21, 22].

Alginate is a green, biocompatible and biodegradable polysaccharide that consists of blocks of 1–4 linked α-L-guluronic and β-D-mannuronic acids [23]. It has been applied as an effective sorbent for heavy metals removal and a green encapsulating biopolymer for chemical and biological compounds; these applications are directly associated to the presence of numerous functional groups (e.g. carboxyl and hydroxyl) distributed along the backbone as coordination

and reaction sites [22, 24]. For example, alginate was combined with chitosan [25], silica [26], bentonite clay [27], cellulose [28], hydroxyapatite [29], graphene oxide [30], maghemite particles [31] and polyethyleneimine (PEI) [32] to form new materials such as bead [33], magnetic composite [34], aerogel [30] and membrane [35]. The incorporation of these compounds contributes to enhancing its own mechanical properties and improving its sorption efficiency for the removal of heavy metals. Among them, PEI is a water-soluble polymer having abundant polar groups (amine group) and hydrophobic groups (vinyl group) that can combine with different materials. Meanwhile, it also can chelate heavy metal ions and has been widely applied for increasing the sorption capacities of modified adsorbents [36]. Recently, Xiong et al. [37] developed a recyclable adsorbent for removal of anionic dyes from wastewater by assembling alginate and PEI onto magnetic microspheres. Sun et al. [38] prepared a novel sorbent (PEI/SA) by functionalizing PEI/sodium alginate with 3-aminopropyltriethoxysilane for the sorption of Cu(II) from aqueous solution. Moreover, our research group has also successfully prepared PEI-impregnated alginate-based beads. Their application to the sorption of palladium demonstrated high metal sorption capacity [39], and also high stability after metal reduction for catalytic application [40]. Alternative conditionings have been designed for chitosan [41] and alginate [42], including porous membranes which could (a) increase in the number of contact sites between sorbent and metal ions and (b) keep highly percolating properties for sorption.

The rationale of this research consisted of evaluating the feasibility of designing highly percolating membranes (authorizing the feed of structured material with simple natural filtration, without pumping) with simple procedure, which does not require energy-consuming procedures for structuring the composite. The second objective of this work corresponded to evaluating the feasibility of using the as-prepared membranes for the recovery of anions.

Therefore, this work investigates the sorption of anions (i.e. Cr(VI) and Se(VI)) on this macroporous alginate-PEI membrane in a batch-like set-up: the membrane is disposed in a cylindrical holder and the solution is pumped through the membrane in a recirculation mode. The effect of pH on metal sorption, the uptake kinetics and the sorption isotherms are successively investigated (in terms of both quantification and modeling). FTIR spectroscopy, SEM-EDX and XPS analysis are also used for discussing the sorption mechanisms. It is noteworthy that a special attention is paid to the possible occurrence of reduction phenomena (Cr(VI) being readily reduced in acidic solutions while Se(VI) are more stable). The interference of other coexisting ions eventually present in the wastewater on the removal of Cr(VI) or Se(VI) is investigated to evaluate the selectivity of membranes. At last, the desorption

of Cr(VI) and Se(VI) is carried out to test the reusability of membranes.

2.3. Materials and Methods

2.3.1. Materials

Alginate powder was purchased from FMC BioPolymer (Ayr, UK). Previous analyses have characterized the biopolymer [43]:

- weight-average molar mass (Mw) of 4.46×10^5 g mol^{-1} (determined by the equation $[\eta]=0.023\times Mw^{0.984}$ [44], where the intrinsic viscosities [η] were measured on an Ubbelohde viscometer with a solvent flow time (0.1 M NaCl) at 25 °C).
- mannuronic to guluronic acid (M/G) ratio of 0.16/0.84 (obtained by ^{13}C NMR using a Bruker Avance 400 spectrometer).

A homogeneous alginate solution (4%, w/w) was prepared by mixing appropriate amounts of alginate powder with demineralized water (under vigorous stirring) at room temperature. Branched polyethylenimine (PEI, 50 % w/w, molecular weight close to 7.5×10^5 g mol^{-1}) and glutaraldehyde (GA, 50 %, w/w in water) solutions were supplied by Sigma–Aldrich (Saint-Louis, USA). The working PEI solution (4%, w/w) was obtained by dilution with demineralized water and pH control to 6.5 using HNO_3 solution. All other pH adjustment was performed using HCl and NaOH solutions.

2.3.2. Membrane fabrication

Figure 2-1 shows the schematic process used for the synthesis of the macroporous alginate-PEI (AP) membranes. Different amounts of PEI and GA are used to obtain two kinds of membranes for Cr(VI) and Se(VI) sorption, respectively.

In the case of Cr sorption, the AP-3% membrane was fabricated by diluting 132 g of 4% alginate solution with pure water to 500 g and stirring until obtaining a homogeneous solution. In a second step, 35 mL of 3% PEI solution was sequentially added to alginate solution (7 times: 5 mL every 10 s) under stirring. After 1 min of strong stirring the solution was rapidly poured into a rectangular mold. Fabricated membranes may have different sizes (thickness) by using different molds. The membrane was gradually formed by fully reacting PEI with alginate over 24 h (Reaction 1, see Figure 2-1). The third step consisted of crosslinking the membrane with glutaraldehyde to strengthen the material: 4 mL of GA (50%, w/w) were added into the mold with 300 mL demineralized water before immersing the membrane (which was previously carefully washed with deionized water four times) at room temperature (Reaction 2, see Figure 2-1). Finally, after 24 h of slow shaking (30 rpm) the membrane was carefully washed with

deionized water before being air-dried for 2 days. The membrane was cut into circular specimens for the next experiments.

In the case of Se sorption, another AP-4% membrane was prepared by diluting 100 g of 4 % alginate solution with demineralized water to 500 g and stirring until obtaining a homogeneous solution. In a second step, 35 mL of 4 % PEI was added into the solution under stirring. Next, the mixture was rapidly poured into a rectangular mold and maintained at room temperature for 24 h to complete the reaction between PEI and alginate and form the membrane. Fabricated membranes can be shaped into different sizes by using different molds. Afterwards, for strengthening the stability of the composite membrane a crosslinking treatment was applied: 2.5 mL of 50 % GA was added into the mold with 300 mL of demineralized water before immersing the membrane (which was previously carefully washed with deionized water, four times) at room temperature. Finally, after 24 h of slow shaking (30 rpm) the membrane was again carefully washed with deionized water and air-dried at room temperature. The membrane was cut into circular segment (disc, 25 mm diameter) for sorption tests.

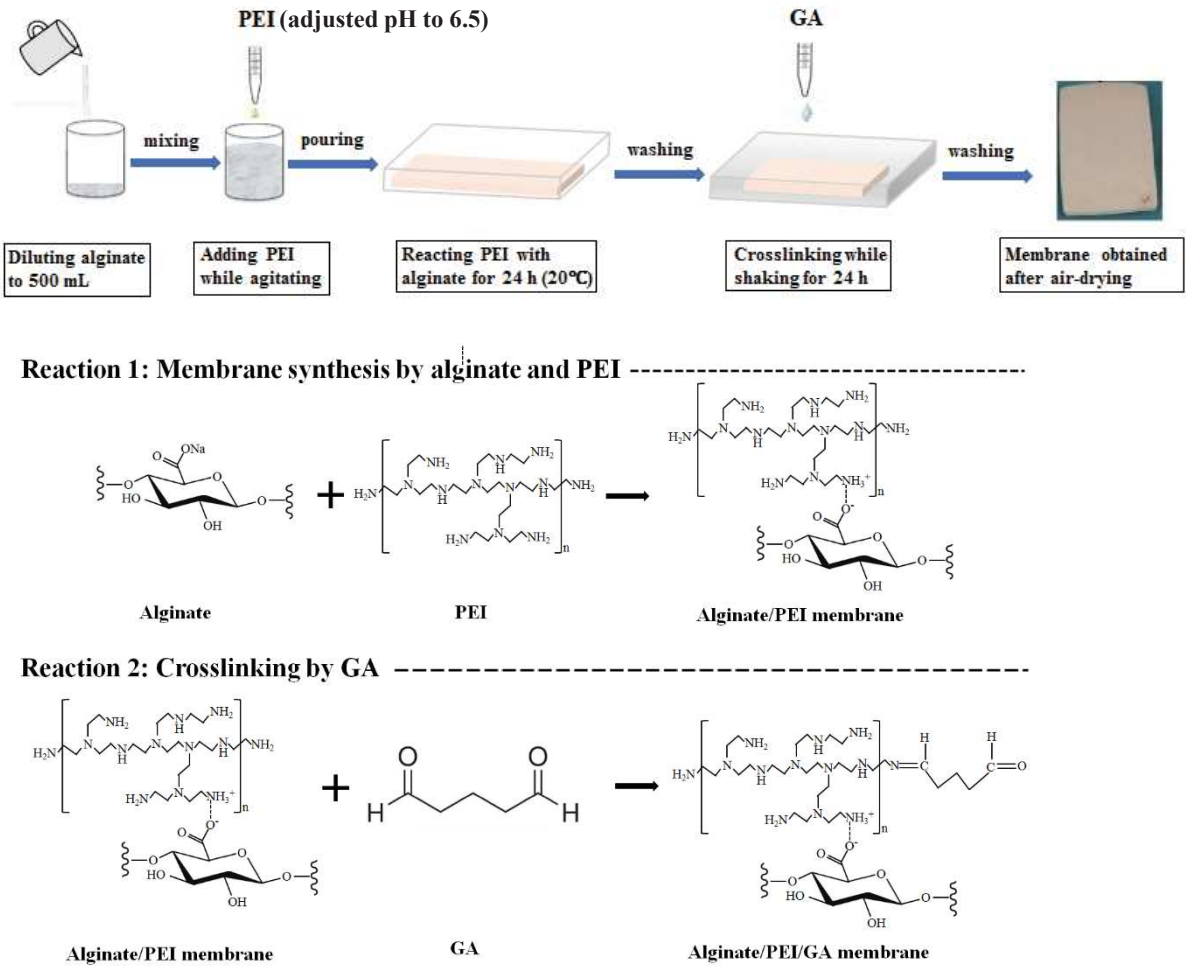

Figure 2-1 Process for membrane manufacturing

2.3.3. Membrane characterization

The porosity of the membranes was obtained by pycnometer measurements using ethanol as the soaking agent, and measuring the total volume of membranes and the amount of ethanol required to fill the porous compartment [45, 46].

The stability of the sorbents was measured by shaking the membrane disc in 20 mL of pure water for 72 h at 150 rpm. Then, the membranes were weighed after drying. Stability (%) was calculated as follows Eq. 2-1:

$$\text{Stability} = \frac{100\ m_{eq}}{m_0} \qquad \textbf{Eq. 2-1}$$

where m_0 (mg) and m_{eq} (mg) are the mass of the membrane disc before and after shaking.

The determination of the water flux through the membranes was conducted at 20 °C and 0.006 bar (calculated from the water height by p = ρgh) and the effective area of the membrane was 4.64 cm^2; then the water was maintained at the same level and the time consumed for passing 100 mL water though the membrane disc was recorded. The water flux (J, mL cm^{-2} min^{-1}) was calculated by the following equation:

$$J = \frac{V_p}{A\ t} \qquad \textbf{Eq. 2-2}$$

where V_p (mL) is the permeate volume, A (cm^2) the membrane effective area and t (min) the time consumed.

In addition, the free draining flow velocity (free percolation without forced pumping) was determined by feeding water at the top of the column increasing flow rate. The limit flow rate for free draining corresponded to the beginning of water accumulation at the top of the membrane. All the above experiments were repeated at least twice to evaluate the experimental error.

The pH point of zero charge (pH_{Pzc}) corresponded to the pH of the solution surrounding the sorbents when the electrical charge density on a surface is zero. Therefore, the charges on the surface will be positive and negative when the pH is lower and higher than the pH_{pzc}, respectively. The pH_{PZC} of the membranes was measured according to the pH-drift method [47, 48]. 50 mL of 0.1 M NaCl solution at different initial pH values (pH_0, in the range 2-10) were mixed with 0.1 g of membrane for 2 days under agitation (150 rpm) at room temperature. Then, the final pH (pH_f) was recorded and plotted against pH_0 and the pH_{PZC} corresponds to the point at which pH_f was equal to pH_0.

The surface morphology of the membrane and its changes after sorption were determined using SEM (Quanta FEG 200, Thermo Fisher Scientific, Mérignac, France). The main elemental analysis of the materials (semi-quantitative analysis) before and after Cr sorption was carried out using EDX accessory (Oxford Instruments France, Saclay, France). FTIR spectra were used to examine the functional groups of the membranes using an FTIR-ATR (Attenuated Total Reflectance tool) Bruker VERTEX70 spectrometer (Bruker, Germany) in the wavenumber range: 4000-400 cm^{-1}. X-ray photoelectron spectroscopy (XPS) analysis was carried on a ESCALAB 250XI spectrometer (Thermo Fisher Scientific, USA) with a monochromatic Al Kα radiation (hυ = 1486.6 eV) and a passing energy of 50 eV.

2.3.4. Sorption experiments

Batch sorption experiments were performed in a continuous treatment device (Figure 2-2), in the recirculation mode, by pumping the metal-containing solution through a flow system composed of a peristaltic pump (Ismatec ISM404B, USA), filter membrane holders and water tanks. Different sizes of filter membrane holders can be selected depending on the different diameter (Ø) of membrane disk used. In the process, the membrane disk has been fixed into the filter membrane holder, and the solution was pumped through the system on a recirculation mode at certain flow rate (i.e., 15 mL min^{-1}). Simultaneously, a gentle agitation was set under water tanks with a plate magnetic stirrer (Variomag Poly 15, Thermo, Germany).

(1) Sorption of Cr(VI) and TCr

The Cr(VI) and Cr(III) stock solutions were prepared by dissolving appropriate amounts of potassium dichromate ($K_2Cr_2O_7$) (Merck KGaA, Darmstadt, Germany) and chromium(III) chloride hexahydrate ($Cl_3Cr{\cdot}6H_2O$) (Sigma-Aldrich, Darmstadt, Germany) into 0.01 M HCl solution, respectively, then further diluted to obtain working solutions.

For the pH effect experiments, 50 mL of 200 mg L^{-1} metal ion solutions at different pH values (in the range 0.5-4, adjusted with HCl or NaOH solution) were contacted with 30 mg of membrane (Ø: 12 mm; height: 4.0± 0.1 mm) for 2 days at room temperature, and the flow rate was maintained at 15 mL min^{-1}. For uptake kinetics, a piece of membrane (mass: 217 mg, Ø: 24.5 mm; height: 6.5 ± 0.1 mm) was contacted with 1 L of 100 mg L^{-1} metal ion solutions at pH 2 at two different flow rates (15 mL min^{-1} and 30 mL min^{-1}, respectively). Four milliliters of solution were collected at predetermined times and immediately filtered using filter papers (Ø 25 mm, Prat-Dumas, France). For the sorption isotherm, 30 mg of membrane were contacted with 50 mL of metal ion solution at different initial concentrations (C_0, ranging from 20 and 300 Cr mg L^{-1}) for 3 days at room temperature. The pH of the solutions was initially set at pH 2 and the flow rate maintained at 15 mL min^{-1}. For the effect of coexisting ions such as Ca^{2+},

Cu^{2+}, Cl^{-}, NO_3^{-}, and SO_4^{2-}) which are commonly present in industrial effluents, 30 mg of macroporous membrane were contacted with 50 mL of Cr(VI) solution containing each of various components at different concentrations (ranging from 0 and 800 mg L^{-1}) for 3 days at room temperature. The concentrations of SO_4^{2-} and Ca^{2+} in electroplating and tannery effluent can reach up to 500 and 800 mg L^{-1}, respectively [49].

The concentration of Cr(VI) was analyzed using UV spectrophotometer (Varian 2050) at 540 nm by the diphenylcarbazide method, while the TCr (total chromium) concentration was determined by inductively coupled plasma atomic emission spectrometry (ICP-AES, JY Activa M, Jobin-Yvon, Horiba, Longjumeau, France) after proper dilutions. The Cr(III) concentration was then obtained by subtracting the amount of Cr(VI) from the TCr (i.e. TCr = Cr(III) + Cr(VI)). The solution pH was measured using a pH-meter cyber scan pH 6000 (Eutech instruments, Nijkerk, The Netherlands).Actually, wastewater usually contains several metal ions (and inorganic anions), so in order to test the suitability of the macroporous membrane in a complex system; different masses (15 mg and 30 mg) of sorbents were applied to treat a synthesized electroplating wastewater and a single Cr-containing wastewater (control group). The synthesized wastewater was simulated from an electroplating unit at Kolkata, India, which contains 54.5 mg L^{-1} of Cr(VI), 6.25 mg L^{-1} of Cu(II), 26.4 mg L^{-1} of Ca(II), 173.26 mg L^{-1} of Na(I), 2.52 mg L^{-1} of K(I) and 1.45 mg L^{-1} of Zn(II) [50]. The synthesized solutions were treated at pH 2 for 2 days.

Desorption and reuse experiments are studied in this work. After the kinetic experiments at the flow rate of 15 mL min^{-1}, metal loaded membranes were washed with demineralized water. Four-mL sample was collected at predetermined times for analyzing residual metal concentration. For evaluating the reversibility of chromate-loaded membranes. The materials were subjected to desorption kinetic experiment using 1 L solution of NaOH at either 0.01 M (pH=11.9) or 0.1 M (pH=12.5) concentrations. To determine the reusability of membranes, experiments on Cr(VI) sorption and desorption process were carried out for 3 cycles. For each cycle, 30 mg of macroporous membrane was contacted with 50 mL of 200 mg L^{-1} Cr(VI) solution for 2 days and then desorbed for 4 h using 50 mL of 0.01 M NaOH solution (after optimization of desorption conditions). After each cycle of sorption-desorption, the membrane was washed by demineralized water four times for reuse in the next cycle.

(2) Sorption of Se(VI)

A 2 g L^{-1} Se(VI) stock solution was prepared by dissolving appropriate amounts of sodium selenate ($Na_2SeO_4.10H_2O$, BDH chemicals Ltd., Poole, England) in water and then further

diluted to obtain working solutions. The effect of pH was conducted in the initial pH range of 1–7 (adjusted by HCl or NaOH) with a fixed Se(VI) concentration of 100 mg L^{-1} and a sorbent dosage of 0.8 g L^{-1}. After reacting 24 h, at pump speed of 15 mL min^{-1}, the equilibrium pH_{eq} of solution was measured by a pH-meter Cyber Scan pH 6000 (Eutech instruments, Nijkerk, the Netherlands). Sorption isotherm was assessed at varying initial concentrations (10-270 mg Se L^{-1}) with a sorbent dose of 0.8 g L^{-1} at pH 2. After the reaction reaches equilibrium, the samples were filtered for measurement. Sorption kinetics of Se(VI) on membrane were investigated using batch tests at three different flow rates (5, 15 and 50 mL min^{-1}; i.e., superficial flow velocities: 0.65, 1.94 and 6.47 m h^{-1}). The tests were carried out by contacting in a recirculation mode 200 mg of the membranes with 500 ml of 50 mg Se L^{-1} solution at pH 2. A 2-ml aliquot was collected at specified time intervals and immediately filtered for Se analysis.

The presence of a large number of protonated amine groups in the membrane in acidic solutions lets suspect a high affinity for anions (including selenate anions). Sorption tests were performed in the presence of increasing concentrations of commonly co-existing anions, such as Cl^-, NO_3^-, and SO_4^{2-}. The concentrations of coexisting anions ranged from 0 to 800 mg L^{-1}. These experiments were carried out by contacting 50 mg of the membranes with 50 mL of 100 mg L^{-1} Se(VI) solution (at pH 2) containing co-existing anions at pH 2. After reacting in recirculation mode at pump speed of 15 mL min^{-1} for 24 h, the supernatant was filtered for analyze the residual concentration.

Four cycles of sorption-desorption were carried out to evaluate the reusability of the membrane. For each sorption experiment, 40 mg of membrane were contacted with 50 mL of 100 mg Se L^{-1} Se (VI) at pH 2, and then the solution was collected and filtered after reaching adsorption equilibrium. For the desorption experiment, the Se-loaded membrane was contacted with a 50 mL 0.01 M NaOH solution for 30 min and then collected and filtered the solution. After washing and drying, the regenerated membrane was used in the next cycle.

For all these experiments, after filtration the samples were analyzed (C_{eq}, mg L^{-1}) and the mass balance equation was used for evaluating sorption performance. The removal percentage (R, %) and the sorption capacity (q_{eq}, mg g^{-1}) were calculated with Eq. 2-3 and Eq. 2-4, respectively.

$$R\ (\%) = \frac{100\,(C_0 - C_{eq})}{C_0} \qquad \textbf{Eq. 2-3}$$

$$q_{eq} = \frac{(C_0 - C_{eq})\,V}{m} \qquad \textbf{Eq. 2-4}$$

where V is the volume of solution (L) and m the dry weight of membrane (g).

The desorption efficiency (De, %) was calculated by the equation: De (%) = (amount of metal desorbed / amount of metal sorbed) ×100.

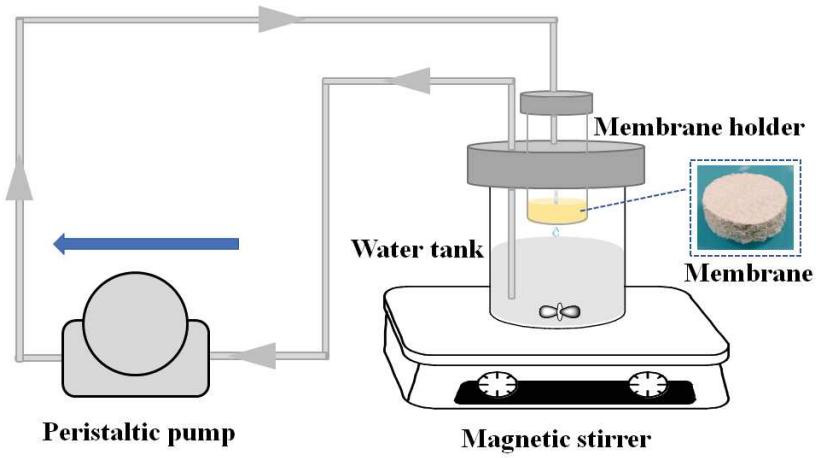

Figure 2-2 Schematic diagram of the continuous treatment device for the sorption experiments.

2.3.5. Modeling

In order to understand the dynamic process of metal ions sorption onto membranes, the experimental sorption kinetics were linear fitted with two common kinetic models, namely Pseudo-first order rate equation (PFORE) and Pseudo-second order rate equation (PSORE), which are commonly used to describe chemical reaction rates in homogeneous or heterogeneous systems [51].

PFORE:

$$q(t) = q_{eq,1}(1 - e^{-k_1 t}) \qquad \textbf{Eq. 2-5}$$

PSORE:

$$q(t) = \frac{q_{eq,2}^2 \times k_2 \times t}{1 + q_{eq,2} \times k_2 \times t} \qquad \textbf{Eq. 2-6}$$

where $q_{eq,i}$ (mg g^{-1}) and q(t) (mg g^{-1}) are the amount of metal adsorbed onto membranes at equilibrium and at time t (i=1 or 2), respectively, and k_1 (min^{-1}) and k_2 (g mg^{-1} min^{-1}) are the rate constants of PFORE and PSORE models, respectively.

In addition, the sorption isotherms can be modeled using various models [52]; however, the most frequently used are the mechanistic Langmuir equation and empirical models such as the Freundlich and the Sips equations. The Langmuir model assumes the sorption processes as a monolayer at the homogeneous surface of the sorbent [53], while the Freundlich model is assigned to non-ideal sorption on heterogeneous surfaces as well as multilayer sorption [54]. The Sips equation also called Langmuir-Freundlich equation) is combination of the two models based on pure mathematical concept.

Langmuir:

$$q_{eq} = \frac{q_m \times b_L \times C_{eq}}{1 + b_L \times C_{eq}}$$ **Eq. 2-7**

Freundlich:

$$q_{eq} = k_F C_{eq}^{1/n_F}$$ **Eq. 2-8**

Sips:

$$q_{eq} = \frac{q_m \times b_S \times C_{eq}^{1/n_S}}{1 + b_S \times C_{eq}^{1/n_S}}$$ **Eq. 2-9**

where C_{eq} (mg L^{-1}) is the equilibrium concentration of metal ions; q_{eq} and q_m (mg g^{-1}) are the equilibrium and the maximum sorption capacities; b_L and b_S (L mg^{-1}) represent the Langmuir and Sips constant, respectively; n_F and n_S are the sorption intensity parameters for Freundlich and Sips equations.

2.3.6. Statistical Analysis

Selected experiments were duplicated and the calculated average values and standard deviations were embodied in the figures. In order to test the repeatability of the sorption performance of membranes, three identical membranes were fabricated at different times and used to remove Cr(VI). Their results are shown in Figure 2-3.

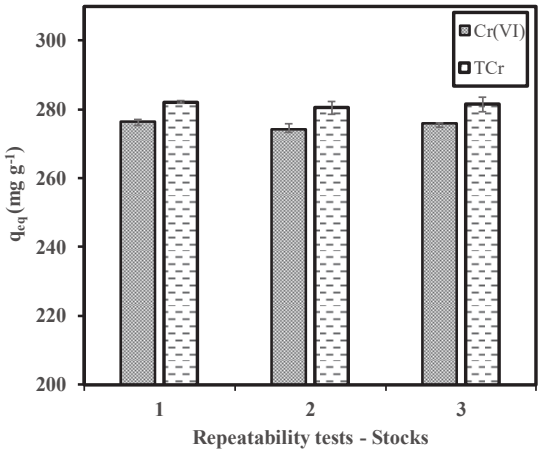

Figure 2-3 Sorption of Cr (VI) and TCr using AP-3% membranes – Comparison of performance for different stocks (mass of membrane = 30 g; volume of solution = 50 mL; pH: 2; Contact time = 48 h).

2.4. Results and discussion

2.4.1. Cr(VI) sorption from aqueous solution

2.4.1.1 Characterization

(1) Percolation characteristics

The basic properties of the membranes are shown in Table 2-1. The porosity of the AP-3% membrane reaches up to 93.4% (± 0.73)%; this is relatively high compared to chitosan/poly(vinyl alcohol) foams, as reported by Wang et al. [55]. This is a favorable property for practical application in continuous sorption in simple percolation mode. The stability of membranes reaches 94.0% (±0.10)%; this means that the material has a high physical stability and maintains its integrity under a high-speed shaking in water. Taking into account that the preferred mode of application consists of immobilizing the membranes in a column set-up, it can be extrapolated that the static immobilization of the membranes in the column fully preserves the material. The water flux of membranes reaches up to 34 mL cm^{-2} min^{-1} at 0.006 bar; this clearly demonstrates the natural highly-percolating property of the sorbents compared to cellulose acetate/PEI microfiltration membranes with water flux of 10-50 mL cm^{-2} min^{-1} at 0.69 bar, as reported by Chen et al. [56]. The free draining flow velocity was found close to 0.62 m h^{-1}.

Table 2-1 Basic properties of the AP-3% membranes.

Property	Porosity (%)	Stability (%)	water flux (mL $cm^{-2}min^{-1}$)
Value	93.41±0.73	94.02±0.10	33.61±0.44

(2) SEM and SEM-EDX analysis

The cross-section morphologies and the distribution of the main elements in the membrane before and after Cr(VI) sorption are characterized by SEM-EDX (Figure 2-4). The SEM images show the porous structure of the material; this is a very opened structure that explains the high porosity and permeability of the sorbent discs. The analysis of specific surface area from N_2 sorption (not shown) confirmed that the material has poor micro- and meso-porosity. Changing the drying process (using either freeze-drying or drying under supercritical CO_2 conditions) did not significantly increase the specific surface of the material: the order of magnitude remains around 1-5 m^2 g^{-1}. The material has a very large macro-porosity that makes the membrane very efficient for natural percolation (without applied pressure) but the specific surface area and porosity (under mesopore size) negligible.

The EDX spectrum presented on Figure 2-4 for raw sorbent (before metal sorption) shows the presence of C and O elements (tracers of organic composition of the sorbent) but also K, Na and Cl elements (associated to the processes of alginate extraction and of shaping/synthesis). The EDX spectrum for the membrane after metal sorption confirms the presence of Cr ions on the sorbent. The obvious increase in percentage of O after Cr(VI) sorption might be attributed to the sorption of negatively charged chromate ions (e.g., $HCrO_4^-$). Cr elements were distributed densely and homogeneously in the whole mass of the sorbent. This also means that the reactive groups are homogeneously distributed in the material (Figure 2-4).

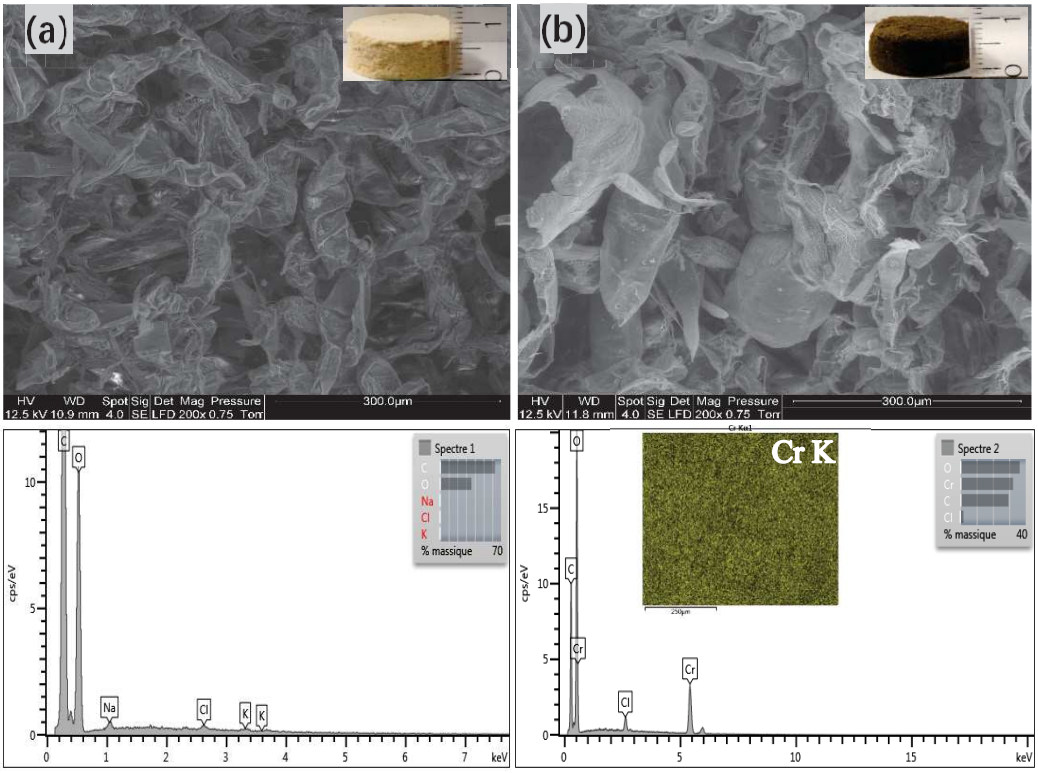

Figure 2-4 SEM image and EDX mapping of membranes (a) before Cr sorption and (b) after Cr sorption (Cr K corresponds to Cr cartography).

(3) FTIR spectroscopy analysis and pH_{PZC}

FTIR is an important technique to analyze the main bands corresponding to the functional groups of the membranes. The raw membranes, the membranes after contacting with 200 mg L^{-1} Cr(VI) at pH 2.0 and the membranes after desorption by 0.01 M NaOH were analyzed by FTIR-ATR spectroscopy (in the range of 4000-400 cm^{-1}). The FTIR spectra and the assignments of the main bands are reported in Figure 2-5 and in Table 2-2, respectively. For raw membrane (Figure 2-5a), the main peaks are identified at 3243 cm^{-1} (N–H and O–H stretching vibrations, including their overlapping) [57], 2928 cm^{-1} (C–H stretching) [58, 59], 1592 cm^{-1} (N–H bending and C=N vibration) [60-62], 1402 cm^{-1} (COO^- symmetric stretching) [63-65], 1315 cm^{-1} (C–N stretching vibration) [66-68], 1087 cm^{-1} and 1028 cm^{-1} (C–O stretching vibration) [69, 70], and 947 cm^{-1} (C–H deformation) [71].

After sorption reaction, the main changes are associated to the broad peaks between 3000 and 3500 cm^{-1} due to the stretching vibration of amine and hydroxyl (or their overlaps). The peaks at 2928 cm^{-1} and 947 cm^{-1} disappeared; assigned to C–H stretching and C–H deformation respectively, this means that their neighbor reactive groups are involved in metal binding or that the sorption of Cr(VI) , associated with a mechanism of reduction of Cr(VI) into Cr(III)

induces the oxidation of some reactive groups [58, 59, 71]. The shift of the peak from 1592 cm^{-1} to 1579 cm^{-1} may be assigned to N–H bending (assigned to the primary amine groups of PEI) [72] and C=N vibration (due to the formation of Schiff bases generated by the reaction between PEI and GA) [62]. The intensity of the peak at 1402 cm^{-1} decreases (this band is assigned to COO^- symmetric stretching of the carboxylate groups in alginate [73]. The peak at 1315 cm^{-1} assigned to C-N stretching [66-68, 74] and resulting from the interaction between amine groups of PEI and aldehyde groups of GA is shifted (with a decrease in its intensity). The intensities of the peaks at 1087 cm^{-1} and 1028 cm^{-1} (assigned to C-O skeletal stretching vibrations [75, 76]) also decrease. Therefore, the sorption of Cr(VI) involves interactions of the metal ions with hydroxyl and carboxylic groups on alginate and amine groups from PEI-GA. However, carboxyl and hydroxyl groups should not be involved in metal binding with chromate species (anions). This could be an indication that Cr(VI) was partially reduced to Cr(III) (probably by amine groups) and then sorbed through coordination with these groups. Indeed, Mohanty et al. [77] also reported that the sorption of Cr(VI) onto *Eichhornia crassipes* took place on hydroxyl groups (characterized by FTIR analysis). Nakano et al. [78] proposed that Cr(VI) was firstly reduced to Cr(III) at low pH and then bound onto tannin gels through the ion exchange of Cr(III) with hydroxyl and/or carboxyl groups. Beside, a mechanism of electrostatic attraction between PEI on the membrane and chromate anions may be involved in Cr(VI) sorption, which was also reported by Yan et al. [79]. Additionally, new peaks appeared at 895 cm^{-1}, 770 cm^{-1} and 467 cm^{-1} corresponding to the stretching vibrations of Cr=O, Cr–O and Cr–N, respectively; this further indicated that Cr(VI) was successfully adsorbed on the membrane surface and the amine groups on PEI-GA play a major role in Cr(VI) binding [80-83]. The changes on the bands of reactive groups may also be explained by the protonation of reactive groups: carboxylate groups are fully protonated (carboxylic acid). However, the comparison of the FTIR spectra for membranes conditioned under neutral and acidic solutions did not show substantial differences in the regions associated to carboxylate/carboxylic groups (not show).

After desorption, the FTIR spectrum goes back to the spectrum of raw membrane. Slight changes may be observed in the positions and intensities, but it did not change much compared to the raw membranes, except for the disappearance of the peak at 1315 cm^{-1} (C–N stretching vibration) and to the presence of a peak in the range 450-550 cm^{-1} (Cr–N stretching vibration). This is probably due to incomplete desorption of Cr. Based on the above analysis, the following possible mechanism of Cr(VI) sorption is proposed: (1) the sorption of Cr(VI) anions by amine groups from PEI-GA; (2) reduction of Cr(VI) to Cr(III) and (3) Cr(III) binding by coordination with hydroxyl and carboxylic groups.

In addition, the pH_{PZC} of the sorbent is close to 5.73. The pK_a values of carboxylic groups in alginate are usually reported at 3.38 and 3.65 for mannuronic acid and guluronic acid, respectively [84]. On the other hand, PEI bears alkaline amine groups with different strengths (associated to primary, secondary and tertiary amine groups in branched polymer): pK_a values are close to 7-8 and 10 [85]. This means that in the pH range selected for this study (i.e., 0.5-4) the overall charge of the sorbent is positive. The cationic behavior of the membrane opens the way for electrostatic attraction (ion-exchange mechanism) of anionic species (such as chromate anions) onto protonated groups.

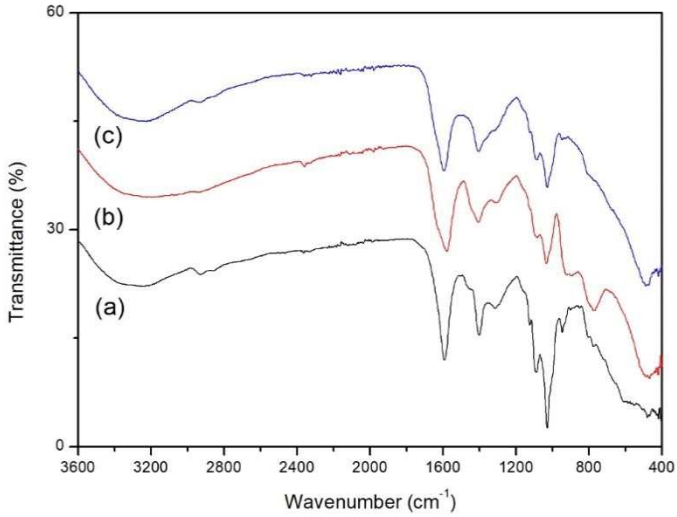

Figure 2-5 FTIR spectra of membranes: (a) raw membrane; (b) membrane after Cr(VI) sorption; (c) membrane after desorption.

Table 2-2 Assignments of main FTIR bands of AP-3% membranes: (A) raw membrane; (B) membrane after Cr(VI) sorption; (C) membrane after metal desorption.

A (cm^{-1})	B (cm^{-1})	C (cm^{-1})	Band Assignment	Reference
3243	3198	3225	N–H and O–H or their overlaps stretching	[57]
2928	——	2935	C–H stretching	[58, 59]
1592	1579	1596	N–H bending and C=N vibration	[60-62]
1402	1405	1405	COO^- symmetric stretching	[63-65]
1315	1311	——	C–N stretching vibration	[66-68]
1087	1083	1086	C–O stretching vibration	[69, 70]
1028	1033	1028	C–O stretching vibration	[69, 76]
947	——	948	C–H deformation	[71]
——	895	——	Cr=O stretching vibration	[80-83]
——	770	——	Cr–O stretching vibration	[80-82]
——	467	488	Cr–N stretching vibration	[82]

2.4.1.2 Effect of pH

The pH is a critical operating parameter for sorption processes because of cross-effects on metal speciation and protonation/deprotonation of reactive groups (i.e., carboxylic groups, amine groups). In the case of Cr(VI), complementary mechanisms of reduction may also influence the interaction of the sorbent with metal ions (both in terms of sorption and desorption) [86]. Several studies reported that the removal efficiency of Cr(VI) was higher for sorbents at low pH [87, 88]. In this work, the effect of pH on the sorption of Cr(VI) and TCr by AP-3% membranes was investigated in the pH range of 0.5-4; Figure 2-6 shows a synthesis of these results. The optimum pH is reached at pH 2 under selected experimental conditions.

It is noteworthy that for most of pH values the curves for Cr(VI) and TCr overlap, except for pH 0.5. It is well known that the presence of organic matter at low pH causes the reduction of Cr(VI) into Cr(III). Chromate ion has a high positive redox potential and easily reduced in the presence of electron donors [89]. Several studies have shown that algal biomass sorbents can be used for the conversion of Cr(VI) into Cr(III) in acidic solution [90, 91]. At this low pH value, the reduction of Cr(VI) plays an important role and the cationic charge of Cr(III) is not favorable for binding on protonated reactive groups of the sorbent (both carboxylic and amine groups are protonated). The sorption capacity for total chromium strongly decreases compared to Cr(VI) removal: the mass balance on TCr gives at pH 0.5 a sorption capacity close to 36 mg TCr g^{-1}. On the other hand, the mass balance equation (i.e. TCr = Cr(III) + Cr(VI)) assessed on Cr(VI) in the solutions shows a removal that combines metal binding but also conversion of Cr(VI) into Cr(III) and the deduced sorption capacity is artificially increased up to 140 mg Cr(VI) g^{-1}). The sorption capacity of Cr(III) using AP-3% membrane was specifically quantified at pH 2: Cr(III) is weakly bound (less than 1.2 mg Cr(III) g^{-1}). This confirms that the difference between the Cr(VI) and TCr at pH 0.5 is essentially due to the proper reduction of the metal.

The pH_{PZC} of the membrane is close to 5.73; this means that the reactive groups are strongly protonated at pH 4 (and below). These protonated groups can only bind anionic species [92]. At very low pH the strong protonation and the high concentration of counter anions (dissociation of the acid used for pH control) strongly compete with chromate anions for binding on carboxylic acids and more specifically on protonated amine groups. As the pH increases the surface remains positively charged but the competition effect of counter anions progressively decreases. However, above pH 2 the sorption capacity tends to decrease. This is directly attributed to the decrease in the protonation of amine groups, which, in turn, decreases

the electrostatic attraction of chromate anions. Indeed, Guo et al. [93] reported that when the solution pH > 2 (C_0: 100 mg L^{-1}), the degree of protonation of -NH_2 decreased, resulting in a decrease in the sorption capacity of chromium(VI) onto PEI-functionalized cellulose aerogel beads. On the other hand, as the pH increases the global cationic charge decreases and at pH 4 the carboxylic groups are partially converted into carboxylate: their anionic charges may contribute to the particle repulsion of anionic species (or, at least, to moderate the attraction of these anionic metal species by protonated amine groups). As a matter of fact, pH 2 is good compromise between attractive effects on chromate anions and repulsive effects of counter anions of the acid media.

This means that another criterion is involved in the control of sorption. The speciation of chromate is a critical parameter for explaining the affinity of the sorbent for the metal. Figure 2-7 shows the speciation of chromate (C_0: 200 mg Cr L^{-1}) as a function of pH (Calculated with the Visual Minteq software [94]). In the selected pH range (i.e., 0.5-4) the predominant species are $HCrO_4^-$ (between 75 % and 87 %) and $Cr_2O_7^{2-}$ (about 12 %). At pH below 1, a neutral species H_2CrO_4 also appears (representing about 13%). Apart of the competitor effect of counter anions (from acid), the formation of neutral species contributes the decrease in sorption properties. Similar research result has also been found in Cr(VI) removal by magnetic cellulose nanocomposite [95].Therefore, the pH 2 is the optimum pH value; further experiments were performed at this pH.

In addition, the values of initial pH (pH_i) and final pH (pH_f) after Cr(VI) sorption were recorded: the pH variation is non-negligible (Figure 2-6). The pH_f hardly changes at pH_i below 2, while the pH_f increases significantly as the pH_i increased from 2.5 to 4.0: the largest variation was observed at pH_i 3.5 (increased 2.5 pH units). Finally, the pH_f was stable and close to 6.0 in the range of pH 3.5-4, which revealed the pH buffering effect of the membrane.

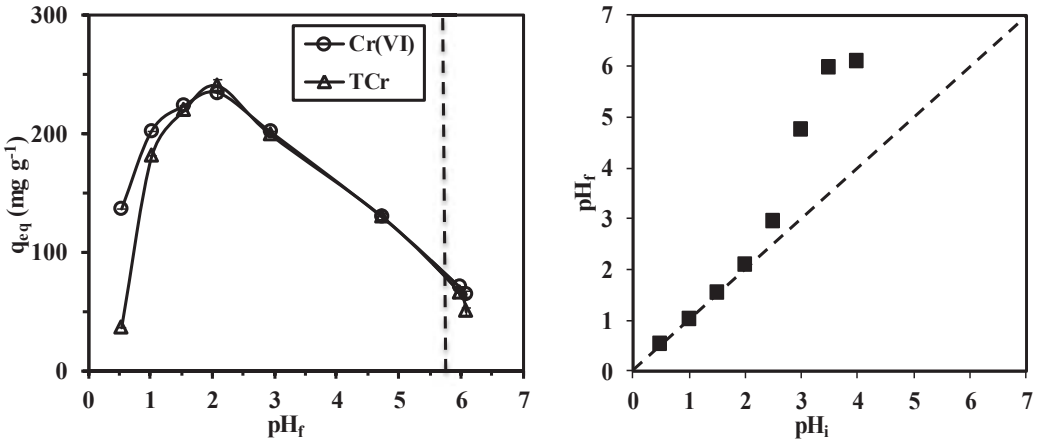

Figure 2-6 Effect of pH on the sorption of Cr(VI) and TCr onto AP-3% membrane (C_0 = 200 mg L^{-1}; V = 50 mL; sorbent mass = 30 mg; contact time = 48 h; flow rate = 15 mL min^{-1} ; temperature = 20 ± 1 °C).

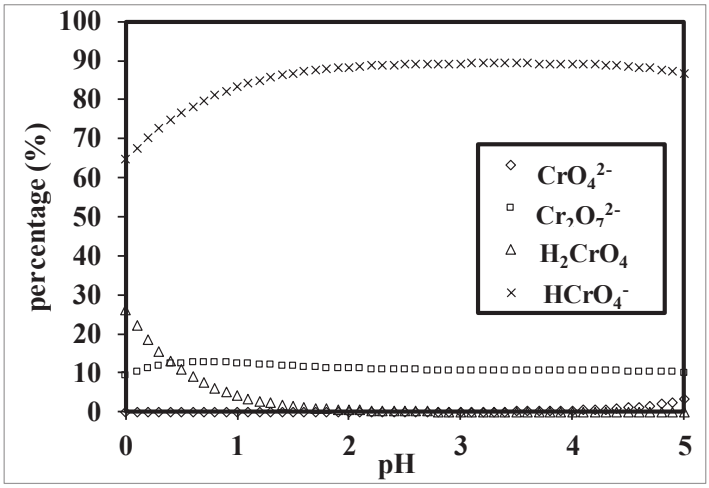

Figure 2-7 The Cr(VI) species distribution under different solution pH (pH ranges from 0 to 5 with the step length of 0.1) when Cr(VI) concentration is 200 mg L^{-1}, simulated by Visual MINTEQ ver. 3.1 [96].

2.4.1.3 Uptake kinetics

Uptake kinetics allows fixing the equilibrium time but also to evaluating the steps that are controlling the transfer of the solute from the solution to the sorbent surface [51]. Indeed, the sorption of metal ions can be controlled by different diffusion mechanisms (including bulk, film and intraparticle diffusions) and by the proper reaction rate (including parallel or complementary mechanisms of oxidation/reduction, precipitation). Figure 2-8 shows the effect flow rate (15 or 30 mL min^{-1}) on the uptake of Cr(VI) and TCr on the membrane at pH 2. Varying the flow rate (and then the superficial flow velocity) could affect the kinetic profiles.

Indeed, the irregular distribution of the channels into the membrane could induce preferential channels and irregular distributions of flow transfer in the material. Forcing the flow rate at higher value may contribute to decrease the preferential channeling. The figure clearly shows that the flow rate does not significantly affect the concentration decay in the solution (at least in the range: 15-30 mL min^{-1}). The kinetic profiles show 3 steps in the process: (a) a fast initial stage (within the first hour of contact) represents 41 to 48 % of total sorption, (b) a second slower phase (ranging between 1 and 6 h) corresponding to 58-66 % of total sorption, and (c) a very slow sorption phase that lasts till 78 h. This long sequence means that the resistance to intraparticle diffusion is contributing to the overall control of the uptake kinetics.

In addition, the uptake kinetics of Cr(VI) and TCr have been modeled using the pseudo-first-order rate equation (PFORE, see Eq. 2-5) and the pseudo-second-order rate equation (PSORE, see Eq. 2-6) which are commonly used to describe chemical reaction rates in homogeneous or heterogeneous systems [51].

The parameters of the models are summarized in Table 2-3. According to the high determination coefficient R^2, the PSORE fits more appropriately the kinetic curves for Cr(VI) and TCr recovery by AP-3% membranes. In addition, the comparison of calculated and experimental values for the equilibrium sorption capacity systematically confirmed that the PFORE describes more realistically the experimental profile. The lines in Figure 2-8 shows the simulation of uptake kinetics with the PSORE and the parameters reported in Table 2-3. The model described correctly the initial and final stages of the curves; however, there are some discrepancies in the intermediary stage (corresponding to the highest curvatures in the experimental profiles).

Table 2-3 Modeling of uptake kinetics of Cr(VI) and TCr onto AP-3% membranes at two different flow rates (15 or 30 mL min^{-1}).

Model	Parameter	F=15 mL min^{-1}		F=30 mL min^{-1}	
		Cr(VI)	TCr	Cr(VI)	TCr
	$q_{eq,exp}$ (mg g^{-1})	300.9	293.6	304.1	293.5
	$q_{eq,cal}$ (mg g^{-1})	291.8	287.8	266.8	265.6
PFORE	$k_1 \times 10^3$ (min^{-1})	1.6	1.6	1.5	1.7
	R^2	0.732	0.705	0.696	0.743
PSORE	$q_{eq,cal}$ (mg g^{-1})	303.0	294.1	303.0	294.1
	$k_2 \times 10^5$ (g mg^{-1} min^{-1})	2.4	2.4	2.8	3.1
	R^2	0.993	0.993	0.994	0.995

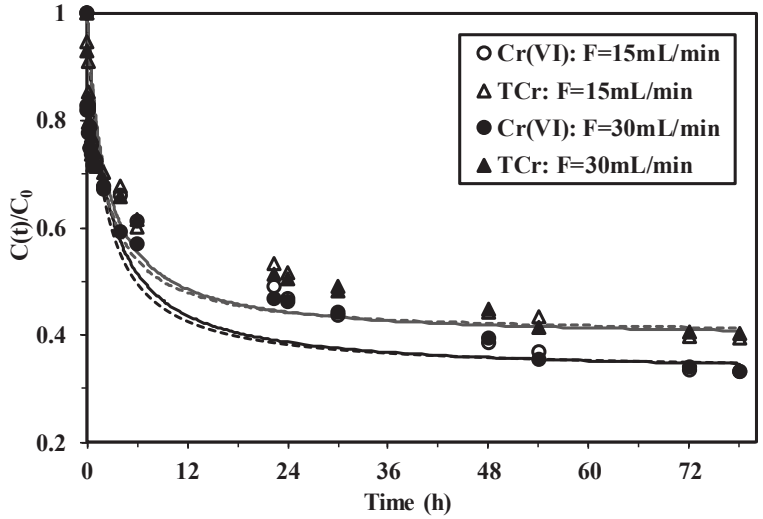

Figure 2-8 Cr(VI) and TCr uptake kinetics using AP-3% membranes – effect of flow rate (C_0 = 200 mg L^{-1}; V = 1 L; sorbent mass = 217 mg; pH: 2; temperature = 20 ± 1 °C – Lines represent the modeling of kinetic profiles with the pseudo-second order rate equation using parameters from Table 2-3).

2.4.1.4 Sorption isotherms

Sorption isotherms represent the equilibrium distribution of the solute between the liquid and solid phases at a fixed temperature (and pH). Playing with increasing concentration allows

determining the maximum sorption capacity of the sorbent but also its affinity for target metal. The initial slope of the curve gives important information on this affinity and on the trend of the sorbent for reaching its saturation. The sorption isotherms are modeled by mechanistic (Langmuir equation, Eq. 2-7) or empirical (Freundlich, Eq. 2-8) equations. In most cases, the saturation plateau (finite sorption capacity) observed on sorption isotherms makes the Langmuir equation more appropriate for describing equilibrium distributions [97]. However, in some cases involving several modes of interaction, different reactive groups, and other phenomena (such as local precipitation or condensation) the Langmuir model requires extensions (using muti-site sorption, or combination of Langmuir and Freundlich equations, such as the Sips equation (Eq. 2-9)). The Sips isotherm (also called the Langmuir-Freundlich isotherm) is a hybrid form of Langmuir and Freundlich equations. The Sips equation follows a trend similar to the Freundlich equation except that it reaches a finite saturation limit when the concentration is sufficiently high [98]. Nonlinear regression analysis was used for fitting model equations. Experimental sorption isotherms (Figure 2-9) were obtained, at pH 2, by variation of the initial chromate sorption between 20 and 300 mg Cr L^{-1}. The parameters of the models (together with their correlation coefficients) are reported in Table 2-4.

The sorption isotherm for Cr(VI) is characterized by a steep initial slope followed by the saturation plateau, which is reached for a residual concentration close to 40-50 mg Cr L^{-1}. This means that AP-3% membrane has a good affinity for chromate anions. Based on Table 2-4, it appears that Cr(VI) sorption isotherm follows both the Freundlich and the Sips equations, while the TCr sorption isotherm is better fitted by both the Langmuir and the Sips equations. Model fitting of the experimental data does not mean that the assumptions of the model are effectively verified but this may help for explaining the metal binding mechanism. The mathematical model designed by Freundlich accounts for describing multilayer adsorption of Cr(VI) molecules, while Langmuir might be attributed to relatively homogeneous binding sites on the surface of the sorbents [99].

Furthermore, the maximum sorption capacities of Cr(VI) and TCr reach 313.7 and 330.7 mg g^{-1}, respectively (Table 2-4). These data showed relatively higher Cr(VI) sorption capacities, compared to most of reported sorbents (Table 2-5). Taking commercial resin as examples, Cr(VI) sorption capacities reached 89.3 and 126.6 mg g^{-1} for Purolite CT-275 and Purolite MN-500 ion-exchange resins, respectively [100]. Xiao et al. [101] also reported a sorption capacity value in a range of 105–120 mg Cr g^{-1} for a series of polystyrene resins (D201, D202, and D301) at initial Cr(VI) concentration of 500 mg L^{-1} and pH 2.

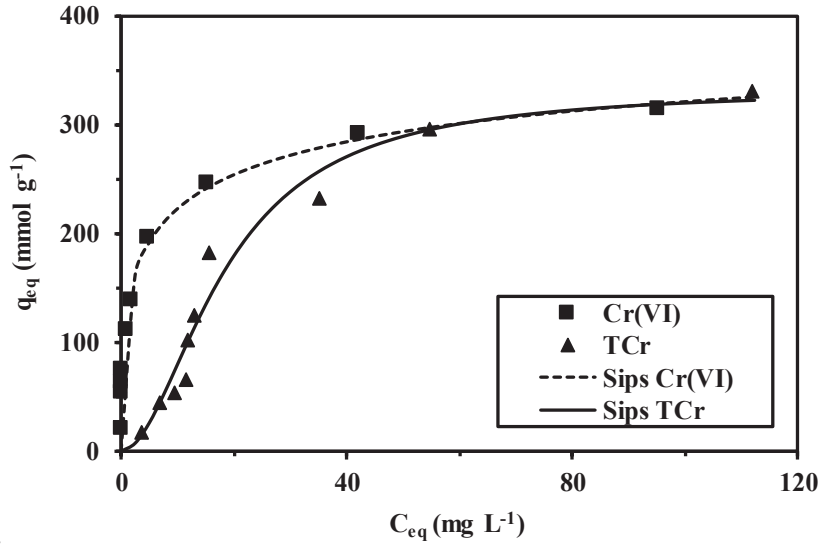

Figure 2-9 Cr(VI) and TCr sorption isotherms on AP-3% membranes at pH 2 (V = 50 mL; sorbent mass = 30 mg; pH: 2; contact time = 78 h; flow rate = 15 mL min^{-1}; temperature = 20 ± 1 °C – Lines represent the modeling of sorption isotherms with the Sips equation and the parameters summarized in Table 3).

Table 2-4 Sorption isotherms – Modeling parameters for Langmuir, Freundlich and Sips equations.

Model	Parameter	Cr(VI)	TCr
	$q_{m,exp}$ (mg g^{-1})	313.7	330.7
Langmuir	$q_{m,cal}$ (mg g^{-1})	297.9	480.7
	b_L (L mg^{-1})	0.539	0.024
	R^2	0.884	0. 923
Freundlich	k_F (mg g^{-1})/(L mg^{-1}) $^{1/n}$	130.4	27.02
	n	4.885	1.803
	R^2	0.968	0.851
Sips	$q_{m,cal}$ (mg g^{-1})	455.3	332.4
	ns	2.521	0.529
	b_S (L mg^{-1})	0.383	0.004
	R^2	0.987	0.954

Table 2-5 Comparison of sorption performances with other sorbents.

Sorbent	pH	$q_{m,Cr(VI)}$ (mg g^{-1})	$q_{m,TCr}$ (mg g^{-1})	Ref.
Alginate–goethite beads	2	27.1	35.9	[102]
Grape stalks entrapped into alginate beads	3	3.6	10	[103]
PEI immobilized acrylate-based magnetic beads	2	138	N.M.	[104]
Biomass of alga *Spirogyra*	2	14.7	N.M.	[105]
PEI-modified biomass	4.6	279	N.M.	[89]
Alginate beads	3	34.5	N.M.	[95]
Bacterial consortia immobilized alginate beads	3	66.7	N.M.	[95]
Sodium alginate-polyaniline nanofibers	2	73.3	N.M.	[106]
Magnetic nano-hydroxyapatite encapsulated alginate beads	2	29.1	N.M.	[107]
Ethylenediamine-modified cross-linked magnetic chitosan resin	2	51.8	N.M	[108]
Purolite CT-275 and Purolite MN-500 ion-exchange resins	3	89.3; 126.6	N.M	[100]
Polystyrene resins (D201, D202, and D301)	2	105-120	N.M	[101]
AP-3% membranes	2	314	331	This study

2.4.1.5 Effect of coexisting ions

Industrial effluents often contain various other anions and cations coexisting with Cr(VI); these ions may compete with reactive groups at the surface of the sorbent, or change metal speciation. This competition may significantly decrease the sorption performance. In order to evaluate the stability of sorption performance in complex solutions, the sorption efficiency of AP-3% membranes for Cr(VI) (and TCr) was compared in the presence of increasing concentrations of anions (e.g., Cl^-, NO_3^- and SO_4^{2-}) and cations (e.g., Cu(II) and Ca(II)) at pH 2. In this case, the surface groups of absorbents are strongly protonated and beneficial to bind anionic species, and the main chromate species are $HCrO_4^-$ (about 87 %) and $Cr_2O_7^{2-}$ (about 12 %) at pH 2. Figure 2-10 shows that monovalent anions, such as chloride and nitrate anions, even in excess, have a rather limited effect on chromate sorption: even at concentration as high as 800 mg L^{-1} the decrease in sorption efficiency does not exceed 2 %. Hu et al. [109] also reported that the competitive effect of chloride and nitrate anions on Cr(VI) sorption by magnetic nanoparticles can be ignored and suggested the two anions are poor ligands which showed a weaker binding affinity for Cr(VI) species (and a low sorption on protonated amine groups). On the opposite

hand, sulfate anions have a strong impact on sorption performance: the decrease in sorption efficiency may reach up to 30 % for Cr(VI) and 44 % for TCr. Sulfate anions being divalent have a stronger affinity (compared to mono-anionic $HCrO_4^-$ species) for protonated amine groups; this may explain the stronger effect of sulfate anions on metal binding. Even with large concentration excess metal cations such as Ca(II) and Cu(II) hardly affect chromate sorption: the loss in sorption efficiency remains below 8 %. This can be easily explained by the protonation of reactive groups (carboxylic groups vs. carboxylate; and protonated primary and secondary amine groups). These protonated groups have poor affinity for metal cations. The carboxylate and free amine groups would predominate at higher pH values (above 4); these conditions would be more favorable for the sorption of metal cations, which, in turn, would have a greater effect on the sorption properties of the membranes. The AP-3% membranes have a remarkable selectivity for anionic metal ions in acidic solutions; on the contrary, the presence of competitor anions (counter anions, or anionic metal complexes) may be taken into account (especially when divalent).

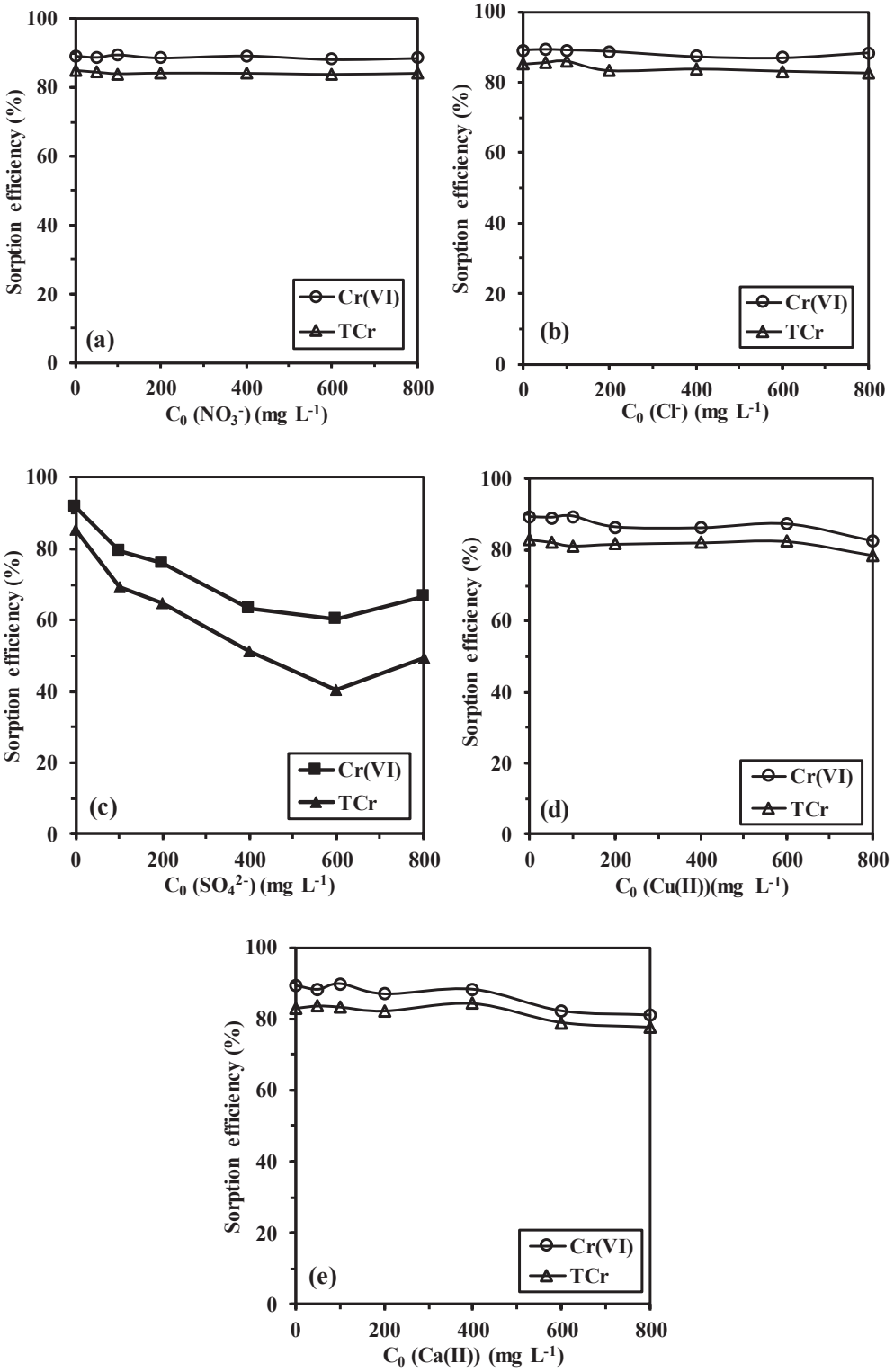

Figure 2-10 Effect of coexisting ions on the removal of Cr(VI) and TCr by AP-3% membranes: (a) NO_3^-, (b) Cl^-, (c) SO_4^{2-}, (d) Cu(II) and (e) Ca(II) (C_0 = 200 mg L^{-1}; V = 50 mL; sorbent mass = 30 mg; pH: 2; contact time = 72 h; flow rate = 15 mL min^{-1}; temperature = 20 ± 1 ºC).

2.4.1.6 Treatment of simulated electroplating wastewater

To test the suitability of the membranes in a complex system, alginate/PEI membrane was used to remediate a simulated electroplating wastewater. Table 2-6 presents the experimental data for the treatment of the wastewater; a single Cr-containing wastewater (containing a similar concentration of chromate) was used as control. The tests were performed using two different masses (15 mg and 30 mg) of alginate/PEI membrane. The C_{eq} of Cr(VI) in the simulated electroplating wastewater and Cr-containing wastewater were 3.07 mg L^{-1} and 2.66 mg L^{-1}, respectively, with a sorbent mass of 15 mg. While increasing the amount of sorbent to 30 mg, Cr(VI) was completely removed for the two solutions. The comparison of the results for the two wastewaters shows that the presence of other metal ions or anions in the solution hardly changes chromate binding and TCr removal. These conclusions are consistent with the results reported in the previous section. On the other hand, the analysis of total chromium (by ICP-AES) shows that chromium does not completely disappear from the solution because of the conversion of chromate into chromium (III), which is poorly sorbed on AP-3% membranes in acidic solutions. Moreover, the experimental results show that the sorbent has poor sorption capacities for other metal cations such as Cu(II), Ca(II), Na(I), K(I), and Zn(II). AP-3% membranes have a great selectivity for chromate under selected experimental conditions. Therefore, the sorbent clearly demonstrate a great potential for removing Cr(VI) from industrial wastewater, as a polishing treatment.

Table 2-6 Comparison of experimental data on the treatment of simulated electroplating wastewater and single Cr-containing wastewater (control group) at two different mass (15 mg and 30 mg) of membranes (V= 50 mL; pH: 2; contact time = 72 h; flow rate = 15 mL min^{-1}; temperature = 20 ± 1 °C).

Waste-water	Simulated electroplating wastewaters			Single Cr-containing solution		
		mass:15 mg	mass:30 mg		mass:15 mg	mass:30 mg
	C_0 (mg L^{-1})	C_{eq} (mg L^{-1})	C_{eq} (mg L^{-1})	C_0 (mg L^{-1})	C_{eq} (mg L^{-1})	C_{eq} (mg L^{-1})
Cr (VI)	53.4	3.07±0.16	0.00	53.8	2.66±0.10	0.00
TCr	55.6	8.93±0.13	7.33±0.44	55.9	7.01±0.23	6.14
Cu(II)	6.71	6.65±0.04	6.64	——	——	——

Waste-water	Simulated electroplating wastewaters			Single Cr-containing solution		
		mass:15 mg	mass:30 mg		mass:15 mg	mass:30 mg
	C_0 (mg L^{-1})	C_{eq} (mg L^{-1})	C_{eq} (mg L^{-1})	C_0 (mg L^{-1})	C_{eq} (mg L^{-1})	C_{eq} (mg L^{-1})
Zn(II)	1.16	1.09±0.03	1.08	——	——	——
Ca(II)	26.5	26.5	26.5	——	——	——
K(I)	20.5	20.3	20.2	——	——	——
Na(I)	27.9	25.3±0.48	24.7	——	——	——

C_0: metal initial concentrations, C_{eq}: metal residual equilibrium concentration.

2.4.1.7 Metal desorption and recycling of AP-3% membranes

Many previous studies have shown that NaOH solution are highly efficient for desorbing Cr(VI) from loaded sorbents [110-112]. Figure 2-11a shows the kinetic profiles for the desorption of chromate ions from Cr-loaded AP-3% membranes using 0.01 M and 0.1 M NaOH solutions. Increasing the concentration of the eluant increases the velocity of metal release: 1 h vs. 2 h for reaching the equilibrium. However, the concentration does not affect the effective desorption efficiency at equilibrium, which does not exceed 45 %. It is noteworthy that during desorption experiments the released concentrations of Cr(VI) and TCr are equal (contrary to the observations made during sorption steps); this is obviously due to the different effects of chromate reduction during sorption (additional reduction on the sorbent) and desorption (no reduction).

The poor desorption of Cr(VI) is probably due to the partial reduction of Cr(VI) to Cr(III) during metal sorption on AP-3% sorption. This is consistent with FTIR analysis that showed an alteration of the biomass (remaining chromium but also partial degradation due to the oxidation of some reactive groups). Similar conclusions were reported in the case of chromate desorption from Cr-loaded mustard oil cake and polypyrrole/Fe_3O_4 magnetic nanocomposite [71]. As described above, the presence of organic matter at low pH causes the reduction of Cr(VI) into Cr(III), which may result in a decrease in desorption efficiency. Therefore, to test whether this was caused by the low pH (i.e., pH 2) during the sorption process, desorption of Cr-loaded membranes using 0.01 M NaOH after Cr(VI) sorption at pH 3 and 3.5 was also investigated. Relevant results are summarized in Table 2-7; they show that Cr(VI) desorption efficiency

hardly changed when the pH used for sorption step was increased. This means that increasing the pH is supposed to reduce the yield of reduction on organic material, but does not affect the desorption efficiency in the present case.

Figure 2-11b shows the comparison of sorption capacities for Cr(VI) and TCr under similar experimental conditions (sorption at pH 2 and desorption using 0.01 M NaOH solutions). The sorption capacity progressively decreases by 19 % at the second cycle (sorption capacity remains as high as 219 mg Cr g^{-1}). However, at the third cycle, AP-3% membrane loses about 60 % of its sorption capacity: residual capacity does not exceed 107 mg Cr g^{-1}. This value remains relatively high compared to the sorption capacities of other biosorbents. However, these data definitively show the difficulty to use this material for numerous cycles of sorption and desorption. The weak desorption of chromate hinders the re-use of the sorbent for more than 3 cycles.

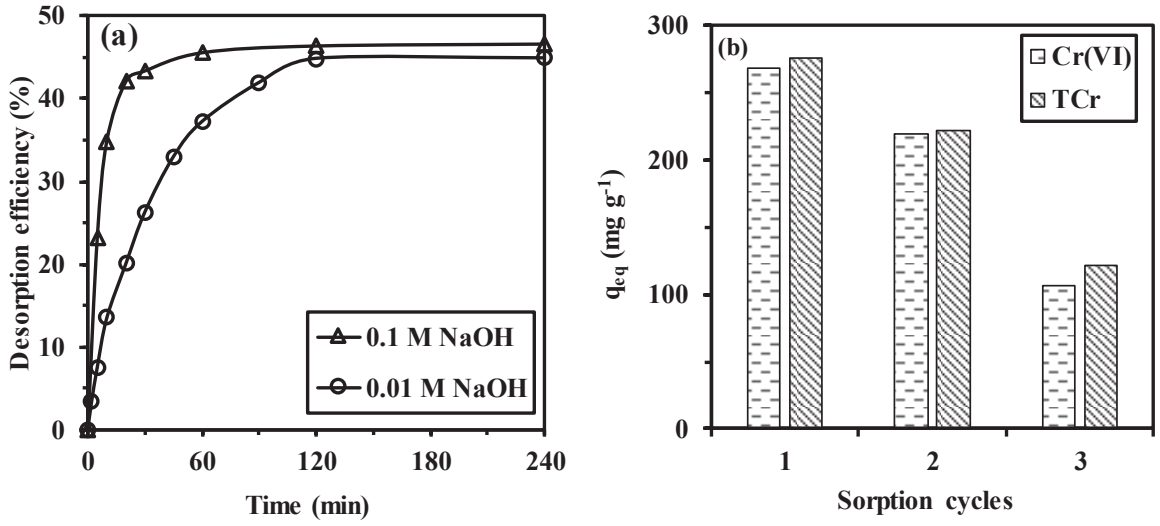

Figure 2-11 Metal desorption from loaded AP-3% membranes and sorbent reycling: (a) desorption kinetics using solution of NaOH at 0.01 M (pH=11.9) and 0.1 M (pH=12.5) concentrations (Metal loading on the sorbent before desorption showed in Figure 6. Desorption step - V: 1 L; time: 4 h; flow rate: 15 mL min^{-1}; temperature: 20 ± 1 °C) and (b) comparison of sorption–desorption performances for 3 successive cycles (Sorption step - C_0: 200 mg L^{-1}; V: 50 mL; sorbent mass: 30 mg; pH: 2; contact time: 48 h; flow rate: 15 mL min^{-1}; temperature: 20 ± 1 °C. Desorption step - desorption agent: 0.01 M NaOH; V: 50 mL; time: 4 h; flow rate: 15 mL min^{-1}; temperature: 20 ± 1 °C).

Table 2-7 Sorption and desorption of metal ions at different pH values.

NO.	pH	Cr(VI)		TCr	
		Sorption ($mg\ g^{-1}$)	Desorption (%)	Sorption ($mg\ g^{-1}$)	Desorption (%)
1	3	110.7±1.47	38.14±0.92	107.5±1.02	38.97±0.63
2	3.5	65.81±0.11	42.16±2.28	55.82±1.34	45.36±0.09

2.4.2. Se(VI) sorption from aqueous solution

2.4.2.1 Characterization

Several measuring methods are carried out to understand the physical and chemical properties of AP-4% membrane. For the mechanical stability of materials, results show that it reaches up to 86% under vigorous vibration conditions (i.e., 150 rpm). This means that the material has a high mechanical stability and can maintain its integrity under a high-speed shaking in water. Considering that the preferred mode of application is fixing the membranes in a column device, the static stability of the membrane (measured under constant feeding for 3 days) in the column device is also measured (up to 97%). This means that the material is stable in fixed-bed column with negligible mass loss.

In addition, the SEM test is used for observing the physical structures and morphologies of the material. The surface and cross-section morphologies of the membrane are shown in Figure 2-12. The material has a porous structure with considerable macro-porosity. This means that the membrane is widely opened, which keeps high-permeability for water transfer. Pycnometer measurements show that the density and porosity of the membrane are 0.048 g cm^3 and 74%, respectively. The water flux of the membrane is 13 mL cm^{-2} min^{-1} at 0.006 bar, which means the superficial flow velocities as high as 7.8 m h^{-1} can be reached under pumping. This clearly demonstrates highly percolating property of the membranes compared to most of reported similar membranes (Table 2-8). Despite lower pressure applied to the membrane (corresponding to natural drainage conditions), the water flux of AP-4% membrane is over-performing compared with reference membranes.

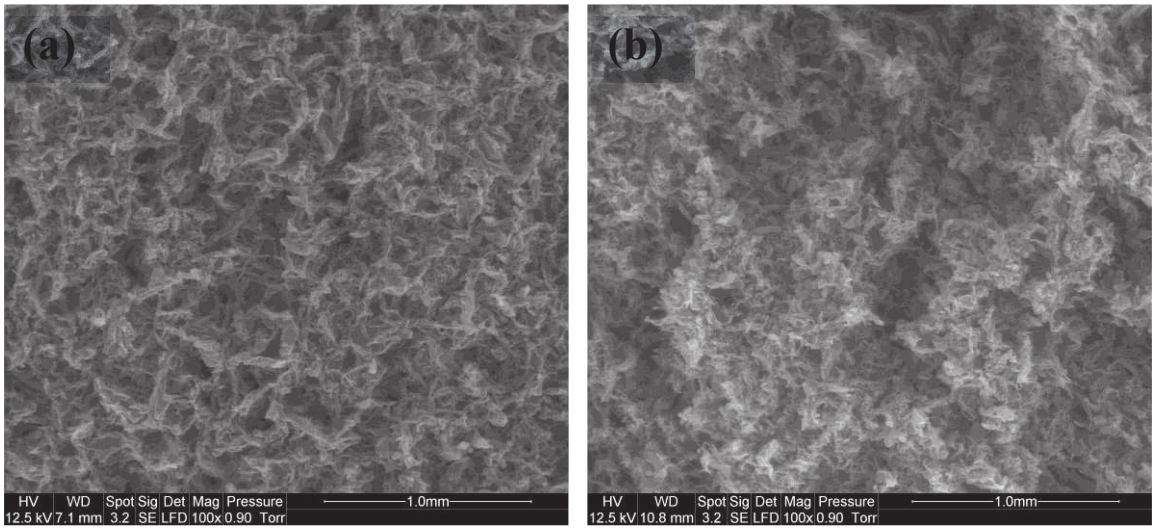

Figure 2-12 Porous structure of membranes (SEM micrographs) (a) Surface and (b) Cross-section (bar: 1 mm).

Table 2-8 Water flux comparison of the different membranes.

Membranes	Pressure (bar)	Water flux (mL cm^{-2} min^{-1})	Reference
PEI-grafted porous membrane	1.2	10.3	[113]
PEI/graphene oxide membrane	5	0.007	[114]
PEI/polyacrylonitrile membrane.	10	0.03	[115]
Polydopamine/PEI-decorated membranes	1	3.3-11.8	[115]
PEI immobilized composite porous membranes	1	0-0.3	[116]
Polydopamine functionalized halloysite nanotube/polyetherimide membranes	3	0.2-0.5	[117]
AP-4% membrane	0.006	13	This study

EDX measurement was recorded for qualitative analysis of the elemental constitution of the membrane (Figure 2-13). The spectrum of raw membrane (Figure 2-13c) shows that the material mainly consists of C and O elements (exceed 95% in total, organic tracers) but also Ca, Na, Cl, K, S, Mg and Al elements (residues of the extraction/shaping process of alginate). Figure 2-13d shows selenium peaks which were absent in the raw membrane, confirming selenium was loaded onto membrane.

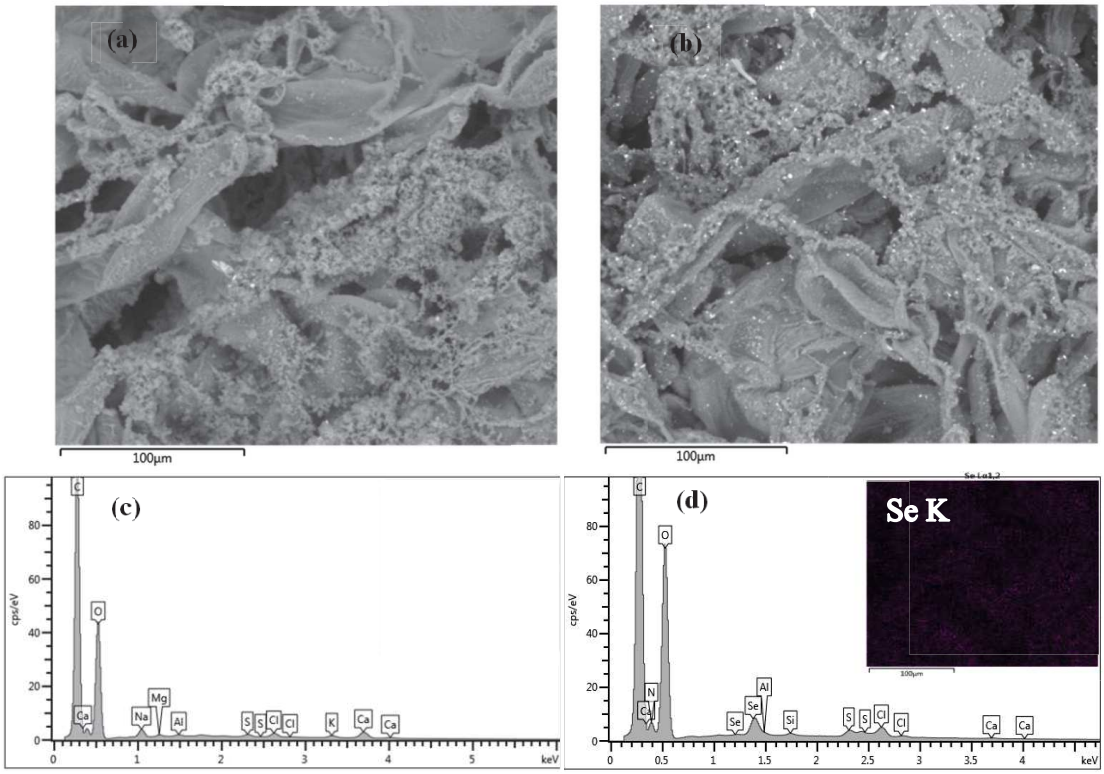

Figure 2-13 SEM micrographs (a/b) (bar: 0.1 mm) and EDX analysis (c/d): for AP-4% membrane (a/c) and Se(VI)-loaded membrane (b/d) (the insert in d: corresponds to Se cartography).

The FT-IR analysis allows identifying the chemical groups present on membrane (Figure 2-14). For the raw membrane, the main band assignments were as follows: the strong and wide band at 3200-3500 cm^{-1} is assigned to the overlapping of O–H and N–H stretching vibration [118], with the weak band around 2927 cm^{-1} is attributed to the stretching vibration of C–H [119]. Strong absorption at 1596 cm^{-1} and medium absorption at 1317 cm^{-1} bands are characteristic peaks of overlapping of C=N and N–H vibration and C–N stretching vibration, respectively. This is attributed to the reaction between amine groups of PEI and aldehyde groups of GA [120-122]. This confirms the formation of Schiff bases during the process of PEI and GA crosslinking; amide groups appear on the membrane, which contribute substantially improving its sorption capacity, especially for anions (e.g., Se(VI)). The band at 1404 cm^{-1} is assigned to the symmetric stretching of COO^{-} group of the alginate [123]. Meanwhile, the bands at 1087 and 1029 cm^{-1} are associated with C–O stretching vibration [124, 125] and 947 and 885 cm^{-1} are C–H bending vibrations [126]. All the above implies that hydroxyl, carboxyl, amino groups in the membrane might play important roles in the binding of selenium ions.

It is noteworthy that the conjugate acid dissociation constant (pK_a) of carboxylic groups in alginate are 3.38 for mannuronic and 3.65 for guluronic acid [127], while the pK_a values of amine groups in PEI are usually reported at 4.5, 6.7 and 11.6 for primary, secondary and tertiary amines, respectively [128]. In addition, the pH_{PZC} of membrane determined in the pH range of 1.0 to 10.0 was found to be 6.3; this means the reactive groups are protonated below pH 6. The charges on the surface of membrane are positive; this opens the way to the sorption of negatively charged selenium anions by electrostatic attraction.

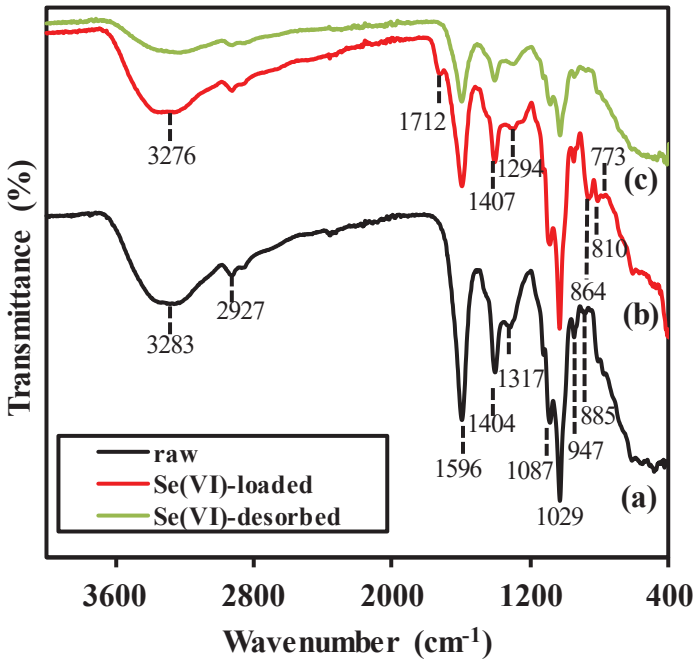

Figure 2-14 FTIR spectra of (a) AP-4% membrane, (b) Se(VI)-loaded AP-4% membrane, and (c) AP-4% regenerated membrane (after Se(VI) desorption).

2.4.2.2 Effect of pH on Se(VI) adsorption by membranes

The pH is a critical parameter in the evaluation (and understanding) of sorption properties of a sorbent for metal ions. Indeed, this parameter has a dual effect on the speciation of metal ions in solution (depending also on the presence of ligands) and on the charge characteristics of sorbent surface. Figure 2-15 shows the effect of pH variation between 1 and 7. Under selected experimental conditions, maximum Se(VI) sorption capacity reaches 61.7 mg g^{-1} at pH 2. Similar sharp optimum (between pH 2.5 and 3.5) was reported for the recovery of both Se(IV) and Se(VI) using eggshell membrane and chicken feather [129]. The pH_{PZC} of 6.3 for membrane means in acidic solution (pH below 6), the overall charge on membrane surface is positive: selenate anions are electrostatically attracted on protonated amine groups. At pH below 2, the competitor anions Cl^- (due to acid dissociation) strongly limits the sorption capacity. In addition,

selenate anions may be protonated. Peng et al. [130] reported the values of pKa_1 and pKa_2 for H_2SeO_4 correspond to strong acid and 1.9, respectively. This means below pH 2, selenate ions are protonated: it will weaken the electrostatic attraction between the reactive groups and sorbate ions. Therefore, sorption capacity decreases. Torres et al. [13] also showed that the contents of uncharged H_2SeO_4 increases at pH below 2.

When the pH increases from 2 to 7, the sorption capacity decreases to 8.3 mg g^{-1}. The protonation of amine groups progressively decreases and the speciation of selenate is displaced to different predominating metal species (but also the protonation state of reactive groups). Figure 2-16(a) shows the speciation of primary and secondary amine groups; tertiary amine groups remain protonated in the studied pH range.

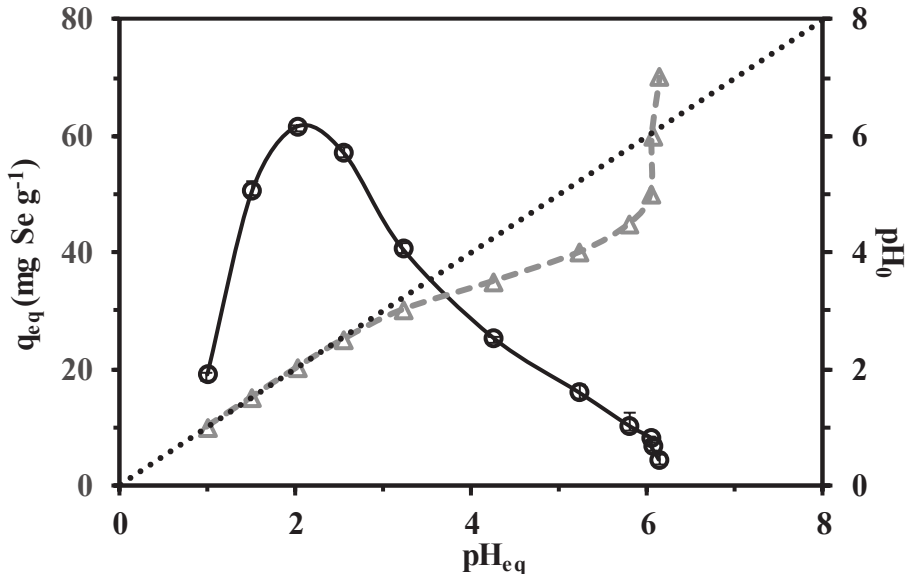

Figure 2-15 Effect of pH on Se(VI) sorption using membrane (C_0 = 100 mg Se L^{-1}; Sorbent dosage = 0.8 g L^{-1}; contact time = 24 h; flow rate = 15 mL min^{-1}; temperature = 20± 1 °C; dashed line represents pH variation during sorption).

The comparison of the distribution of SeO_4^{2-} and $HSeO_4^-$ species with the sorption efficiency suggests that selenium binding drastically increases when divalent a nionic species predominates over monovalent species (in the range pH 1-2). In this pH range, primary amine groups are fully protonated.

Above pH 2, despite the predominance of monovalent selenate species the sorption capacity strongly decreases. This can be associated to the progressive decrease of the protonation of primary amine groups. The pK_a of primary amine groups is close to 4.5. The partial cross-linking of amine groups with aldehyde groups (of the cross-linker agent) may affect the acid-

base properties of these amines but the reactive groups remain basic enough for maintaining convenient protonation/deprotonation pattern.

In the range pH 3.5-5.5, the sorption capacity decreases more weakly: primary amine groups are deprotonating but secondary amine groups (with less affinity for selenate anions) may contribute to weak sorption. At pH above 5.5, the secondary amine groups begin to deprotonate and a new stronger decrease in sorption capacity is observed.

These observations tend to demonstrate that the probable mechanism involved in metal binding consist of the electrostatic attraction of preferentially SeO_4^{2-} (divalent anion) onto protonated primary amine groups (preferentially to secondary amine groups). This means also that an appropriate crosslinking ratio (between primary amine groups and aldehyde groups) should take into account the necessary stabilization of the sorbent but also the availability of primary amine groups. In the case of the sorption of anionic Se species on non-living *Eichornis crassipes* and *Lemna minor*, the possible contribution of Coulombic interaction with protonated hydroxyl groups (in acidic solutions) has been also reported [131].

Figure 2-15 also shows the pH change during the sorption process. Between pH 2 and 3.5, the pH remains stable, despite the sorption of the metal; protons capture and selenate binding are low enough compared to the actual amount of protons to maintain unchanged the pH. In the range pH 3.5-6, the equilibrium pH tends to substantially decrease: protons are released due to deprotonation of amine groups and to the dissociation of HSO_4^-/SeO_4^{2-}. These trends are confirmed in Figure 2-16b pH variations during sorption are compared to pH variations from background slat solutions (results collected from titration data in the determination of pH_{PZC}). The pH variation is negligible in the optimum pH range of sorption but substantially increases at pH higher than 3-4. The pH variation is less marked in the case of Se sorption solution (compared with background salt solution). These trends confirm that pH variation is not only due to the proper acid-base properties of the sorbent but that the interaction with selenate species contribute to moderate pH variation.

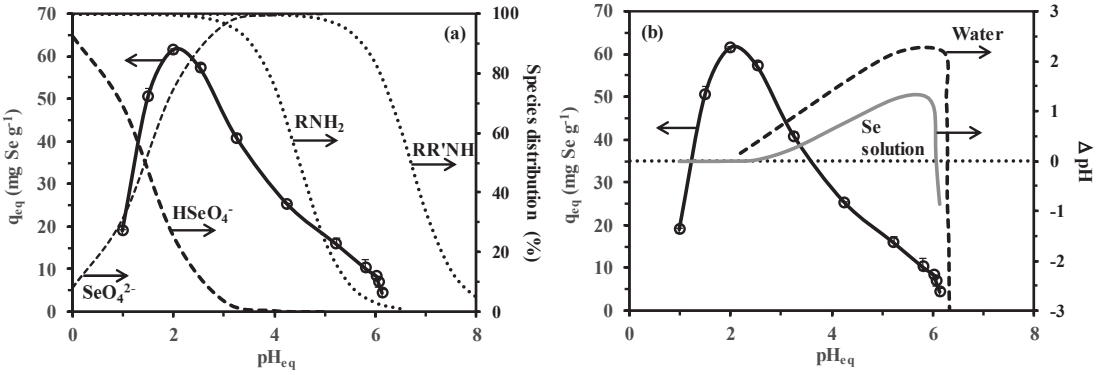

Figure 2-16 (a) Effect of Se speciation and protonation of amine groups (primary, secondary) on Se(VI) sorption capacity, (b) pH variation during sorption compared to pH variation in background salt (relationship with sorption capacity)(Se speciation was calculated using Visual Minteq [132]).

Figure 2-17 shows the plot of the distribution ratio ($\log_{10}D = q_{eq}/C_{eq}$, L g^{-1}) *vs.* equilibrium pH (log-log plot). The slope of linear sections is frequently associated with the stoichiometry of the ion-exchange between sorbed species and counter-ion released from the sorbent. The optimum pH is confirmed close to pH 2. Two segments roughly linear can be identified corresponding to the increase of sorption with pH (from 1 to 2) with a slope close to 0.7 (the points at pH 1 are shifting the slope to higher value compared to the points between pH 1.5 and 2; slope close to 0.3). The average value close to 0.5 could be associated with the binding of SeO_4^{2-} (consistently with the predominating species in this pH range); this means that two protonated amine groups are involved in the binding of one selenate ion (selenate/amine molar ratio close to 0.5). At pH higher than 2, the sorption capacity decreases and the slope of the curve is close to 0.27, as an evidence of the change in the interaction mode between amine groups and selenium species and to the effect of acid-base characteristics of the sorbent. Further experiments were performed at pH 2.

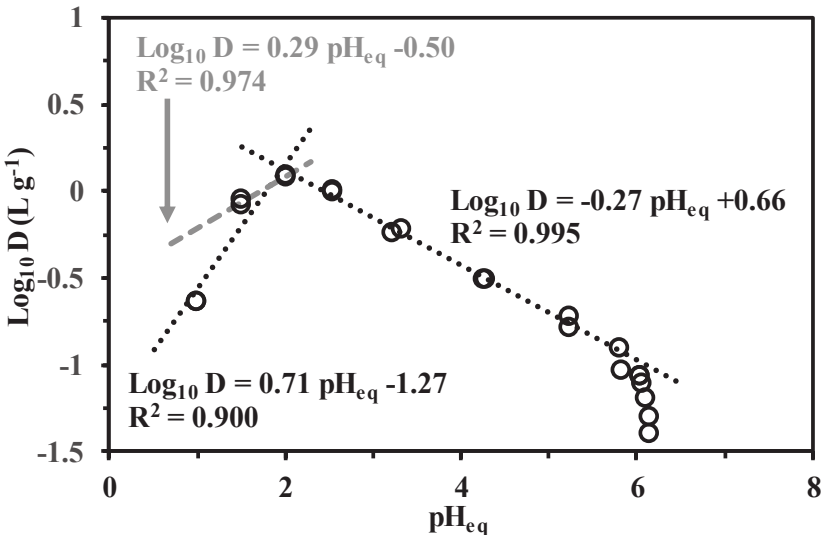

Figure 2-17 Variation of the distribution ratio (Log_{10} D plot) with equilibrium pH.

2.4.2.3 Effect of flow rate on uptake kinetics

The uptake kinetics can be controlled by the diffusion mass transfer process and the proper sorption reaction at the liquid/solid interface [133]. In fixed-bed columns, the flow rates may have potential impact on mass transfer (through resistance to film diffusion, to intraparticle diffusion) but also on eventual preferential channeling. In the case of non-homogeneous distribution and size of channels, the solution may pass through the largest pores (at the expense of longer transfer zone and earlier breakthrough or longer time required for reaching the equilibrium, and even a non-saturation of certain parts of the membrane). Imposing a higher flow rate may help accessing the completely reactive volume of the membrane. This may be explained by the fact that a lower flow rate (5 mL min^{-1}) slows down the flow inside the membrane (which blocks the hydrodynamic transfer of the solution in the whole mass of the membrane), and increases the resistance of air bubbles (which may limit the contact of the solution with reactive groups) [134]. In order to verify this effect and to determine the minimum flow rate (or superficial flow velocity) experiments were compared at different flow rates (i.e., 5, 15 and 50 mL min^{-1}). In the case of membranes immobilized in column but under recirculation mode, the system is globally analogous to the stirred reactor and the flow velocity is analogous to the agitation speed parameter, complicated by the possible occurrence of channel effects. Figure 3 shows the kinetic profiles for the sorption of Se(VI); the contact time for equilibrium was set to 24 h. The residual concentration is not affected by the flow rate; under selected experimental conditions, the recovery yield reaches 46% (sorption capacity close to 60 mg Se g^{-1}). The equilibrium time is almost unchanged when varying the flow rate between 15 and 50 mL min^{-1}; 30 min are sufficient while at the lowest flow rate (i.e., 5 mL min^{-1}), the

equilibrium time increases up to 120 min. The limit flow rate for avoiding channeling effects is close to 15 mL min^{-1} (i.e; superficial flow velocity: 1.93 m h^{-1}).

The proper reaction rate may be approached using the pseudo-first order rate equation (PFORE) or the pseudo-second order rate equation (PSORE) which are commonly used to model chemical reactions [135]. These equations (Eq. 2-5 and Eq. 2-6), initially designed for modelling homogeneous chemical reactions, have been successfully used for describing heterogeneous systems. However, in these cases, the rate coefficients are considered apparent rate constants that integrate the contribution of diffusion mechanisms.

The parameters of the PFORE and PSORE for Se(VI) sorption kinetics using three different flow rates are listed in Table 2-9; they were determined by non-linear regression using Mathematica® software. In Figure 2-18, the solid lines represent the simulated curves for PFORE and PSORE using the calculated parameters summarized in Table 2-9. The comparison of the determination coefficients (R^2) shows that the PFORE equation fits better kinetic profiles. This is confirmed by the superimposition of fitted curves with experimental points. However, it is noteworthy that the calculated values for the equilibrium sorption capacity (i.e., $q_{eq,i}$) PSORE are more accurate than for PFORE. Here the preferential fit of experimental data with the PFORE probably can be explained by the electrostatic attraction mechanism between anionic selenate species and protonated amine groups. The apparent rate coefficients strongly increase with the flow rate: between 5 and 15 mL min^{-1}, the k_1 coefficient varies proportionally (i.e., from 3.30×10^{-2} to 9.93×10^{-2} min^{-1}) while above at 50 mL min^{-1}, the coefficient progression tends to level off (at 17.2×10^{-2} min^{-1}). Similar trends are observed for the evolution of the apparent rate coefficient for PSORE (i.e., k_2 in Table 2-9).

Table 2-9 Effect of flow rate on Se(VI) uptake kinetics – Comparison of fitting equations.

Models	Parameters	F=5 mL min^{-1}	F=15 mL min^{-1}	F=50 mL min^{-1}
	$q_{eq,exp}$ (mg g^{-1})	60.9	60.1	60.9
	$q_{eq,cal}$ (mg g^{-1})	59.0	56.7	57.4
PFORE	$k_1 \times 10^2$ (min^{-1})	3.30	9.93	17.2
	R^2	0.997	0.992	0.996
	$q_{eq,cal}$ (mg g^{-1})	63.8	59.4	59.5
PSORE	$k_2 \times 10^3$ (g mg^{-1} min^{-1})	0.69	2.46	4.49
	R^2	0.984	0.990	0.988

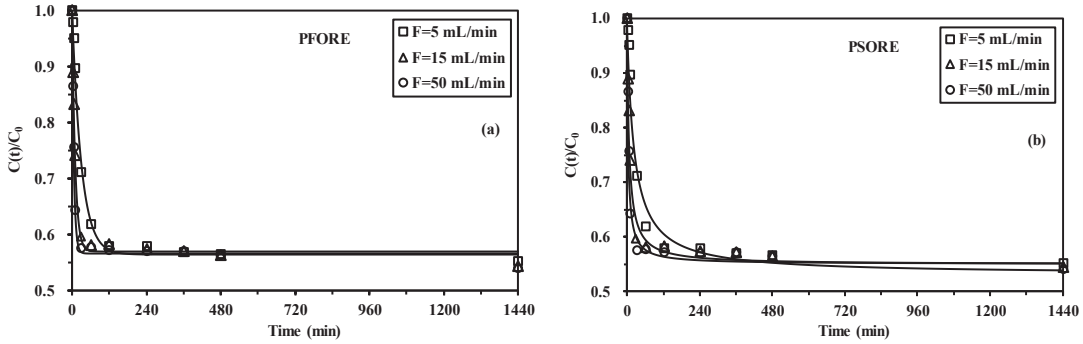

Figure 2-18 Se(VI) uptake kinetics – Effect of flow rate (C_0 = 50 mg Se L^{-1}; SD = 0.4 g L^{-1}; pH_0: 2; T = 20 ± 1 °C; solid line: fit of kinetic profile with the PFORE (a) and the PSORE(b)).

2.4.2.4 Adsorption isotherms

The sorption isotherm, which plots the sorption capacity in function of residual concentration at fixed temperature and pH, provides important information on the affinity of the sorbent for the solute. At pH 2 the sorption isotherm for Se(VI) is shown in Figure 4. The sorption capacity steeply increases at low metal concentration (below 25 mg Se L-1) before progressing more weakly. A pseudo-saturation plateau is reached around 83 mg Se g^{-1} (for residual concentrations higher than 150 mg Se L^{-1}). The sorption isotherms can be modeled using Langmuir (see Eq. 2-7), Freundlich (see Eq. 2-8) and Sips models (see Eq. 2-9).

The lines in Figure 2-19 show the fits of experimental data with the three models and the parameters reported in Table 2-10 (parameters were determined by non-linear regression analysis). The three models fit well the data in the pseudo linear section (henry domain) of the sorption isotherm. The Langmuir equation respects the shape of the curve up to a residual concentration close to 103 mg Se L^{-1} and then diverges and underestimates the sorption capacity in the saturation domain. The maximum sorption capacity at saturation of the monolayer is consistent with the effective maximum sorption capacity (i.e., 82.3 mg Se g^{-1} vs. 83 mg Se g^{-1}). The Freundlich equation underestimates sorption capacity in the intermediary domain (highest curvature) and overestimates the q_{eq} in the saturation domain; this is a power-type function non-consistent with the progressive saturation of the sorbent. Best fit is obtained with the Sips equation; using a third parameter logically improves the quality of mathematical fit. However, the maximum sorption capacity is substantially overestimated (close to 105 mg Se g^{-1}). The qualitative evaluation of modeled profiles is consistent with the comparison of determination coefficients in Table 2-10.

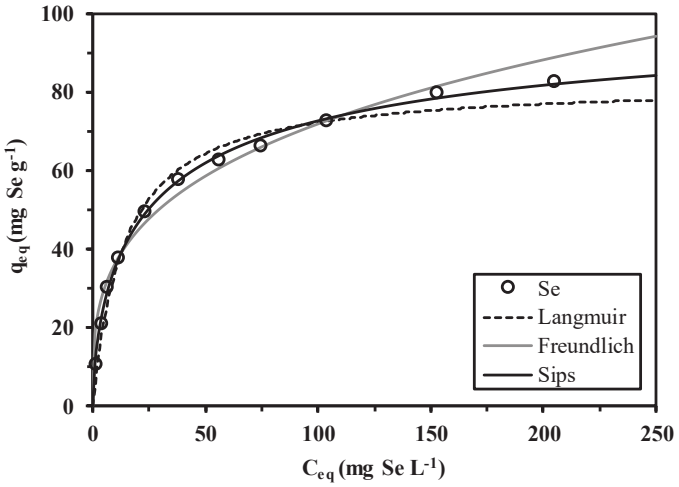

Figure 2-19 Se(VI) sorption isotherms using membranes (SD = 0.8 g L^{-1}; contact time = 24 h; pH: 2; flow rate = 15 mL min^{-1}; T = 20± 1 °C).

Table 2-10 Se(VI) sorption isotherms – Modeling.

Model	Parameter	
Langmuir	$q_{mL,cal}$ (mg g^{-1})	82.4
	b_L (L mg^{-1})	0.072
	R_L	0.04-0.59
	R^2	0.978
Freundlich	k_F (mg g^{-1})/(L mg^{-1})$^{1/n}$	18.46
	n_F	3.385
	R^2	0.965
Sips	$q_{mS,cal}$ (mg g^{-1})	105.2
	b_S (L mg^{-1})	0.115
	n_S	1.548
	R^2	0.997

The basic characteristics of the sorption process (obeying the Langmuir equation) can be described by the dimensionless equilibrium parameter, R_L, which is calculated using Eq. 2-10 [136].

$$R_L = \frac{1}{1 + b_L \times C_0}$$ **Eq. 2-10**

where C_0 is the initial concentration (mg Se L^{-1}).

The values of R_L allow qualifying the sorption as unfavorable ($R_L > 1$), linear ($R_L = 1$), favorable ($0 < R_L < 1$) or irreversible ($R_L = 0$) processes [137]. Under selected experimental conditions, the values of R_L vary in the range 0.04–0.59; this confirms that Se(VI) sorption on AP-4% membranes is a favorable process.

Table 2-11 compares a series of sorption performances reported in the literature using the q_m Langmuir capacity. Some sorbents such as thiourea-formaldehyde resin [138], chloride hydrocalumite Friedel phase [139] polyamine synthetic resin [140] have remarkable maximum sorption capacities (i.e., 526, 196 mg and 134 Se g^{-1}, respectively); however, in most cases, AP-4% membranes have comparable or higher sorption capacities than alternative sorbents.

Table 2-11 Se(VI) adsorption capacities of a series of sorbents reported in literature.

Sorbents	pH	C_0[a] (mg L^{-1})	q_m (mg g^{-1})	Ref.
Fe–Mn hydrous oxides	4	5-500	19.8	[141]
Thiourea-formaldehyde resin	5M HCl	100-500	526	[138]
Purolite S108 resin	3.56	0-856	3.23	[142]
Oxidized multi-walled carbon nanotubes	7	0.5-2	1.87	[143]
Al(III)/SiO_2 binary oxide system	5	0-237	11.3	[144]
Chloride hydrocalumite Friedel phase	8	36-1086	196	[139]
Al_2O_3 impregnated chitosan beads	6	0-3.8[b]	20.1	[145]
Chitosan	6	0-15[b]	2.01	[146]
MgO nanosheets	10.5	1-100	10.3	[146]
LDH/chitosan nanocomposite	6	0-16[b]	4.5	[147]
Silica magnetite nanoparticles	n.r.	0-200	46.1	[148]
Functionalized silica magnetite NPs	n.r.	0-200	27.6	[148]
Cladophora hutchinsiae	5	10-400	74.9	[8]
Chitosan/clay composite	4	0-10[b]	8	[149]
Polyamine-type weakly basic IX resin	6	30-240	134.2	[140]
Eggshell membrane	-	-	37.0	[129]
Chicken feather	-	-	20.7	[129]
AP-4% Membranes	2	10-270	83.0	This study

[a]Initial concentration range; [b]equilibrium concentrations (estimated from the graphs); n.r.: not reported.

2.4.2.5 Effect of coexisting anions

Coexisting anions such as sulfate, nitrate and chloride are frequently present in natural water streams or industrial effluents. Therefore, considering their potential impact on selenium removal is critical for evaluating the effectiveness of AP-4% membranes for Se(VI) recovery. The sorption capacity of AP-4% membranes for Se(VI) was tested in the presence of increasing concentrations of these competitor anions (50-800 mg L^{-1}). Figure 2-20 shows that the three anions inhibited Se(VI) sorption to different extents. Indeed, AP-4% membranes being positively charged in acid solutions have obvious affinity for binding anions. Monovalent anions, such as chloride and nitrate, have comparable and limited effect on Se(VI) sorption. Under selected experimental conditions, the sorption capacity decreases from 57.7 mg Se g^{-1} to 42.1-43.6 mg Se g^{-1} (loss in sorption capacity close to 25%) when Cl^- or NO_3^- concentration reaches up to 800 mg L^{-1} (i.e., 22.5 mM for Cl^- and 12.9 mM for NO_3^-), which are 17.3 and 9.9 times excess compared to selenium molar concentration (1.3 mM), respectively. In the case of divalent sulfate anions, Se(VI) sorption is almost completely inhibited at [sulfate] = 800 mg L^{-1} (i.e., 8.3 mM, 6.4 times excess): the sorption capacity decreases to 5 mg Se g^{-1} (i.e., loss exceeds 91%). Figure 2-21 shows the impact of competitor anions on Se(VI) distribution ratio (log-log plot). Chloride and nitrate anions have similar behavior with a slope of the plot close to -0.16-0.17 while for sulfate anions the slope was close to -1 (i.e., -0.96). These differences clearly illustrate the different competitor mechanism between these anions. Similar phenomenon reported in the adsorption of Se(VI) by iron-oxide-coated sand [150] The divalent charge of sulfate anions (analogous to the expected bound selenate species, SeO_4^{2-}) may explain the strong competitor effect on selenate uptake (direct competitor effect or ion-exchange between sulfate and selenate anions) [151, 152]. The chemical analogy between SO_4^{2-} and SeO_4^{2-} was also reported for explaining the strong impact of the competitor anion on Se(VI) recovery using a polyamine weakly basic ionic exchange resin [140]. In the case of hematite modified magnetic nanoparticles [153], the sorption of selenate anions was inhibited by anions (in the range of concentrations: 0-10 mM) according the series: chloride≈nitrate (negligible) < sulfate < carbonate- << silicate <<< phosphate. In the case of Mg-Al LDH sorbent, the sorption of selenate was also more reduced by sulfate or phosphate anions compared with nitrate effect; while for selenate the presence of phosphate increased Se(VI) recovery compared with nitrate and contrary to the negative effect of sulfate anions. The presence of small amounts of sulfate (i.e., 10 ppm) was sufficient for strongly limiting the sorption of selenite and selenate on nanocrystalline-impregnated chitosan beads [145].

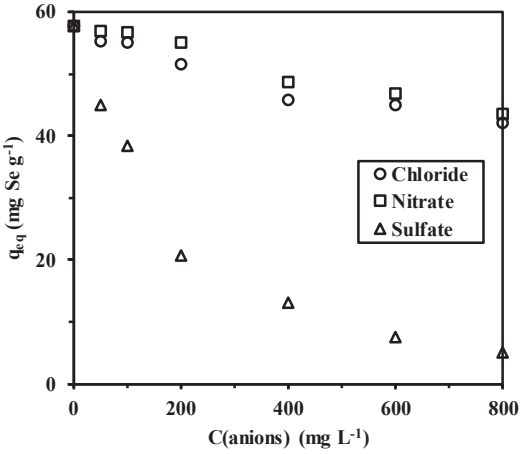

Figure 2-20 Effect of coexisting anions on Se(VI) adsorption by membranes (C_0 = 100 mg L^{-1}; SD = 1 g L^{-1}; contact time = 24 h; pH: 2; flow rate = 15 mL min^{-1}; temperature = 20 ± 1 °C).

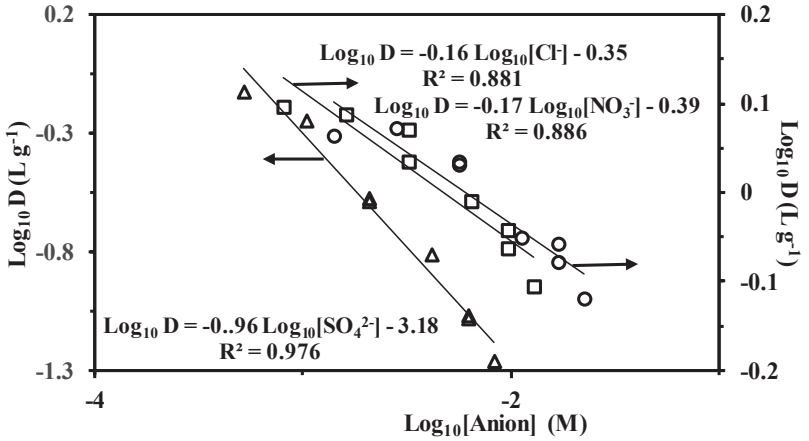

Figure 2-21 Variation of the distribution ratio D with competitor anion concentration (Log-Log plot) at pH 2.

2.4.2.6 Desorption and recyclability study

Membrane recyclability is a vital parameter for assessing the cost-effectiveness of wastewater treatment. The competitor effect of phosphate was used for promoting the acidic desorption of Se(VI) from Se-loaded marine biomass [131] or the regeneration of Al/Si-Fe/Si coprecipitates [154]. Hydrochloric acid (1 M) solution was used for removing Se(VI) from polyamine-type weakly basic ion exchange resin [140]. In the case of functionalized cellulose, selenate was quantitatively recovered from loaded sorbent using 3 M HCl/2 % $KClO_3$ solutions [155]. Ma et al. [153] used 0.01 M NaOH solutions for Se desorption from hematite modified magnetic nanoparticles.

In this study, four consecutive sorption-desorption cycles were carried out using 0.01M NaOH solution as the eluent to desorb Se(VI). As shown in Figure 2-22, the sorption capacity increases slightly from 63 mg g^{-1} to 66 mg g^{-1} from the first cycle to fourth cycle (under selected experimental conditions). The desorption efficiency is enhanced after the first cycle and then remains over 96% in the subsequent cycles. These results indicate that the membrane has an excellent reusability and that NaOH regeneration allows stable sorption and desorption performances for Se(VI) removal for at least four cycles. It is noteworthy that the same sorbent was used for chromate recovery from acidic solutions [43]; in this case, chromate desorption was much less efficient (not exceeding 40-50 %). Therefore, the recycling of the sorbent was rather limited: the sorption capacity after three cycles was reduced by 60 %. These differences between selenate and chromate anions may be explained by the stronger ability of chromate to be reduced in acidic solutions in the presence of organic compounds. The partial degradation (by oxidation) of the sorbent and the *in situ* reduction of Cr(VI) (to form Cr(III)) may explain this progressive depreciation of sorption efficiency. Though selenate can be reduced to selenite, this phenomenon is probably less active compared with chromate/chromium redox reaction (redox potentials: +1.33 V for Cr(VI)/Cr(III) against +1.06 V for Se(VI)/Se(IV) and +0.903 V for Se(VI)/Se(0)).

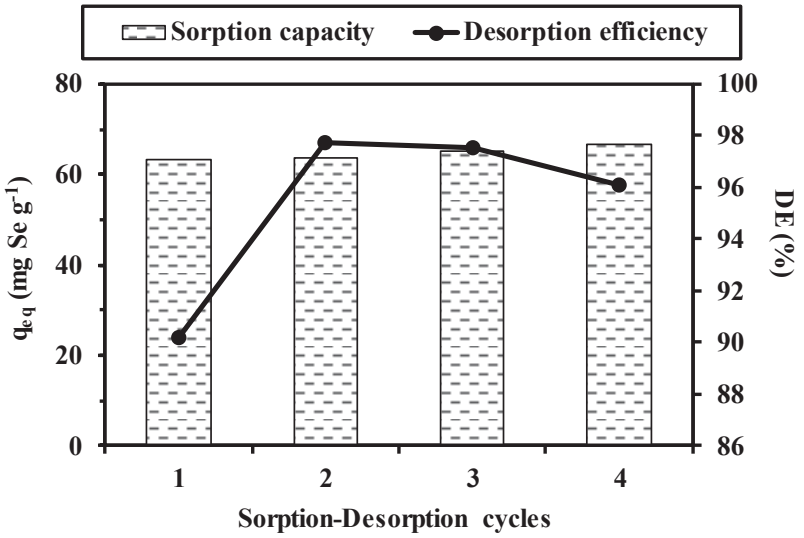

Figure 2-22 Metal desorption and sorbent recycling - Se(VI) sorption capacity and desorption efficiency (Sorption step - C_0 = 100 mg Se L^{-1}; SD = 0.8 g L^{-1}; pH: 2; flow rate = 15 mL min^{-1}; temperature = 20 ± 1 °C. Desorption step - desorption agent: 0.01 M NaOH; V = 50 mL; time = 30 min; flow rate = 15 mL min^{-1}; temperature = 20 ± 1 °C).

2.4.2.7 Adsorption mechanism discussion

The analysis of pH effect, the selenium speciation and the measurement of pH_{pzc} value suggest that selenate anionic species are immobilized at the surface of the sorbent (on protonated amine groups, preferentially primary amine groups) through electrostatic attraction mechanism. The stoichiometric ratio (i.e., close to 0.5) means that, at the optimum pH, selenate requires two protonated amine groups. In addition, the strong interference of sulfate on selenate sorption confirms that the main bound species are probably SeO_4^{2-} and $HSeO_4^-$.

EDX spectra (Figure 2-13) show selenium ions are found to be uniformly distributed on the surface of material after Se(VI) treatment; this provides direct evidence for homogeneous selenium sorption onto AP-4% membrane. The significant increase in the intensity of O element after Se(VI) sorption, is directly associated to the binding of the oxyanion [156, 157]. Analytical tools may contribute to confirm the interaction mode.

FTIR spectra and the changes in the main bands (before and after Se(VI) sorption and desorption) are recorded in Figure 2-14. After Se(VI) sorption, the band at 3283 cm^{-1} (assigned to O–H and N–H stretching vibration) shifts to 3276 cm^{-1}. Simultaneously, a new band at 1712 cm^{-1} (attributed to C=O stretching vibration) is observed after Se(VI) adsorption; this may be explained by the partial oxidation of some reactive groups [158]. The intensities of the bands at 1596 cm^{-1} and 1404 cm^{-1} decrease; these bands are assigned to C=N and N–H vibration in PEI-GA and COO^- symmetric stretching in alginate, respectively. The band at 1317 cm^{-1} (attributed to C-N stretching vibration) shifts to 1294 cm^{-1}. These changes reveal that hydroxyl and carboxyl groups on alginate and amino groups from PEI-GA may be involved in Se(VI) binding (mainly amine groups) and possible subsequent reduction process. The appearance of a strong band at 864 cm^{-1} which can mask the band of 885 cm^{-1} after sorption could be attributed to the presence of Se–O bond as reported by Peak and Sparks [159] and Chubar [160], which illustrated the formation of complexes between selenate and the sorbent. Moreover, changes of bands at 810 cm^{-1} and 773 cm^{-1} may also be caused by selenate sorption followed by in situ reduction [161, 162]. Indeed, Elder et al. [163] also reported that the IR spectra of free SeO_3^{2-} in solution exhibits a peak at 810 cm^{-1} (symmetric stretching vibration) while the intensity of the peak at 740 cm^{-1} decreases (asymmetric stretching vibration). After selenium desorption, the spectrum of the material shows only minor changes compared with the spectrum of raw AP-4% membrane. The broad band (overlapping of O–H and N–H stretching vibrations) is shifted to 3220 cm^{-1} after desorption by NaOH solution. It is noteworthy that the bands between 900 and 750 cm^{-1} (on the spectrum of Se-loaded AP-4% membrane) are shifted back to their original

positions on the spectrum of raw AP-4% membrane; this confirms that selenium is almost completely desorbed, and that the material is perfectly regenerated.

The XPS analyses of raw, Se-loaded and Se-desorbed membranes are carried out to obtain more detailed information on sorption mechanisms through the determination of functional groups and Se oxidation state. Figure 2-23 shows XPS survey spectra of the membranes. Small peaks appear around binding energies (BEs) of 58.7 eV and 164.7 eV for Se 3d and Se 3p on Se(VI)-loaded membrane, indicating the accumulation of Se on the sorbents. Table 2-12 and Figure 2-24 reports the identification of the most representative elements (i.e., C, N, O and Se) observed on the XPS survey spectra for raw, Se(VI) loaded and desorbed membranes. Due to the overlapping of the S 2p and the Se 3p, it appears preferable discussing Se 3d band. The spectrum of Se 3d was fitted by two peaks at binding energies of 59.2 and 60.1 eV, which can be assigned to the oxidation states of Se(IV) and Se(VI), with peak areas (atomic fractions) of 60% and 40%, respectively. This means that Se(VI) ions were partially reduced to Se(IV) on AP-4% membranes (see Table 2-12).

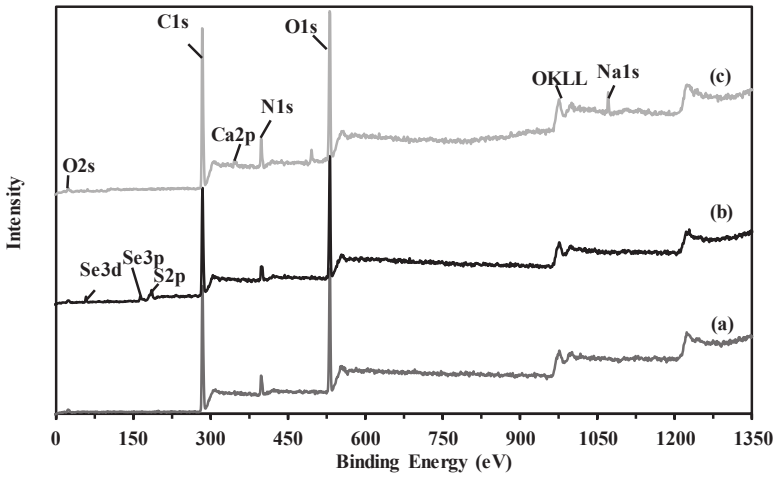

Figure 2-23 The XPS survey spectra of (a) raw membrane, (b) Se(VI)-loaded membrane and (c) Se(VI)-desorbed membrane.

The C 1s spectra of raw membrane can be deconvoluted into four individual component peaks with BEs of 284.8, 286.0, 287.6 and 289.1 eV, which are assigned to C–C/C=C/adventitious carbon, C–N/C=N/C–OH/C–O–C, C=O and carboxylate groups, respectively. These assignments reflect the functional groups in the alginate/PEI/GA. The peak area of C–N/C=N/C–OH/C–O–C slightly increased from 41% to 43% after sorption may be due to that these groups participate in Se(VI) binding. Furthermore, the deconvolution of the O 1s spectra of the samples shows two peaks with BEs of 531.0 and 532.5 eV (for raw membrane). These peaks can be assigned to O element in C=O/carboxylate and C–OH/C–O–C, respectively. After

Se(VI) sorption, the peak area of C=O slightly increases from 23% to 24% while the peak area of C–OH/C–O–C decreases from 77 % to 76%. These weak changes may be related to a fractional degradation associated with the reduction of Se(VI) at pH 2; these groups react as electron donors, according Eq. 2-11. These observations are consistent with the changes on FTIR spectra.

$$\sim C–OH + Se(oxidized) + H^+ \rightarrow \sim C=O + Se(reduced) + H_2O \quad \textbf{Eq. 2-11}$$

Figure 2-24 also shows the N 1s XPS spectra and the shifts and changes in intensity of the different forms of N reactive groups (before and after Se sorption). The N 1s spectrum of AP-4% membrane is decomposed into three individual components at BEs of 399.1, 400.4 and 401.7 eV, which can be assigned to N into C-NH/amine, -C=N- (generated during the reaction of PEI and GA, see Scheme 1), and $–NH_3^+$ (ionic), respectively. Obviously, after Se(VI) sorption, the peak area of C-NH/amine decreases from 53% to 46% while the peak area of $–NH_3^+$ (ionic) increases from 22% to 31%. These changes are other evidences for the protonation of amine groups, so that the Se(VI) anions could be bound to the membrane by the electrostatic attraction of positive amine groups. Moreover, these changes could be also related to the reduction process of Se(IV). Yan et al. [164] reported that amine groups of PEI could be involved in the reduction of Cr(VI) to Cr(III) as electron donors. Qiu et al. [165] found similar results in the study of Cr(VI) removal by PEI-modified ethyl cellulose: both the amine groups of PEI and the hydroxyl groups of ethyl cellulose contributed to the reduction of Cr(VI) reduction. This series of chemical reactions occurring during Se(VI) sorption on AP-4% membrane are also consistent with kinetic profiles: (a) first fast step of sorption, followed by (b) slower mass transfer into the thin scaffold foils of the material together with the proper reduction phenomenon.

After selenium desorption by NaOH solution, the atomic fraction of $–NH_3^+$ decreases from 31% to 11% (due to deprotonation); deprotonation contributes to decreasing the affinity of the sorbent for selenium anionic species (based on XPS analysis, mainly selenite) and to improve selenium desorption.

The plausible mechanism of Se(VI) sorption onto AP-4% membrane consists of:

(a) first binding of Se(VI) anions by electrostatic attraction on protonated amine groups of the sorbent (preferentially primary amines), followed by

(b) the *in situ* reduction of Se(VI) to Se(IV) (with the help of H^+ and electron-donor groups like amines, aldehyde, and/or hydroxyls).

It is noteworthy that despite this sorption and reduction mechanisms (similarly to chromate), the recycling of the sorbent is remarkably high compared to chromate case.

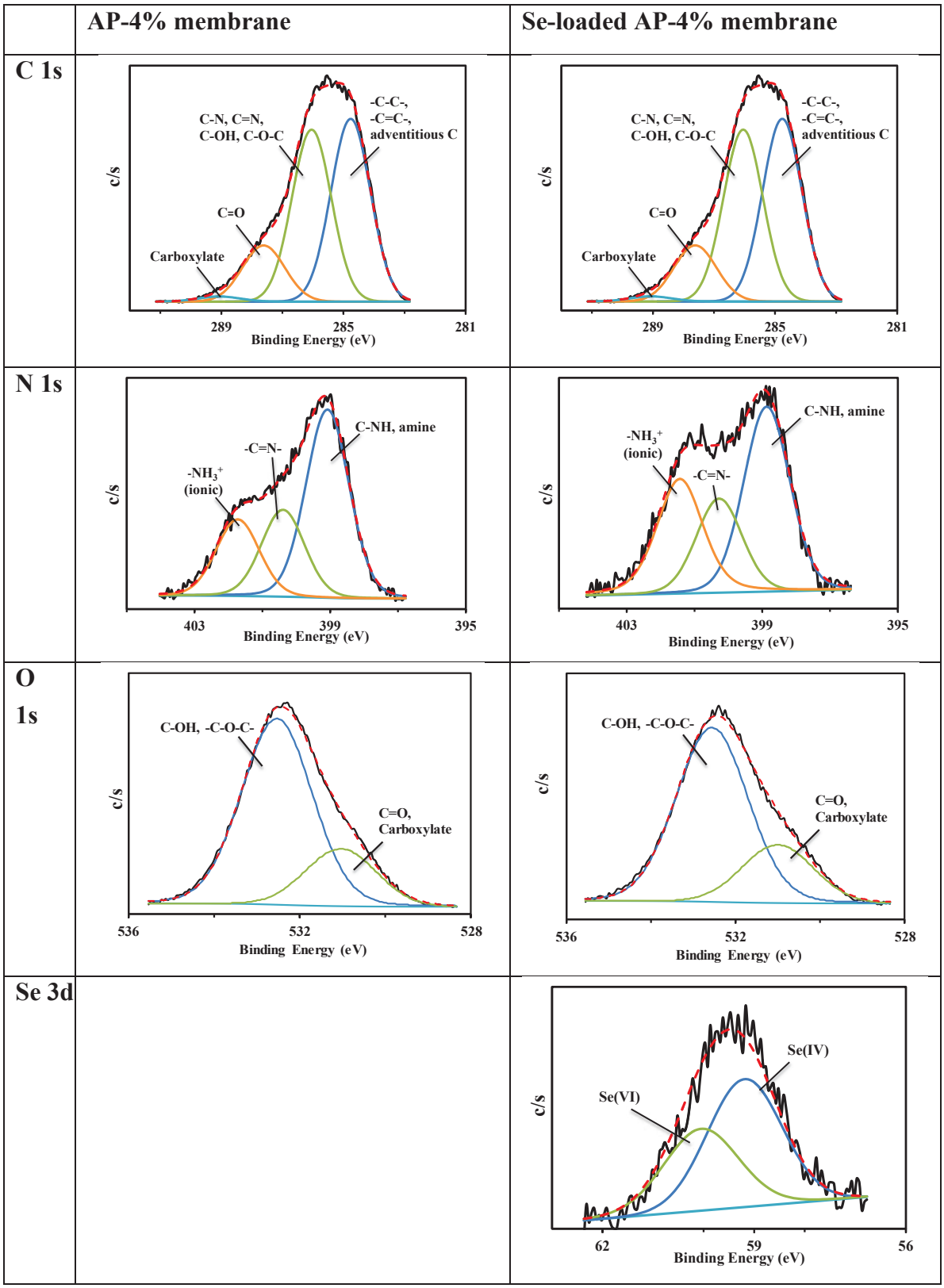

Figure 2-24 High resolution C 1s, O 1s, N 1s, and Se 3d core level XPS spectrum of AP-4% membrane and Se(VI)-loaded AP-4% membrane.

Table 2-12 XPS analysis of sorbent (before and after Se(VI) sorption, and after metal desorption) – Binding energies (BE, eV), atomic fractions (AF, %) and assignments [166].

Sample	A-PEI Membrane		A-PEI membrane after Se(VI) sorption		A-PEI membrane after Se(VI) desorption		Assignments
	BE (eV)	AF (%)	BE (eV)	AF (%)	BE (eV)	AF (%)	
C 1s	284.8	44	284.8	41	284.8	48	C-C, C=C, adventitious carbon
	286.0	41	286.1	43	286.0	37	C-N, C=N, C-OH, C-O-C
	287.6	14	287.6	13	287.6	13	C=O
	289.1	1	288.7	3	288.7	2	Carboxylate
N 1s	399.1	53	398.9	46	398.9	63	C-NH, amine
	400.4	25	400.3	23	400.1	26	C=N
	401.7	22	401.4	31	401.7	11	NH_3^+ (ionic)
O 1s	531.0	23	531.0	24	530.9	34	C=O and Carboxylate
	532.5	77	532.6	76	532.5	66	C-OH, C-O-C
Se 3d	–	–	59.2	60			Se(IV)
	–	–	60.1	40			Se(VI)

2.5. Principales conclusions

Cette première étude concerne la synthèse de membranes alginate / PEI à haut pouvoir de percolation, au travers d'un procédé de préparation mettant en œuvre un séchage peu sophistiqué, et leurs propriétés de fixation des ions chromates et sélénates. Ces deux types de contaminants (chromates et sélénates) se caractérisent par des comportements différents : les ions chromates sont facilement réduits (en Cr(III)) en milieu acide en présence de composés organiques alors que les ions sélénates sont plus stables. L'effet du pH est étudié, mettant en évidence le même pH optimal (i.e., pH 2) en lien avec les caractéristiques de charge des membranes (protonation des fonctions aminées) et la spéciation des ions métalliques (anions). L'étude des cinétiques en mode statique (recirculation d'un volume fini de la solution au travers de la membrane) est menée en faisant varier le débit de la solution ; ce paramètre présente un effet mineur sur les profils cinétiques pour autant qu'une valeur minimale de ce débit (de l'ordre de 10-15 mL min^{-1}, soit une vitesse superficielle de 1.2-1.8 m h^{-1}) soit imposée afin de forcer la solution dans les canaux poreux de plus grande tortuosité ou de plus petits diamètres (en raison de l'hétérogénéité des membranes). Les isothermes d'adsorption sont également acquises à pH 2. Le cas des ions chromates met en évidence des propriétés remarquables ; les capacités maximales de fixation de l'ordre de 6 mmol Cr g^{-1} classent le matériau parmi les meilleurs adsorbants. Ces performances sont bien meilleures que pour les ions sélénates pour laquelle la capacité de fixation n'excède pas 1 mmol Se g^{-1}. Si les isothermes d'adsorption du Cr(VI) et du Se(VI) sont correctement décrites par l'isotherme de Langmuir, le profil sigmoïdal pour le cas du chrome total s'accommode mieux du modèle mathématique de Sips.

L'effet d'anions compétiteurs (chlorure, nitrate et sulfate) s'exprime essentiellement dans le cas des sulfates dont le caractère divalent facilite l'interaction avec le support au détriment de la fixation des ions métalliques, contrairement aux anions monovalents.

Les différences entre les ions chromates et les ions sélénates s'expriment également en termes de désorption des anions métalliques et de recyclage de l'adsorbant. Ainsi, alors que pour les ions chromates l'efficacité de fixation du chrome décroit progressivement avec le nombre de cycles, dans le cas des ions sélénates le matériau maintient remarquablement ses performances d'adsorption et de désorption pour un minimum de 4 cycles. Même si l'analyse XPS met en évidence des phénomènes de réduction partielle dans le cas des ions sélénates, il semblerait que ces phénomènes présentent une acuité plus marquée pour la fixation des ions chromates soit directement par "l'empoisonnement" de la surface de l'adsorbant soit par dégradation (oxydation) des groupes réactifs (ou des éléments de structure du matériau).

2.6. References

[1] G. Lytras, C. Lytras, D. Argyropoulou, N. Dimopoulos, G. Malavetas, G. Lyberatos, A novel two-phase bioreactor for microbial hexavalent chromium removal from wastewater, Journal of hazardous materials, 336 (2017) 41-51.
[2] J. Konczyk, C. Kozlowski, W. Walkowiak, Removal of chromium(III) from acidic aqueous solution by polymer inclusion membranes with D2EHPA and Aliquat 336, Desalination, 263 (2010) 211-216.
[3] S. Xu, S. Pan, Y. Xu, Y. Luo, Y. Zhang, G. Li, Efficient removal of Cr(VI) from wastewater under sunlight by Fe(II)-doped TiO_2 spherical shell, Journal of hazardous materials, 283 (2015) 7-13.
[4] A.K. Shanker, C. Cervantes, H. Loza-Tavera, S. Avudainayagam, Chromium toxicity in plants, Environment international, 31 (2005) 739-753.
[5] A.D. Lemly, Aquatic selenium pollution is a global environmental safety issue, Ecotoxicology and Environmental Safety, 59 (2004) 44-56.
[6] S. Santos, G. Ungureanu, R. Boaventura, C. Botelho, Selenium contaminated waters: An overview of analytical methods, treatment options and recent advances in sorption methods, Science of the Total Environment, 521 (2015) 246-260.
[7] WHO, Guidelines for drinking-water quality, WHO, Geneva, Switzerland, 2017.
[8] M. Tuzen, A. Sari, Biosorption of selenium from aqueous solution by green algae (*Cladophora hutchinsiae*) biomass: Equilibrium, thermodynamic and kinetic studies, Chemical Engineering Journal, 158 (2010) 200-206.
[9] Y. Nakamaru, K. Tagami, S. Uchida, Distribution coefficient of selenium in Japanese agricultural soils, Chemosphere, 58 (2005) 1347-1354.
[10] M.R. Awual, M.M. Hasan, T. Ihara, T. Yaita, Mesoporous silica based novel conjugate adsorbent for efficient selenium(IV) detection and removal from water, Microporous and Mesoporous Materials, 197 (2014) 331-338.
[11] K. Mondal, G. Jegadeesan, S.B. Lalvani, Removal of selenate by Fe and NiFe nanosized particles, Industrial & Engineering Chemistry Research, 43 (2004) 4922-4934.
[12] P. Gurunathan, S. Hari, S.B. Suseela, R. Sankararajan, A. Mukannan, Production, characterization and effectiveness of cellulose acetate functionalized ZnO nanocomposite adsorbent for the removal of Se (VI) ions from aqueous media, Environmental Science and Pollution Research, 26 (2019) 528-543.
[13] J. Torres, V. Pintos, L. Gonzatto, S. Dominguez, C. Krerner, E. Kremer, Selenium chemical speciation in natural waters: Protonation and complexation behavior of selenite and selenate in the presence of environmentally relevant cations, Chemical Geology, 288 (2011) 32-38.
[14] Y. Fu, J. Wang, Q. Liu, H. Zeng, Water-dispersible magnetic nanoparticle-graphene oxide composites for selenium removal, Carbon, 77 (2014) 710-721.
[15] B. Galán, D. Castañeda, I. Ortiz, Removal and recovery of Cr(VI) from polluted ground waters: a comparative study of ion-exchange technologies, Water research, 39 (2005) 4317-4324.

[16] S. Aber, A. Amani-Ghadim, V. Mirzajani, Removal of Cr(VI) from polluted solutions by electrocoagulation: Modeling of experimental results using artificial neural network, Journal of hazardous materials, 171 (2009) 484-490.
[17] C. Blöcher, J. Dorda, V. Mavrov, H. Chmiel, N. Lazaridis, K. Matis, Hybrid flotation—membrane filtration process for the removal of heavy metal ions from wastewater, Water research, 37 (2003) 4018-4026.
[18] Ihsanullah, F.A. Al-Khaldi, B. Abu-Sharkh, A.M. Abulkibash, M.I. Qureshi, T. Laoui, M.A. Atieh, Effect of acid modification on adsorption of hexavalent chromium (Cr(VI)) from aqueous solution by activated carbon and carbon nanotubes, Desalination and Water Treatment, 57 (2016) 7232-7244.
[19] M. Mahmood-ul-Hassan, V. Suthor, E. Rafique, M. Yasin, Removal of Cd, Cr, and Pb from aqueous solution by unmodified and modified agricultural wastes, Environmental monitoring and assessment, 187 (2015) 19.
[20] A.G. Thanos, E. Katsou, S. Malamis, V. Drakopoulos, P. Paschalakis, E.A. Pavlatou, K.J. Haralambous, Cr(VI) removal from aqueous solutions using aluminosilicate minerals in their Pb-exchanged forms, Applied Clay Science, 147 (2017) 54-62.
[21] S. Sarode, P. Upadhyay, M. Khosa, T. Mak, A. Shakir, S. Song, A. Ullah, Overview of wastewater treatment methods with special focus on biopolymer chitin-chitosan, International journal of biological macromolecules, (2018).
[22] V. Gopalakannan, S. Periyasamy, N. Viswanathan, Synthesis of assorted metal ions anchored alginate bentonite biocomposites for Cr(VI) sorption, Carbohydrate polymers, 151 (2016) 1100-1109.
[23] H.C. Vu, A.D. Dwivedi, T.T. Le, S.-H. Seo, E.-J. Kim, Y.-S. Chang, Magnetite graphene oxide encapsulated in alginate beads for enhanced adsorption of Cr(VI) and As(V) from aqueous solutions: role of crosslinking metal cations in pH control, Chemical Engineering Journal, 307 (2017) 220-229.
[24] Y. Huang, H. Wu, T. Shao, X. Zhao, H. Peng, Y. Gong, H. Wan, Enhanced copper adsorption by DTPA-chitosan/alginate composite beads: mechanism and application in simulated electroplating wastewater, Chemical Engineering Journal, 339 (2018) 322-333.
[25] T. Gotoh, K. Matsushima, K.-I. Kikuchi, Preparation of alginate–chitosan hybrid gel beads and adsorption of divalent metal ions, Chemosphere, 55 (2004) 135-140.
[26] R.D.C. Soltani, G.S. Khorramabadi, A. Khataee, S. Jorfi, Silica nanopowders/alginate composite for adsorption of lead(II) ions in aqueous solutions, Journal of the Taiwan Institute of Chemical Engineers, 45 (2014) 973-980.
[27] W.S. Tan, A.S.Y. Ting, Alginate-immobilized bentonite clay: adsorption efficacy and reusability for Cu(II) removal from aqueous solution, Bioresource technology, 160 (2014) 115-118.
[28] Y.-L. Lai, M. Thirumavalavan, J.-F. Lee, Effective adsorption of heavy metal ions (Cu^{2+}, Pb^{2+}, Zn^{2+}) from aqueous solution by immobilization of adsorbents on Ca-alginate beads, Toxicological and Environ Chemistry, 92 (2010) 697-705.
[29] F. Googerdchian, A. Moheb, R. Emadi, Lead sorption properties of nanohydroxyapatite–alginate composite adsorbents, Chemical Engineering Journal, 200 (2012) 471-479.

[30] C. Jiao, J. Xiong, J. Tao, S. Xu, D. Zhang, H. Lin, Y. Chen, Sodium alginate/graphene oxide aerogel with enhanced strength–toughness and its heavy metal adsorption study, International journal of biological macromolecules, 83 (2016) 133-141.
[31] A. Idris, N.S.M. Ismail, N. Hassan, E. Misran, A.-F. Ngomsik, Synthesis of magnetic alginate beads based on maghemite nanoparticles for Pb(II) removal in aqueous solution, Journal of Industrial and Engineering Chemistry, 18 (2012) 1582-1589.
[32] C. Bertagnolli, A. Grishin, T. Vincent, E. Guibal, Recovering heavy metal ions from complex solutions using polyethylenimine derivatives encapsulated in alginate matrix, Industrial & Engineering Chemistry Research, 55 (2016) 2461-2470.
[33] S. Wang, T. Vincent, C. Faur, E. Guibal, Modeling competitive sorption of lead and copper ions onto alginate and greenly prepared algal-based beads, Bioresource technology, 231 (2017) 26-35.
[34] M.M. Lakouraj, F. Mojerlou, E.N. Zare, Nanogel and superparamagnetic nanocomposite based on sodium alginate for sorption of heavy metal ions, Carbohydrate polymers, 106 (2014) 34-41.
[35] J.H. Chen, Q.L. Liu, S.R. Hu, J.C. Ni, Y.S. He, Adsorption mechanism of Cu(II) ions from aqueous solution by glutaraldehyde crosslinked humic acid-immobilized sodium alginate porous membrane adsorbent, Chemical Engineering Journal, 173 (2011) 511-519.
[36] T.A. Saleh, M. Tuzen, A. Sarı, Polyethylenimine modified activated carbon as novel magnetic adsorbent for the removal of uranium from aqueous solution, Chemical Engineering Research and Design, 117 (2017) 218-227.
[37] B. Xiong, N. Wang, Y. Chen, H. Peng, Self‐assembly of alginate/polyethyleneimine multilayer onto magnetic microspheres as an effective adsorbent for removal of anionic dyes, Journal of Applied Polymer Science, 135 (2018) 45876.
[38] X. Sun, J.H. Chen, Z. Su, Y. Huang, X. Dong, Highly effective removal of Cu(II) by a novel 3-aminopropyltriethoxysilane functionalized polyethyleneimine/sodium alginate porous membrane adsorbent, Chemical Engineering Journal, 290 (2016) 1-11.
[39] S. Wang, T. Vincent, C. Faur, E. Guibal, A comparison of palladium sorption using polyethylenimine impregnated alginate-based and carrageenan-based algal beads, Applied Sciences, 8 (2018) 264.
[40] S. Wang, T. Vincent, C. Faur, E. Rodríguez-Castellón, E. Guibal, A new method for incorporating polyethyleneimine (PEI) in algal beads: High stability as sorbent for palladium recovery and supported catalyst for nitrophenol hydrogenation, Materials Chemistry and Physics, 221 (2019) 144-155.
[41] M. Beppu, E. Arruda, R. Vieira, N. Santos, Adsorption of Cu(II) on porous chitosan membranes functionalized with histidine, Journal of Membrane Science, 240 (2004) 227-235.
[42] Q. Li, Y. Li, X. Ma, Q. Du, K. Sui, D. Wang, C. Wang, H. Li, Y. Xia, Filtration and adsorption properties of porous calcium alginate membrane for methylene blue removal from water, Chemical Engineering Journal, 316 (2017) 623-630.
[43] Y. Mo, S. Wang, T. Vincent, J. Desbrieres, C. Faur, E. Guibal, New highly-percolating alginate-PEI membranes for efficient recovery of chromium from aqueous solutions, Carbohydrate polymers, 225 (2019) 115177.

[44] M.R. Torres, A.P.A. Sousa, E. Filho, F. Dirce, J.P.A. Feitosa, R.C.M. de Paula, M.G.S. Lima, Extraction and physicochemical characterization of *Sargassum vulgare* alginate from Brazil, Carbohydrate Research, 342 (2007) 2067-2074.
[45] S. Wang, M.F. Hamza, T. Vincent, C. Faur, E. Guibal, Praseodymium sorption on Laminaria digitata algal beads and foams, Journal of Colloid and Interface Science, 504 (2017) 780-789.
[46] P. Eiselt, J. Yeh, R.K. Latvala, L.D. Shea, D.J. Mooney, Porous carriers for biomedical applications based on alginate hydrogels, Biomaterials, 21 (2000) 1921-1927.
[47] S. Wang, T. Vincent, C. Faur, E. Guibal, Algal foams applied in fixed-bed process for lead(II) removal using recirculation or one-pass modes, Marine drugs, 15 (2017) 315.
[48] M.V. Lopez-Ramon, F. Stoeckli, C. Moreno-Castilla, F. Carrasco-Marin, On the characterization of acidic and basic surface sites on carbons by various techniques, Carbon, 37 (1999) 1215-1221.
[49] S. Gupta, B. Babu, Removal of toxic metal Cr(VI) from aqueous solutions using sawdust as adsorbent: Equilibrium, kinetics and regeneration studies, Chemical Engineering Journal, 150 (2009) 352-365.
[50] B. Singha, S.K. Das, Biosorption of Cr(VI) ions from aqueous solutions: kinetics, equilibrium, thermodynamics and desorption studies, Colloids and surfaces B: Biointerfaces, 84 (2011) 221-232.
[51] Z. Reddad, C. Gerente, Y. Andres, P. Le Cloirec, Adsorption of several metal ions onto a low-cost biosorbent: kinetic and equilibrium studies, Environmental science & technology, 36 (2002) 2067-2073.
[52] C. Tien, Adsorption Calculations and Modeling, Butterworth-Heinemann, Newton, MA, 1994.
[53] S. Sheshmani, A. Ashori, S. Hasanzadeh, Removal of Acid Orange 7 from aqueous solution using magnetic graphene/chitosan: A promising nano-adsorbent, International Journal of Biological Macromolecules, 68 (2014) 218-224.
[54] M.M. Motsa, B.B. Mamba, J.M. Thwala, T.A.M. Msagati, Preparation, characterization, and application of polypropylene-clinoptilolite composites for the selective adsorption of lead from aqueous media, Journal of Colloid and Interface Science, 359 (2011) 210-219.
[55] X. Wang, Y.S. Chung, W.S. Lyoo, B.G. Min, Preparation and properties of chitosan/poly (vinyl alcohol) blend foams for copper adsorption, Polymer International, 55 (2006) 1230-1235.
[56] Z. Chen, M. Deng, Y. Chen, G. He, M. Wu, J. Wang, Preparation and performance of cellulose acetate/polyethyleneimine blend microfiltration membranes and their applications, Journal of Membrane Science, 235 (2004) 73-86.
[57] J. Zhang, S. Chen, H. Zhang, X. Wang, Removal behaviors and mechanisms of hexavalent chromium from aqueous solution by cephalosporin residue and derived chars, Bioresource technology, 238 (2017) 484-491.
[58] S. Deng, Y.-P. Ting, Characterization of PEI-modified biomass and biosorption of Cu(II), Pb(II) and Ni(II), Water Research, 39 (2005) 2167-2177.
[59] M. Naebe, J. Wang, A. Amini, H. Khayyam, N. Hameed, L.H. Li, Y. Chen, B. Fox, Mechanical property and structure of covalent functionalised graphene/epoxy nanocomposites, Scientific reports, 4 (2014) 4375.

[60] J.B. Lindén, M. Larsson, S. Kaur, W.M. Skinner, S.J. Miklavcic, T. Nann, I.M. Kempson, M. Nydén, Polyethyleneimine for copper absorption II: kinetics, selectivity and efficiency from seawater, RSC Advances, 5 (2015) 51883-51890.
[61] S.S. Abolmaali, A.M. Tamaddon, R. Dinarvand, Nano-hydrogels of methoxy polyethylene glycol-grafted branched polyethyleneimine via biodegradable cross-linking of Zn^{2+}-ionomer micelle template, Journal of nanoparticle research, 15 (2013) 2134.
[62] S.H. Rahaman, R. Ghosh, T.-H. Lu, B.K. Ghosh, Chelating N, N′ -(bis (pyridin-2-yl) alkylidene) propane-1, 3-diamine pseudohalide copper(II) and cadmium(II) coordination compounds: Synthesis, structure and luminescence properties of [M (bpap)(X)] ClO_4 and [M (bpap)$(X)_2$][M= Cu, Cd; X= N_3^-, NCS^-], Polyhedron, 24 (2005) 1525-1532.
[63] K.S. Katti, D. Sikdar, D.R. Katti, P. Ghosh, D. Verma, Molecular interactions in intercalated organically modified clay and clay–polycaprolactam nanocomposites: experiments and modeling, Polymer, 47 (2006) 403-414.
[64] B. Mandal, S.K. Ray, Synthesis of interpenetrating network hydrogel from poly (acrylic acid-co-hydroxyethyl methacrylate) and sodium alginate: modeling and kinetics study for removal of synthetic dyes from water, Carbohydrate Polymers, 98 (2013) 257-269.
[65] S.B. Kuila, S.K. Ray, Separation of benzene–cyclohexane mixtures by filled blend membranes of carboxymethyl cellulose and sodium alginate, Separation and Purification Technology, 123 (2014) 45-52.
[66] X. Zhang, J. Zhang, Z. Liu, C. Robinson, Inorganic/organic mesostructure directed synthesis of wire/ribbon-like polypyrrole nanostructures, Chemical Communications, (2004) 1852-1853.
[67] X. Zhang, X. Pei, Q. Wang, The tribological properties of acid-and diamine-modified carbon fiber reinforced polyimide composites, Materials Chemistry and Physics, 115 (2009) 825-830.
[68] R. Mishra, R. Kumar, S. Kumar, J. Majeed, M. Rashid, S. Sharma, Synthesis and in vitro antimicrobial activity of some triazole derivatives, Journal of the Chilean Chemical Society, 55 (2010) 359-362.
[69] G. Lawrie, I. Keen, B. Drew, A. Chandler-Temple, L. Rintoul, P. Fredericks, L. Grøndahl, Interactions between alginate and chitosan biopolymers characterized using FTIR and XPS, Biomacromolecules, 8 (2007) 2533-2541.
[70] A. Esmaeili, N. Khoshnevisan, Optimization of process parameters for removal of heavy metals by biomass of Cu and Co-doped alginate-coated chitosan nanoparticles, Bioresource technology, 218 (2016) 650-658.
[71] M. Bhaumik, A. Maity, V. Srinivasu, M.S. Onyango, Enhanced removal of Cr(VI) from aqueous solution using polypyrrole/Fe_3O_4 magnetic nanocomposite, Journal of hazardous materials, 190 (2011) 381-390.
[72] J. Wang, Z. Li, Enhanced selective removal of Cu(II) from aqueous solution by novel polyethylenimine-functionalized ion imprinted hydrogel: Behaviors and mechanisms, Journal of hazardous materials, 300 (2015) 18-28.
[73] S. Thakur, S. Pandey, O.A. Arotiba, Development of a sodium alginate-based organic/inorganic superabsorbent composite hydrogel for adsorption of methylene blue, Carbohydrate polymers, 153 (2016) 34-46.

[74] A. Chandramohan, R. Bharathikannan, M. Kandhaswamy, J. Chandrasekaran, R. Renganathan, V. Kandavelu, Synthesis, spectral, thermal and NLO properties of *N, N* - Dimethyl anilinium picrate, Crystal Research and Technology: Journal of Experimental and Industrial Crystallography, 43 (2008) 173-178.
[75] C. Zhang, Q. Ping, Y. Ding, Y. Cheng, J. Shen, Synthesis, characterization, and microsphere formation of galactosylated chitosan, Journal of Applied Polymer Science, 91 (2004) 659-665.
[76] N. Viswanathan, C.S. Sundaram, S. Meenakshi, Removal of fluoride from aqueous solution using protonated chitosan beads, Journal of Hazardous materials, 161 (2009) 423-430.
[77] K. Mohanty, M. Jha, B. Meikap, M. Biswas, Biosorption of Cr(VI) from aqueous solutions by *Eichhornia crassipes*, Chemical Engineering Journal, 117 (2006) 71-77.
[78] Y. Nakano, K. Takeshita, T. Tsutsumi, Adsorption mechanism of hexavalent chromium by redox within condensed-tannin gel, Water research, 35 (2001) 496-500.
[79] Y. Feng, Y. Wang, Y. Wang, X.F. Zhang, J. Yao, In-situ gelation of sodium alginate supported on melamine sponge for efficient removal of copper ions, Journal of colloid and interface science, 512 (2017) 7-13.
[80] A.S.K. Kumar, T. Gupta, S.S. Kakan, S. Kalidhasan, V. Rajesh, N. Rajesh, Effective adsorption of hexavalent chromium through a three center (3c) co-operative interaction with an ionic liquid and biopolymer, Journal of Hazardous materials, 239 (2012) 213-224.
[81] A.S.K. Kumar, N. Rajesh, Exploring the interesting interaction between graphene oxide, Aliquat-336 (a room temperature ionic liquid) and chromium(VI) for wastewater treatment, RSC Advances, 3 (2013) 2697-2709.
[82] S.M. El-Medani, O.A. Ali, R.M. Ramadan, Photochemical reactions of group 6 metal carbonyls with N-salicylidene-2-hydroxyaniline and bis-(salicylaldehyde) phenylenediimine, Journal of Molecular Structure, 738 (2005) 171-177.
[83] S. Kalidhasan, A.S.K. Kumar, V. Rajesh, N. Rajesh, An efficient ultrasound assisted approach for the impregnation of room temperature ionic liquid onto Dowex 1× 8 resin matrix and its application toward the enhanced adsorption of chromium(VI), Journal of Hazardous materials, 213 (2012) 249-257.
[84] A. Haug, Dissociation of alginic acid, Acta Chem. Scand, 15 (1961) 950-952.
[85] J.D. Ziebarth, Y. Wang, Understanding the protonation behavior of linear polyethylenimine in solutions through Monte Carlo simulations, Biomacromolecules, 11 (2009) 29-38.
[86] X. Sun, L. Yang, Q. Li, J. Zhao, X. Li, X. Wang, H. Liu, Amino-functionalized magnetic cellulose nanocomposite as adsorbent for removal of Cr(VI): synthesis and adsorption studies, Chemical Engineering Journal, 241 (2014) 175-183.
[87] P. Miretzky, A.F. Cirelli, Cr(VI) and Cr(III) removal from aqueous solution by raw and modified lignocellulosic materials: a review, Journal of hazardous materials, 180 (2010) 1-19.
[88] U.O. Aigbe, R. Das, W.H. Ho, V. Srinivasu, A. Maity, A novel method for removal of Cr(VI) using polypyrrole magnetic nanocomposite in the presence of unsteady magnetic fields, Separation and Purification Technology, 194 (2018) 377-387.

[89] S. Deng, Y.P. Ting, Polyethylenimine-modified fungal biomass as a high-capacity biosorbent for Cr(VI) anions: sorption capacity and uptake mechanisms, Environmental science & technology, 39 (2005) 8490-8496.
[90] D. Park, Y.-S. Yun, J.M. Park, Reduction of hexavalent chromium with the brown seaweed Ecklonia biomass, Environmental science & technology, 38 (2004) 4860-4864.
[91] H. Guha, K. Jayachandran, F. Maurrasse, Microbiological reduction of chromium(VI) in presence of pyrolusite-coated sand by *Shewanella alga* Simidu ATCC 55627 in laboratory column experiments, Chemosphere, 52 (2003) 175-183.
[92] L. Zhou, Y. Liu, S. Liu, Y. Yin, G. Zeng, X. Tan, X. Hu, X. Hu, L. Jiang, Y. Ding, Investigation of the adsorption-reduction mechanisms of hexavalent chromium by ramie biochars of different pyrolytic temperatures, Bioresource technology, 218 (2016) 351-359.
[93] D.-M. Guo, Q.-D. An, Z.-Y. Xiao, S.-R. Zhai, Z. Shi, Polyethylenimine-functionalized cellulose aerogel beads for efficient dynamic removal of chromium(VI) from aqueous solution, RSC Advances, 7 (2017) 54039-54052.
[94] J. Gustafsson, Visual MINTEQ, Version 3.1, Sweden, https://vminteq.lwr.kth.se/, (2013).
[95] J. Samuel, M. Pulimi, M.L. Paul, A. Maurya, N. Chandrasekaran, A. Mukherjee, Batch and continuous flow studies of adsorptive removal of Cr(VI) by adapted bacterial consortia immobilized in alginate beads, Bioresource technology, 128 (2013) 423-430.
[96] J. Gustafsson, Visual MINTEQ, Version 3.1 Division of Land and Water Resources, Royal Institute of Technology, Stockholm, Sweden http://www2. lwr. kth. se/English/Oursoftware/vminteq/download. html, (2013).
[97] J. Ng, W. Cheung, G. McKay, Equilibrium studies of the sorption of Cu(II) ions onto chitosan, Journal of Colloid and Interface Science, 255 (2002) 64-74.
[98] E. Repo, J.K. Warchol, T.A. Kurniawan, M.E. Sillanpää, Adsorption of Co(II) and Ni(II) by EDTA-and/or DTPA-modified chitosan: kinetic and equilibrium modeling, Chemical Engineering Journal, 161 (2010) 73-82.
[99] K.Y. Foo, B.H. Hameed, Insights into the modeling of adsorption isotherm systems, Chemical Engineering Journal, 156 (2010) 2-10.
[100] A. Baran, E. Bıçak, Ş.H. Baysal, S. Önal, Comparative studies on the adsorption of Cr(VI) ions on to various sorbents, Bioresource Technology, 98 (2007) 661-665.
[101] K. Xiao, F. Xu, L. Jiang, Z. Dan, N. Duan, The oxidative degradation of polystyrene resins on the removal of Cr(VI) from wastewater by anion exchange, Chemosphere, 156 (2016) 326-333.
[102] N. Lazaridis, C. Charalambous, Sorptive removal of trivalent and hexavalent chromium from binary aqueous solutions by composite alginate–goethite beads, Water Research, 39 (2005) 4385-4396.
[103] C. Escudero, N. Fiol, I. Villaescusa, J.-C. Bollinger, Effect of chromium speciation on its sorption mechanism onto grape stalks entrapped into alginate beads, Arabian Journal of Chemistry, 10 (2017) S1293-S1302.
[104] G. Bayramoğlu, M.Y. Arica, Adsorption of Cr(VI) onto PEI immobilized acrylate-based magnetic beads: isotherms, kinetics and thermodynamics study, Chemical Engineering Journal, 139 (2008) 20-28.

[105] V. Gupta, A. Shrivastava, N. Jain, Biosorption of chromium(VI) from aqueous solutions by green algae *Spirogyra* species, Water Research, 35 (2001) 4079-4085.
[106] R. Karthik, S. Meenakshi, Removal of Cr(VI) ions by adsorption onto sodium alginate-polyaniline nanofibers, International Journal of Biological Macromolecules, 72 (2015) 711-717.
[107] S. Periyasamy, V. Gopalakannan, N. Viswanathan, Hydrothermal assisted magnetic nano-hydroxyapatite encapsulated alginate beads for efficient Cr(VI) uptake from water, Journal of Environmental Chemical Engineering, 6 (2018) 1443-1454.
[108] X.-j. Hu, J.-s. Wang, Y.-g. Liu, X. Li, G.-m. Zeng, Z.-l. Bao, X.-x. Zeng, A.-w. Chen, F. Long, Adsorption of chromium(VI) by ethylenediamine-modified cross-linked magnetic chitosan resin: isotherms, kinetics and thermodynamics, Journal of Hazardous materials, 185 (2011) 306-314.
[109] J. Hu, G. Chen, I.M. Lo, Removal and recovery of Cr(VI) from wastewater by maghemite nanoparticles, Water research, 39 (2005) 4528-4536.
[110] K. Hui, C.Y.H. Chao, S. Kot, Removal of mixed heavy metal ions in wastewater by zeolite 4A and residual products from recycled coal fly ash, Journal of hazardous materials, 127 (2005) 89-101.
[111] S. Debnath, A. Maity, K. Pillay, Magnetic chitosan–GO nanocomposite: Synthesis, characterization and batch adsorber design for Cr(VI) removal, Journal of Environmental Chemical Engineering, 2 (2014) 963-973.
[112] T.V. Reddy, S. Chauhan, S. Chakraborty, Adsorption isotherm and kinetics analysis of hexavalent chromium and mercury on mustard oil cake, Environmental Engineering Research, 22 (2016) 95-107.
[113] X.H. Ruan, Y. Xu, X.H. Liao, G.H. He, X.M. Yan, Y. Dai, N. Zhang, L. Du, Polyethyleneimine-grafted membranes for simultaneously adsorbing heavy metal ions and rejecting suspended particles in wastewater, AIChE Journal, 63 (2017) 4541-4548.
[114] Q. Nan, P. Li, B. Cao, Fabrication of positively charged nanofiltration membrane via the layer-by-layer assembly of graphene oxide and polyethylenimine for desalination, Applied Surface Science, 387 (2016) 521-528.
[115] C.C. Feng, J. Xu, M.M. Li, Y.Y. Tang, C.J. Gao, Studies on a novel nanofiltration membrane prepared by cross-linking of polyethyleneimine on polyacrylonitrile substrate, Journal of Membrane Science, 451 (2014) 103-110.
[116] C.J. Liu, L.A. Cheng, Y.F. Zhao, L.P. Zhu, Interfacially crosslinked composite porous membranes for ultrafast removal of anionic dyes from water through permeating adsorption, Journal of Hazardous Materials, 337 (2017) 217-225.
[117] R.S. Hebbar, A.M. Isloor, K. Ananda, A.F. Ismail, Fabrication of polydopamine functionalized halloysite nanotube/polyetherimide membranes for heavy metal removal, Journal of Materials Chemistry A, 4 (2016) 764-774.
[118] V. Jaiswal, S. Saxena, I. Kaur, P. Dubey, S. Nand, M. Naseem, S.B. Sing, P.K. Srivastava, S.K. Barik, Application of four novel fungal strains to remove arsenic from contaminated water in batch and column modes, Journal of Hazardous Materials, 356 (2018) 98-107.
[119] X.W. Li, X.H. Dai, J. Takahashi, N. Li, J.W. Jin, L.L. Dai, B. Dong, New insight into chemical changes of dissolved organic matter during anaerobic digestion of dewatered sewage

sludge using EEM-PARAFAC and two-dimensional FTIR correlation spectroscopy, Bioresource Technology, 159 (2014) 412-420.
[120] J.B. Linden, M. Larsson, S. Kaur, W.M. Skinner, S.J. Miklavcic, T. Nann, I.M. Kempson, M. Nyden, Polyethyleneimine for copper absorption II: kinetics, selectivity and efficiency from seawater, Rsc Advances, 5 (2015) 51883-51890.
[121] X.R. Zhang, X.Q. Pei, Q.H. Wang, The tribological properties of acid- and diamine-modified carbon fiber reinforced polyimide composites, Materials Chemistry and Physics, 115 (2009) 825-830.
[122] S.Y. Wang, T. Vincent, C. Faur, E. Guibal, A comparison of palladium sorption using polyethylenimine impregnated alginate-based and carrageenan-based algal beads, Applied Sciences-Basel, 8 (2018).
[123] Q. Xiao, X.H. Gu, S. Tan, Drying process of sodium alginate films studied by two-dimensional correlation ATR-FTIR spectroscopy, Food Chemistry, 164 (2014) 179-184.
[124] Y.F. Xu, Y. Wang, J.J. Liang, Y. Huang, Y.F. Ma, X.J. Wan, Y.S. Chen, A hybrid material of graphene and poly (3,4-ethyldioxythiophene) with high conductivity, flexibility, and transparency, Nano Research, 2 (2009) 343-348.
[125] D.W. Cho, B.H. Jeon, C.M. Chon, Y. Kim, F.W. Schwartz, E.S. Lee, H. Song, A novel chitosan/clay/magnetite composite for adsorption of Cu(II) and As(V), Chemical Engineering Journal, 200 (2012) 654-662.
[126] L. Ayed, K. Chaieb, A. Cheref, A. Bakhrouf, Biodegradation and decolorization of triphenylmethane dyes by *Staphylococcus epidermidis*, Desalination, 260 (2010) 137-146.
[127] A.B. Hegge, T. Andersen, J.E. Melvik, E. Bruzell, S. Kristensen, H.H. Tonnesen, Formulation and bacterial phototoxicity of curcumin loaded alginate foams for wound treatment applications: Studies on curcumin and curcuminoides XLII, Journal of Pharmaceutical Sciences, 100 (2011) 174-185.
[128] B.N. Dickhaus, R. Priefer, Determination of polyelectrolyte pK_a values using surface-to-air tension measurements, Colloids and Surfaces a-Physicochemical and Engineering Aspects, 488 (2016) 15-19.
[129] S.I. Ishikawa, S. Sekine, N. Miura, K. Suyama, K. Arihara, M. Itoh, Removal of selenium and arsenic by animal biopolymers, Biological Trace Element Research, 102 (2004) 113-127.
[130] H.Y. Peng, N. Zhang, M. He, B.B. Chen, B. Hu, Simultaneous speciation analysis of inorganic arsenic, chromium and selenium in environmental waters by 3-(2-aminoethylamino) propyltrimethoxysilane modified multi-wall carbon nanotubes packed microcolumn solid phase extraction and ICP-MS, Talanta, 131 (2015) 266-272.
[131] C. Evelina Rodriguez-Martinez, Z. Ivonne Gonzalez-Acevedo, M. Teresa Olguin, H. Frias-Palos, Adsorption and desorption of selenium by two non-living biomasses of aquatic weeds at dynamic conditions, Clean Technologies and Environmental Policy, 18 (2016) 33-44.
[132] J.P. Gustafsson, Visual MINTEQ, ver. 3.1, in, KTH, Royal Institute of Technology, (url: https://vminteq.lwr.kth.se/; accessed May 2017), Stockholm, Sweden, 2013.
[133] J.P. Simonin, On the comparison of pseudo-first order and pseudo-second order rate laws in the modeling of adsorption kinetics, Chemical Engineering Journal, 300 (2016) 254-263.

[134] C. Vincent, A. Hertz, T. Vincent, Y. Barre, E. Guibal, Immobilization of inorganic ion-exchanger into biopolymer foams - Application to cesium sorption, Chemical Engineering Journal, 236 (2014) 202-211.
[135] Y.S. Ho, G. McKay, Pseudo-second order model for sorption processes, Process Biochemistry, 34 (1999) 451-465.
[136] T.W. Weber, R.K. Chakravorti, Pore and solid diffusion models for fixed-bed adsorbers, AIChE Journal, 20 (1974) 228-238.
[137] S. Bhowmick, S. Chakraborty, P. Mondal, W. Van Renterghem, S. Van den Berghe, G. Roman-Ross, D. Chatterjee, M. Iglesias, Montmorillonite-supported nanoscale zero-valent iron for removal of arsenic from aqueous solution: Kinetics and mechanism, Chemical Engineering Journal, 243 (2014) 14-23.
[138] N. Gezer, M. Gulfen, A.O. Aydin, Adsorption of selenite and selenate ions onto thiourea-formaldehyde resin, Journal of Applied Polymer Science, 122 (2011) 1134-1141.
[139] Y. Wu, Y. Chi, H. Bai, G. Qian, Y. Cao, J. Zhou, Y. Xu, Q. Lu, Z.P. Xu, S. Qiao, Effective removal of selenate from aqueous solutions by the Friedel phase, Journal of Hazardous Materials, 176 (2010) 193-198.
[140] T. Nishimura, H. Hashimoto, M. Nakayama, Removal of selenium(VI) from aqueous solution with polyamine-type weakly basic ion exchange resin, Separation Science and Technology, 42 (2007) 3155-3167.
[141] M. Szlachta, N. Chubar, The application of Fe-Mn hydrous oxides based adsorbent for removing selenium species from water, Chemical Engineering Journal, 217 (2013) 159-168.
[142] R.-X. Zhou, J.-H. Zhao, Z.-M. Wei, Simulation and optimization of the selenium recovery process using the continuous counter-current decantation ion exchange system, Chemical Engineering Journal, 191 (2012) 386-393.
[143] R. Kamaraj, S. Vasudevan, Decontamination of selenate from aqueous solution by oxidized multi-walled carbon nanotubes, Powder Technology, 274 (2015) 268-275.
[144] Y.T. Chan, W.H. Kuan, T.Y. Chen, M.K. Wang, Adsorption mechanism of selenate and selenite on the binary oxide systems, Water Research, 43 (2009) 4412-4420.
[145] J.S. Yamani, A.W. Lounsbury, J.B. Zimmerman, Adsorption of selenite and selenate by nanocrystalline aluminum oxide, neat and impregnated in chitosan beads, Water Research, 50 (2014) 373-381.
[146] W. Cui, P. Li, Z. Wang, S. Zheng, Y. Zhang, Adsorption study of selenium ions from aqueous solutions using MgO nanosheets synthesized by ultrasonic method, Journal of Hazardous Materials, 341 (2018) 268-276.
[147] M. Li, A. Dopilka, A.N. Kraetz, H. Jing, C.K. Chan, Layered double hydroxide/chitosan nanocomposite beads as sorbents for selenium oxoanions, Industrial & Engineering Chemistry Research, 57 (2018) 4978-4987.
[148] Y.N. Larimi, M.H. Mallah, M.A. Moosavian, J. Safdari, Kinetic and equilibrium study of selenium removal from wastewater in mag-molecular process, Desalination and Water Treatment, 57 (2016) 933-948.
[149] N. Bleiman, Y.G. Mishael, Selenium removal from drinking water by adsorption to chitosan-clay composites and oxides: Batch and columns tests, Journal of Hazardous Materials, 183 (2010) 590-595.

[150] S.L. Lo, T.Y. Chen, Adsorption of Se(IV) and Se(VI) on an iron-coated sand from water, Chemosphere, 35 (1997) 919-930.
[151] L.V. Constantino, J.N. Quirino, A.M. Monteiro, T. Abrao, P.S. Parreira, A. Urbano, M.J. Santos, Sorption-desorption of selenite and selenate on Mg-Al layered double hydroxide in competition with nitrate, sulfate and phosphate, Chemosphere, 181 (2017) 627-634.
[152] H. Dong, Y. Chen, G. Sheng, J. Li, J. Cao, Z. Li, Y. Li, The roles of a pillared bentonite on enhancing Se(VI) removal by ZVI and the influence of co-existing solutes in groundwater, Journal of Hazardous Materials, 304 (2016) 306-312.
[153] Z. Ma, C. Shan, J. Liang, M. Tong, Efficient adsorption of selenium(IV) from water by hematite modified magnetic nanoparticles, Chemosphere, 193 (2018) 134-141.
[154] Y.T. Chan, Y.T. Liu, Y.M. Tzou, W.H. Kuan, R.R. Chang, M.K. Wang, Kinetics and equilibrium adsorption study of selenium oxyanions onto Al/Si and Fe/Si coprecipitates, Chemosphere, 198 (2018) 59-67.
[155] M. Min, C. Shen, L. Fang, B. Zhu, J. Li, L. Yao, Y. Jiang, C. Xiong, Design of a selective regenerable cellulose microcolumn for selenium efficient recovery and economic determination, Chemical Engineering Research & Design, 117 (2017) 773-783.
[156] N.K. Asmel, A.R.M. Yusoff, S.K. Lakkaboyana, Z.A. Majid, S. Salmiati, High concentration arsenic removal from aqueous solution using nano-iron ion enrich material (NIIEM) super adsorbent, Chemical Engineering Journal, 317 (2017) 343-355.
[157] B. Chen, Z. Zhu, Y. Guo, Y. Qiu, J. Zhao, Facile synthesis of mesoporous Ce-Fe bimetal oxide and its enhanced adsorption of arsenate from aqueous solutions, Journal of Colloid and Interface Science, 398 (2013) 142-151.
[158] C. Sellitti, J.L. Koenig, H. Ishida, Surface characterization of graphitized carbon-fibers by attenuated total reflection Fourrier-transform infrared spectroscopy, Carbon, 28 (1990) 221-228.
[159] D. Peak, D.L. Sparks, Mechanisms of selenate adsorption on iron oxides and hydroxides, Environmental Science & Technology, 36 (2002) 1460-1466.
[160] N. Chubar, EXAFS and FTIR studies of selenite and selenate sorption by alkoxide-free sol-gel generated Mg-Al-CO_3 layered double hydroxide with very labile interlayer anions, Journal of Materials Chemistry A, 2 (2014) 15995-16007.
[161] J. Ma, Y. Wang, L. Zhou, S. Zhang, Preparation and characterization of selenite substituted hydroxyapatite, Materials Science & Engineering C-Materials for Biological Applications, 33 (2013) 440-445.
[162] W. Zhang, Y. Chai, N. Cao, Y. Wang, Synthesis and characterization of selenium substituted hydroxyapatite via a hydrothermal procedure, Materials Letters, 134 (2014) 123-125.
[163] R.C. Elder, P.E. Ellis, Selenite complexes with pentaamminecobalt(III) - O-bound and Se-bound forms, Inorganic Chemistry, 17 (1978) 870-874.
[164] Y.-Z. Yan, Q.-D. An, Z.-Y. Xiao, S.-R. Zhai, B. Zhai, Z. Shi, Interior multi-cavity/surface engineering of alginate hydrogels with polyethylenimine for highly efficient chromium removal in batch and continuous aqueous systems, Journal of Materials Chemistry A, 5 (2017) 17073-17087.

[165] B. Qiu, J. Guo, X. Zhang, D. Sun, H. Gu, Q. Wang, H. Wang, X. Wang, X. Zhang, B.L. Weeks, Z. Guo, S. Wei, Polyethylenimine facilitated ethyl cellulose for hexavalent chromium removal with a wide pH range, Acs Applied Materials & Interfaces, 6 (2014) 19816-19824.
[166] J.F. Moulder, Handbook of X-ray photoelectron spectroscopy, Physical electronics, (1995) 230-232.

Chapter 3 Investigation of mercury(II) and copper(II) sorption in single and binary systems by alginate/polyethylenimine membranes

3.1. Introduction Générale

L'étude illustrée par le Chapitre II a permis de mettre en évidence les propriétés d'adsorption des membranes PEI/alginate pour des solutions mono-élémentaires de Cr(VI) et Se(VI) par un mécanisme d'échange d'ions/attraction électrostatique mettant en jeu des interactions entre les anions métalliques et les fonctions aminées protonées.

Dans le Chapitre III, l'attention est portée sur l'étude de l'adsorption du mercure et du cuivre, à la fois en solutions mono-élémentaires mais aussi en solution mixte. Ces deux ions métalliques sont caractérisés par des comportements différents en termes de spéciation et par une grande stabilité en terme de stabilité redox (dans les conditions expérimentales sélectionnées aucun de ces deux ions métalliques ne subit de réduction, contrairement aux cas de Cr(VI) et Se(VI)). Ainsi, en milieu HCl, le mercure en solution peut former des complexes anioniques alors que le cuivre reste sous sa forme libre. Comparer le comportement de ces deux ions métalliques permettra donc de mettre en évidence l'impact de la spéciation non seulement sur les performances d'adsorption (incluant la caractérisation des propriétés de sélectivité) mais aussi sur les mécanismes d'adsorption mis en jeu. Afin de mettre en évidence les mécanismes réactionnels impliqués dans la fixation de ces ions métalliques,, une première partie de l'étude analyse les matériaux par spectroscopie FTIR et par MEB couplée à la spectroscopie de rayons X à dispersion d'énergie . Puis l'effet du pH sur l'adsorption des deux ions métalliques est analysé, pour des solutions mono-élémentaires, en corrélant la spéciation des métaux et l'état ionique des groupements fonctionnels présents en surface de l'adsorbant. La comparaison des profils peut représenter une première indication sur les conditions opératoires à mettre en œuvre pour faciliter la séparation des ions métalliques. L'étude se poursuit par une investigation des cinétiques de fixation et des isothermes d'adsorption à pH 5. Dans un premier temps, les isothermes sont réalisées avec des solutions mono-élémentaires, avant de tester l'adsorption en solutions binaires en faisant varier les conditions de concentrations molaires pour les deux ions métalliques (Hg(II)/Cu(II) : 4/1, 1/1 et 1/4). Cette partie complète l'approche séparative initiée dans le cadre de l'étude de l'effet du pH. Si le choix du pH permet d'anticiper, dans des conditions optimales, la séparation des deux ions métalliques, cette partie de l'étude permet en effet d'évaluer la préférence éventuelle des membranes PEI/Alginate pour l'un des deux métaux (y compris dans des conditions moins favorables de séparation par le pH). Cette partie est complétée par une approche de modélisation des isothermes d'adsorption (en solution mono-élémentaires et en solutions binaires), réalisée en particulier en traçant les surfaces tridimensionnelles des isothermes d'adsorption (après régression non-linéaire afin de déterminer les paramètres du modèle de Sips étendu aux solutions binaires).

Ce chapitre fait l'objet d'un article qui est prévu d'être soumis dans Journal of Hazardous Materials : 5. **Yayuan Mo**, Thierry Vincent, Catherine Faur, and Eric Guibal. Investigation of Hg(II) and Cu(II) sorption in single and binary systems by alginate/polyethylenimine membranes. In preparation.

3.2. Introduction

Industrialization and technological development have made life easier than before, while also exposing our global environment and human civilization to high levels of pollution. Pollution of water by heavy metals is one of the global problems, since effluents containing various toxic metals has been directly or indirectly discharged from some industrial processes such as electroplating, smelting, printing and mining into the natural environment [1, 2]. The commonly contained heavy metals in effluents like Pb (II), Cu (II), Cr (VI), Hg (II), and As (V) are harmful to human health and ecosystems because of their highly toxicity, bioaccumulation and persistence, even at low concentrations [3, 4]. These metals often exist in the forms of cations and anions (including oxyanions and chloro-anions) in aqueous solution with different or even opposite properties. It is interesting to find an economical and effective method or material for the removal and recovery of these metals from aqueous systems.

Sorption, one of wastewater treatment methods which can minimize the hazardous effects of metals in the aqueous environment, has been shown to be an economically feasible alternative for the removal of metals [5, 6]. Alginate as a non-toxic, abundant, cheap, renewable, biocompatible, and biodegradable biopolymer containing a number of free hydroxyl and carboxyl groups, which is available to use for metal ions binding and new sorbent preparation [7]. Many reports have formulated conditioned alginate into various forms alginate-based materials like hydrogels, beads and fibers by means of functional modifications such as crosslinking and applied them to absorb metal ions since their inherent properties including gelling ability, tailorable morphology, further functionalization and strong affinity of metal ions [8-10]. According to these increasing literatures, improving the stability of alginate-based materials, achieving the facile solid-liquid separation and enhancing the recyclability and reusability are become the challenges in industrial applications [11, 12].

Recently, we have prepared alginate/polyethylenimine (A-PEI) membranes though reacting anionic carboxyl groups of negatively charged alginate solution with cationic amine groups of positively charged PEI to form membrane gel, followed by a stabilizing crosslinking via a Schiff-base reaction of primary amine groups (on PEI) using glutaraldehyde (GA) [13]. The fabrication procedure is easy to achieve without complicated operating conditions and high energy consuming like freeze-drying process. Remarkably, the as-prepared membrane with high permeability are able to achieve outstanding natural drainage properties combined with high affinity for oxyanions Cr(VI) and Se(VI) recovery from aqueous solution [13, 14]. In the other side, it is still interesting to explore the applicability of this percolating membranes towards other forms of metal ions with different electrical properties such as cations and chloride anions. In this study, two representative metals

Cu(II) and Hg(II) are selected as models of pollutants to study the sorption performance of the A-PEI membrane in not only mono-component solution but also binary mixture since multi-metal systems are more meaningful and closer with actual wastewaters. Theoretically, Cu(II) is a widespread heavy metal presented in stable cationic status in aqueous solution which can be bound on amine groups through chelation and electrostatic attracted by negative charged groups, while Hg(II) will be able to form chloride anions (such as $HgCl_3^-$, $HgCl_4^{2-}$) in the present of chloride ions and this anions can be easily attracted by protonated amine groups through electrostatic interaction [15, 16]. In addition, copper ions are usually accompanied by mercury ions presented in effluents from a variety of industrial processes like chlor-alkali production, battery manufacturing and cosmetic preparations so on [17].

Thus, the main objectives of this work are to (1) assess the sorption and competitive sorption behaviors of the A-PEI membranes for the recovery of Cu(II) and Hg(II) in the single and binary metal ion systems at different pH values and different initial concentrations; (2) explore mechanism of the cationic Cu(II) ions and chloro-anionic Hg(II) ions binding onto the membranes using FTIR and SEM-EDX techniques and isotherms and kinetics modeling. Moreover, the selectivity of the membrane towards Cu(II) and Hg(II) is analyzed by plotting the three-dimensional surfaces of the adsorption isotherms, which is extremely valuable for the further engineering application of the as-prepared membrane in the heavy metals treatment.

3.3. Materials and methods

3.3.1. Chemicals and materials

Metal salts like chloride (II) nitrate ($HgCl_2$, 99.5%) and copper (II) nitrate ($Cu(NO_3)_2$, 99.5%) were purchased from Fluka (Switzerland). Sodium alginate powder (commercial reference: Protanal 200S, molar mass (M_w) = 4.46×10^5 g mol^{-1}, M/G ratio of 0.16/0.84) was provided by FMC BioPolymer (Ayr, UK). Branched polyethylenimine (PEI, M_w =7.5×10^5 g mol^{-1}) and glutaraldehyde (GA) in 50 % w/w aqueous solution were purchased from Sigma–Aldrich (Saint-Louis, USA). All chemicals used in this study were of analytical grade and demineralized (DI) water was used in the whole study.

3.3.2. Synthesis of membranes

The procedure of A-PEI membrane sorbents synthesis was reported previously [13]. Four grams of alginate powder were dissolved in 100 mL of DI water under vigorous stirring to obtain a homogeneous alginate mixture (4%, w/w). Diluting 100 g of 4 % alginate mixture into a total amounts of 500 g solution with DI water. In the next step, 35 mL of 4 % PEI (pH = 6.5) was added into the solution under strong stirring (7 times: 5 mL every 10 s). After stirring well, the mixture was rapidly poured into a rectangular container and maintained at room temperature for 24 h to complete the reaction between PEI and alginate and form the membrane. Fabricated membranes can be shaped into different sizes by using different containers. After that, the composite membrane

was carefully washed three times and further crosslinking by immersing into 300 mL of DI water with 2.5 mL of 50 % GA and slow shaking at 30 rpm for 24 h. Finally, the A-PEI membrane obtained by thoroughly washed and air-dried at room temperature.

3.3.3. Characterization

FTIR spectra of materials were scanned in the region of 4000-400 cm^{-1} in an FTIR Bruker VERTEX70 spectrometer (Bruker, Germany) though a Smart Orbit Accessory for Single-Reflection Attenuated Total Reflectance (ATR). The surface morphologies and elemental compositions of materials were examined by a scanning electron microscope (SEM, Quanta FEG 200, Thermo Fisher Scientific, Mérignac, France) equipped with an Energy dispersive X-ray accessory (EDX, Oxford Instruments France, Saclay, France).

3.3.4. Sorption experiments

The Cu(II) (10 mmol L^{-1}) or Hg(II) (10 mmol L^{-1}) stock solution was prepared by dissolving appropriate amounts of $HgCl_2$ or $Cu(NO_3)_2$ into DI water, respectively, then further diluted to obtain working solutions. The working mono-component solution was obtained by separately diluting 10 mmol L^{-1} of Cu(II) and Hg(II) stock solution to the desired concentration, while the binary Cu(II) and Hg(II) solution were obtained by mixing the required amounts of Cu(II) and Hg(II) stock solution in the working medium. Before contacting with the sorbents, the pH of each metal solution was adjusted to the required value using 1 M HCl or NaOH solution. Batch sorption experiments were performed in a continuous treatment device (see section 2.3.4, Figure 2-2).

The solution pH effect was firstly investigated in the initial pH range of 1-6 by contacting 0.5 g L^{-1} of sorbent with 0.5 mmol L^{-1} of mono-component (Cu(II) or Hg(II)) solution or 1.0 mmol L^{-1} of [Hg-Cu] (Hg(II) and Cu(II) at equimolar concentrations) binary solution, respectively. After 3 days of agitation (100 rpm), the equilibrium pH values were recorded on a pH-meter Cyber Scan pH 6000 (Eutech instruments, Nijkerk, the Netherlands).The samples were subsequently filtered by filter papers (Ø 25 mm, 1.-2 µm pore size, Prat-Dumas, France); all the residual metal ion concentration was analyzed by inductively coupled plasma atomic emission spectrometry (ICP-AES, JY Activa M, Jobin-Yvon, Horiba, Longjumeau, France).

The kinetics parameters were performed only in the single system with a recirculation mode; a given amount of sorbent (i.e., 210 mg) was contact with 1L of 0.25 mmol L^{-1} metal ions (Cu(II) or Hg(II)) solution at pH 5. Samples were collected at regular time intervals and filtered for metal ion analysis.

The series sorption isotherm experiments were evaluated in single and binary systems at pH 5 with a sorbent dose of 0.6 g L^{-1} for 3 days to reach equilibrium. For the single system, batch sorption tests were performed on varying initial concentrations 0.1 to 2 mmol L^{-1} Cu(II) or Hg(II) solution; while for binary systems, the tests were performed in three parts: one part contains Cu(II) and Hg(II) in concentrations each varying from 0.1 to 2 mmol L^{-1} with molar ratio of 1:1; another two parts

contain Cu(II) and Hg(II) in concentrations each varying from 0.1 to 2.8 mmol L^{-1} with molar ratios of 1:4, 4:1.

The amounts of metal adsorbed per unit of sorbent or sorption capacity (q_{eq}, mmol g^{-1}) was calculated under a given amount of sorbent (m, g) with a given volume (V, L) though the equation: $q_{eq} = (C_0\text{-}C_{eq})*V/m$, where C_0 and C_{eq} are the initial and residual concentrations (mmol L^{-1}), respectively; while the desorption efficiency (DE, %) was obtained by the comparison of the amounts of metal successively adsorbed and desorbed: DE (%) = (amount of metal desorbed / amount of metal sorbed) *100.

All experiments were performed at room temperature (20±1 ◦C), and mostly of experiments were conducted in parallel and the results were presented as the average values and standard deviation (SD).

3.4. Results and discussion

3.4.1. Sorbent characterization

FTIR is the most widely used technique for characterizing the main bands corresponding to the functional groups of materials [18]. The raw sorbent, the sorbents after reacting with Hg(II) and Cu(II) at pH 5.0 in both single and binary systems are analyzed by FTIR-ATR spectroscopy (in the range of 4000-400 cm^{-1}). The FTIR spectra and the assignments of the main peaks are presented in Figure 3-1 and Table 3-1. Based on Figure 3-1, the main peaks of raw membrane are characterized at 3280 cm^{-1} (N–H and O–H stretching vibrations, including their overlapping), 2927 cm^{-1} (C–H stretching), 1593 cm^{-1} (N–H bending and C=N vibration), 1406 cm^{-1} (COO^- symmetric stretching), 1316 cm^{-1} (C–N stretching vibration), 1089 cm^{-1} and 1030 cm^{-1} (C–O stretching vibration), and 947 cm^{-1} (C–H deformation) [13]. After metal ions sorption reaction in both single and binary systems, several similar changes are observed:

(a) shift of the strong and wide peak at 3280 cm^{-1} due to the stretching vibration of amine and hydroxyl groups [19]. It is noteworthy that the change of Cu(II)-loaded membrane is less marked compare to that of Hg(II)-loaded membrane. This means the involvement of amine and hydroxyl groups with Hg(II) is stronger in the case of mercury sorption;

(b) shift of the peak at 2928 cm^{-1} (C–H stretching vibration); this means that C–H groups or their neighbor reactive groups are involved in metals binding process [20];

(c) shift and intensity decrease of the peak at 1316 cm^{-1} (C–N stretching vibration, resulting from the interaction between amine groups of PEI and aldehyde groups of GA), which related with both metals binding;

(d) slight decrease of the intensity of the peaks at 1406 cm^{-1} and 1030 cm^{-1} are assigned to COO^- symmetric stretching and C-O skeletal stretching vibrations of the carboxylate groups in alginate [21]. This means carboxylate groups play a role in the sorption of Hg(II) and Cu(II).

In addition, it is noteworthy that the intensity of the peak at 1592 cm^{-1} have a slight decrease after Hg(II) sorption and Hg-Cu sorption; this may be caused by the vibrations of N–H (assigned to the primary amine groups of PEI) and C=N (due to the formation of Schiff bases generated by the reaction between PEI and GA) [22, 23]. The intensity decrease may be explained by the contribution of protonated amine groups in the specific binding of mercury species.

These analyses have thus shown that O–H, N–H, C–H, C–O and C–N identified on the membrane might participate in the process of Hg(II) and Cu(II) ions sorption, with a specific involvement of protonated amine groups in the case of mercury sorption.

SEM-EDX measurement is applied for analyzing the surface morphologies and elemental compositions of the membranes before and after metal ions sorption (shown in Figure 3-2). The SEM images show that the prepared membrane has a porous structure with macro-porosity. It is apparent that there are aggregates in the material after reaction with Hg(II) regardless of the single or binary system; this indicates that the membrane has a great affinity on mercury ions. Indeed, the EDX spectrum of raw membrane displays the presence of C and O elements (exceed 96% in total, organic tracers) but also S, Na, Ca, Cl, Si, Mg and Al elements (residues of the extraction/shaping process of alginate), while after Hg(II) sorption the species of elements on the membrane dramatically decreases and even only C, O, Hg and Cl remains; this reveals that mercury ions are strong competitive compared to other elements onto the membrane. Simultaneously, the large increase in the content of chloride ions from 0.2% to 2.7-3% means that the fixation of mercury onto the membrane are in the form of a complex of mercury chloride; this also confirms that mercury is bound to the membrane in the form of chloro-mercury ions. On the contrary, the change of element composition on the membrane after Cu(II) sorption is less obvious compare to Hg sorption, except that the completely disappears of sodium ions, which may be caused by the ion exchange interaction between Cu^{2+} and Na^+ ions. The mapping of Cu element also shows the homogeneous distribution of Cu ions binding on the membrane. In conclusion, the presences of mercury and copper peaks in the membrane confirm their successful loading onto the membrane. Copper ions are distributed densely and homogeneously on the surface of the sorbent, while Hg elements are found uniformly distributed on the surface of material even with a few aggregates.

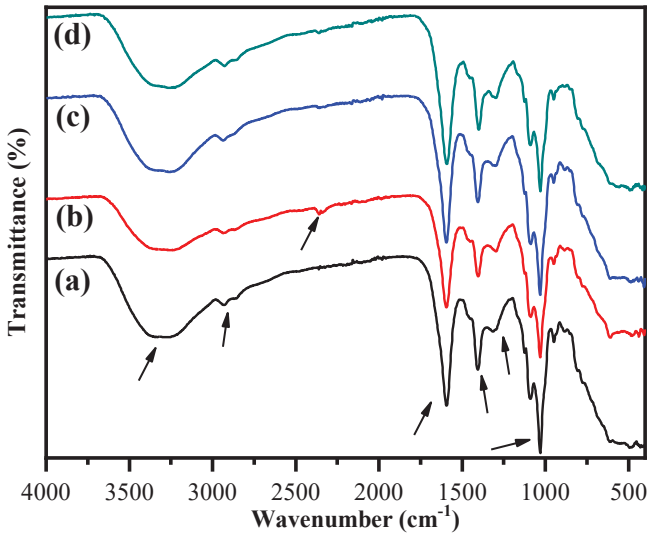

Figure 3-1 FTIR spectra of membranes (a) raw; (b) after Hg(II) sorption; (C) after Cu(II) sorption and (d) after Hg(II)-Cu(II) sorption.

Table 3-1 Assignments of main FTIR bands of membranes (a) raw; (b) after Hg(II) sorption; (C) after Cu(II) sorption and (d) after Hg(II)-Cu(II) sorption.

(a) (cm^{-1})	(b) (cm^{-1})	(c) (cm^{-1})	(d) (cm^{-1})	Band Assignment	Reference
3280	3236	3254	3242	N–H and O–H or their overlaps stretching	[19]
2927	2936	2937	2931	C–H stretching	[20]
1593	1595	1595	1596	N–H bending and C=N vibration	[24]
1406	1403	1405	1405	COO^- symmetric stretching	[25]
1316	1296	1297	1296	C–N stretching	[23]
1089	1087	1087	1088	C–O stretching	[26]
1030	1030	1031	1031	C–O stretching	[21]
948	949	949	950	C–H deformation	[27]

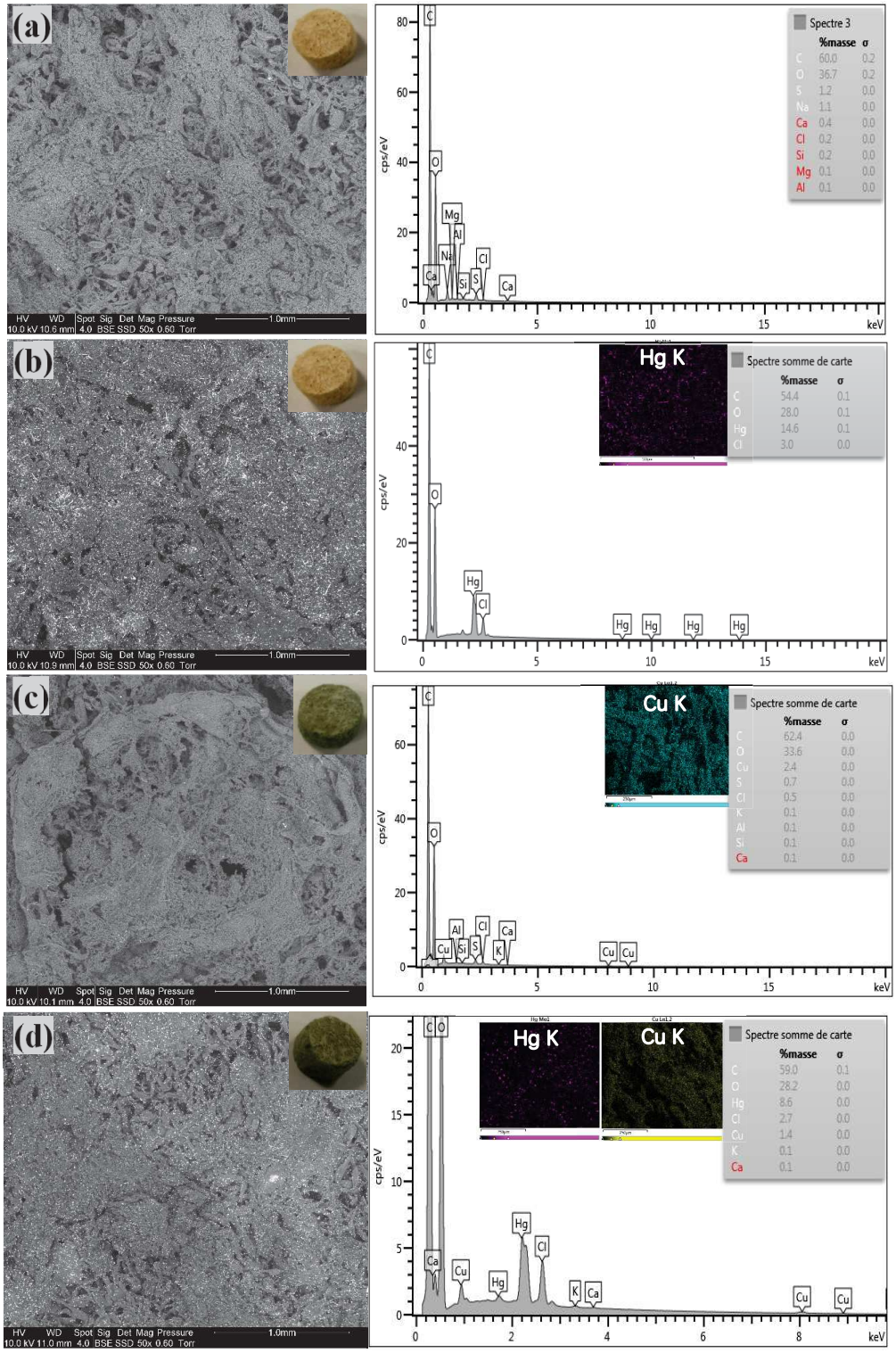

Figure 3-2 SEM image and EDX mapping of membranes (a) raw; (b) after Hg(II) sorption; (C) after Cu(II) sorption and (d) after Hg(II)-Cu(II) sorption.

3.4.2. Effect of pH

Solution pH may affect the sorption behavior by changing the charge characteristics of sorbent and speciation of adsorbate [28]. The pH effect of this study on metal ions binding onto the membrane was investigated in both single and binary systems. To avoid the precipitation phenomenon of metal ions, pH variation was limited to 6 and the results are presented in Figure 3-3. From the figure, it clearly demonstrates that the solution pH (varying from 1 to 6) has a significant impact on Cu(II) ions binding, while for the Hg(II) recovery, the change on sorption capacities of metals is slight with the pH regardless of in single or binary systems. It is remarkable that the membrane sorbents maintain a high affinity to Hg(II) ions under the widely selected pH range, and its sorption capacity is higher than that of Cu(II). This significant difference between Hg(II) and Cu(II) sorption can be correlated with the properties of the active functional groups on sorbents and the physicochemical properties of the metals (such as ionic radii and ionic charge) [29-32]. For example, Vieira et al. [33] studied the sorption of binary mixtures of Cu and Hg ions using chitosan membranes. They reported that the adsorption capacity for Hg(II) was higher than for Cu(II) is probably due to the higher ionic radii of Hg(II) (i.e., 1.02 Å) compared to Cu(II) (i.e., 0.73 Å).

More particularly, Cu(II) ions are mostly present in cationic form under the pH range 1 to 6 [34]. For Cu sorption, it is obvious that at low pH (below pH 2) the sorption capacity (not exceed 0.006 mmol g^{-1}) can be negligible in both single and binary systems and subsequent present an increasing trend as the pH increases from 2 to 6. This may be associated to the protonation of functional groups such as carboxylic groups (existed in alginate) at the surface of membranes. As previously reported, the pK_a values of carboxylic groups in alginate are usually reported at 3.38 and 3.65 for mannuronic acid and guluronic acid, respectively [35]. Thus, the deprotonation of the carboxylic groups ($COOH \rightarrow COO^- + H^+$) progressively increases with the increasing pH (especially when pH higher than 3.6), which are favorable to the sorption of Cu(II) cations [36]. Indeed, the steep increase of Cu(II) sorption capacity in both single and binary systems is observed around pH 3.6 shown in Figure 3-3; similar conclusions also be reported by Wang et al. [23]. On the other hand, many studies have reported PEI to be a specific ligand for various metal ions and Cu(II) can be bound on the donating nitrogen atoms of PEI by chelation in near-neutral solutions [37, 38].Therefore, Cu(II) ions also can be chelated on nitrogen with the pH increase to 6. Moreover, the maximum Cu(II) sorption capacities reach to 0.44 mmol g^{-1} in single solution and 0.37 mmol g^{-1} in binary solution at the initial of pH 6. This indicates that the presence of Hg(II) ions will compete with Cu(II) ions and weaken the ability of Cu(II) ions binding onto the membrane.

In the case of Hg(II), Figure 3-3 shows that the membrane can efficiently remove Hg(II) from both single and binary component systems within a wide pH range (1-6) and the presence of Cu(II) ions with the same concentration has no significant effect on Hg sorption capacity: the Hg(II) sorption capacities slightly increased from 0.76 mmol g^{-1} (at pH 1) to 0.84 mmol g^{-1} (around pH 5) in these systems. This phenomenon may be caused by the special property of Hg(II) which can form chloro-

complexes in the presence of Cl^- ions. As reported by Ranganathan [39], the different accumulations of Cl^- ions can cause the formation of various species of Hg complex including $HgCl_2$, $HgCl^+$, $HgCl_3^-$ and $HgCl_4^{2-}$. Figure 3-4 shows the speciation of mercury (C_0: 0.5 mmol L^{-1}) as a function of pH in the corresponding concentration of chloride ion (calculated with the Visual Minteq). In this case, it can be seen that the predominant mercury species are $HgCl_2$, $HgCl_3^-$ and $HgCl_4^{2-}$ under the selected pH range (i.e., 0-4). It is noteworthy that the uncharged species $HgCl_2$ presents in significant amount (representing 90-98%) in the range of pH 2−4. However, the sorption capacities of Hg(II) ions are almost unchanged in different pH though the proportion of neutral ($HgCl_2$) and negatively charged species ($HgCl_3^-$ and $HgCl_4^{2-}$) significant changed; this indicates that all these three species (including neutral $HgCl_2$) are absorbed by the membrane. The SEM-EDX analysis of Hg(II)-loaded membranes after metals sorption at initial pH 5 (i.e. pH_{eq} 3.6) also confirmed the $HgCl_2$ is taken up by the membrane. Apparently, these chloro-anions ($HgCl_3^-$ and $HgCl_4^{2-}$) are readily bound in protonated amine groups of PEI (the apparent pKa's of PEI are 4.5, 6.7 and 11.6 for primary, secondary and tertiary amines, respectively) by electrostatic interactions [40]. However, for the neutral $HgCl_2$ species, their uptakes in the sorbents can be explained by the possibility of the interaction between these species with the carboxylic acid moiety of alginate and the donating nitrogen atoms of PEI, which is in accordance with the findings obtained by FTIR. Indeed, Sarkar et al. [41] in the study of Hg(II) adsorption by calcium alginate hydrogels pointed out that the uncharged $HgCl_2$ is free to interact with the available sites of the carboxylic acid moiety by hydrogen bonding or van der Waal's forces. Devi et al. [42] in the study of Hg(II) adsorption by chemically synthesized polyaniline also revealed that mercury-chloride anions can be bound on the protonated amine groups whereas neutral $HgCl_2$ species interact with unprotonated nitrogen. In addition, it is noteworthy that at extremely acidic condition (pH =1), the sorption capacity has a little decrease; this may be caused by the excess of chloride ions leading to a competition effect which in turn limited uptake ability [43]. More interestingly, at low pH (pH 1 to 2) the membrane sorbent exhibits a high affinity for Hg (0.76-0.81 mmol g^{-1}), while the uptake for Cu are less than 0.006 mmol g^{-1}; this indicates that the membrane is superior acid-resistant and has an extraordinarily high selectivity of Hg over Cu in an acidic environment.

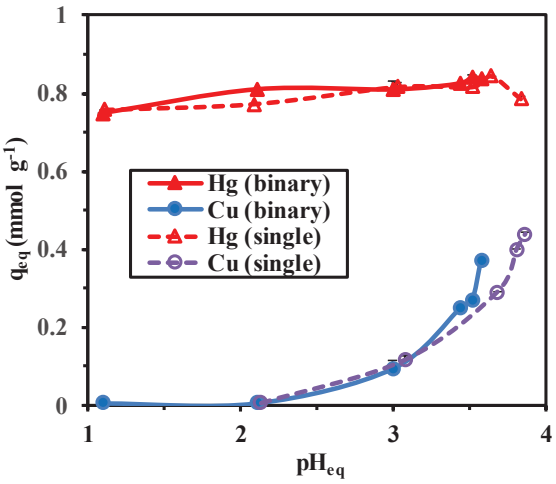

Figure 3-3 Effect of pH on metal ions sorption in both single and binary systems (Metal concentration: 0.5 mmol L^{-1} of Cu(II) or Hg(II) single solution and 1.0 mmol L^{-1} of mixed [Hg(II):Pb(II)=1:1] solution; Sorbent dosage = 0.5 g L^{-1}; contact time = 3 days; temperature = 20± 1 °C).

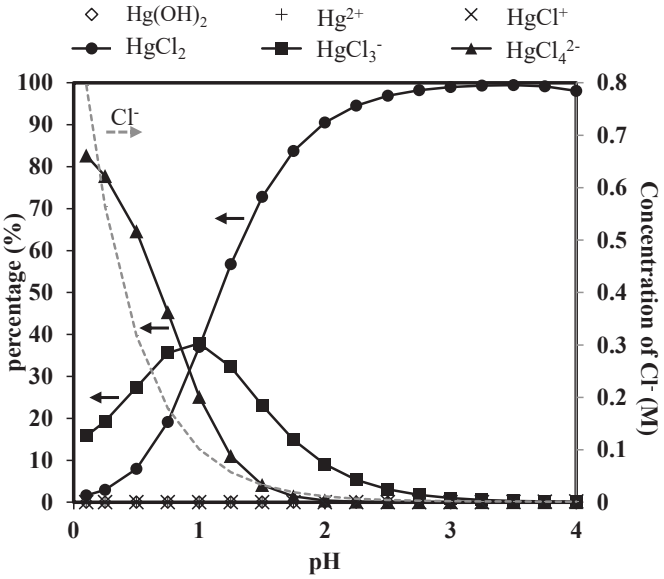

Figure 3-4 Hg speciation under different pH conditions with the presence of chloride ions (Hg(II) concentration is 0.5 mM, calculated by Visual Minteq).

3.4.3. Uptake kinetics

In order to evaluate the global sorption performances of membranes, it is important to investigate the uptake kinetics for determining equilibrium time but also identifying the controlling steps in the process. Indeed, the sorption kinetics may be controlled by various diffusion pathways (including bulk, film and intraparticle diffusion), different reaction mechanism (including

participation, chelation and electrostatic interactions) or their simultaneous contributions [44, 45]. Deng et al. [46] reported the polyacrylonitrile fibers have a fast sorption rate for Cu(II) and Hg(II) (without Cl-) mainly due to the high collision possibility with chelate groups which was controlled by the diffusion and migration process of metal ions in the solution to the active site. While Gavilan et al. [15] found that the time required for achieving the complete recovery of Hg(II) (in the presence of Cl^-) using thiocarbamoyl derivative of chitosan or for reaching the equilibrium was quite long (up to 3 - 4 days of contact) due to the resistance of intraparticle diffusion. In this study, Figure 3-5 presents the kinetic profiles for Cu(II) and Hg(II) sorption; the reaction time for equilibrium was set to 3 days. Under selected experimental conditions Cu(II) sorption by the membrane is faster than Hg(II): in the first 2 min, the recovery yields of Cu(II) and Hg(II) are 30 % (q_e = 0.39 mmol g^{-1}) and 6.3% (q_e = 0.08 mmol g^{-1}), respectively. For Cu(II) sorption, the equilibrium was reached in 24 h with a sorption capacity of 0.65 mmol g^{-1}. In the case of the Hg(II), the equilibrium was reached in 72 h, and the maximum sorption capacity is 0.93 mmol g^{-1}.

The pseudo-first order rate equation (PFORE) and the pseudo-second order rate equation (PSORE) were used to analyze the experiment process [47]. The equations of PFORE and PSORE were initially designed for modeling the chemical reaction rates in homogeneous systems. The application of these equations was extended to the description of heterogeneous systems:

PFORE:

Eq. 3-1

$$q(t) = q_{eq,1}(1 - e^{k_1 t})$$

PSORE:

Eq. 3-2

$$q(t) = \frac{q_{eq,2}^2 \times k_2 \times t}{1 + q_{eq,2} \times k_2 \times t}$$

where $q_{eq,i}$ (mmol g^{-1}) and q(t) (mmol g^{-1}) are the amount of metal ions adsorbed onto membranes at equilibrium and at time t (i=1 or 2), respectively, and k_1 (min^{-1}) and k_2 (g mmol g^{-1} min^{-1}) are the rate constants of PFORE and PSORE models, respectively.

The kinetic parameters of the PFORE and PSORE models for sorption of metal ions onto the membrane are presented in Table 3-2; the determination coefficients (R^2) of Cu(II) and Hg(II) in PSORE model are both 0.999, indicating the PSORE equation fits better kinetic profiles than PFORE equation. This is confirmed by the calculated equilibrium sorption capacity ($q_{eq,cal}$) for PSORE are more accurate than for PFORE and the superimposition of PSORE fitted curves with experimental points presented in Figure 3-5. Moreover, the comparison of calculated rate constants of PSORE for Cu(II) and Hg(II) also confirmed that Cu(II) sorption by the membrane is faster than

Hg(II). This may be due to the fact that the molecular weight of the chloro-mercury complex is much higher than that of the Cu(II) cation, resulting in a lower diffusion rate under the same membrane sorption.

Table 3-2 Kinetic parameters of the PFORE and PSORE models for sorption of metal ions.

Models	Parameters	Hg(II)	Cu(II)
	$q_{eq,exp}$ (mmol g^{-1})	0.931	0.650
PFORE	$q_{eq,cal}$ (mmol g^{-1})	0.593	0.307
	k_1 (min^{-1})	0.001	0.003
	R^2	0.928	0.984
PSORE	$q_{eq,cal}$ (mmol g^{-1})	0.926	0.653
	k_2 (g $mmol^{-1}$ min^{-1})	0.016	0.066
	R^2	0.999	0.999

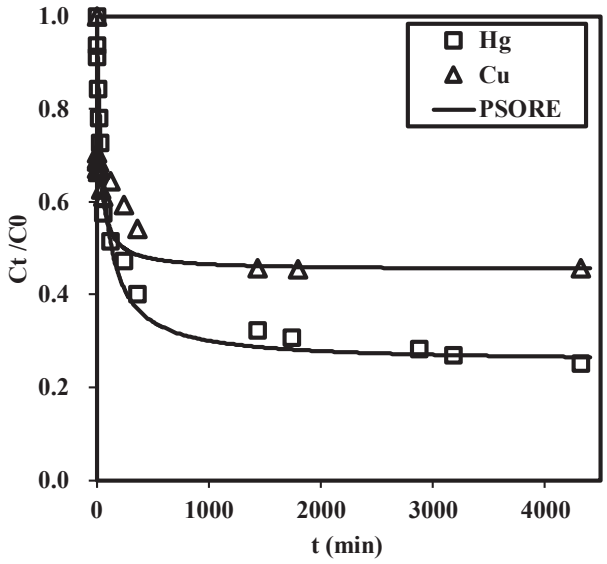

Figure 3-5 Modeling of kinetic profiles (Metal concentration: 0.25 mmol L^{-1} of Cu(II) or Hg(II) single solution; Sorbent dosage = 0.2 g L^{-1}; initial pH = 5; T: 20± 1 °C; solid line: fit of kinetic profile with the PSORE).

3.4.4. Sorption isotherms

The sorption isotherm plots the sorption capacity as a function of residual concentration at fixed temperature and pH value. The isotherm experiments in this study have been performed on both single and binary systems at pH 5. Analysis of isotherm data provides important information on the affinity of the sorbent for the solute [48]. Several classical models like Langmuir, Freundlich and Sips are proposed for fitting the experimental data. Figure 3-6 illustrates the sorption and competitive sorption behaviors for Hg(II) and Cu(II) in single and binary systems and all corresponding parameters are presented in Table 3-3 and Table 3-4.

For the single system, the Langmuir equation is based on the assumption that the sorption processes is a monolayer and occur on the homogeneous surface of the sorbent, while the Freundlich is assigned to multilayer sorption with non-uniform distribution of sorption heat and affinities on the heterogeneous surface [49]. The Sips isotherm is a combination of Langmuir and Freundlich model: at the low concentration stage, the Sips isotherm assumes the form of the Freundlich model, while at high concentration, it is similar to the Langmuir isotherm with a finite saturation limit [50, 51]. Their equations were used to describe as follows.

Langmuir:

$$q_{eq} = \frac{q_{m,L} \times b_L \times C_{eq}}{1 + b_L \times C_{eq}} \qquad \textbf{Eq. 3-3}$$

Freundlich:

$$q_{eq} = k_F C_{eq}^{1/n_F} \qquad \textbf{Eq. 3-4}$$

Sips:

$$q_{eq} = \frac{q_{m,S} \times b_S \times C_{eq}^{1/n_S}}{1 + b_S \times C_{eq}^{1/n_S}} \qquad \textbf{Eq. 3-5}$$

where C_{eq} (mmol L^{-1}) is the equilibrium concentration of metals; q_{eq} and $q_{m,j}$ (mmol g^{-1}) are the equilibrium concentration and the maximum sorption capacities calculated from Langmuir and Sips equations; the parameters k_F and n_F are the Freundlich constants, and b_j represent sorption intensity parameter for Freundlich and Sips equations (j=L or S).

As Figure 3-6 shows, the sorption capacity of Hg(II) or Cu(II) in the single system is characterized by a steep initial slope followed by the saturation plateau. Interestingly, the saturation plateau for Hg(II) sorption is reached 1.39 mmol g^{-1}, while the saturated sorption capacity of Cu(II) is only

0.56 mmol g^{-1}; this means that the affinity of membrane for Hg(II) is much higher than Cu(II). Moreover, the three selected models fit well with the experimental data based on obtaining R^2 values (around 0.91-0.99) shown in Table 3-3. Best fit is obtained with the Sips equation; using a third parameter logically improves the quality of mathematical fit. However, the maximum sorption capacities for Hg(II) and Cu(II) in the single system reach to 1.60 mmol g^{-1} and 0.66 mmol g^{-1} respectively, which are higher than the values obtained from experiments.

Since the isotherms for both Hg(II) and Cu(II) sorption onto the membrane obey the single-component Sips model, competitive Sips model was adopted to modeled the sorption data in binary system. The equation of competitive Sips model can also be expressed as [52]:

Sips (in binary system): $q_{e,j} = \frac{q_{m,CS} \times b_{CS,i} \times C_{e,i}^{1/n_{CS,i}}}{1+\sum_{j=1}^{2} b_{CS,j} \times C_{e,j}^{1/n_{CS,j}}} \quad (i \neq j)$ **Eq. 3-6**

where $q_{m,CS}$ (mg g^{-1}) is the total maximum sorption capacity of Hg(II) and Cu(II) calculated from competitive Sips equation .

Based on Figure 3-6, in the case of Hg(II), all sorption isotherms in Hg–Cu binary solutions are almost superimposed to the mono-component Hg(II) sorption isotherm under the selected experimental conditions. While for Cu(II) sorption, the sorption capacity will obviously decrease in the presence of Hg(II) ions. In addition, the obtained parameters of the competitive Sips model for binary system are summarized in Table 3-4.

The experimental data show a good compliance with the competitive Sips model in terms of R^2 (0.97) and the obtained total sorption capacity of Hg(II) and Cu(II) is 2.19 mmol g^{-1}. To obtain a good prediction for sorption behaviors of Hg(II) and Cu(II) under binary sorption conditions, these results are also plotted in three-dimensional sorption surfaces using Origin software (OriginLab, v. 9.0, MA, Northampton, USA) which presented in Figure 3-7 together with experimental data. It is obvious that the increase of Hg(II) concentration led to a dramatic fall in the sorption capacity of Cu(II). On the contrary, as the concentration of Cu(II) increased, no obvious decrease was found in Hg(II) sorption by the membrane: these predicted results are consistent with those obtained from the binary sorption experiments.

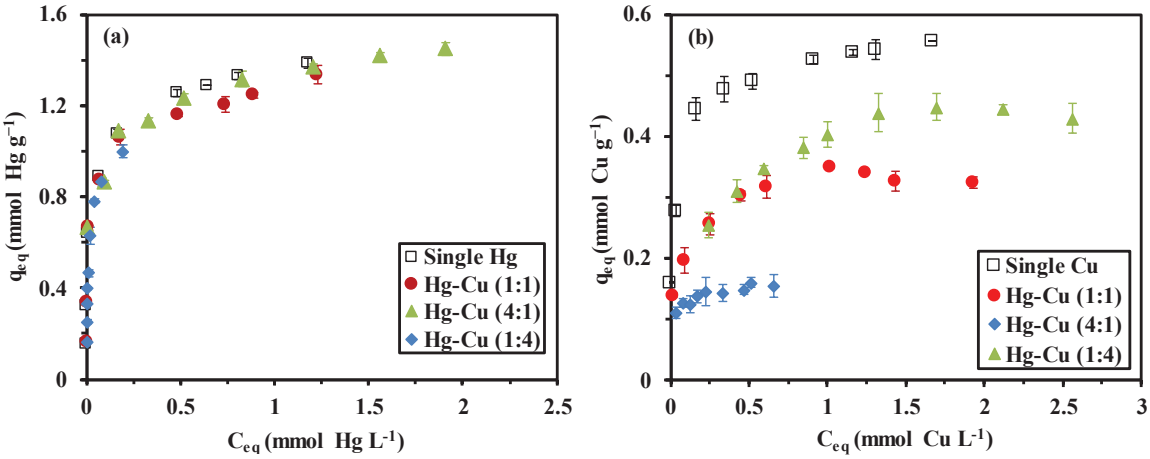

Figure 3-6 Sorption and competitive sorption behaviors of (a) Hg(II) and (b) Cu(II) in single and binary systems (Sorbent dosage = 0.6 g L^{-1}; initial pH: 5; contact time = 78 h; T = 20± 1 °C; Hg(II) or Cu(II) concentration: 0.1-2 mmol L^{-1} in single and Hg-Cu(1:1) solution; 0.1-2.8 mmol L^{-1} in Hg-Cu(4:1) and Hg-Cu(1:4). Note: Hg-Cu: the molar ratio of Hg(II) and Cu(II)).

Table 3-3 Sorption isotherms in single system – Modeling parameters for Langmuir, Freundlich and Sips equations.

Model	Parameter	Hg(II)	Cu(II)
	$q_{max,exp}$ (mmol g^{-1})	1.39	0.56
Langmuir	$q_{mL,cal}$ (mmol g^{-1})	1.28	0.53
	b_L (L $mmol^{-1}$)	87.8	40.8
	R^2	0.94	0. 91
Freundlich	k_F (mmol g^{-1})/(L $mmol^{-1}$) $^{1/n}$	1.42	0.53
	n_F	4.81	5.82
	R^2	0.95	0.94
Sips	$q_{mS,cal}$ (mmol g^{-1})	1.60	0.66
	b_S (L $mmol^{-1}$)	5.37	4.31
	ns	1.97	2.09
	R^2	0.99	0.99

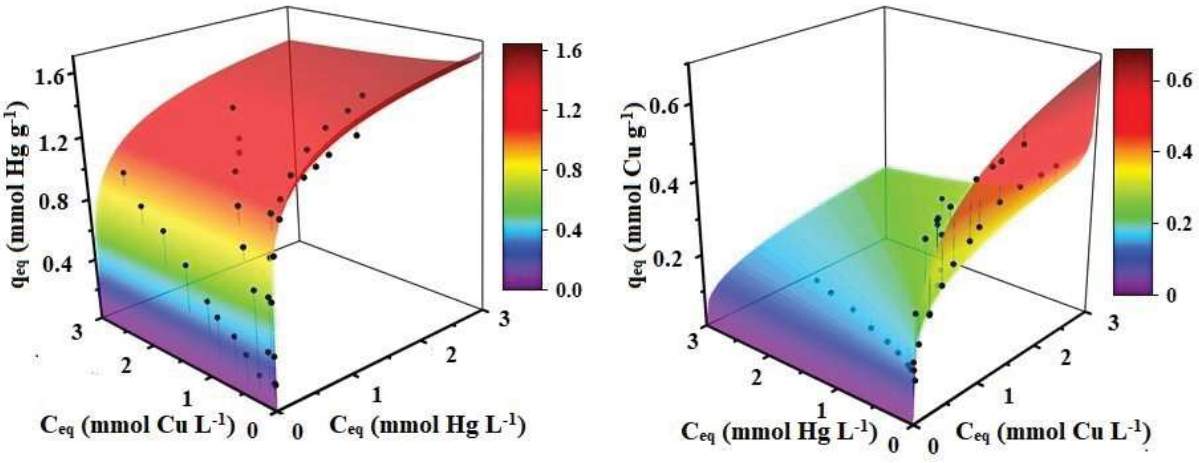

Figure 3-7 Three-dimensional sorption surface showing competitive Sips model prediction and experimental data points.

Table 3-4 Sorption isotherms in Hg-Cu binary system

Parameters	$q_{m,CS}$ (mmol g^{-1})	$b_{SC,\,Hg}$ (L mmol $^{-1}$)	$b_{SC,\,Cu}$ (L mmol $^{-1}$)	$n_{SC,\,Hg}$	$n_{SC,\,Cu}$	R^2
Values	2.19	1.94	0.32	2.57	3.18	0.97

3.4.5. Comparison of sorption performances with various sorbents

Table 3-5 lists the comparison of maximum sorption capacities of A-PEI membrane with various similar sorbents reported in the literature, which suggests that the as-prepared membrane in this study shows a relatively high sorption capacity on metals ions, especially for Hg(II). It is noteworthy that the A-PEI membrane have an important advantage related to their efficient Hg uptake in a very wide pH range (from 1 to 6) since the pH has no significant impact on the Hg(II) sorption under selected condition. Moreover, the membrane shows an extraordinarily high selectivity to Hg ions in acidic condition from Hg-Cu mixture which exhibits the membrane has a great potential in the recovery of Hg(II) from aqueous solutions, such as contaminated industrial effluents.

Table 3-5 Comparison of sorption performances with various similar sorbents

Sorbent	pH	$q_{m,Hg(II)}$ (mmol g^{-1})	$q_{m,Cu(II)}$ (mmol g^{-1})	Ref.
Wool-grafted-poly(cyano-acetic acid α-amino-acrylic-hydrazide) chelating fibers	5	0.77	1.73	[53]
Modified poly(ethylene terephthalate) cheating fibers	5	0.6	1.5	[54]
PVA/PEI complexing membrane	Cu:5; Hg:2.5	1.08	0.69	[55]
Schiff-base-grafted guar gum adsorbent	5	0.2	N.M.	[56]
Thiourea-modified magnetic chitosan microspheres	5	3.11	1.05	[57]
Immobilized [A336][MTBA] in PVA–alginate gel beads	5.8	0.25	--	[58]
Thiourea modified Hg(II) ion-imprinted cellulosic cotton fibers	5	0.55	N.M.	[59]
PEI modified cellulose nanofibrils	5	--	0.82	[60]
Magnetic silica coated iron carbide/alginate bead	4	--	0.59	[61]
Magnetic chitosan-phenylthiourea resin	5	0.67	--	[62]
Chitosan–thioglyceraldehyde Schiff base cross-linked magnetic resin	5	0.49	1.19	[63]
A-PEI membrane	5	1.39	0.56	This study

3.5. Principales conclusions

Les membranes alginate/PEI ont été testées pour l'adsorption des métaux de base Hg(II) et Cu(II) en solutions monocomposé et en mélange binaire. L'analyse par spectroscopie FTIR des adsorbants montre, après sorption, certains déplacements des bandes caractéristiques des fonctions aminées (notamment pour le mercure) même si l'allure générale des spectres reste peu affectée par l'adsorption des deux ions métalliques. L'analyse MEB-EDX confirme la présence des deux ions métalliques adsorbés individuellement ou en mélange. Le cuivre est réparti de façon homogène sur

tout la masse de l'absorbant alors que le mercure est distribué en surface du matériau, de façon homogène malgré la présence de quelques agrégats. Il convient de remarquer que dans le cas du mercure, l'analyse semi-quantitative par EDX met en évidence la présence de Cl, simultanément à Hg. Cela tend à indiquer la fixation du mercure sous la forme d'un complexe de chlorure de mercure (vraisemblablement anionique sur la base de la spéciation du métal en solution HCl).

L'étude de l'effet du pH sur la fixation des deux ions métalliques caractérise les comportements très différents des deux métaux , avec formation de complexes chloro-anioniques avec le mercure alors que le cuivre reste libre en solution. Cela se traduit en particulier par une adsorption très efficace et quasi constante du mercure entre pH 1 et 6 la capacité de fixation variant de 0,73 mmol Hg g^{-1} à pH 1,1 à 0,84 mmol Hg g^{-1} à pH 3,8. Le mécanisme de sorption est attribué à la fixation des espèces anioniques sur les fonctions aminées protonées. Pour Cu(II), l'adsorption est en revanche négligeable à pH très acide (<0,006 mmol $^{g-}$1 à pH < 2) car la protonation des fonctions aminées repousse électrostatiquement les cations Cu^{2+}, tandis que les fonctions carboxyliques ne sont pas favorables à la complexation du Cu(II). Quand le pH augmente au-delà de 2,1, l'adsorption du cuivre augmente progressivement en lien avec la déprotonation des groupes fonctionnels, mais même à pH 3.9 la capacité d'adsorption ne dépasse pas 0,44 mmol Cu g^{-1}. Ces résultats confirment que l'adsorbant peut être considéré comme sélectif du mercure vis-à-vis du cuivre à pH inférieur à 2.

La comparaison des cinétiques de fixation (modélisées par l'équation de pseudo-second ordre) montre une vitesse de sorption légèrement plus importante pour le cuivre (k_2, constante apparente de vitesse: 0,066 g $mmol^{-1}$ min^{-1}) que pour le mercure (k_2: 0,016 g $mmol^{-1}$ min^{-1}).

Les isothermes d'adsorption obtenues en solutions mono-élémentaires ou mixtes sont caractérisées par une adsorption très favorable (pente très importante pour les plus faibles concentrations résiduelles, suivie d'un plateau de saturation atteint pour des concentrations résiduelles comprises entre 1,0 et 1,4 mmol Hg L^{-1}). L'équation de Sips permet une bonne simulation des profils à la fois en solution mono-élémentaire et en solutions mixtes. Si l'adsorption du mercure n'est pas affectée par la présence du cuivre, à l'inverse, la fixation du cuivre est fortement impactée par la présence de concentrations croissantes de mercure. Même à pH 5, malgré le caractère favorable de l'adsorption du cuivre, les membranes PEI/Alginate ont une préférence très marquée pour le mercure. Cette sélectivité vis-à-vis du mercure est confirmée par la comparaison des surfaces tridimensionnelles des isothermes du mercure et du cuivre (construites par l'équation de Sips étendue).

La préférence de la membrane PEI/Alginate pour le mercure est directement liée au mécanisme d'adsorption et à la prévalence de formes complexes anioniques du mercure tandis que la disponibilité des formes amines primaires pour le cuivre reste limité du fait des interactions entre l'alginate et la PEI, et de la réticulation de la PEI.

3.6. References

[1] A.K. Krishna, M. Satyanarayanan, P.K. Govil, Assessment of heavy metal pollution in water using multivariate statistical techniques in an industrial area: a case study from Patancheru, Medak District, Andhra Pradesh, India, Journal of hazardous materials, 167 (2009) 366-373.
[2] N. Saha, M.S. Rahman, M.B. Ahmed, J.L. Zhou, H.H. Ngo, W. Guo, Industrial metal pollution in water and probabilistic assessment of human health risk, Journal of environmental management, 185 (2017) 70-78.
[3] A.S. Luna, A.L.H. Costa, A.C.A.d. Costa, C.A. Henriques, Competitive biosorption of cadmium(II) and zinc(II) ions from binary systems by Sargassum filipendula, Bioresource Technology, 101 (2010) 5104-5111.
[4] G. Ru, H. Zheng, X. Chang, Q. He, L. Zhang, Z. Tu, J. Shi, Chemically modified activated carbon with 1-acylthiosemicarbazide for selective solid-phase extraction and preconcentration of trace Cu(II), Hg(II) and Pb(II) from water samples, Journal of Hazardous Materials, 172 (2009) 324-329.
[5] R. Qu, C. Sun, F. Ma, Y. Zhang, C. Ji, Q. Xu, C. Wang, H. Chen, Removal and recovery of Hg(II) from aqueous solution using chitosan-coated cotton fibers, Journal of Hazardous Materials, 167 (2009) 717-727.
[6] S. Hokkanen, A. Bhatnagar, M. Sillanpää, A review on modification methods to cellulose-based adsorbents to improve adsorption capacity, Water research, 91 (2016) 156-173.
[7] X. Gao, M. Li, Y. Zhao, Y. Zhang, Mechanistic study of selective adsorption of Hg^{2+} ion by porous alginate beads, Chemical Engineering Journal, 378 (2019) 122096.
[8] I.S. Fernando, D. Kim, J.-W. Nah, Y.-J. Jeon, Advances in functionalizing fucoidans and alginates (bio) polymers by structural modifications: A review, Chemical Engineering Journal, 355 (2019) 33-48.
[9] S. Wang, T. Vincent, C. Faur, E. Guibal, A comparison of palladium sorption using polyethylenimine impregnated alginate-based and carrageenan-based algal beads, Applied Sciences, 8 (2018) 264.
[10] M. Farokhi, F. Jonidi Shariatzadeh, A. Solouk, H. Mirzadeh, Alginate Based Scaffolds for Cartilage Tissue Engineering: A Review, International Journal of Polymeric Materials and Polymeric Biomaterials, 69 (2020) 230-247.
[11] S. Wang, T. Vincent, C. Faur, E. Rodríguez-Castellón, E. Guibal, A new method for incorporating polyethyleneimine (PEI) in algal beads: High stability as sorbent for palladium recovery and supported catalyst for nitrophenol hydrogenation, Materials Chemistry and Physics, 221 (2019) 144-155.
[12] X. Li, Y. Qi, Y. Li, Y. Zhang, X. He, Y. Wang, Novel magnetic beads based on sodium alginate gel crosslinked by zirconium(IV) and their effective removal for Pb^{2+} in aqueous solutions by using a batch and continuous systems, Bioresource technology, 142 (2013) 611-619.
[13] Y. Mo, T. Vincent, C. Faur, E. Guibal, Se(VI) sorption from aqueous solution using alginate/polyethylenimine membranes: Sorption performance and mechanism, International Journal of Biological Macromolecules, 147 (2020) 832-843.
[14] Y. Mo, S. Wang, T. Vincent, J. Desbrieres, C. Faur, E. Guibal, New highly-percolating alginate-PEI membranes for efficient recovery of chromium from aqueous solutions, Carbohydrate Polymers, 225 (2019) 115177.
[15] K.C. Gavilan, A.V. Pestov, H.M. Garcia, Y. Yatluk, J. Roussy, E. Guibal, Mercury sorption on a thiocarbamoyl derivative of chitosan, Journal of Hazardous Materials, 165 (2009) 415-426.

[16] W. Zhang, J. Song, Q. He, H. Wang, W. Lyu, H. Feng, W. Xiong, W. Guo, J. Wu, L. Chen, Novel pectin based composite hydrogel derived from grapefruit peel for enhanced Cu(II) removal, Journal of hazardous materials, 384 (2020) 121445.
[17] H. Bessbousse, T. Rhlalou, J.-F. Verchère, L. Lebrun, Sorption and filtration of Hg(II) ions from aqueous solutions with a membrane containing poly(ethyleneimine) as a complexing polymer, Journal of Membrane Science, 325 (2008) 997-1006.
[18] M. Traoré, J. Kaal, A.M. Cortizas, Application of FTIR spectroscopy to the characterization of archeological wood, Spectrochimica Acta Part A: Molecular and Biomolecular Spectroscopy, 153 (2016) 63-70.
[19] S. Deng, R. Ma, Q. Yu, J. Huang, G. Yu, Enhanced removal of pentachlorophenol and 2, 4-D from aqueous solution by an aminated biosorbent, Journal of hazardous materials, 165 (2009) 408-414.
[20] L.C. Oliveira, E. Pereira, I.R. Guimaraes, A. Vallone, M. Pereira, J.P. Mesquita, K. Sapag, Preparation of activated carbons from coffee husks utilizing $FeCl_3$ and $ZnCl_2$ as activating agents, Journal of hazardous materials, 165 (2009) 87-94.
[21] G. Lawrie, I. Keen, B. Drew, A. Chandler-Temple, L. Rintoul, P. Fredericks, L. Grøndahl, Interactions between alginate and chitosan biopolymers characterized using FTIR and XPS, Biomacromolecules, 8 (2007) 2533-2541.
[22] H. Liu, T. Kuila, N.H. Kim, B.-C. Ku, J.H. Lee, In situ synthesis of the reduced graphene oxide–polyethyleneimine composite and its gas barrier properties, Journal of Materials Chemistry A, 1 (2013) 3739-3746.
[23] S. Wang, T. Vincent, J.-C. Roux, C. Faur, E. Guibal, Pd(II) and Pt(IV) sorption using alginate and algal-based beads, Chemical Engineering Journal, 313 (2017) 567-579.
[24] J.B. Lindén, M. Larsson, S. Kaur, W.M. Skinner, S.J. Miklavcic, T. Nann, I.M. Kempson, M. Nydén, Polyethyleneimine for copper absorption II: kinetics, selectivity and efficiency from seawater, RSC Advances, 5 (2015) 51883-51890.
[25] Q. Xiao, X.H. Gu, S. Tan, Drying process of sodium alginate films studied by two-dimensional correlation ATR-FTIR spectroscopy, Food Chemistry, 164 (2014) 179-184.
[26] H. Xiong, S. Tang, H. Tang, P. Zou, The structure and properties of a starch-based biodegradable film, Carbohydrate polymers, 71 (2008) 263-268.
[27] W. Zhang, Y. Chai, N. Cao, Y. Wang, Synthesis and characterization of selenium substituted hydroxyapatite via a hydrothermal procedure, Materials Letters, 134 (2014) 123-125.
[28] K.Z. Elwakeel, A.S. Al-Bogami, Influence of Mo(VI) immobilization and temperature on As(V) sorption onto magnetic separable poly p-phenylenediamine-thiourea-formaldehyde polymer, Journal of hazardous materials, 342 (2018) 335-346.
[29] C. Mahamadi, T. Nharingo, Competitive adsorption of Pb^{2+}, Cd^{2+} and Zn^{2+} ions onto *Eichhornia crassipes* in binary and ternary systems, Bioresource technology, 101 (2010) 859-864.
[30] A. Ahmadpour, M. Zabihi, M. Tahmasbi, T.R. Bastami, Effect of adsorbents and chemical treatments on the removal of strontium from aqueous solutions, Journal of hazardous materials, 182 (2010) 552-556.
[31] A. El-Bayaa, N. Badawy, E.A. AlKhalik, Effect of ionic strength on the adsorption of copper and chromium ions by vermiculite pure clay mineral, Journal of hazardous materials, 170 (2009) 1204-1209.
[32] E. Fosso-Kankeu, A. Mulaba-Bafubiandi, B. Mamba, T. Barnard, Prediction of metal-adsorption behaviour in the remediation of water contamination using indigenous microorganisms, Journal of environmental management, 92 (2011) 2786-2793.

[33] R.S. Vieira, E. Guibal, E.A. Silva, M.M. Beppu, Adsorption and desorption of binary mixtures of copper and mercury ions on natural and crosslinked chitosan membranes, Adsorption, 13 (2007) 603-611.
[34] A. Wołowicz, Z. Hubicki, The use of the chelating resin of a new generation Lewatit MonoPlus TP-220 with the bis-picolylamine functional groups in the removal of selected metal ions from acidic solutions, Chemical Engineering Journal, 197 (2012) 493-508.
[35] P. Krys, F. Testa, A. Trochimczuk, C. Pin, E. Guibal, Encapsulation of ammonium molybdophosphate and zirconium phosphate in alginate matrix for the sorption of rubidium(I), Journal of Colloid & Interface Science, 409 (2013) 141-150.
[36] J.N. Nkoh, J. Yan, R.-K. Xu, R.-y. Shi, Z.-n. Hong, The mechanism for inhibiting acidification of variable charge soils by adhered Pseudomonas fluorescens, Environmental Pollution, 260 (2020) 114049.
[37] M.J. Hudson, Z. Matejka, Extraction of copper by selective ion exchangers with pendent ethyleneimine groups - investigation of active states, Separation Science and Technology, 24 (1989) 1417-1426.
[38] H. Bessbousse, T. Rhlalou, J.-F. Verchère, L. Lebrun, Removal of heavy metal ions from aqueous solutions by filtration with a novel complexing membrane containing poly (ethyleneimine) in a poly (vinyl alcohol) matrix, Journal of Membrane Science, 307 (2008) 249-259.
[39] K. Ranganathan, Adsorption of Hg(II) ions from aqueous chloride solutions using powdered activated carbons, Carbon, 41 (2003) 1087-1092.
[40] J.D. Ziebarth, Y. Wang, Understanding the protonation behavior of linear polyethylenimine in solutions through Monte Carlo simulations, Biomacromolecules, 11 (2014) 29-28.
[41] K. Sarkar, Z. Ansari, K. Sen, Detoxification of Hg(II) from aqueous and enzyme media: pristine vs. tailored calcium alginate hydrogels, International Journal of Biological Macromolecules, 91 (2016) 165-173.
[42] P.R. Devi, S. Kumar, R. Verma, M. Sudersanan, Sorption of mercury on chemically synthesized polyaniline, Journal of Radioanalytical and Nuclear Chemistry, 269 (2006) 217-222.
[43] E. Guibal, K.C. Gavilan, P. Bunio, T. Vincent, A. Trochimczuk, Cyphos IL 101 (tetradecyl (trihexyl) phosphonium chloride) immobilized in biopolymer capsules for Hg(II) recovery from HCl solutions, Separation Science and Technology, 43 (2008) 2406-2433.
[44] F. Quattrini, J. Galceran, C. David, J. Puy, G. Alberti, C. Rey-Castro, Dynamics of trace metal sorption by an ion-exchange chelating resin described by a mixed intraparticle/film diffusion transport model. The Cd/Chelex case, Chemical Engineering Journal, 317 (2017) 810-820.
[45] E.P. Kuncoro, J. Roussy, E. Guibal, Mercury recovery by polymer‐enhanced ultrafiltration: comparison of chitosan and poly (ethylenimine) used as macroligand, Separation Science and Technology, 40 (2005) 659-684.
[46] A. Esposito, A. Reverberi, Copper adsorption on calcium alginate beads: equilibrium pH-related models, Hydrometallurgy, 65 (2002) 43-57.
[47] Z. Reddad, C. Gerente, Y. Andres, P. Le Cloirec, Adsorption of several metal ions onto a low-cost biosorbent: kinetic and equilibrium studies, Environmental science & technology, 36 (2002) 2067-2073.
[48] C.L. Carnahan, J.S. Remer, Nonequilibrium and equilibrium sorption with a linear sorption isotherm during mass transport through an infinite porous medium: some analytical solutions, Journal of Hydrology, 73 (1984) 227-258.
[49] K.Y. Foo, B.H. Hameed, Insights into the modeling of adsorption isotherm systems, Chemical Engineering Journal, 156 (2010) 2-10.

[50] J. Febrianto, A.N. Kosasih, J. Sunarso, Y.H. Ju, N. Indraswati, S. Ismadji, Equilibrium and kinetic studies in adsorption of heavy metals using biosorbent: A summary of recent studies, Journal of Hazardous Materials, 162 (2009) 616-645.
[51] C. Yan, G. Li, P. Xue, Q. Wei, Q. Li, Competitive effect of Cu(II) and Zn(II) on the biosorption of lead(II) by Myriophyllum spicatum, Journal of Hazardous Materials, 179 (2010) 721-728.
[52] S. Wang, T. Vincent, C. Faur, E. Guibal, Modeling competitive sorption of lead and copper ions onto alginate and greenly prepared algal-based beads, Bioresource technology, 231 (2017) 26-35.
[53] M. Monier, N. Nawar, D. Abdel-Latif, Preparation and characterization of chelating fibers based on natural wool for removal of Hg(II), Cu(II) and Co(II) metal ions from aqueous solutions, Journal of hazardous materials, 184 (2010) 118-125.
[54] M. Monier, D. Abdel-Latif, Modification and characterization of PET fibers for fast removal of Hg (II), Cu (II) and Co (II) metal ions from aqueous solutions, Journal of hazardous materials, 250 (2013) 122-130.
[55] H. Bessbousse, T. Rhlalou, J.-F. Verchère, L. Lebrun, Sorption and filtration of Hg(II) ions from aqueous solutions with a membrane containing poly (ethyleneimine) as a complexing polymer, Journal of Membrane Science, 325 (2008) 997-1006.
[56] S. Thakur, S. Kumari, P. Dogra, G.S. Chauhan, A new guar gum-based adsorbent for the removal of Hg(II) from its aqueous solutions, Carbohydrate polymers, 106 (2014) 276-282.
[57] L. Zhou, Y. Wang, Z. Liu, Q. Huang, Characteristics of equilibrium, kinetics studies for adsorption of Hg(II), Cu(II), and Ni(II) ions by thiourea-modified magnetic chitosan microspheres, Journal of hazardous materials, 161 (2009) 995-1002.
[58] Y. Zhang, D. Kogelnig, C. Morgenbesser, A. Stojanovic, F. Jirsa, I. Lichtscheidl-Schultz, R. Krachler, Y. Li, B.K. Keppler, Preparation and characterization of immobilized [A336][MTBA] in PVA–alginate gel beads as novel solid-phase extractants for an efficient recovery of Hg(II) from aqueous solutions, Journal of hazardous materials, 196 (2011) 201-209.
[59] M. Monier, I. Kenawy, M. Hashem, Synthesis and characterization of selective thiourea modified Hg(II) ion-imprinted cellulosic cotton fibers, Carbohydrate polymers, 106 (2014) 49-59.
[60] N. Zhang, G.-L. Zang, C. Shi, H.-Q. Yu, G.-P. Sheng, A novel adsorbent TEMPO-mediated oxidized cellulose nanofibrils modified with PEI: Preparation, characterization, and application for Cu(II) removal, Journal of hazardous materials, 316 (2016) 11-18.
[61] F. Ahmadpoor, S.A. Shojaosadati, S.Z. Mousavi, Magnetic silica coated iron carbide/alginate beads: Synthesis and application for adsorption of Cu(II) from aqueous solutions, International Journal of Biological Macromolecules, 128 (2019) 941-947.
[62] M. Monier, D. Abdel-Latif, Preparation of cross-linked magnetic chitosan-phenylthiourea resin for adsorption of Hg(II), Cd(II) and Zn(II) ions from aqueous solutions, Journal of hazardous materials, 209 (2012) 240-249.
[63] M. Monier, Adsorption of Hg^{2+}, Cu^{2+} and Zn^{2+} ions from aqueous solution using formaldehyde cross-linked modified chitosan–thioglyceraldehyde Schiff's base, International Journal of Biological Macromolecules, 50 (2012) 773-781.

Chapter 4 Selenium(VI) and copper(II) adsorption using polyethyleneimine-based resins: effect of glutaraldehyde crosslinking and storage condition

4.1. Introduction Générale

La comparaison des performances de fixation du cuivre et du mercure à la section précédente a permis d'illustrer l'effet de la spéciation des ions métalliques (formation favorable d'espèces chloro-anioniques de mercure) sur les mécanismes de fixation. La réticulation des fonctions aminées de la PEI par le glutaraldéhyde se traduit par la formation de liaisons imines qui diminue la quantité de fonctions amine primaires libres susceptibles de chélater des cations métalliques. Afin de clarifier et confirmer cette analyse, une étude complémentaire a été menée sur de la polyethylèneimine réticulée par le glutaraldéhyde (conditionnée sous forme de poudre). Dans cette étude, différents taux de réticulation de la PEI ont été testés (48%, 57 %, 63 % et 72%) pour produire quatre matériaux dont les propriétés d'adsorption ont été comparées pour la fixation du Se(VI) et Cu(II). Ces deux métaux représentent les cas respectifs d'espèces anioniques et cationiques. Ces taux de réticulation permettent de couvrir différents scénarios de réticulation (défaut/excès de glutaraldehyde) avec comme conséquence une disponibilité variable des fonctions aminées libres.

Les adsorbants et leur interaction avec les ions métalliques ont été caractérisés par spectroscopie infrarouge et par spectrométrie photo électronique X.

L'effet du pH sur les cinétiques d'adsorption du Se(VI) et du Cu(II) a été comparé pour les quatre adsorbants, avant d'acquérir les isothermes d'adsorption du Se(VI) à pH 2 et du Cu(II) à pH 3.

Une étude complémentaire a porté sur l'évaluation de la sélectivité de cet adsorbant pour la fixation du Se(VI) (associé aux ions As(V)) et du Cu(II) (associé aux ions Pb(II)) en mélange binaire.

Au fil de cette étude, l'observation des résines exposées à l'air a permis de mettre en évidence une évolution de leur couleur ; cela traduit une instabilité relative des résines. Afin de vérifier l'impact de cette instabilité sur l'adsorption des ions métalliques, des tests comparatifs d'adsorption (dans des conditions expérimentales comparables) ont été réalisés sur ces quatre adsorbants après un stockage de 20 jours dans un flacon ouvert et dans un flacon scellé. L'effet de ces conditions de stockage a été mesuré sur les performances de fixation (cinétiques et capacités à l'équilibre) du Se(VI) et du Cu(II).

Cette étude complémentaire permet d'abonder la connaissance de l'effet des paramètres de fabrication des membranes PEI/Alginate en anticipant les effets éventuels du taux de réticulation sur les performances d'adsorption des métaux : cette réticulation est nécessaire pour structurer l'hydrogel avant l'étape de séchage et pour renforcer la stabilité du matériau en milieu acide. Ce taux de greffage est toutefois critique : un excès de réticulation peut induire une plus grande fragilité de la mousse sous contrainte mécanique (la densité de liaisons de réticulation diminue la

"souplesse" ou flexibilité des mousses), ainsi qu'une réduction de la disponibilité des fonctions aminées libres nécessaires pour la complexation des cations. Cette étude contribue à mesurer cet effet et à anticiper les taux de réticulation admissibles pour la réalisation des membranes PEI/Alginate.

4.2. Introduction

Amine-rich adsorbents present high adsorption affinity towards both anions and cations in aqueous solutions *via* different mechanisms. Owing to the presence of primary (1/4), secondary (2/4), and tertiary amine (1/4) groups, branched polyethylenimine (PEI)-based materials are continuously being developed for the removal of aqueous contaminants including anions such as chromate, palladium-chloro complexes, and platinum-chloro complex through electrostatic attraction at low pH or metal cations such as copper, lead, and zinc through coordination/chelation onto free amine groups. However, limited by its high solubility in water, PEI has to be immobilized before application. Glutaraldehyde (GA) has been extensively used to immobilize/crosslink PEI through the reaction between primary amine groups of PEI and GA, forming "Schiff's base" [1]. Lindén et al [2] reported that GA crosslinking significantly improved the mechanical and chemical stability of PEI coatings that formed on silica surfaces. PEI-GA resins reported by Kaur et al. [3] showed excellent selectivity for Cu(II) binding and metal recovery from complex solutions. But excessive crosslinking will inevitably reduce the number of available primary amine groups and thus decrease the binding properties of PEI [4]. Although many studies regarding the modification of materials using PEI followed by GA or the direct use of PEI-GA resins for the removal of aqueous contaminants have been published previously [5, 6], information is lacking on how much GA crosslinking impacts the binding towards different metals onto PEI.

The removal of copper (Cu) and selenium (Se) has attracted attention because these metals represent health hazards for living organisms. The U.S. Environmental Protection Agency (EPA) mandated a maximum acceptable level for Se in drinking water of 0.05 mg L^{-1} while for Cu the limit was set to 1.3 mg L^{-1}. Selenium can occur in both organic and inorganic forms (including different oxidation states with different toxicities). Due to their high solubility and bioavailability, the inorganic species, selenite and selenate anions, are the dominant species in natural water [7]. Though both anions could bioaccumulate in organisms, selenate is more difficult to remove due to its more stable structure in aqueous solutions than selenite [8]. In the case of Cu, free aqueous Cu(II) is the dominant species in acidic solutions. Therefore, Cu(II) can react with the amino groups of the PEI-GA through coordination, and the Se(VI) anions can be retained through the electrostatic attraction when nitrogen atoms are protonated in acidic solutions. However, it is well-known that metal (cations)–nitrogen bonds are inherently weaker on tertiary amine groups than on primary or secondary amine groups [9]. Therefore, understanding the effect of GA crosslinking, which consumes primary amine groups, on the adsorption performance of PEI for Cu(II) cations is of importance. Moreover, its impact on selenate (anions) binding is also worthy studying. Because

these two contaminants can represent a variety of ions in aqueous solutions such as oxyanions or metal complex anions and metal cations, respectively. In addition, primary and secondary amine groups are reported to be unstable when exposed to air as they can easily react with CO_2/H_2O. Therefore, when stored in open condition for a certain time, the conversion of amine groups to carbamate and/or bicarbonate occurs [10], which might have detrimental, beneficial or minimal effects on the adsorption performance of PEI towards aqueous contaminants. However, to our knowledge, neither of the effects of crosslinking or the storage conditions on the adsorption properties of PEI-based materials has been studied so far.

This study investigates the effect of different levels of GA crosslinking and storage conditions on the adsorption properties of PEI-GA resins for Se(VI) (selenate anions) and Cu(II) (cations). Moreover, copper is commonly associated with lead in the wastewater from manufacture of printed circuit boards, battery, etc. [11], while selenium can coexist with arsenic in the leachates of sedimentary rocks [12]. Therefore, the selectivity of the adsorbents for Se(VI) in Se(VI)-As(V) system and Cu(II) in Cu(II)-Pb(II) system has been also studied. The results of this study should be useful for the synthesis and storage of various PEI-based or amine-rich adsorbents applied for the removal of aqueous contaminants including anions and cations.

4.3. Materials and methods

4.3.1. Materials

Branched polyethyleneimine (PEI, 50% (w/w) in water), glutaraldehyde (GA, 50% (w/w) in water), copper nitrate and lead nitrate were purchased from Sigma-Aldrich (Taufkirchen, Germany). Other reagents were supplied by Chem-Lab NV (Zedelgem, Belgium).

4.3.2. Preparation of adsorbents

For preparing PEI-GA resins, 40 g of PEI solution (50%, w/w) were dissolved into 400 mL of pure water. Thereafter, different amounts, namely, 10 g, 16 g, 20 g, and 30 g of GA (50%, w/w) were added, respectively, under strong agitation (≈ 300 rpm) of PEI solution for 30 seconds. The mixtures were sealed and kept at room temperature (19 ºC–25 ºC) for 16 h to ensure completion of the reaction, which is shown in Figure 4-1(a). The reaction can face three different scenarios:

(1) when there is deficient GA, the crosslinking is formed with one GA molecule and two primary amine groups on PEI;

(2) when there is excess GA, there is formation of only one Schiff base, with one aldehyde group of GA, the other aldehyde group remains free;

(3) when GA amount is sufficient, the reaction is between (1) and (2) (co-existence of Schiff base and crosslinked groups).

The obtained PEI-GA resins were thoroughly washed by immersing them in 1 L of deionized water under 50 rpm of agitation for 10 min and filtrated. The washing step was repeated 5 times for each sample. The solids were then freeze-dried at −52 °C/0.1 mbar, for two days, ground to pass through

0.25-mm screen (Retsch, ZM 200, Retsch Technology, Haan, Germany) and stored in seal-packaging by plastic films or in open condition under room atmosphere with a temperature range of 19 ºC–25 ºC and relative humidity of 36%–48%. The obtained adsorbents prepared using 10 g, 16 g, 20 g, and 30 g of GA are marked as PEI-GA1, PEI-GA2, PEI-GA3 and PEI-GA4, respectively. Figure 1(b) shows that with the increase of GA amount applied for crosslinking from 10 g to 30 g, the color of the resins turned from yellow to orange-red. Moreover, different storage condition resulted in different colors of the resins after 20 days. The experiment below will show if the storage condition affects their adsorption for Se(VI) and Cu(II). The yield of conversion was calculated based on the mass of obtained resin (i.e., $m_{PEI\text{-}GA}$) divided by the mass of the PEI and GA introduced for resin preparation (i.e., $m_{PEI}+m_{GA}$). Taking PEI-GA1 as an example, the mass of PEI and GA used for adsorbent preparation was 20.00 g and 5.00 g, respectively, while that of the obtained resins after freeze-drying was 12.11 g. The average yield equaled to $12.11/(20+5)\times100=48.4\%$. The synthesis process was repeated to obtain freshly prepared materials. Average values and standard deviations (SD) were calculated, which turned out to be 48.0 ± 3.8% for PEI-GA1, 56.7 ± 3.1% for PEI-GA2, 62.5 ± 1.9% for PEI-GA3 and 72.0 ± 0.8% for PEI-GA4.

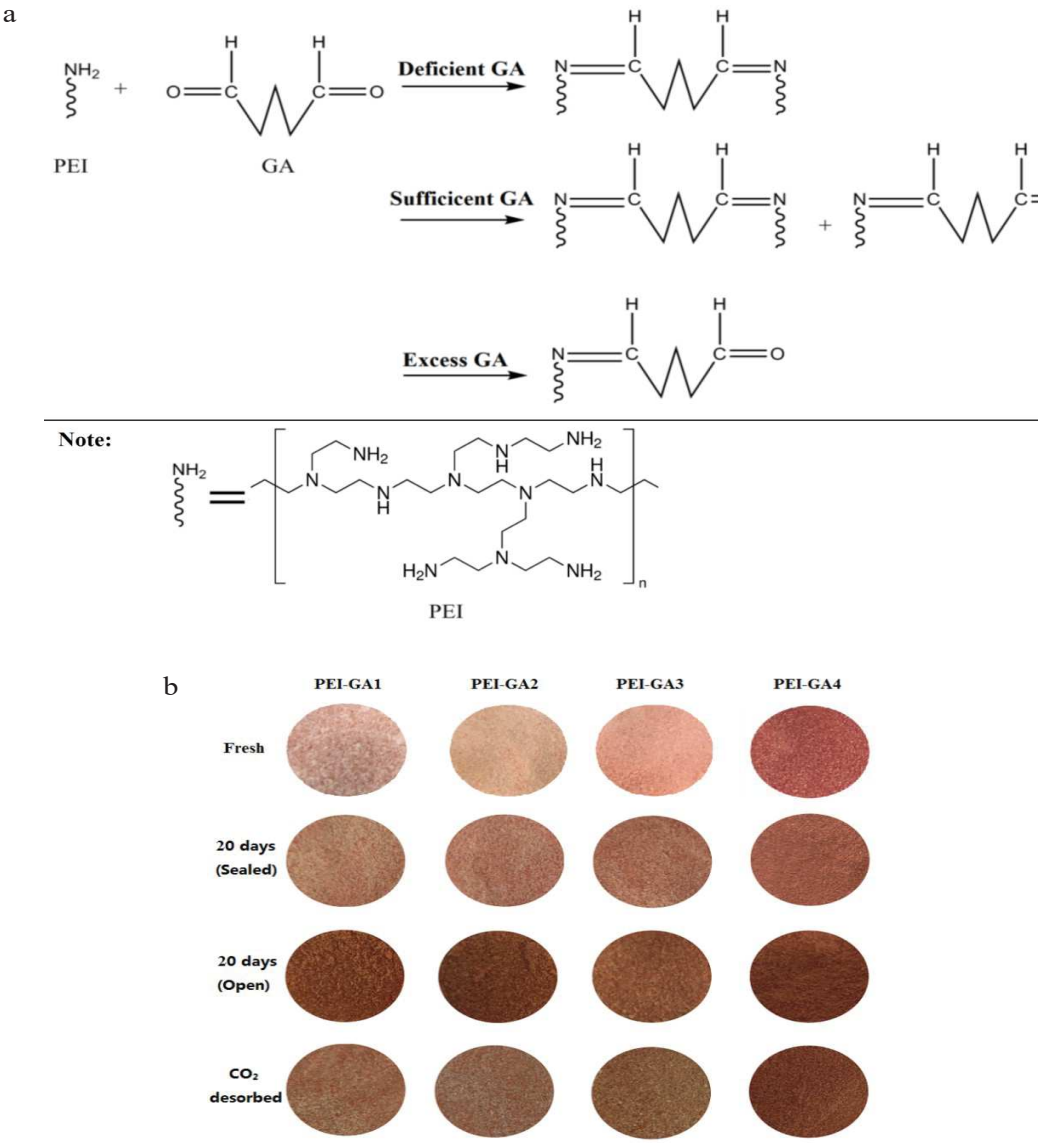

Figure 4-1 (a) The reaction of PEI with GA; (b) Images of PEI-GA resins under different conditions.

4.3.3. Characterization of materials

For characterization, freshly resins were prepared and stored in sealed condition before being analyzed within 5 days. Se(VI)-loaded resins were prepared by contacting 0.5 L of 0.5 mmol L^{-1} Se(VI) solution with 100 mg of resins for 600 min, while Cu(II)-loaded ones were obtained by

contacting 0.5 L of 1.0 mmol L^{-1} Cu(II) solution with 200 mg of resins for 48 h. Those contaminant-loaded adsorbents were freeze-dried at −52 °C/0.1 mbar for 24 h and stored in sealed condition before being characterized.

Elemental analyses were carried out with an Elementar Vario EL cube (Hanau, Germany).

FT-IR spectrometry analysis was performed in the range 4000–400 cm^{-1} using an FTIR-ATR (Attenuated Total Reflectance tool) Bruker VERTEX70 spectrometer (Bruker, Ettlingen, Germany).

X-ray photoelectron spectroscopy (XPS) measurements were carried out with a K-Alpha+ spectrometer (ThermoFisher Scientific, East Grinstead, UK).

Scanning electron microscopy (SEM) was performed using an environmental scanning electron microscope Quanta FEG 200 (FEI France, Thermo Fisher Scientific, Mérignac, France).

The pH_{PZC} values of PEI-GA resins that are freshly prepared or stored in open condition after 20 days were measured using the pH-drift method. Briefly, 50 mL of 0.1 M NaCl solution with initial pH (pH_0) range of 5-12 were mixed with 0.1 g of the adsorbent for 48 hours under agitation with a speed of 150 rpm at room temperature. Thereafter, final pH (pH_f) was measured and plotted against pH_0. The values of pH_{PZC} correspond to the point at which pH_f was equal to pH_0.

4.3.4. Adsorption experiments

The adsorption experiments were carried out by contact of a given amount of adsorbents (m, g) with a given volume (V, L) of metal-containing solution (C_0, mg L^{-1}) at room temperature with a range of 16 ºC - 25 ºC. At desired time intervals, 2 mL of samples were collected, filtrated and analyzed using inductively coupled plasma atomic emission spectrometry (ICP-AES, JY Activa M, Jobin-Yvon, Horiba, Longjumeau, France). It is noted that unless otherwise specified, all the adsorbents used were those freshly prepared and stored in sealed condition less than 10 days.

4.3.5. Modeling and selectivity

1.3.5.1. Modeling

Uptake kinetics has been modeled using the pseudo-first order rate equation (PFORE) and the pseudo-second order rate equation (PSORE).

PFORE:

Eq. 4-1

$$q(t) = q_{eq,1}(1 - e^{-k_1 t})$$

PSORE :

Eq. 4-2

$$q(t) = \frac{q_{eq,2}^2 \times k_2 \times t}{1 + q_{eq,2} \times k_2 \times t}$$

where q_t and q_{eq} (mmol g^{-1}) are the adsorption capacities adsorbed at t and at equilibrium, respectively. The parameters k_1 and k_2 are the apparent rate constants of PFORE (min^{-1}), and PSORE (g $mmol^{-1}$ min^{-1}), respectively.

Sorption isotherms represent the solute distribution at equilibrium between the liquid and the solid phase for different initial metal concentrations: the adsorption capacity (q) is plotted vs. the residual metal concentration (C_{eq}). One of the most commonly used models for describing solute adsorption to soils is the Langmuir model (Eq. 4-3).

Langmuir:

$$q_{eq} = \frac{K \times q_m \times C_{eq}}{1 + K \times C_{eq}} \quad \textbf{Eq. 4-3}$$

where q_m and K are the Langmuir parameters corresponding to the adsorption capacity at saturation of the monolayer (mmol g^{-1}) and K is the affinity coefficient (L $mmol^{-1}$).

The parameters were obtained by non-linear regression analysis using Origin 9.0 (Origin software Inc., San Clemente, CA, USA).

1.3.5.2. Selectivity

The separation factor ($\alpha_{i/j}$, i and j referring to co-existing contaminants in binary system) is calculated for defining the possible preference of the adsorbent for a given contaminant in the binary adsorption system by the following equation:

$$\alpha_{i/j} = \frac{q_{eq,i} \times C_{eq,j}}{q_{eq,j} \times C_{eq,i}} \quad \textbf{Eq. 4-4}$$

If $\alpha_{i/j}>1$, i is preferred; alternatively, j is preferred.

4.4. Results and discussion

4.4.1. SEM and Elemental analysis

Figure 4-2 shows the SEM images of PEI-GA adsorbents. It is noted that all the adsorbents were crushed to pass a 0.25-mm screen using a Retsch ZM 200 centrifugal mill. Generally, the adsorbents consist of small particles with a size less than 0.2 mm; however, some aggregation of these small particles are observed for all the adsorbents, except for PEI-GA4. The aggregation is probably due to the hydrogen-bonding interactions between amine groups, especially primary amines, that gathers the tiny particles. This is the first clue that most of primary amine groups have been consumed by GA in PEI-GA4.

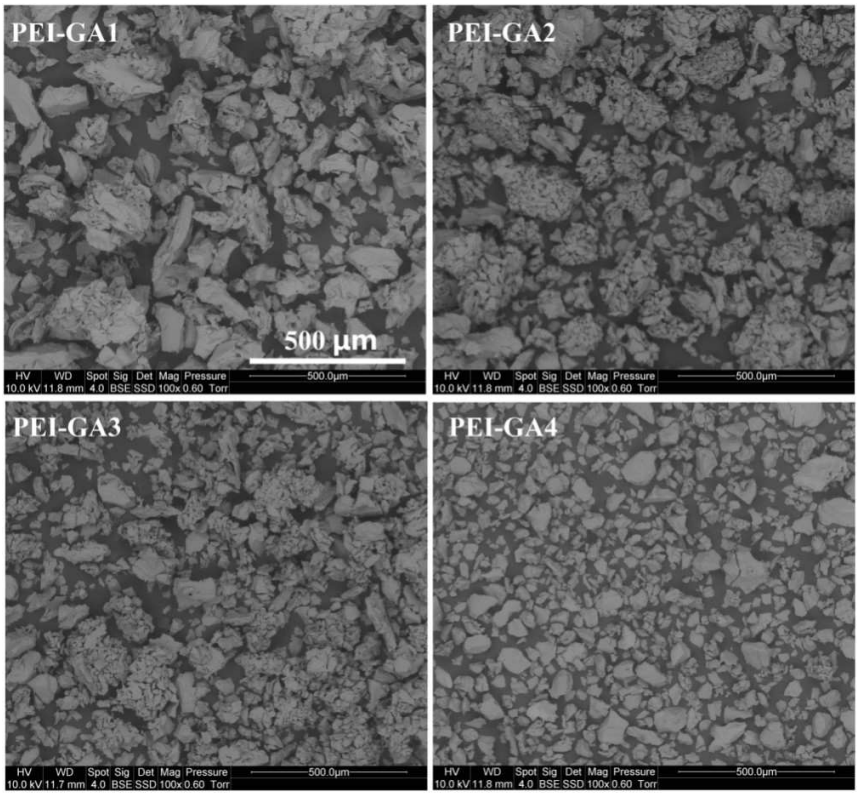

Figure 4-2 SEM images of the PEI-GA resins.

Based on the elemental composition of PEI and GA, the elemental composition of PEI-GA resins only consists of C, H, O, and N.

The SEM images and elemental maps for N, Se and Cu of Se(VI)-loaded and Cu(II)-loaded resins are shown in Figure 4-3 and Figure 4-4. After sorption, much less aggregates are found from SEM images. This is because that most amine groups are protonated after interacting with acidic contaminant solutions, resulting in the electrostatic repulsion which separates those aggregated particles. Moreover, N distribution is roughly homogeneous in the whole mass of the adsorbents. This means the resins are homogeneous and PEI is uniformly dispersed. The distribution of Se or Cu is clearly correlated to that of N, suggesting that N plays an important role in binding Se(VI) and Cu(II).

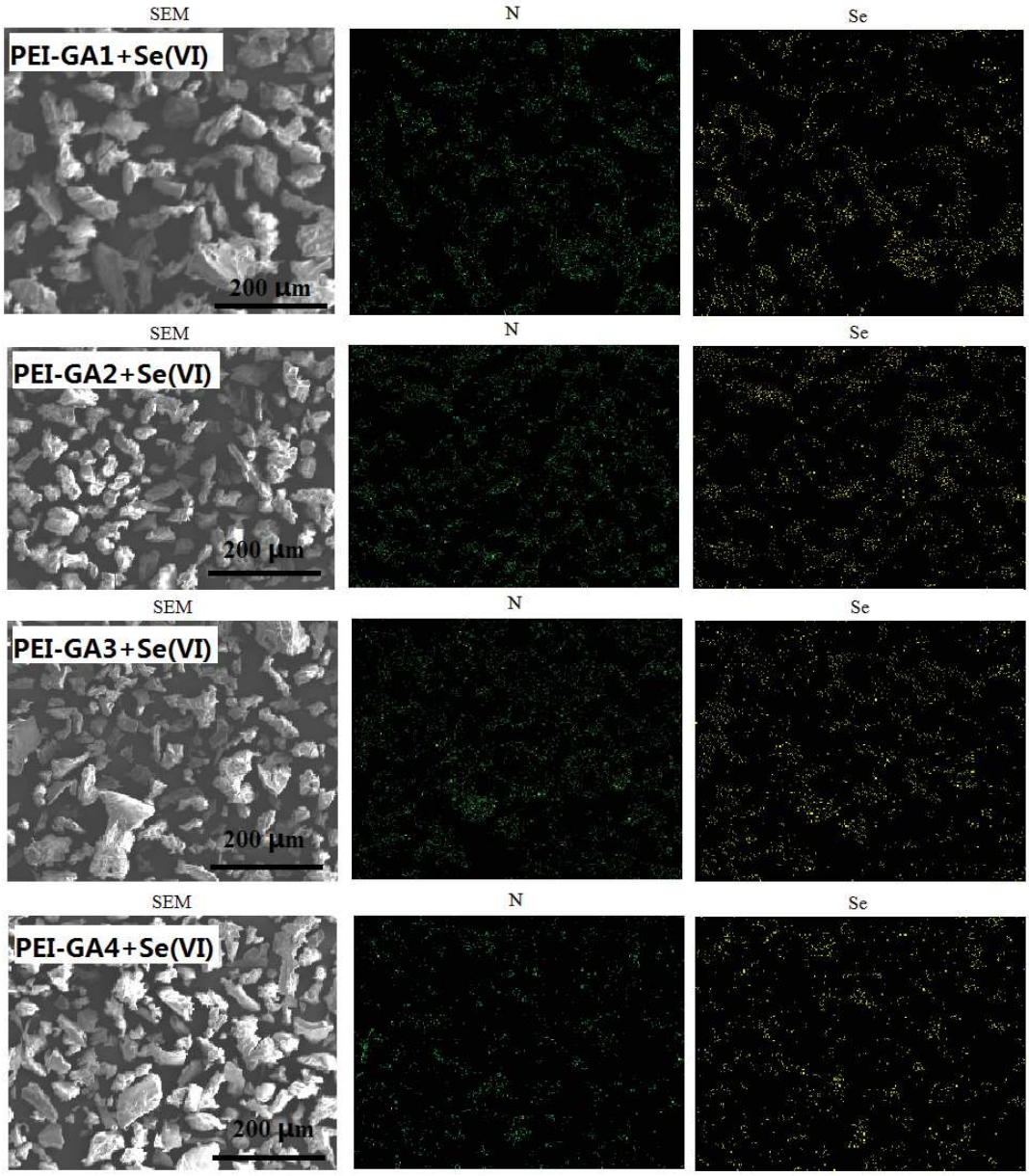

Figure 4-3 SEM images and elemental map for N and Se of Se(VI)-loaded PEI-GA resins.

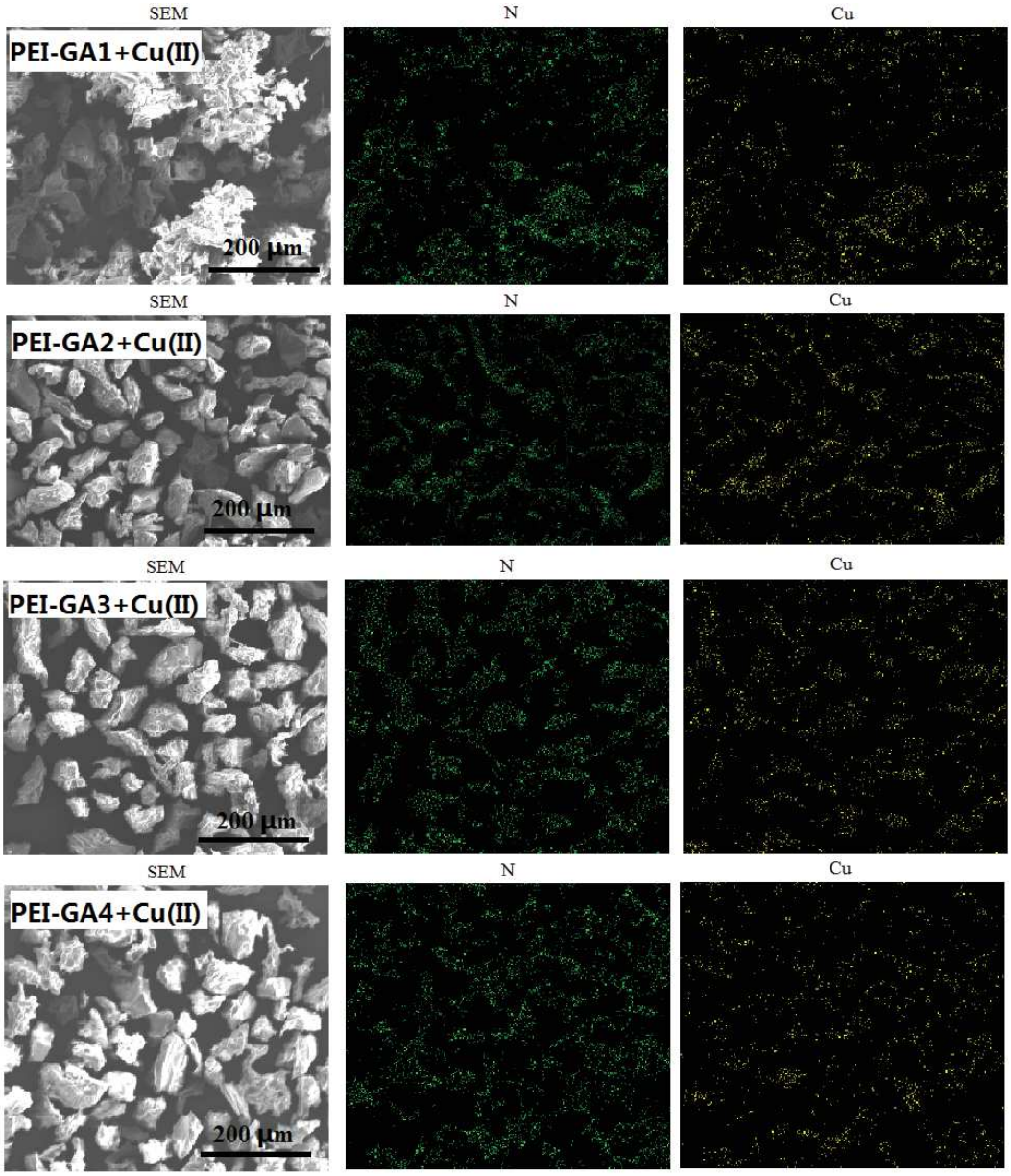

Figure 4-4 SEM images and elemental map for N and Cu of Cu(II)-loaded PEI-GA resins.

Elemental analysis (Table 4-1) shows that for raw samples, C content increases with increasing GA amount, while an opposite trend is found for N content. For PEI-GA1, GA amount is deficient, resulting in a large amount of PEI loss; the yield of conversion is the lowest among the four adsorbents. Therefore, its N content is only slightly higher than that of other samples. However, for PEI-GA4, there is an excess of GA; therefore, one Schiff base is formed with one aldehyde group of the GA and the other aldehyde group remains free. In this case, GA takes a larger part in the final product compared to the other three adsorbents, leading to a lower N content. When there

is deficient GA, the crosslinking is formed with one GA molecule and two primary amine groups on PEI, meaning that, in this case (for example, PEI-GA1), no oxygen should be found.

Surprisingly, O element can be found in the four adsorbents. This could be attributed to the eventual capture of CO_2 and H_2O (when the air is humid) during the synthesis. Figure 4-5 shows the proposed reactions between PEI and CO_2 and H_2O. After storing in open condition for 20 days, a very small decrease on N content is observed; this is due to the capture of with CO_2 and H_2O (or their reaction), increasing the mass of the adsorbents and thus reducing the proportion of N content. After CO_2 desorption process, the content of C, N and O increases/or decreases back towards the original values, indicating that the changes during storage are mostly reversible. It is worth studying how this change affects the binding properties of these adsorbents for Cu(II) and Se(VI).

Table 4-1 Elemental analysis of PEI-GA adsorbents (wt.%).

Element	Condition	PEI-GA1	PEI-GA2	PEI-GA3	PEI-G4
C	Freshly prepared	62.13 ± 1.22	61.03 ± 0.64	61.27 ± 0.70	63.41 ± 0.83
	After 20 days[a]	53.79 ± 0.39	52.40 ± 0.58	51.20 ± 1.08	54.75 ± 0.86
	After desorption step	59.75 ± 2.00	60.18 ± 0.08	61.00 ± 0.19	61.87 ± 0.85
N	Freshly prepared	22.67 ± 0.85	22.27 ± 0.52	21.20 ± 1.18	18.41 ± 0.48
	After 20 days	21.89 ± 1.06	20.91 ± 1.05	20.66 ± 1.37	17.2 ± 1.24
	After desorption step	22.10 ± 0.53	22.07 ± 0.80	21.45 ± 1.09	18.10 ± 1.06
O	Freshly prepared	4.06 ± 1.52	6.02 ± 0.15	7.12 ± 0.09	8.34 ± 0.03
	After 20 days	14.54 ± 1.14	17.28 ± 1.64	19.00 ± 0.08	18.75 ± 1.97
	After desorption step	7.91 ± 1.75	7.41 ± 0.92	6.98 ± 0.35	10.42 ± 2.74
H	Freshly prepared	11.14 ± 0.25	10.69 ± 0.28	10.42 ± 0.56	9.85 ± 0.38
	After 20 days	9.78 ± 0.46	9.41 ± 0.02	9.14 ± 0.21	9.31 ± 0.13
	After desorption step	10.25 ± 0.28	10.35 ± 0.20	10.57 ± 1.25	9.60 ± 0.81

[a]: in open condition.

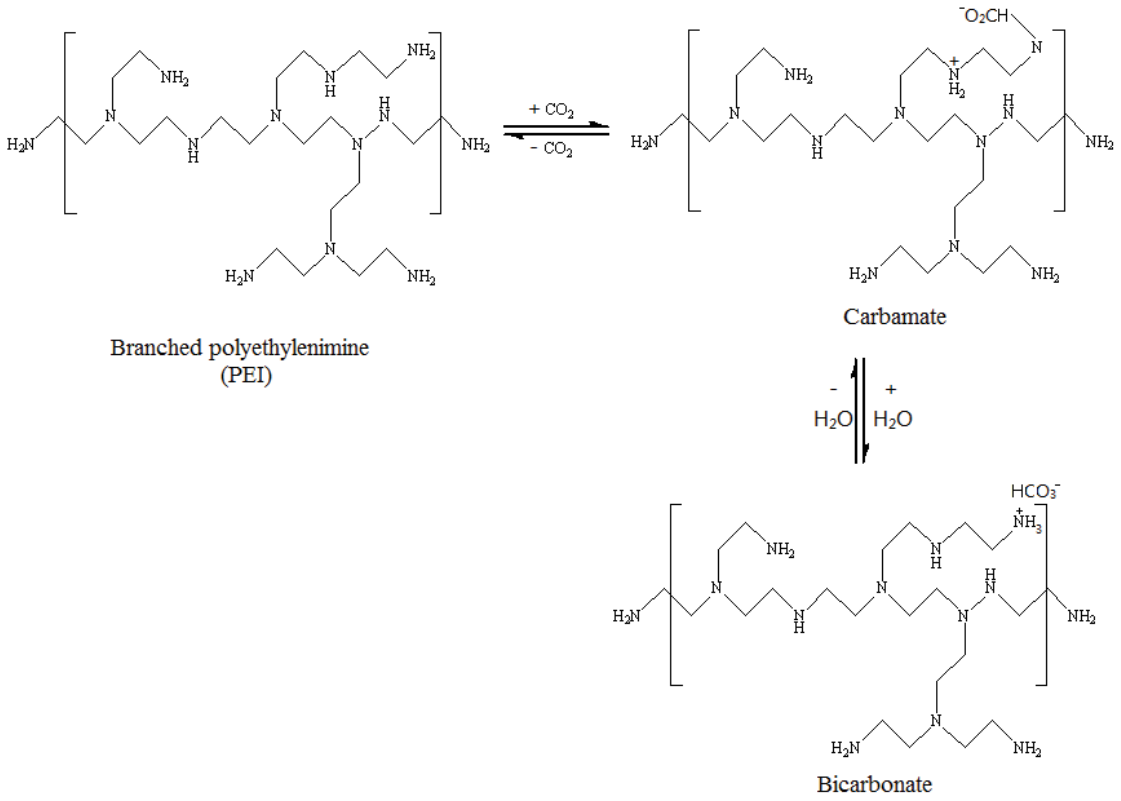

Figure 4-5 Reaction between polyethyleneimine and CO_2/H_2O.

4.4.2. FTIR

The functional groups present on the adsorbents can be identified using FTIR spectroscopy. Moreover, by comparing the spectra before and after adsorption of contaminants, it is possible to explain the mechanisms of the adsorption process through the identification of functional groups involved in metal binding. The corresponding FTIR spectra of the freshly prepared and contaminant-loaded adsorbents and those after 20-day storage and CO_2 desorption process are shown in Figure 4-6. The assignments of the main bands in spectra are reported in Table 4-2 to Table 4-5. The tables show that contaminant-free spectra of the four freshly prepared adsorbents present very similar profiles. Taking PEI-GA1 as an example, the broad absorption peaks observed between 3500–3000 cm^{-1} corresponds to the overlapping of –OH and –NH peaks [13]. The peaks at 2928 and 2812 cm^{-1} represent C–H stretching vibrations of CH_2 and CH groups, respectively [14]. The peak at 1655 cm^{-1} is due to the formation of C=N bonds [15], indicating that crosslinking has taken place between primary amine groups of PEI and GA, forming "Schiff's base" [1]. The peak at 1570 cm^{-1} can be assigned to the N–H bending vibration of primary amines [16]. It is noteworthy that, in the figures, the intensity of this peak becomes less and less noticeable as the

GA amount increases and almost disappears for PEI-GA4, suggesting that GA crosslinks most of the primary amine groups on PEI-GA4. Besides, peaks at 1458 and 1281cm^{-1} correspond to C–H bending vibration [17]. Peaks at 1102 and 1053 cm^{-1} are assigned to C–O asymmetric stretching [18]. The C–O peaks should not be found in the raw adsorbents, since the molecular formula of PEI-GA does not have C–O bond, unless it is contaminated. As discussed above, PEI could react with CO_2 and has been reported to be high-capacity adsorbent for CO_2 capture [19]. The result here is a second evidence that the adsorbents partially react with CO_2 and/or H_2O during preparing process. For both primary and secondary amines, the adsorption of CO_2 involves hydrogen bonding with surface silanols or neighboring alkylamines, possibly through various arrangements upon the formation of carbamic acid.

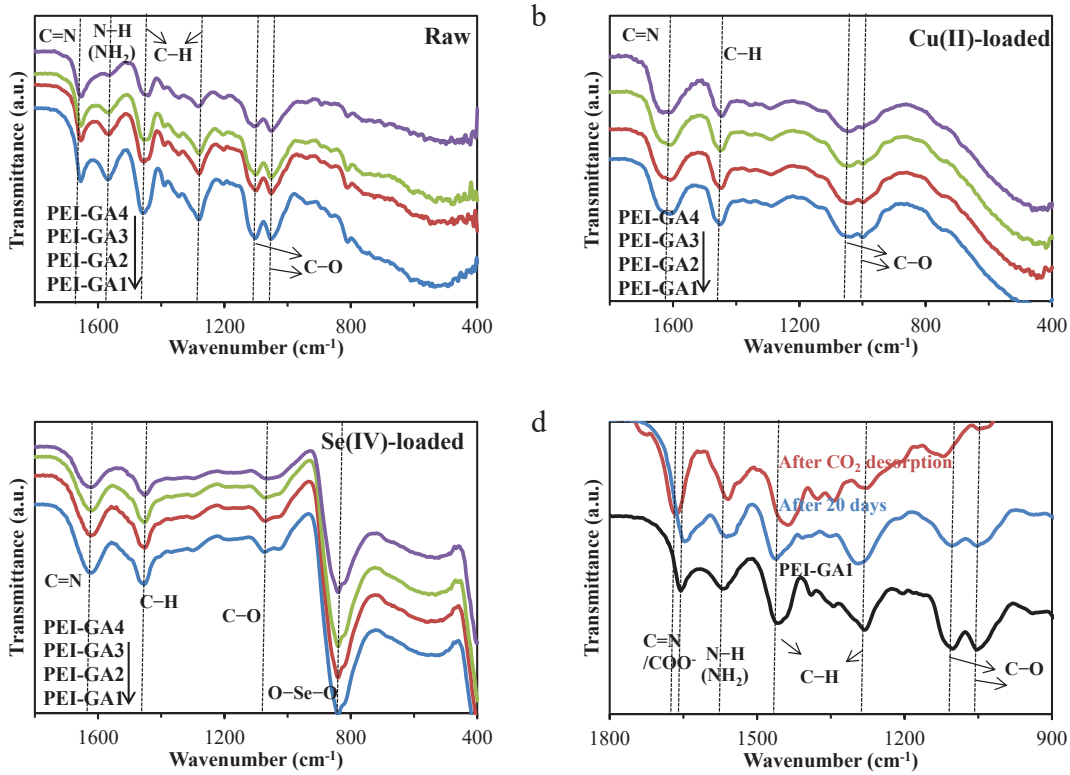

Figure 4-6 FTIR spectra of (a) raw PEI-GA, (b) and (c) before and after Cu(II) and Se(VI) adsorption and (d) PEI-GA1 after 20 days of storage and after CO_2 desorption process.

Table 4-2 Assignment of vibrational bands (wavenumber, cm^{-1}) for PEI-GA1 (raw and contaminant-loaded).

Vibration	Wavenumber cm^{-1}	Ref.	Raw	Cu(II)-loaded	Se(VI)-loaded	After 20 days

–NH/–OH stretching	3500-3000	[1]	3261	3352	3333	3252
C–H stretching vibrations of CH_2	2928	[2]	2928	2941	3007 (weak)	2935
C–H stretching vibrations of CH	2812	[2]	2812	–	2884 (weak)	2829
C=N stretching	1635	[3]	1655	1611	1621	1647
N–H bending vibration of primary amines	1570	[4]	1570	–	–	1562
C–H bending	1473	[5, 6]	1458	1450	1453	1461
C–H bending	1281	[5, 6]	1281	1288 (weak)	–	1295
C–O asymmetric stretching	1102	[7]	1102	–	1074	1105
C–O asymmetric stretching	1053	[7]	1053	1037	–	1052
SeO_3 pyramidal groups	840	[8]	–	–	840 (strong)	–

Table 4-3 Assignment of vibrational bands (wavenumber, cm^{-1}) for PEI-GA2 (raw and contaminant-loaded).

Vibration	Wavenumber	Ref.	Raw	Cu(II)-loaded	Se(VI)-loaded	After 20 days
–NH/–OH stretching	3500-3000	[1]	3261	3351	3258	3251
C–H stretching vibrations of CH_2	2928	[2]	2928	2941	3006	2934
C–H stretching vibrations of CH	2812	[2]	2807	–	2845	2824
C=N stretching	1635	[3]	1655	1609	1621	1648
N–H bending vibration of primary amines	1570	[4]	1566	–	–	1562
C–H bending	1473	[5, 6]	1455	1448	1452	1457
C–H bending	1281	[5, 6]	1280	1289	–	1288
C–O asymmetric stretching	1102	[7]	1101	–	1071	1103
C–O asymmetric stretching	1053	[7]	1052	1039	–	1054

Vibration	Wavenumber	Ref.	Raw	Cu(II)-loaded	Se(VI)-loaded	After 20 days
SeO_3 pyramidal groups	840	[8]	–	998	840	–

Table 4-4 Assignment of vibrational bands (wavenumber, cm^{-1}) for PEI-GA3 (raw and contaminant-loaded).

Vibration	Wavenumber	Ref.	Raw	Cu(II)-loaded	Se(VI)-loaded	After 20 days
–NH/–OH stretching	3500-3000	[1]	3264	3350	3267	3229
C–H stretching vibrations of CH_2	2928	[2]	2929	2936	3012	2935
C–H stretching vibrations of CH	2812	[2]	2805	–	2843	2819
C=N stretching	1635	[3]	1655	1610	1620	1652
N–H bending vibration of primary amines	1570	[4]	1566	–	–	1558
C–H bending	1473	[5, 6]	1454	1450	1453	1457
C–H bending	1281	[5, 6]	1280	1289	–	1285
C–O asymmetric stretching	1102	[7]	1100	–	1072	1102
C–O asymmetric stretching	1053	[7]	1053	1051	–	1051
SeO_3 pyramidal groups	840	[8]	–	999	840	–

Table 4-5 Assignment of vibrational bands (wavenumber, cm^{-1}) for PEI-GA4 (raw and contaminant-loaded).

Vibration	Wavenumber	Ref.	Raw	Cu(II)-loaded	Se(VI)-loaded	After 20 days
–NH/–OH stretching	3500-3000	[1]	3272	3343	3237	3245
C–H stretching vibrations of CH_2	2928	[2]	2926	2939	2850	2931
C–H stretching vibrations of CH	2812	[2]	2812	–	–	2820
C=N stretching	1635	[3]	1654	1632	1623	1650
C–H bending	1473	[4]	1441	1444	1454	1442

Vibration	Wavenumber	Ref.	Raw	Cu(II)-loaded	Se(VI)-loaded	After 20 days
C–H bending	1281	[5, 6]	1283	1293	–	1288
C–O asymmetric stretching	1102	[5, 6]	1106	–	–	1100
C–O asymmetric stretching	1053	[7]	1050	1044	1064	1054
SeO_3 pyramidal groups	840	[7]	–	–	840	–

After storing in open condition for 20 days, taking PEI-GA1 samples as an example (shown in Figure 4-6d), the intensity of peak at 1570 cm $^{-1}$ corresponding to N–H bending vibration of primary amines decreases slightly, while the peak at around 1655 cm^{-1} becomes much wider. This can be due to the overlapping of COO^- stretching at 1610 cm^{-1} [20]. These results indicate the formation of COO^- groups by the reaction of free amine groups with CO_2. The same trend is also found for the other adsorbents (shown in Figure 4-7). After a thermal treatment under nitrogen atmosphere, the peak at 1655 cm^{-1} red-shifts and becomes less wide compared to resins stored after 20 days. This might be due to the disappearance of COO^- groups. The contamination could affect the adsorption properties of PEI-GA for metal adsorption, which will be discussed below.

After Cu(II) binding, the band around 1570 cm^{-1} specific to primary amine groups completely disappears. This significant change confirms the involvement of N–H of primary amines groups in Cu(II) adsorption onto the adsorbents. Other changes are associated to slight shifts of the bands. Taking PEI-GA1 as an example, the bands shift at 3261, 2928, 1655 and 1053 cm^{-1}, which are ascribed to the stretching vibrations of N–H [21], C–H [14], C=N [15] and C–O [18], respectively. The disappearance of peaks at 2812 and 1102 cm^{-1}, corresponding to C–H stretching and C–O stretching, respectively, was also observed. This could be due to the reaction of carbamate with H_2O in humid condition to form bicarbonate or carbamic acid [22].

In the case of the Se(VI)-adsorbed samples, a new peak at 840 cm^{-1}, assigned to the vibrations of SeO_3 pyramidal groups with C3v point symmetry [23], appears regardless of adsorbents, confirming the binding of SeO_4^{2-}. In addition, the stretching of C=N is shifted toward lower wavenumbers. Other changes consist of the disappearance of peaks corresponding to N–H bending vibration of primary amines, C–H bending and asymmetric stretching vibration of C–O–C.

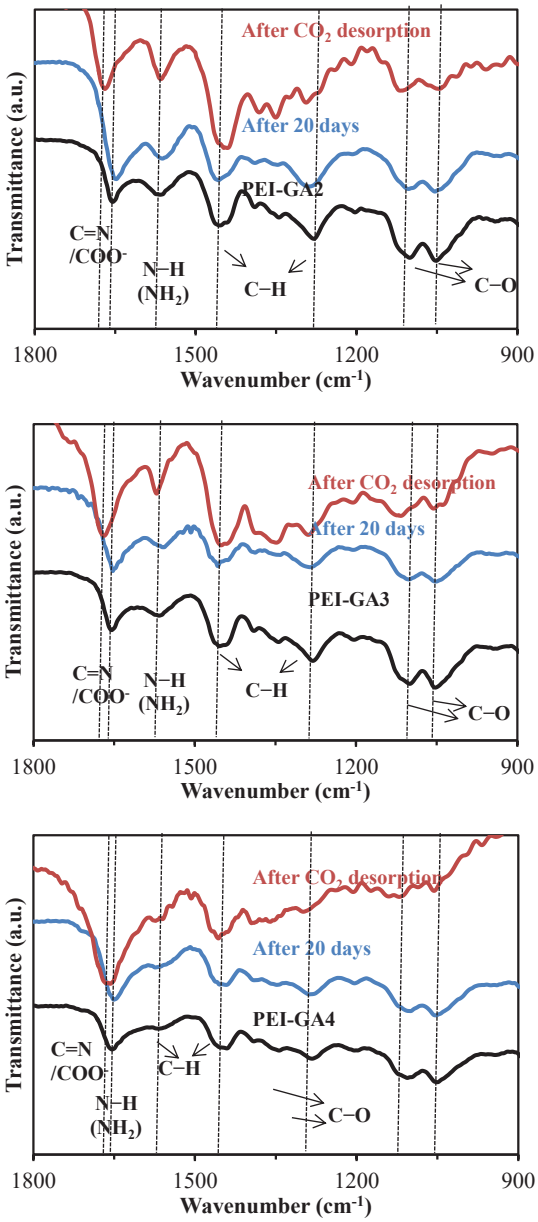

Figure 4-7 FTIR spectra of fresh PEI-GA2, PEI-GA3 and PEI-GA4, these after 20 days of storage and after CO_2 desorption process.

In addition, the pH_{PZC} of freshly prepared PEI-GA1, PEI-GA2, PEI-GA3 and PEI-GA4 are 9.95, 10.11, 9.80 and 9.69, respectively. After 20-day storage, these values decreased to 9.54, 9.72, 9.46 and 9.43, respectively. This decrease on pH_{PZC} values are probably due to the formation of groups with a lower pK_a value, further (besides the result of FTIR) confirming the formation of COO^- groups, whose pKa value is close to 4. The experiments below (see section 4.4.5) will discuss how this change affects the adsorption properties of the resins for Cu(II) and Se(VI).

4.4.3. XPS

To further confirm the contamination of PEI-GA resins when stored in open condition for a certain time, XPS was used to investigate surface composition of PEI-GA resins before and after exposure to the air after 20 days. As expected, XPS of freshly prepared materials (Figure 4-8a) reveals the presence of N, C and O. The N 1s peak is broad and can be resolved into two components: (a) a high binding energy (399 eV) attributed to amine or amide groups and (b) a lower binding energy one (398.9 eV) assigned to the N in the tertiary amine groups (>N–) [24]. The amount of tertiary amine groups increases with the increasing GA amount, due to the reaction between aldehyde groups on GA and free amine groups on PEI. The binding energy around 284.8 eV and 285.8 eV could be due to C–C bond and C–N or C–O–C bond, respectively [5, 6]. The contribution at around 287.3–280.0 eV represents C=O functions, which could be attributed to uncrosslinked aldehyde groups of GA or a slight adsorption of CO_2 because of the presence of abundant free amine groups during preparation process.

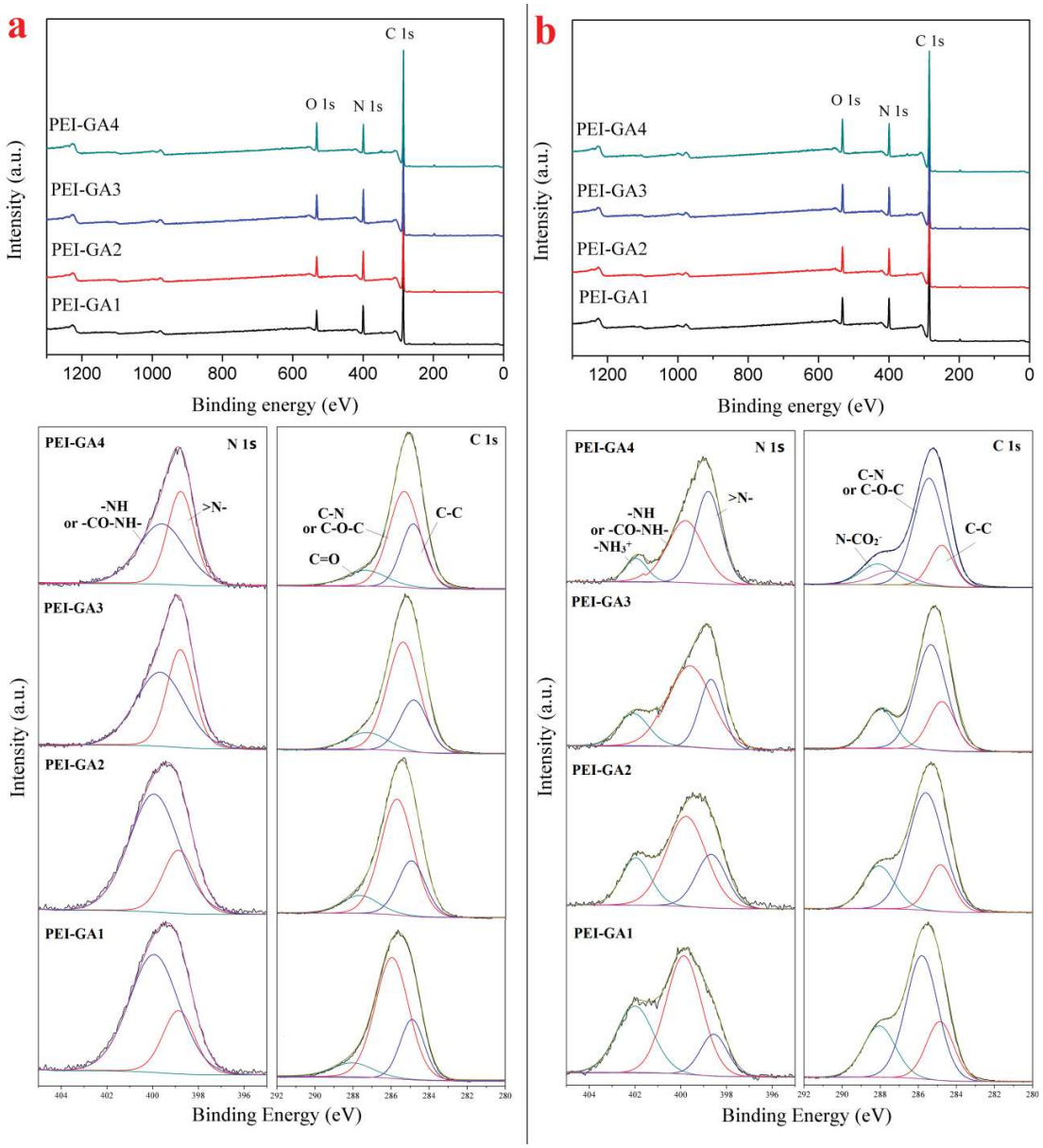

Figure 4-8 X-ray photoelectron spectra of PEI-GA resins (a) freshly prepared and (b) after 20-day storage in open condition.

After 20-day storage in open condition, new peaks, shown in Figure 4-8b, appear at around 288.1 eV for C 1s representative for carboxylate and 402.1 eV for N 1s due to protonated nitrogen associated with the formation of the carbamate ion. These peaks firmly confirm the interaction of CO_2 and PEI-GA resins.

4.4.4. Effect of pH on adsorption kinetics

Raw wastewaters containing Cu(II) or Se(VI) are commonly acidic, such as Cu(II) in printed circuit board wastewater (pH 1) [25], mix electroplating wastewater (pH 1.6) [26], and smelter wastewater (pH<1) [27]. To ensure no formation of metal hydroxide precipitates and avoid using too much pH-adjusting reagents such as NaOH, CaO, etc. when applied practically, the effect of pH was conducted in acidic condition with the pH range of 2–3. Figure 4-9 shows the effect of pH on Se(VI) and Cu(II) adsorption kinetics. In general, the adsorption of Se(VI) presents an anionic behavior, slightly decreasing as the pH increased from 2 to 3. The trend is attributed to the predominant selenium species in solution and the surface charges of adsorbents. The pK_a values of primary, secondary, and tertiary amine groups on PEI were reported as 4.5, 6.7, and 11.6, respectively [28]. The pH_{PZC} (Table 4-6) of the resins is in the range of 9.69 to 10.11. Since the initial pH range of the present study is between 2.0 and 3.0 (corresponding to final pH between 2.1 to 4.3), the reactive groups are strongly protonated. These protonated groups can only bind anionic species. Therefore, as is shown in Figure 2-16(a) (see Chapter 2), the adsorption decreases as the percentage of the aqueous species $HSeO_4^-$ decreases. Erosa at al. [29] observed a gradual decrease on Se(VI) adsorption as pH increased from 2 to 10 using weakly basic anion exchangers that possess primary, secondary and/or tertiary amino groups. This decrease on Se(VI) binding was due to the decline on the degree of amine protonation and the decrease of the fraction of $HSeO_4^-$. Similarly, Yamani et al. [30] reported that the adsorption of Se(VI) onto chitosan-based beads decreased at alkaline pH. The difference of Se(VI) adsorption among the adsorbents is negligible, especially among PEI-GA1, PEI-GA2 and PEI-GA3. The level of GA crosslinking for PEI causes different contents of primary amine groups in the adsorbents, but does not affect significantly the total amount of amine groups (or N content), except for PEI-GA4 (confirmed by elemental analysis). Therefore, the lowest Se(VI) adsorption capacities of PEI-GA4 can be directly explained by the lower N content compared with the other adsorbents.

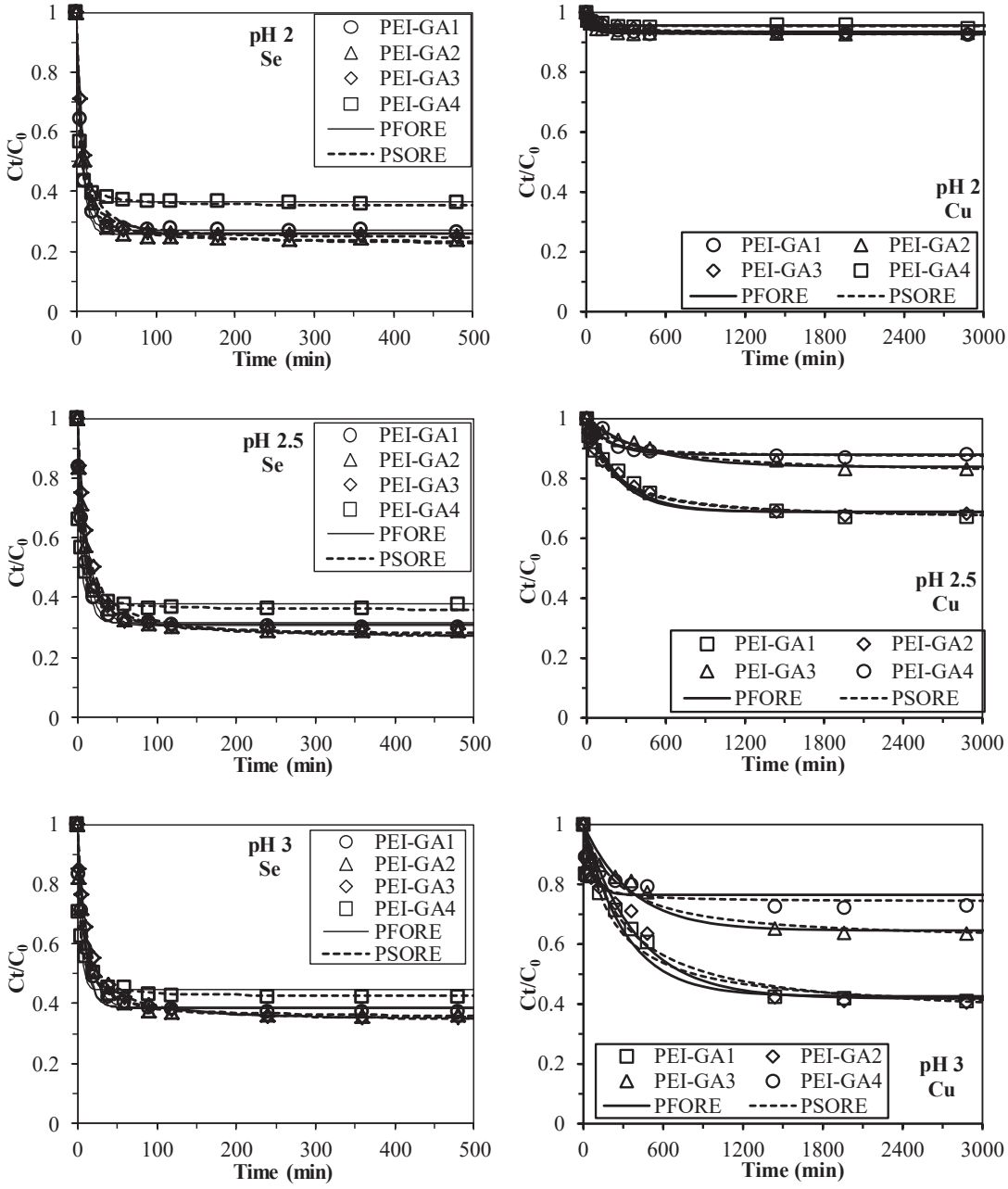

Figure 4-9 Effect of pH on Se(VI) and Cu(II) adsorption-kinetics modeling using PFORE and PSORE (Volume = 0.5 L; Adsorbent mass = 100 mg for Se(VI) and 200 mg for Cu(II); Room temperature (19-25 ^{o}C); C_0 = 0.5 mmol L^{-1} for Se(VI) and 1 mmol L^{-1} for Cu(II)).

Table 4-6 pH_{PZC} of PEI-GA (freshly prepared and stored in open condition after 20 days).

	Condition	PEI-GA1	PEI-GA2	PEI-GA3	PEI-G4
pH_{PZC}	Freshly prepared	9.95	10.11	9.80	9.70
	After 20 days	9.54	9.72	9.46	9.43

The trend found for Cu(II) cations is completely opposite: the adsorption efficiency is strongly affected by solution pH. Negligible adsorption is found when initial pH value is 2.0 and the adsorption efficiency increases significantly when initial pH increases to 3.0, corresponding to equilibrium pH value of 3.63 for PEI-GA1, 3.64 for PEI-GA2, 3.59 for PEI-GA3 and 3.42 for PEI-GA4. The amine groups on the adsorbents are fully protonated in all solutions within selected pH range, resulting in the electrostatic repulsion of Cu(II). As pH increases, this electrostatic repulsion reduces, leading to better adsorption performance. The main adsorption interaction can be summarized as the coordination bonding between Cu(II) and primary and secondary amine groups on PEI-GA. The binding potential of tertiary amine groups on the adsorbents is limited due to the lower stability constants of complexes with tertiary amines than those with primary or secondary amines [31]. The amount of primary amine groups on the adsorbents decreases gradually as the level of crosslinking between PEI and GA increases. This can explain the big gap of the adsorption efficiency among PEI-GA2, PEI-GA3 and PEI-GA4. Interestingly, apart from the first 10 h of reaction, the equilibrium adsorption efficiencies of PEI-GA1 and PEI-GA2 are almost the same. This could be due to that the amount of GA added for crosslinking for PEI-GA1 is not enough and a certain amount of PEI is not crosslinked or well immobilized; therefore, during washing step, some free PEI may be released and thus the adsorption capacity is not as high as it is expected.

The pseudo-second order rate equation (PSORE) and the pseudo-first order rate equation (PFORE) were used to fit experimental data. The plots shown in Figure 4-9 indicate that both PFORE and PSORE can be used to fit kinetic profiles. However, the parameters shown in Table 4-7 for Cu(II) and Table 4-8 for Se(VI) suggest that the PSORE fits the data slightly better with all the values of determination coefficient (r^2) more than 0.90. The apparent rate constants k_1 and k_2 of PEI-GA4 for both contaminants are higher than those for the other three adsorbents; this could be due to poorer mass transfer property caused by the aggregation of PEI-GA1, PEI-GA2 and PEI-GA3 particles, which has been discussed in section 4.4.1.

Table 4-7 Kinetics constants for the adsorption of Cu(II) at pH 3.

Models	**Parameters**	PEI-GA1	PEI-GA2	PEI-GA3	PEI-GA4
	$q_{eq,exp}$ (mmol L^{-1})	1.33	1.34	0.82	0.61
PFORE	$q_{eq,cal}$ (mmol L^{-1})	1.29	1.31	0.80	0.53
	$k_1 \times 10^3$ (min^{-1})	3.2	2.5	2.8	15.6
	r^2	0.87	0.87	0.87	0.78
PSORE	$q_{eq,cal}$ (mmol L^{-1})	1.41	1.47	0.89	0.58
	$k_2 \times 10^3$ (g $mmol^{-1}$ min^{-1})	3.3	2.3	4.4	5.2
	r^2	0.91	0.90	0.91	0.87

Table 4-8 Kinetics constants for the adsorption of Se(VI) at pH 2.

Models	**Parameters**	PEI-GA1	PEI-GA2	PEI-GA3	PEI-GA4
	$q_{eq,exp}$ (mmol L^{-1})	4.69	4.82	4.78	4.12
PFORE	$q_{eq,cal}$ (mmol L^{-1})	4.63	4.68	4.69	4.03
	$k_1 \times 10^3$ (min^{-1})	139.8	148.6	98.2	227.6
	r^2	0.99	0.95	0.99	0.99
PSORE	$q_{eq,cal}$ (mmol L^{-1})	4.82	4.87	4.95	4.14
	$k_2 \times 10^3$ (g $mmol^{-1}$ min^{-1})	50.0	55.1	30.9	117.0
	r^2	0.98	0.98	0.99	0.99

In order to further confirm the effect of GA crosslinking on adsorption capacities of PEI-GA resins for Se(VI) and Cu(II), adsorption isotherms were conducted at pH 2 for Se(VI) and pH 3 for Cu(II). The results shown in Figure 4-10 are in good agreement with those obtained by adsorption kinetics. The maximum adsorption capacity (q_m) calculated from Langmuir model of PEI-GA1 for Se(VI) is 5.25 mmol g^{-1}, very close to 5.14 mmol g^{-1} of PEI-GA2 and 5.05 mmol g^{-1} of PEI-GA3 and slightly higher than 4.24 mmol g^{-1} of PEI-GA4. However, q_m of PEI-GA1 and PEI-GA2 for Cu(II) are 1.57 and 1.40 mmol g^{-1}, respectively, much higher than 0.87 mmol g^{-1} of PEI-GA3 and 0.69 mmol g^{-1} of PEI-GA4.

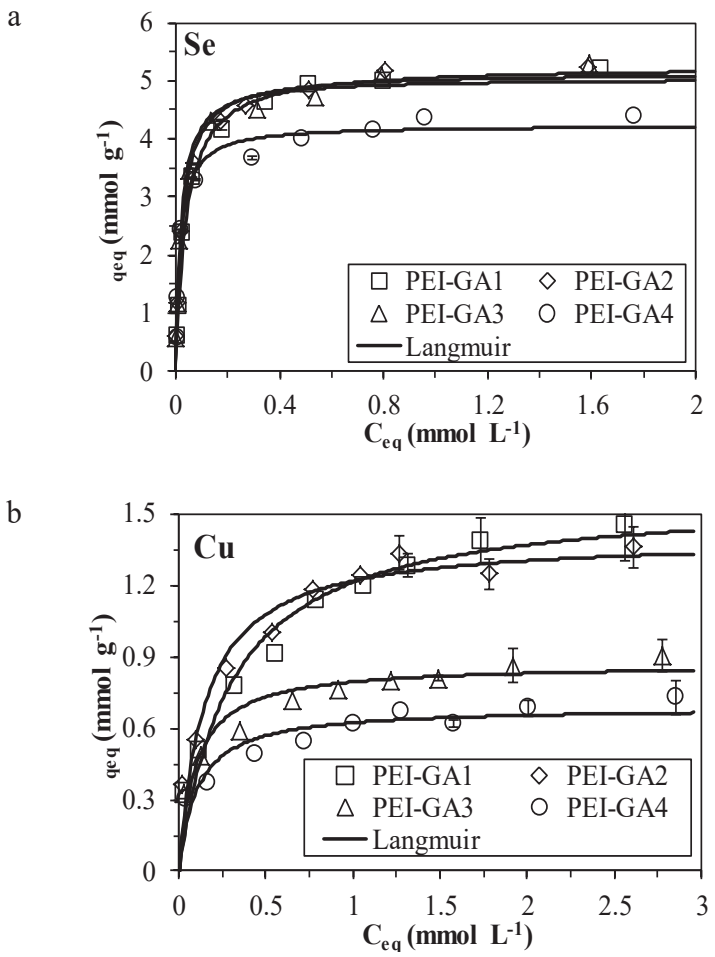

Figure 4-10 (a) Se(VI) and (b) Cu(II) adsorption isotherms using PEI-GA resins (Volume = 50 mL; Room temperature; adsorbent mass = 20 mg; C_0 = 0.1-3.5 mmol L^{-1}; contact time = 24 h for Se(VI) and 48 for Cu(II); pH 2 for Se(VI) and pH 3 for Cu(II)).

4.4.5. Effect of different storage conditions on adsorption capacity

The chemical stability of the functional groups on the adsorbents is essential for further application. When exposed to the air for a long time, the active amine groups on the adsorbents could be converted into carbamate and/or bicarbonate [10], which might have detrimental, beneficial or minimal effects on their adsorption capacity for aqueous contaminants. The storage stability of the adsorbents was tested by comparing the adsorption capacity of PEI-GA freshly prepared and stored in sealed condition or in open condition after 20 days. Figure 4-11 shows that the adsorption efficiency for Se(VI) is slight affected by the storage conditions. No significant difference is observed between the adsorbents prepared freshly and stored in sealed condition after 20 days; for

those stored in open condition, only a slight decrease on adsorption capacity can be found regardless of adsorbent type. This decrease might be caused by the decrease of N content which has been confirmed by elemental analysis. For Cu(II), the adsorption capacity of freshly prepared PEI-GA1, PEI-GA2, PEI-GA3 and PEI-GA4 is 1.33, 1.33, 0.82 and 0.61 mmol g^{-1}, respectively. After storing in open condition for 20 days, those values decrease significantly to 1.02, 0.91, 0.60 and 0.56 mmol g^{-1}, respectively, while those of the adsorbents stored in sealed condition only decrease to 1.30, 1.26, 0.80 and 0.57 mmol g^{-1}, respectively. The reason causing the decrease on adsorption could probably be that primary and secondary amine groups that are active for Cu(II) adsorption on PEI-GA adsorbents stored in open condition react with CO_2/H_2O to form carbamate/bicarbonate. Although carbonyl groups can potentially adsorb Cu(II), their adsorption affinity for Cu(II) at pH 3 is intrinsically lower than that of primary and secondary amine groups. Monier et al. [32] reported a Cu(II) adsorption capacity of 68 mg g^{-1} of amine-based adsorbent (chitosan resin) at pH 3. This is much higher than that of carboxyl-based materials under the similar condition, such as 28 mg g^{-1} of zirconium oxide immobilized alginate beads [33] and 10.2 mg g^{-1} of alginate beads [34]. For Se(VI) adsorption, the adsorption is only associated with amount of nitrogen. Thus, it is hardly affected by the formation of carbamate/or bicarbonate, since N content does not change significantly. Another interesting finding is that the adsorption kinetics of all the adsorbents in open condition for Cu(II) is slower than that of sealed ones. Except for PEI-GA4, the other three adsorbents stored under open condition still present a slow growing trend, while those stored in sealed condition already achieve equilibrium at 24 h. However, the reason causing the slower kinetics remains unclear. One possibility is that the formation of carbamate/or bicarbonate results in a tighter polymer network which makes it more difficult for contaminants to diffuse to the adsorption sites. To conclude, the results indicate that the storage condition plays an important role on Cu(II) adsorption onto adsorbents containing primary or secondary amine groups.

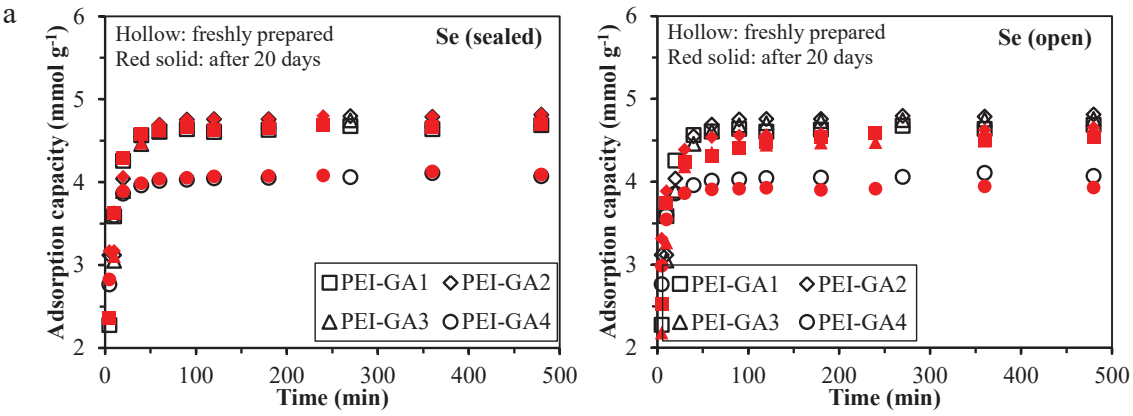

b

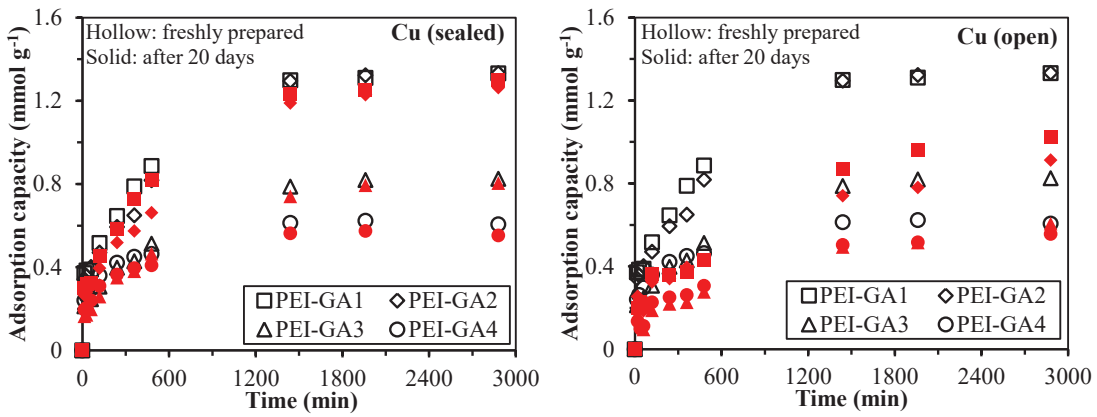

Figure 4-11 Effect of storage condition on adsorption capacity of PEI-GA for (a) Se(VI) and (b) Cu(II) (Volume = 0.5 L; Room temperature (19-25 °C); Adsorbent mass = 100 mg for Se(VI) and 200 mg for Cu(II); C_0 = 0.5 mmol L^{-1} for Se(VI) and 1 mmol L^{-1} for Cu(II); pH_0: 2 for Se(VI) and 3 for Cu(II)). Note: freshly prepared adsorbents were the materials stored in sealed condition within 5 days.

To confirm whether the the decrease on Cu(II) adsorption is caused by CO_2 and if the contamination is reversible. The re-dried, CO_2-loaded and CO_2-desorbed adsorbent were compared for Cu(II) adsorption at pH 3. Figure 4-12 shows that the re-drying process does not recover the adsorption performance significantly, confirming that humidity is not the main cause of decrease on contaminant removal. The adsorbents immersed in pure CO_2 show a sharp decrease Cu(II) adsorption capacities and after the desorption process, the adsorption properties recover significantly. The results further confirm that the decrease on adsorption capacity for Cu(II) is mainly caused by the contamination of CO_2.

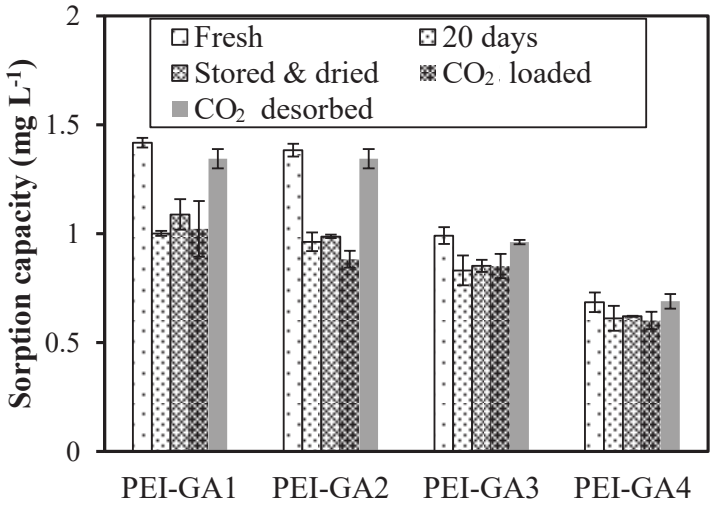

Figure 4-12 Comparison of adsorption properties of PEI-GAs (freshly prepared, re-dried, stored after 20 days in open condition and CO_2 desorbed) for Cu(II) adsorption.

4.4.6. Adsorption in binary system

To investigate the selectivity of PEI-GA adsorbents for Se(VI) and Cu(II), studies are carried out in Se-As and Cu-Pb binary systems, respectively. The results of competitive adsorption of Se(VI) and As(V) from the binary solutions with different pHs are shown in Figure 4-13. All the adsorbents have a greater affinity for Se(VI) over As(V) at pH 2. It is also noteworthy that for the three adsorbents, the equilibrium adsorption capacity is only slightly affected by the presence of As(V) at selected pH values (Figure 4-14). Moreover, As(V) is hardly removed along with Se(VI), indicating that all of the adsorbents can selectively remove Se(VI) from Se-As system at pH 2. This can be explained by the limited adsorption performance of these adsorbents for As(V) at pH 2 (Figure 4-15). When solution pH increases to pH 3, the adsorption of As(V) increases, especially for the first 10 minutes. However, these values decrease dramatically after a longer contact time. This is due to the progressive decrease of available reactive groups and the strong competition between Se(VI) and As(V) for occupying free adsorption sites. Therefore, As(V) ions start to be replaced by Se(VI) and released into the solution. For example, within 10 min, the maximum adsorption capacity of PEI-GA1, PEI-GA2, PEI-GA3 and PEI-GA4 for As(V) reaches 0.67 mmol g^{-1}, 0.49 mmol g^{-1}, 0.52 mmol g^{-1}, and 0.34 mmol g^{-1}, respectively. However, these values decrease to 0.40 mmol g^{-1}, 0.28 mmol g^{-1}, 0.26 mmol g^{-1}, and 0.16 mmol g^{-1}, respectively, after 360 min of reaction, while those for Se(VI) maintain around 4.01 mmol g^{-1}, 4.10 mmol g^{-1}, 3.95 mmol g^{-1}, and 3.56 mmol g^{-1}, respectively. The same phenomenon is observed for Cu(II) and Pb(II) adsorption from binary solutions. The adsorption capacity of Pb(II) in binary system is negligible at pH 2 and pH 2.5, while at pH 3, it reaches 0.21–0.35 mmol g^{-1} within the first hour

but decreases to less than 0.16 mmol g^{-1} after a longer reaction time. The results are also confirmed by separation factors ($\alpha_{Se/As}$ and$\alpha_{Cu/Pb}$), which are much higher than 1. For competitive adsorption of Se(VI) and As(V), the values of $\alpha_{Se/As}$ are in the same order of magnitude regardless of resin type, locating between 300 and 500 at pH 2. They all decrease to less than 50 when pH increases from 2 to 3. In terms of Cu(II) and Pb(II), no difference is found between the values of $\alpha_{Cu/Pb}$ for 4 kinds of PEI-GA resins at pH 2. However, when pH increases to 2.5, the adsorption of Cu(II) increases dramatically, while that for Pb(II) remains almost the same, resulting in much higher $\alpha_{Cu/Pb}$ values. Since PEI-GA1 and PEI-GA2 possess higher adsorption capacity for Cu(II), they present superior selectivity for Cu(II) over Pb(II) at this pH. As pH continues increasing to 3, these values decrease significantly as the adsorption capacity for Pb(II) starts growing up. To conclude, all the resins have a preference for Se(VI) over As(V) and Cu(II) over Pb(II). GA crosslinking hardly affects the preference for Se(VI), but it decreases the selectivity for Cu(II) over Pb(II) when pH is between 2.5 and 3.

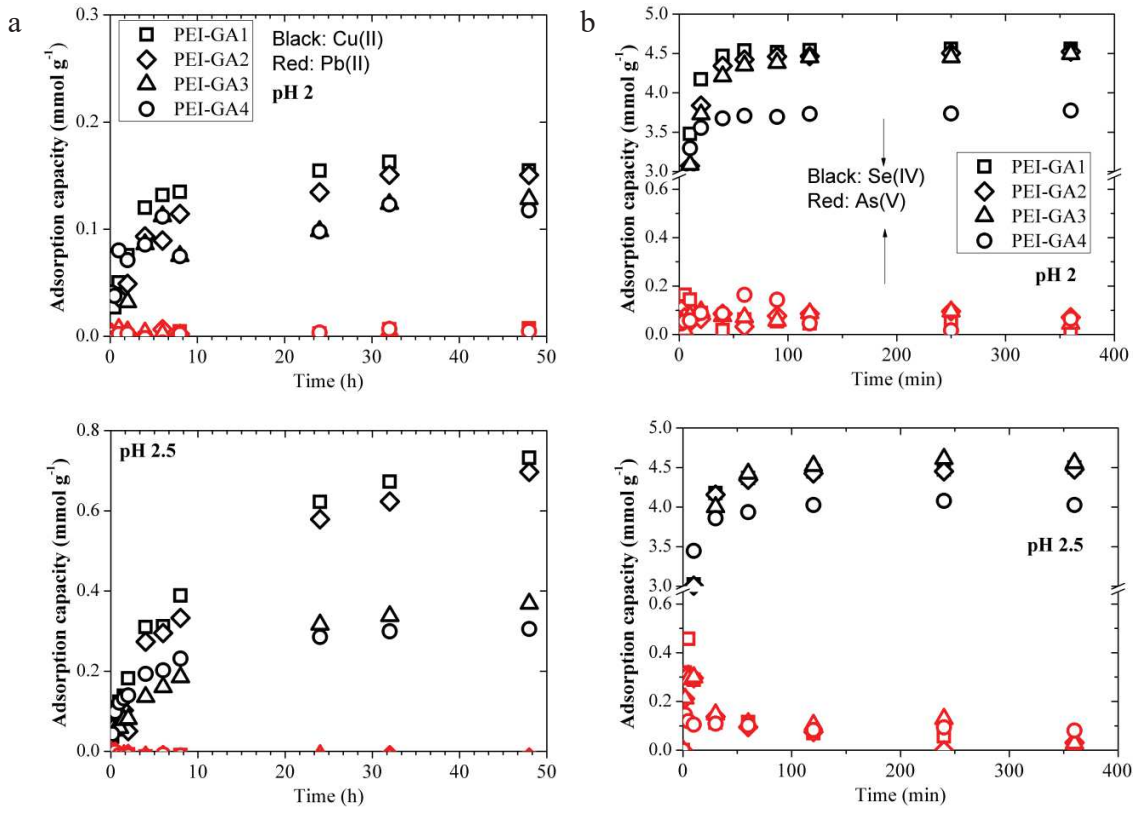

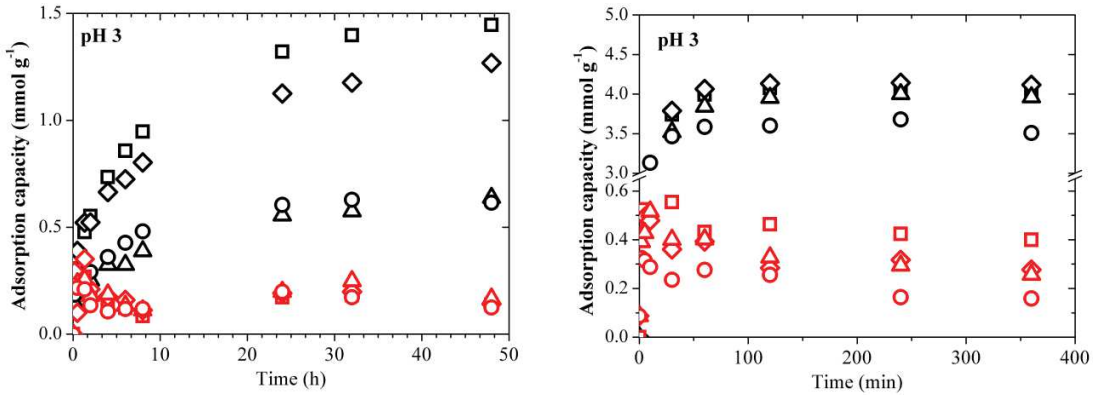

Figure 4-13 Adsorption kinetics of (a) Se(VI) and As(V) and (b) Pb(II) and Cu(II) from binary solutions (Volume = 0.5 L; Room temperature; Adsorbent mass = 100 mg; C_0 = 0.5 mmol L^{-1} for Se(VI) and As(V) and 1 mmol L^{-1} for Cu(II) and Pb(II)).

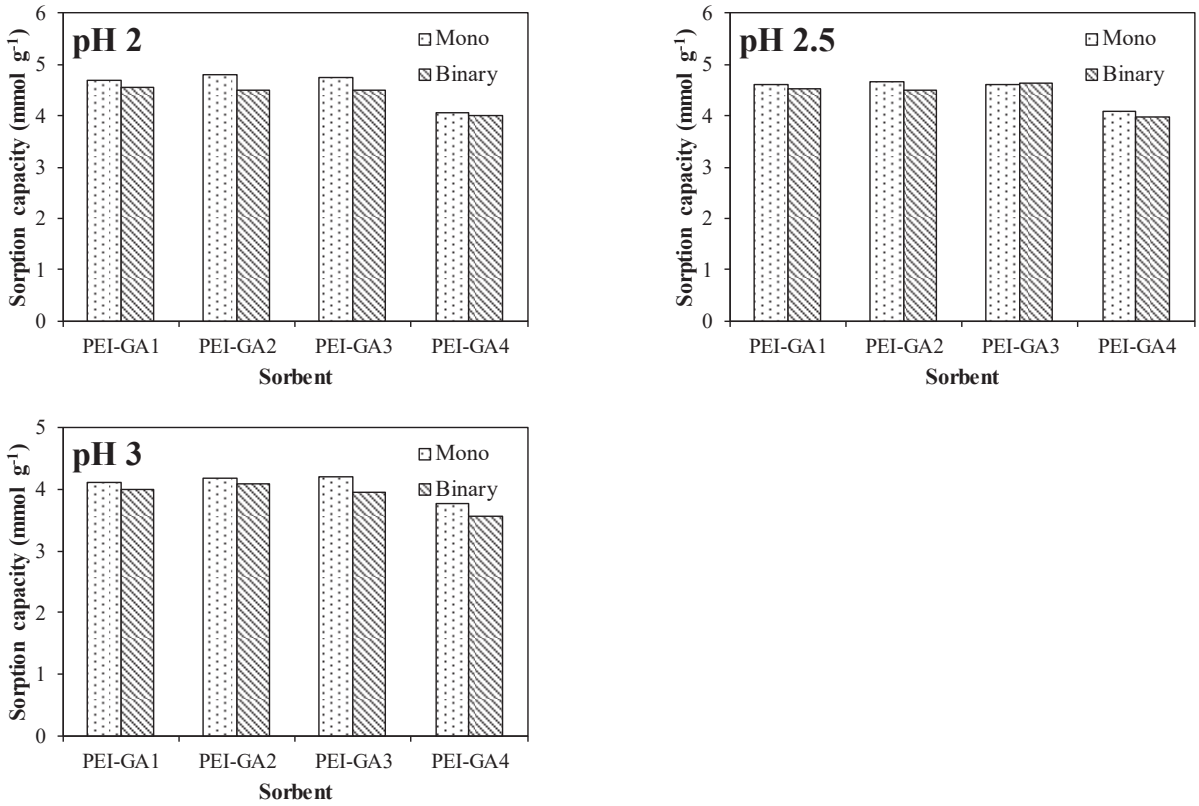

Figure 4-14 Equilibrium adsorption capacity of PEI-GA adsorbents for Se(VI) in mono-component and bi-component solutions.

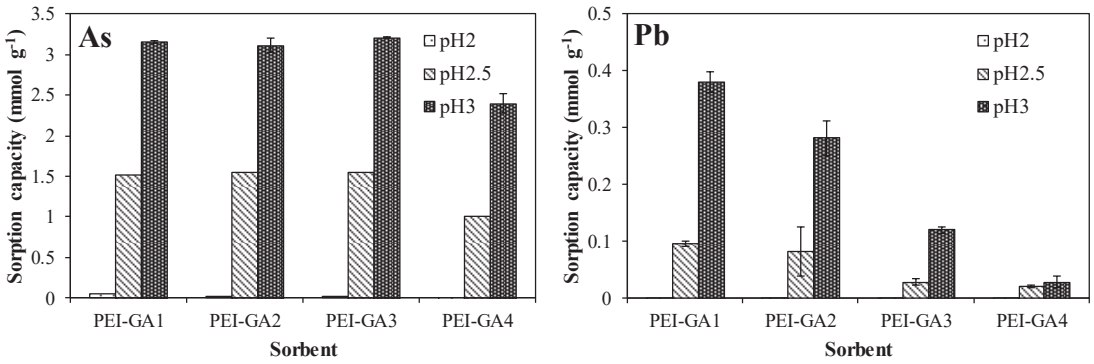

Figure 4-15 Equilibrium adsorption capacity of PEI-GA adsorbents for As(V) and Pb(II) in mono-component solutions.

The properties of the adsorbates (e.g., concentration, ionic size and ionic charge, etc.) and the characteristics of the adsorbents (e.g., the structure and functional groups) are the factors affecting the different binding affinities for metals in multi-metal system. For Cu(II) and Pb(II) adsorption, based on Pearson's theory [35], the hard acids prefer to associate with hard bases and soft acids prefer to associate with soft bases. Both Pb(II) and Cu(II) are considered as intermediate or borderline metal ions; the softness coefficients for Pb(II) is 0.41, very close to 0.38 for Cu(II) and the absolute hardness η_A of Pb(II) (8.5 eV) is slightly higher than that of Cu(II) (8.3 eV). Hence, the selective binding of Cu(II) over Pb(II) onto PEI-GA adsorbents should not be caused by the simple hard–soft concept. Therefore, the reason resulting in the selectivity is probably due to that copper, a transition element, is able to form more stable metal-ligand complexes compared to lead, a non-transition element [36]; Cu(II) forms stable 4-coordinate square planar complexes with amines in aqueous solutions [37], while Pb(II) prefers 4-coordinate octahedral complexes. The stability constant logarithm of metal-ammonia complexes is much higher for Cu(II) (4.12) than for Pb(II) (1.6) [38, 39]. These properties cause a poor adsorption performance of PEI-GA adsorbents for Pb(II); even in mono-metal system (Figure 4-15), the adsorption capacity of PEI-GA1, PEI-GA2, PEI-GA3 and PEI-GA4 for Pb(II) at pH 3 is only 0.38, 0.28, 0.12 and 0.03 mmol g^{-1}, respectively, much less than those for Cu(II). Such preference of Cu(II) adsorption onto GA crosslinked PEI can also be found in Cu(II)-Zn(II) binary system, where 4.5 wt% of Cu(II) was adsorbed, while almost no Zn(II) was adsorbed [40]. The selectivity for Se(VI) over As(V) can be simply explained by the fact that at low pH (such as pH 2), As(V) existed mostly as H_3AsO_4; with the increase of pH, the fraction of $H_2AsO_4^-$ increases and competes with $HSeO_4^-$ and SeO_4^{2-}. Briefly, under selected conditions, Cu(II) and Se(VI) can be successfully separated from Cu(II)-Pb(II) and Se(VI)-As(V) binary solutions, respectively, using PEI-GA resins, regardless of the amount of GA applied for crosslinking.

4.5. Principales conclusions

L'étude a permis de démontrer que le taux de réticulation a un effet modéré sur l'adsorption des ions Se(VI) (qui ne s'exprime réellement que pour le taux de réticulation le plus élevé, soit avec un ratio molaire PEI/GA supérieur à 2). Par ailleurs, le stockage de l'adsorbant à l'air libre ou en flacon scellé, étudié sur 20 jours, n'a qu'un impact mineur sur ses performances d'adsorption. Cela peut s'expliquer par le fait que les ions Se(VI) sont exclusivement fixés par interaction électrostatique entre les amines protonées à pH 2 et les anions sélénates. C'est donc la teneur en azote qui fixe l'affinité de l'adsorbant pour Se(VI) : la réticulation qui affecte la disponibilité des groupes réactionnels dans le cas de mécanismes de complexation ne joue pas un rôle important pour l'échange ionique. Les charges protonées restent accessibles (sauf pour les taux de réticulation les plus élevés pour lesquels l'encombrement stérique peut diminuer la performance de fixation). Cette réactivité des fonctions protonées n'est pas non plus affectée par le vieillissement du support en atmosphère non-contrôlée : la dénaturation du support est interprétée comme une conversion de fonctions aminées en groupes carbamate après exposition à l'air (CO_2/H_2O). Il convient de remarquer que l'adsorbant présente des capacités de fixation particulièrement élevées pour le sélénium (supérieures à 5 mmol Se g^{-1}), qui fait du PEI/GA l'un des supports les plus actifs de la littérature pour la récupération du sélénium en milieu acide.

Dans le cas du Cu(II), tant la réticulation que l'exposition à l'air influent drastiquement sur les performances de fixation. La réticulation diminue le nombre de groupements aminés libres et disponibles pour la chélation des ions cuivre. Cette étude illustre la progressivité de cette chute des performances avec le taux de réticulation. Par ailleurs, la formation de carbamates à la surface de l'adsorbant, par conversion des fonctions aminées, impacte significativement la fixation du Cu(II) en diminuant la disponibilité des groupements fonctionnels. Il convient de remarquer que cette conversion est réversible : une thermo-désorption sous atmosphère d'azote permet de rétablir suffisamment de groupements fonctionnels pour restaurer les capacités de fixation.

Les tests menés en solutions mixtes montrent que l'adsorbant présente une nette sélectivité pour Se(VI) par rapport à As(V) en particulier à pH 2 et pour Cu(II) par rapport à Pb(II). La préférence du matériau pour le sélénium est directement expliquée par la prédominance de formes neutres de l'arsenic(V) à pH 2 alors que le sélénium prédomine sous forme anionique, plus favorable à l'échange d'ions/attraction électrostatique sur les amines protonées. C'est une nouvelle illustration de l'importance de la spéciation des ions métalliques. Dans le cas du couple Cu(II)/Pb(II), la fixation s'effectuant par complexation, il est possible de corréler cette préférence pour le cuivre avec les constantes de complexation de ces ions métalliques avec l'ammoniaque (i.e., log $K(Cu/NH_3) = 4.12 > \log K(Pb/NH_3) = 1.6$), ainsi qu'au mode de coordination (tétra-coordination du cuivre dans une configuration de type "square planar" alors que le plomb est tétra-coordiné dans un système "octahédral").

4.6. References

[1] D. Hu, R. Jiang, N. Wang, H. Xu, Y.-G. Wang, X.-k. Ouyang, Adsorption of diclofenac sodium on bilayer amino-functionalized cellulose nanocrystals/chitosan composite, Journal of hazardous materials, 369 (2019) 483-493.
[2] J.B. Lindén, M. Larsson, S. Kaur, A. Nosrati, M. Nydén, Glutaraldehyde-crosslinking for improved copper absorption selectivity and chemical stability of polyethyleneimine coatings, Journal of Applied Polymer Science, 133 (2016) 43954.
[3] S. Kaur, I. Kempson, H. Xu, M. Nydén, M. Larsson, Bio-template assisted synthesis of porous glutaraldehyde-polyethyleneimine particulate resin for selective copper ion binding and recovery, RSC Advances, 8 (2018) 12043-12052.
[4] M. Ghoul, M. Bacquet, M. Morcellet, Uptake of heavy metals from synthetic aqueous solutions using modified PEI—silica gels, Water Research, 37 (2003) 729-734.
[5] X. Li, Z. Wang, J. Ning, M. Gao, W. Jiang, Z. Zhou, G. Li, Preparation and characterization of a novel polyethyleneimine cation-modified persimmon tannin bioadsorbent for anionic dye adsorption, Journal of environmental management, 217 (2018) 305-314.
[6] S. Wang, T. Vincent, C. Faur, E. Rodríguez-Castellón, E. Guibal, A new method for incorporating polyethyleneimine (PEI) in algal beads: High stability as sorbent for palladium recovery and supported catalyst for nitrophenol hydrogenation, Materials Chemistry and Physics, 221 (2019) 144-155.
[7] K. Fukushi, S. Miyashita, T. Kasama, Y. Takahashi, S. Morodome, Superior removal of selenite by periclase during transformation to brucite under high-pH conditions, Journal of hazardous materials, 371 (2019) 370-380.
[8] H.K. Hansen, S.F. Peña, C. Gutiérrez, A. Lazo, P. Lazo, L.M. Ottosen, Selenium removal from petroleum refinery wastewater using an electrocoagulation technique, Journal of hazardous materials, 364 (2019) 78-81.
[9] F.A. Cotton, G. Wilkinson, Advanced inorganic chemistry, Wiley New York, 1988.
[10] R. Vinodh, A. Abidov, M. Palanichamy, W.S. Cha, H.T. Jang, Constrained growth of solid amino alkyl siloxane (an organic–inorganic hybrid): The ultimate selective sorbent for CO_2, Journal of Industrial and Engineering Chemistry, 65 (2018) 156-166.
[11] C. Liu, R. Bai, Q. San Ly, Selective removal of copper and lead ions by diethylenetriamine-functionalized adsorbent: behaviors and mechanisms, Water Research, 42 (2008) 1511-1522.
[12] C.B. Tabelin, A. Hashimoto, T. Igarashi, T. Yoneda, Leaching of boron, arsenic and selenium from sedimentary rocks: II. pH dependence, speciation and mechanisms of release, Science Of The Total Environment, 473 (2014) 244-253.
[13] X.-F. Sun, S.-G. Wang, W. Cheng, M. Fan, B.-H. Tian, B.-Y. Gao, X.-M. Li, Enhancement of acidic dye biosorption capacity on poly (ethylenimine) grafted anaerobic granular sludge, Journal of hazardous materials, 189 (2011) 27-33.
[14] T. Kuila, S. Bose, A.K. Mishra, P. Khanra, N.H. Kim, J.H. Lee, Effect of functionalized graphene on the physical properties of linear low density polyethylene nanocomposites, Polymer Testing, 31 (2012) 31-38.
[15] J. Li, S. Yuan, J. Zhu, B. Van der Bruggen, High-flux, antibacterial composite membranes via polydopamine-assisted PEI-TiO_2/Ag modification for dye removal, Chemical Engineering Journal, 373 (2019) 275-284.
[16] G. Zhang, P. Zhao, L. Hao, Y. Xu, Amine-modified SBA-15 (P): A promising adsorbent for CO_2 capture, Journal of CO_2 Utilization, 24 (2018) 22-33.

[17] M. Sharifi, S.-M. Robatjazi, M. Sadri, J.M. Mosaabadi, Immobilization of organophosphorus hydrolase enzyme by covalent attachment on modified cellulose microfibers using different chemical activation strategies: Characterization and stability studies, Chinese journal of chemical engineering, 27 (2019) 191-199.
[18] J. Ren, N.M. Musyoka, H.W. Langmi, B.C. North, M. Mathe, W. Pang, M. Wang, J. Walker, In-situ IR monitoring of the formation of Zr-fumarate MOF, Applied Surface Science, 404 (2017) 263-267.
[19] X. Xu, C. Song, J.M. Andresen, B.G. Miller, A.W. Scaroni, Novel polyethylenimine-modified mesoporous molecular sieve of MCM-41 type as high-capacity adsorbent for CO_2 capture, Energy & Fuels, 16 (2002) 1463-1469.
[20] N.M. Sanchez-Ballester, I. Soulairol, B. Bataille, T. Sharkawi, Flexible heteroionic calcium-magnesium alginate beads for controlled drug release, Carbohydrate polymers, 207 (2019) 224-229.
[21] R. Kiruba, S. Vinod, A. Zaibudeen, R.V. Solomon, J. Philip, Stability and rheological properties of hybrid γ-Al_2O_3 nanofluids with cationic polyelectrolyte additives, Colloids and Surfaces A: Physicochemical and Engineering Aspects, 555 (2018) 63-71.
[22] R.P. Wijesiri, G.P. Knowles, H. Yeasmin, A.F. Hoadley, A.L. Chaffee, CO_2 Capture from Air Using Pelletized Polyethylenimine Impregnated MCF Silica, Industrial & Engineering Chemistry Research, 58 (2019) 3293-3303.
[23] A. Bachvarova, Y. Dimitriev, R. Iordanova, Glass formation in the systems Ag_2SeO_3–MnOm and $CuSeO_3$–MnOm (MnOm= B_2O_3, MoO_3), Journal of non-crystalline solids, 351 (2005) 998-1002.
[24] Y. Ma, W.-J. Liu, N. Zhang, Y.-S. Li, H. Jiang, G.-P. Sheng, Polyethylenimine modified biochar adsorbent for hexavalent chromium removal from the aqueous solution, Bioresource technology, 169 (2014) 403-408.
[25] Y.-H. Chou, J.-H. Yu, Y.-M. Liang, P.-J. Wang, C.-W. Li, S.-S. Chen, Recovery of Cu (II) by chemical reduction using sodium dithionite, Chemosphere, 141 (2015) 183-188.
[26] M. Kul, K.O. Oskay, Separation and recovery of valuable metals from real mix electroplating wastewater by solvent extraction, Hydrometallurgy, 155 (2015) 153-160.
[27] H.K. Hansen, C. Gutiérrez, J. Ferreiro, A. Rojo, Batch electrodialytic treatment of copper smelter wastewater, Minerals Engineering, 74 (2015) 60-63.
[28] I. Willner, Y. Eichen, A.J. Frank, M.A. Fox, Photoinduced electron-transfer processes using organized redox-functionalized bipyridinium-polyethylenimine-titania colloids and particulate assemblies, The Journal of Physical Chemistry, 97 (1993) 7264-7271.
[29] M.D. Erosa, W. Höll, J. Horst, Sorption of selenium species onto weakly basic anion exchangers: I. Equilibrium studies, Reactive and Functional Polymers, 69 (2009) 576-585.
[30] J.S. Yamani, A.W. Lounsbury, J.B. Zimmerman, Adsorption of selenite and selenate by nanocrystalline aluminum oxide, neat and impregnated in chitosan beads, Water research, 50 (2014) 373-381.
[31] D.A. Baldwin, E.A. Betterton, J.M. Pratt, The chemistry of vitamin B 12. Part 22. Steric effects in the co-ordination of amines by cobalt (III) corrinoids, Journal of the Chemical Society, Dalton Transactions, (1983) 2217-2222.
[32] M. Monier, D. Ayad, Y. Wei, A. Sarhan, Adsorption of Cu(II), Co(II), and Ni(II) ions by modified magnetic chitosan chelating resin, Journal of Hazardous Materials, 177 (2010) 962-970.
[33] O.-H. Kwon, J.-O. Kim, D.-W. Cho, R. Kumar, S.H. Baek, M.B. Kurade, B.-H. Jeon, Adsorption of As(III), As(V) and Cu(II) on zirconium oxide immobilized alginate beads in aqueous phase, Chemosphere, 160 (2016) 126-133.

[34] B. An, H. Lee, S. Lee, S.-H. Lee, J.-W. Choi, Determining the selectivity of divalent metal cations for the carboxyl group of alginate hydrogel beads during competitive sorption, Journal of hazardous materials, 298 (2015) 11-18.
[35] R.G. Pearson, Acids and bases, Science, 151 (1966) 172-177.
[36] A.A. Atia, A.M. Donia, S.A. Abou-El-Enein, A.M. Yousif, Studies on uptake behaviour of copper (II) and lead (II) by amine chelating resins with different textural properties, Separation and Purification Technology, 33 (2003) 295-301.
[37] R.R. Navarro, K. Sumi, M. Matsumura, Improved metal affinity of chelating adsorbents through graft polymerization, Water Research, 33 (1999) 2037-2044.
[38] A.E. Martell, R.M. Smith, Critical stability constants, Springer, 1974.
[39] R.B. Martin, Practical hardness scales for metal ion complexes, Inorganica Chimica Acta, 339 (2002) 27-33.
[40] A. Movahedi, A. Lundin, N. Kann, M. Nydén, K. Moth-Poulsen, Cu (I) stabilizing crosslinked polyethyleneimine, Physical Chemistry Chemical Physics, 17 (2015) 18327-18336.

Chapter 5 Palladium nanoparticles supported on amine-functionalized alginate membranes for hydrogenation of 3-nitrophenol

5.1. Introduction Générale

Les chapitres précédents ont largement illustré l'affinité des membranes PEI/Alginate pour la fixation des anions métalliques grâce au mécanisme d'échange d'ions/attraction électrostatique entres les amines protonées et ces anions. C'est un procédé particulièrement utile pour l'extraction de métaux toxiques (arseniate, selenate, chromate ou complexes chloroanioniques du mercure). Cette propriété peut être mise à profit dans le cadre de la récupération de métaux valorisables. Les métaux précieux représentent une cible de choix pour ce type d'application en raison de leur aptitude à former des complexes anioniques en milieu acide chlorhydrique (notamment Au(III), Pd(II) ou Pt(IV)).

Ce chapitre a plus particulièrement examiné l'adsorption du palladium, mais en orientant cette étude vers la réalisation de catalyseurs supportés. En effet, le palladium est bien connu dans le milieu de la catalyse hétérogène pour son activité étendue (pour un large spectre de réactions catalytiques). Après avoir brièvement étudié l'adsorption du Pd(II) sur les membranes de PEI/Alginate, il a été procédé à une réduction du Pd(II) fixé sur le support (partiellement converti en Pd(0)) afin de synthétiser des membranes Pd/PEI/Alginate pour étudier une réaction simple d'hydrogénation du 3-nitrophénol (3-NP) en 3-aminophénol (3-AP) en présence de formiate de sodium (comme donneur d'hydrogène). Cette réaction a été choisie pour sa simplicité de mise en œuvre et de suivi analytique. La seule ambition de cette partie est de démontrer la faisabilité d'application de ces supports pour une application en catalyse hétérogène ; cette réaction n'a aucun intérêt industriel mais elle est communément mise en œuvre en pré-étude de caractérisation de nouveaux supports. Elle est donc fréquemment documentée dans la littérature. Ce travail s'en distingue toutefois car la mise en forme du matériau ouvre la voie à une application en mode dynamique avec des conditions hydrodynamiques (percolation) facilitées, et une bonne stabilité (comme le confirmera l'étude).

Dans la partie synthèse et caractérisation, les membranes sont analysées par MEB-EDX (distribution du palladium, observation de la porosité, à différents stades de la fabrication), MET (MEB en mode émulateur de microscope électronique à transmission, pour l'évaluation de la distribution et de la taille des nanoparticules de Pd), XPS (en vue d'évaluer le taux de réduction du palladium), et de flux de percolation.
La partie centrée sur la catalyse supportée du 3-NP (initialement étudiée en mode recirculation, réacteur parfaitement agité) s'attache à évaluer l'impact des conditions de fabrication des membranes Pd/PEI/Alginate, notamment en termes de quantité de Pd et de dispersion des NPs de palladium en jouant respectivement sur la concentration de la solution de palladium utilisée pour charger la membrane et sur le flux de la solution d'ion métallique. Ces deux critères sont

supposés influencer les phénomènes d'agrégation (formation d'amas de Pd alors que l'on recherche une bonne dispersion de particules nanométriques) mais aussi la formation d'un gradient de distribution du Pd (sur la face d'entrée de la solution, à faible débit). Afin d'évaluer de manière précise l'impact de ces différents paramètres opératoires de fabrication, les profils ont été modélisés au moyen d'une équation cinétique de pseudo premier ordre. La stabilité de l'adsorbant est ensuite caractérisée en opérant le traitement de 30 batchs successifs pour évaluer la perte d'activité catalytique avant de tester à faible débit d'alimentation les membranes catalytiques Pd/PEI/Alginate en mode d'alimentation directe (sans recirculation).

5.2. Introduction

The use of platinum group metals (PGMs) has attracted increasing attention during the last decades due to their outstanding catalytic properties. Palladium, in particular, has been the basis for producing electronic devices and automotive catalysts owing to its high catalytic activity in various chemical reactions. Previous studies have fully reported the use of metal nanoparticles for methylene blue removal [1], nitrophenol hydrogenation [2-5], formaldehyde degradation [6], etc. One of the major drawbacks of Pd for catalytic applications is its high cost and thus, recovering such metal from waste sources should prove lucrative. Many studies have been focusing on the recovery of Pd(II) from acidic solutions (the leaching liquors commonly contain a certain amount of acid to efficiently leach Pd(II) from waste catalysts) [7]. On the other hand, there is still much scope left for improving its application potential as catalysts. For example, the aggregation and poor reusability of the palladium nanoparticles still limits their use. Therefore, a stabilizer is commonly needed to enhance the stability of the palladium nanoparticles [8]. Those stabilizers can be inorganic or organic supports that have moderate affinity towards metal nanoparticles. To date, nanoparticles were mostly immobilized in inorganic supports such as SDS-intercalated LDH [9], magnetic supports [10], mesoporous silica, zeolites and activated carbon [11]. Unfortunately, it is easy for the metal nanoparticles immobilized on those inorganic supports to leach out during reaction process [12]. Moreover, the re-use of nanoparticles is still limited as recovery techniques are typically energy intensive and laborious. Conventional separation processes such as filtration not only make the treatment procedure more time-consuming, but also easily cause catalyst loss [13]. One possible way to solve this problem is to decorate the catalyst in magnetic materials [14] . Another way is to apply polymers as the supports owing to their simplified synthesis, good stability and easy recovery [15, 16].

Alginate is a natural biopolymer extracted from seaweeds. One of the advantages of applying alginate is that this material is versatile in terms of shaping and conditioning owing to gelation processes. It can be shaped into nanoparticles [17], gel beads [18-20], membranes [21, 22], fibers [23], and membranes [24] for various applications in different fields. Particularly, alginate has demonstrated its efficiency as immobilizers through alginate-Ca gelation for nanoparticles, such as Ag and Au [25], Ni/Fe [26], Pd [27] and Fe_2O_3 [28]. Polyethyleneimine (PEI) is well known for its metal chelating characteristic owing to the presence of a large

number of amine groups (primary, secondary and tertiary amine groups in branched PEI). Therefore, alginate-Ca/PEI composite can both coordinate with Pd nanoparticles and act as stabilizers for these nanoparticles. In addition, a post-treatment using glutaraldehyde (GA) may contribute to strengthen the alginate-Ca/PEI composite; the Schiff-base reaction between PEI and GA prevents the degradation of alginate-Ca/PEI composite in complex systems with an excess of ions such as K(I) or Na(I) (due to the formation of soluble Na-alginate or K-alginate, etc.). Actually, the simultaneous crosslinking mechanisms between interpenetrating polymers lead to stable complex structures. This method has been recently applied to elaborate alginate/PEI beads for Pd(II) binding immobilize Pd [29], and nanoparticles on alginate/PEI-GA beads in our group. However, although the catalyst is recoverable owing to its large size (around 3 mm) and stable even in complex systems, its catalytic activity for 3-nitrophenol hydrogenation is much lower than the values reported for more conventional catalysts due to poor mass transfer property. Compared to conventional shaking or agitating systems, the use of a fixed-bed column system could enable continuous water treatment by feeding the wastewater into the end of the reactor and obtaining the treated water from the other end. In the case of large and homogeneous (in size and shape) support, the natural percolation of the liquid into the packing makes the process very effective from a mass transfer point of view. Another advantage of this system is that it requires no solid-liquid separation after treatment. A specific shaping of the catalysts (such as macroporous membranes) would be favorable for their application in this kind of system, avoiding head loss and clogging effects. Therefore, a more porous membrane-like support is highly required to decrease the mass transfer resistance, simplify the reaction equipment and improve the reaction rate.

To address these requirements, highly porous membranes that exhibit outstanding percolating characteristics are synthesized. For the first time, the membranes are prepared through the reaction between alginate and partially protonated PEI solution. The challenge also consisted of using a very simple air-drying process for conditioning the membranes instead of more sophisticated drying processes (such as freeze-drying and drying under supercritical CO_2 conditions). To prevent air-drying shrinkage that might cause cracks and water tightness of the membranes, the membrane was crosslinked with GA solution: aldehyde functions react with free amine groups on PEI. The as-prepared membranes are packed in tubular reactors and tested for Pd(II) recovery from acidic solution. The metal loaded membranes are collected for preparation of the catalysts by *in situ* reduction of loaded Pd(II) into Pd(0). The hydrogenation of nitrophenol is an ideal model reaction to access the catalytic activity of a variety of metallic nanoparticles. In addition, nitrophenol is considered as highly toxic organic pollutant in industrial wastewater or agricultural runoff and its reduced product (3-aminophenol, 3-AP) is an important intermediate for producing antipyretic drugs. Therefore, the hydrogenation of 3-NP by formic acid was used as a model reaction to evaluate the catalytic activity of the catalysts. Nitrophenol is reported to be easily reduced to aminophenol by $NaBH_4$ in the presence of metals in solution; the metal nanoparticles catalyze this reaction by facilitating electron relay from the donor BH_4^- to acceptor nitrophenol to overcome the kinetic barrier. However, to avoid using

the toxic and high-cost $NaBH_4$ chemical in the water treatment process, the hydrogen donor was replaced by formic acid, since this reagent is non-toxic and can be handled and stored easily [30]. Gowda et al. [31] reported that formic acid in the presence of 10% Pd-C is a rapid, versatile and selective reducing system for a wide range of nitro compounds. Therefore, this study aims to evaluate the possibility of using novel alginate/PEI membranes as a stabilizer for Pd nanoparticles and determine the catalytic activity of the catalyst packed in tubular reactors for 3-NP hydrogenation by HCOOH. The first part of the work characterizes the materials using techniques such as SEM, TEM, XPS analyses and physical measurements of porosity, water flux and satiability under agitation. In the second step, the study focuses on the influence of a series of experimental parameters (pH, metal content on the catalyst, molar ratio between the feed and the hydrogen donor; i.e., HCOOH) on the kinetics of hydrogenation of 3-nitrophenol.

5.3. Materials and methods

5.3.1. Materials

Manugel GMB alginate was obtained from FMC BioPolymer (Girvan, UK). Branched polyethyleneimine (PEI, 50% (*w/w*) in water), formic acid (99%) and glutaraldehyde (GA, 50% (*w/w*) in water) were purchased from Sigma-Aldrich (Taufkirchen, Germany). Nitric acid (65% w/w) and palladium (II) chloride were obtained from R.D. H (Seelze, Germany). Hydrazine hydrate $N_2H_4 \cdot H_2O$ (reagent grade, 55% ± 5%) was purchased from Sigma Aldrich (Taufkirchen, Germany) and 3-nitrophenol (3-NP) were supplied by Fluka (Buchs, Switzerland). The metal stock solution was prepared by dissolving 1 g of $PdCl_2$ in 1 L of 1.1 M HCl solution, while 3-nitrophenol stock solution was prepared by dissolving 1 g into 1 L of ~~pure~~ water with 1 drop of NaOH solution (10 M).

5.3.2. Preparation of membranes

The process for preparing alginate/PEI (AP) membranes is as follows. One hundred milliliters of 4 % alginate solution were first mixed with 400 mL of water. Thereafter, 35 mL of 4 % PEI (dissolved in slightly acidic nitric acid solutions) was slowly added into the solution while agitating. The mixture was then poured into a container and maintained at 20±1°C for 24 h for completing the gelation. Varying the sizes of containers allows manufacturing membranes with different thicknesses. After that, the membrane was washed 4 times using deionized water, added with 2.5 mL of GA (50%, w/w) and maintained at 20±1°C for 24 h. Finally, the membrane was thoroughly washed and air-dried at 20±1°C.

5.3.3. Immobilization of Pd(II)

The process of experimental set-up used for metal sorption: the membrane was cut into cylinders using a cutter mold and packed in a plastic tube that was fixed above a container filled with the Pd(II) solution. The solution was recirculated through the membrane using a peristaltic pump (Ismatec, ISM 404, Wertheim, Germany) for 24 h. When the height of the water column is around 0.5 cm, the lid is then tightened to seal the recirculation system to maintain a constant water pressure on the membrane (constant level of solution at the top of the column). Time

starts when the first drop reaches the membrane. The sorption isotherm experiment was conducted using solutions containing different concentrations of Pd(II). One liter of solution (at pH 1, controlled with H_2SO_4) was recirculated through AP membrane. Specifically, to study the effect of Pd(II) loaded amount, 1 L of Pd(II) solution at different concentrations (i.e., 10-50 mg Pd L^{-1}) was recirculated through a membrane disc (255 mg, dried weight). The flow rate of the pump was set at 30 mL min^{-1}. The effect of flow rate was studied by the contact of 1 L of a Pd(II) solution (28 mg L^{-1}) with 255 mg of the membrane at three different flow rates (i.e., 5, 30 and 50 mL min^{-1}). For the effect of membrane mass, three different masses of the membrane cylinders with a same diameter (2.43 cm) but different height were applied for Pd(II) recovery from solutions containing a concentration of 28 mg Pd L^{-1}. The flow rate was fixed at 50 mL min^{-1}.

5.3.4. Reduction of Pd(II) into Pd(0)

Before reduction, the Pd(II)-loaded membranes were thoroughly washed. A previous study [32] showed that a small size (~3 nm) of Pd nanoparticles could be obtained by reduction with hydrazine hydrate ($N_2H_4 \cdot H_2O$) in alkaline solution. Therefore, in this study, the reduction of Pd(II) to Pd(0) loaded on the membranes was performed by gentle stirring (50 mov/min) in a solution (200 mL) containing freshly-prepared hydrazine hydrate (0.03 M) and NaOH (0.5 mM) at 60 ^oC for 5 h. The color of the membranes changed from yellowish-brown to dark-gray, suggesting the formation of metallic palladium nanoparticles on the surface of the membranes.

5.3.5. Characterization of materials

Scanning electron microscopy (SEM) and SEM-EDX (SEM coupled with energy dispersive X-ray diffraction analysis) were performed using an environmental scanning electron microscope Quanta FEG 200 (FEI France, Thermo Fisher Scientific, Mérignac, France), equipped with an Oxford Inca 350 energy dispersive X- ray micro-analyzer (Oxford Instruments France, Saclay, France). TEM micrographs were obtained on the SEM using the TEM-emulation mode. Materials were grinded, sieved (below 250 microns), and dispersed in ethanol solution. A micro-drop of the homogenous suspension was deposited at the surface of a grid C film on (S160, 200 mesh Ni grid, Agar Scientific, Stansted, UK). XPS studies were carried on a Physical Electronics spectrometer (PHI Versa Probe II Scanning XPS Microprobe, Physical Electronics, Chanhassen, MN, USA) with monochromatic X-ray Al Kα radiation (100 μm, 100 W, 20 kV, 1,486.6 eV) and a dual beam charge neutralizer. The spectrometer energy scale was calibrated using Cu $2p_{3/2}$, Ag $3d_{5/2}$, and Au $4f_{7/2}$ photoelectron lines at 932.7 eV, 368.2 eV and 84.0 eV, respectively. Under a constant pass energy mode at 23.5 eV condition, the Au $4f_{7/2}$ line was recorded with 0.73 eV FWHM at a binding energy (BE) of 84.0 eV. XPS spectra were analyzed using PHI SmartSoft software and processed using MultiPak 9.3 package. The binding energy values were referenced to adventitious carbon C 1*s* signal (284.8 eV). Recorded spectra were systematically fitted using Gauss–Lorentz curves. Atomic concentration percentages of the characteristic elements of the surfaces were determined taking into account the corresponding area sensitivity factor for the different measured spectral regions. Samples were

finely grinded (below 125 μm) to get an analysis representative of the whole mass of the materials.

The apparent density and porosity of the membranes were measured by pycnometer method using ethanol as a soaking agent. Water flux (mL cm^{-2} min^{-1}) was calculated from the flux at a unit time on a unit membrane area (the height of the membranes was maintained at 8.0 ± 0.2 mm); the pressure calculated from the water height was 0.006 bar (calculated by the depth of the water on the top of the membrane). The pH_{PZC} of the membranes was measured by titration method. Two hundred milligrams of sorbent were mixed with 40 mL of 0.1 M NaCl solution for 48 h; the initial pH values (pH_0) were adjusted between 2 and 10 using a pH meter (inoLab pH 7110, WTW, Germany). The final pH (pH_{eq}) was recorded and plotted against initial pH; the pH_{PZC} corresponds to the pH where the plot crosses the first bisector (i.e., $pH_{eq} = pH_0$). Stability of the membranes was determined by recording the mass of AP membrane before (around 255 mg, dry weight) and after shaking in water at 150 rpm for 2 days. The mass loss (%) was calculated after the drying of the structured membrane.

5.3.6. Catalytic hydrogenation of 3-nitrophenol

3-nitrophenol (3-NP) hydrogenation was reduced by recirculating a 3-NP solution (100 mL, 50 mg L^{-1}) containing 0.2% formic acid through a catalyst disc (weight: 255 ± 10 mg). Samples were collected and acidified with sulfuric acid (1 mL sample with 20 μL 5% H_2SO_4) before being analyzed using a UV spectrophotometer (Varian 2050) at 332 nm [33]. According to a previous study [34], the hydrogenation of 3-NP by formic acid can be expressed as Figure 5-1. Different parameters may influence the conversion of 3-NP into 3-AP (3-aminophenol), such as the pH of the solution (controlled by NaOH or HNO_3), the molar ratio between the hydrogen donor and the feed (HCOOH/3-NP), and the flow rate. The reuse of the catalyst was also investigated for 30 cycles. Full experimental conditions are systematically reported in the caption of figures.

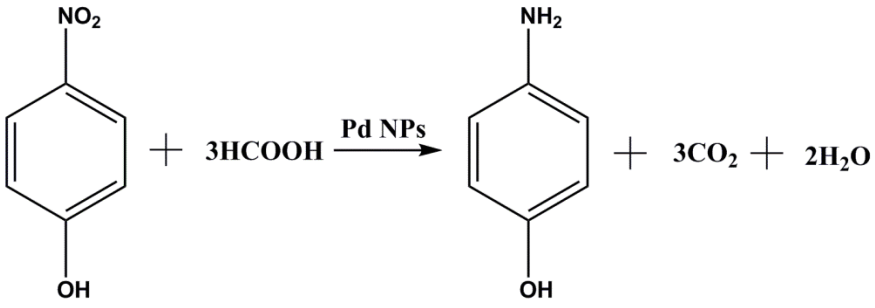

Figure 5-1 Hydrogenation of 3-NP into 3-AP with formic acid (as hydrogen donor).

5.3.7. Statistical analysis

Selected experiments were duplicated. Average values and standard deviations were calculated. Moreover, 3-NP hydrogenation using catalysts prepared from different membranes was carried out to evaluate the reproducibility of the manufacturing procedure. The overlapped plots shown in Figure 5-2 indicate that the synthesis of AP/Pd catalyst is reproducible.

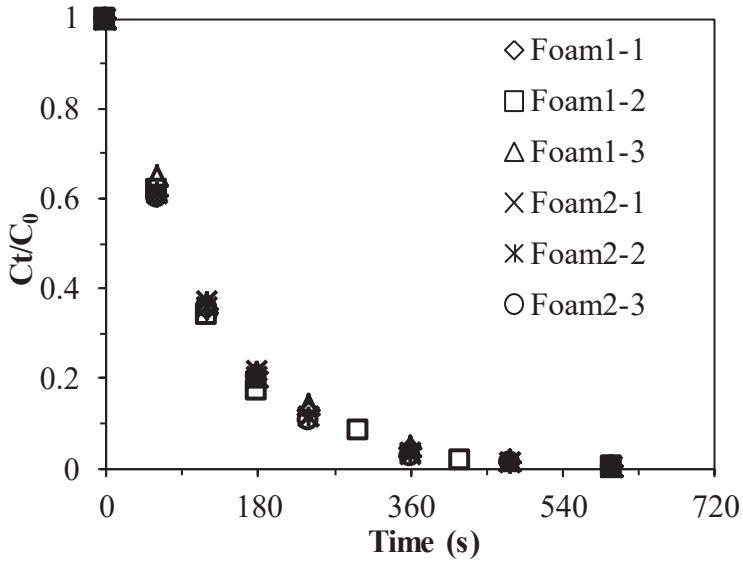

Figure 5-2 3-NP reduction using AP/Pd catalysts prepared by different foams (Pd amount: 27 mg; C_0 (3-NP): 50 mg L^{-1}; Flow rate: 60 mL min^{-1}; $C_{(HCOOH)}$: 0.2%). Note: Foam1 and Foam2 represent foams prepared at different time, while Foam1-1, Foam1-2, Foam1-3 represent different catalysts prepared by Foam1 and likewise as Foam2-1, Foam2-2 and Foam2-3.

5.4. Results and discussion

5.4.1. Characterization of materials

(1) Membrane stability (mechanical agitation) and physico-chemical properties

Table 5-1 gives the measured values of several physicochemical properties of the membranes before and after metal loading process. The pH_{PZC} is 6.29 for the raw AP membranes. At pH < pH_{PZC}, positively charged surface of AP membranes can attract the chloro-anionic species of palladium [35]. The density is 0.0637 g cm^{-3}; after sorption, density slightly increases up to 0.0644 g cm^{-3}, which is probably related to more compact structure of the membranes (see SEM images, Figure 5-3). Therefore, Pd(II)-loaded AP membrane also presents a slightly lower porosity than the raw material. Despite strong shaking, both free and metal loaded membranes maintain a low mass loss around 3%; this high stability enables the reusability of AP/Pd catalyst. The stability of Pd nanoparticles on the catalyst is a key criterion for designing a heterogeneous catalyst. For example, Vincent et al. [35] reported the beneficial use of ionic liquid for stabilizing palladium in alginate-based catalysts (Pd(II) being reduced after binding to the ionic liquid immobilized in alginate capsules): the strong interaction between phosphonium cation and anionic chloropalladate species prevents the leaching of palladium and increase the life of the catalyst.

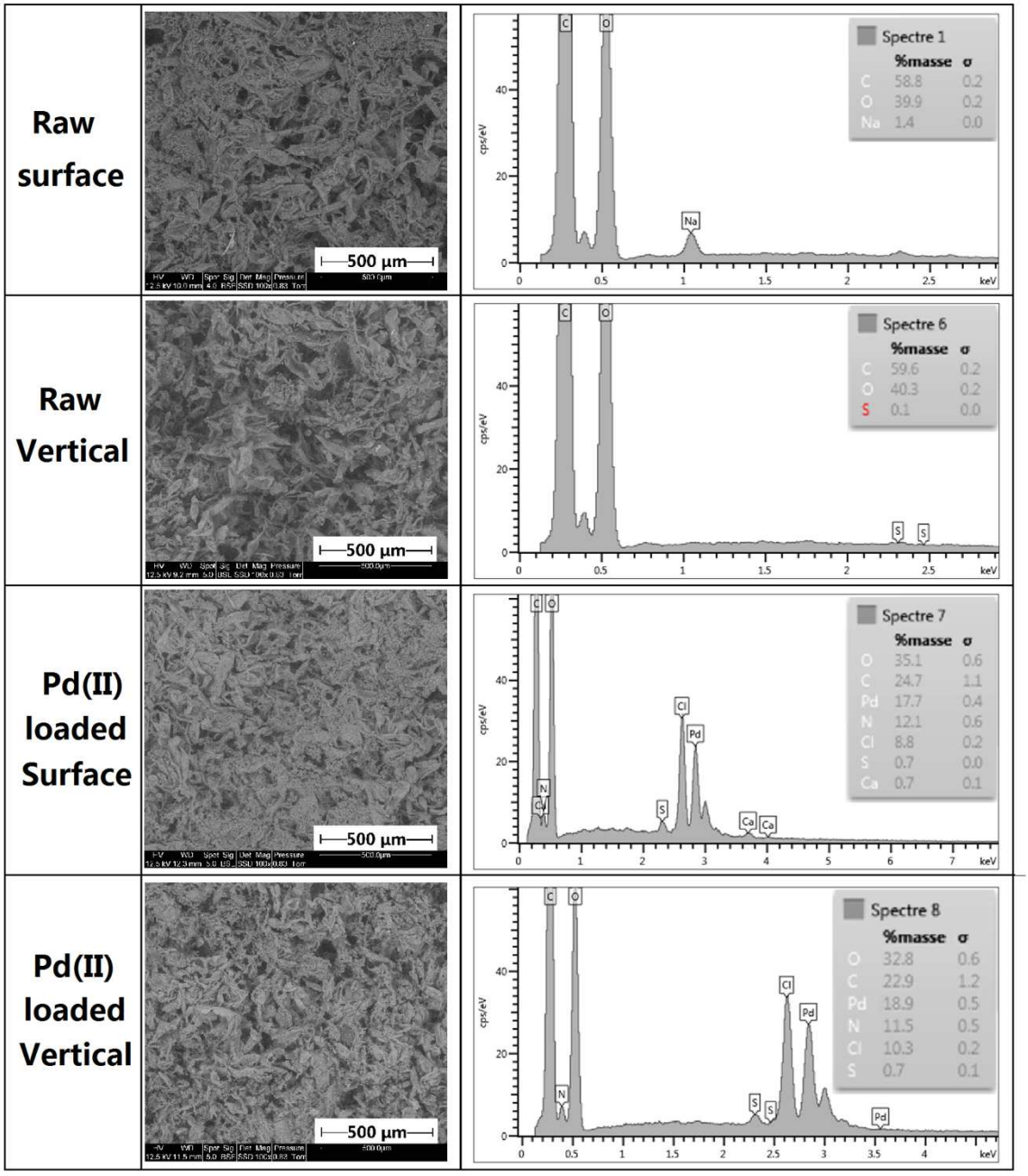

Figure 5-3 SEM-EDX micrographs of raw and Pd(II) loaded membranes.

Table 5-1 Physico-chemical characteristics of raw and Pd(II) loaded AP membranes.

Properties	AP membrane	Pd(II) loaded AP membrane
pH_{PZC}	6.29	–
Water flux (mL cm^{-2} min^{-1})	24.81±0.48	19.27±1.34
Porosity (%)	70.93±1.60	69.79±0.22
Density (g cm^{-3})	0.0637±0.0005	0.0644±0.0005
Stability (mass loss, %)	2.98±0.14	2.91±0.26

The BET analysis of the membrane is not reported here. Preliminary tests showed that specific surface area (SSA) does not exceed 2-3 m^2 g^{-1}. This means that the hyper-macroporous material has limited micro/mesoporosity (which would contribute to the SSA). Complementary tests showed that a final drying under more sophisticated drying conditions (freeze-drying or drying under supercritical CO_2 conditions) did not significantly changed the SSA.

(2) Morphological observations

SEM imaging (Figure 5-3) shows the interconnected porous network that randomly distributed on the surface and vertical section of the raw membranes, contributing to their high-percolating properties. After loading Pd(II), the pore wall of the membranes becomes more compact. This result is in agreement with the decrease in porosity and water flux after the sorption process. This change in structure could be due to the pressure of the circulation sorption system and the re-drying process after metal sorption. In addition, the reaction of amine groups with anionic chloropalladate species may contribute to form additional interchain bonds. EDX analysis mainly shows the presence of C and O elements. The resolution and the sensitivity are not sufficient to achieve the identification of N peak within the forest of peaks (including C and O strong peaks), despite the presence of numerous amine functions on PEI. After Pd(II) sorption, a large peak of Pd is found in/on the membranes. The semi-quantitative analysis shows that the surface of the catalyst bears up to 17.7% (w/w) of palladium, while the metals reaches up to 18.9 % in the internal part of the material: the catalyst is homogeneous in terms of distribution of Pd. The EDX element mapping (Figure 5-4) further confirms that the Pd(II) is well dispersed. Besides, Cl element appears in the membranes. This can be the first evidence that Pd(II) is bound under the form of chloro-palladium complexes. A small amount of S element is also detected (0.7%), because the pH was adjusted using H_2SO_4 and SO_4^{2-}/or HSO_4^- could also bind to amine groups. The semi-quantitative analysis of Pd should simply be considered indicative. Indeed, the mass balance on Pd concentrations before and after sorption, shows much lower values (27.2 mg Pd loaded on 255 mg of membrane; after sorption and metal reduction the final weight is close to 308 mg; i.e., a Pd loading close to 8.8 %, w/w).

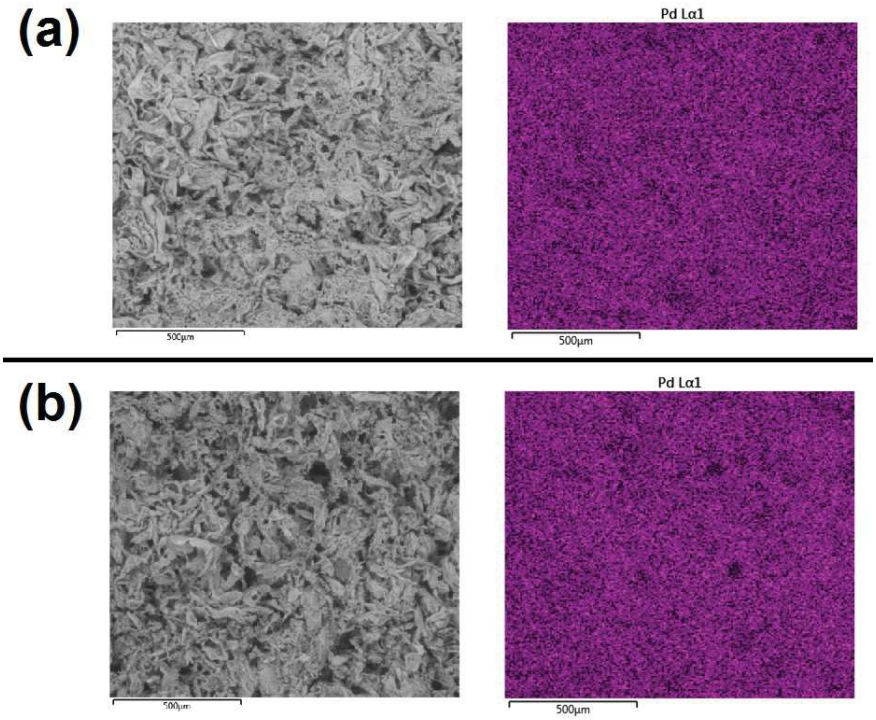

Figure 5-4 Pd cartography of Pd(II) loaded membranes: (a) surface and (b) vertical section.

(3) Sizing of Pd nanoparticles on the catalytic membranes

The high-magnification mode on SEM allows observing (a) the presence of Pd(II) (the high atomic weight of Pd gives a good contrast for identifying the localization of metal binding zones at the surface of the material), (b) the distribution of Pd nanoparticles (small spots). Figure 5-5a shows a rugged surface of Pd(II) loaded AP membranes. After reduction using hydrazine hydrate, Pd(II) is, at least partially, converted into Pd nanoparticles (small spots on Figure 5-5b, of lower individual surface area than the surface area of Pd(II) loaded zones, in Figure 5-5a). It is noteworthy that these nanoparticles are remarkably well distributed; this can be explained by the good dispersion of PEI in the alginate/PEI material. Similar trends were observed for algal/PEI beads catalysts: when PEI is incorporated as GA-crosslinked microparticles the distribution of small Pd nanoparticles is less homogenous than when the algal beads were impregnated with PEI (before being crosslinked with GA) [36].

Despite a few aggregates of individual Pd nanoparticles, the TEM images presented on Figure 5-5c again confirms the good dispersion of these particles. The size of Pd particles (shown on Figure 5-5d) mainly ranges between 4.5 and 10.5 nm (i.e., average value: 7.61 ± 1.93 nm), slightly larger than those free particles previously reported [37, 38]; however, with the advantage of immobilization for a readily recycling or re-use. It was reported that Pd nanoparticles with a size of 6-8 nm are appropriate for alkene hydrogenation reactions [39].

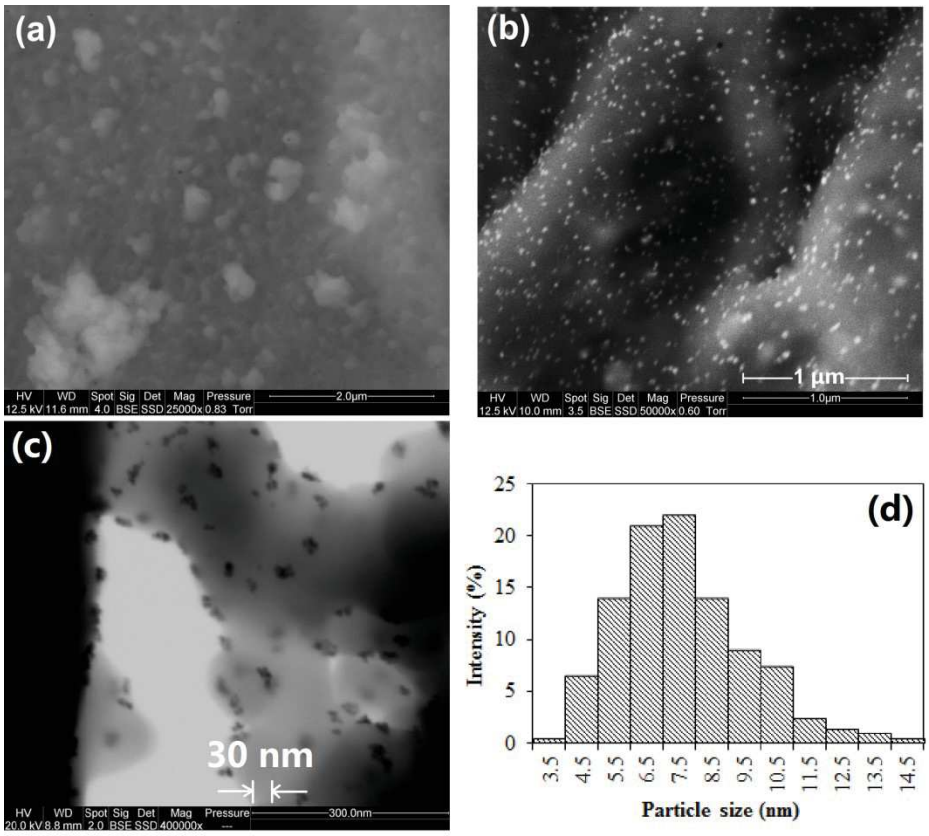

Figure 5-5 SEM micrographs of (a) Pd(II)-loaded and (b) surface of Pd nanoparticles -loaded membranes, (c) TEM micrographs of Pd nanoparticles -loaded membranes and (d) size distribution of Pd particles.

(4) XPS characterization – Modes of interaction and oxidation states of Pd

Figure 5-6 shows the XPS survey of the materials (raw membrane, AP; AP after Pd(II) loading, AP-Pd(II); AP-Pd(II) reduced, as the catalyst; and catalyst after 30 cycles of usage). The survey curves confirm the presence of N element (as a marker for PEI incorporation) and O element (marker of the biopolymer). The sorption of Pd is characterized by the characteristic signals of Pd *3d* bands (and additional weaker signals, such as Pd 4*p*, Pd 3*p*, Pd 3*s* or Pd MNN). It is noteworthy that after Pd(II) sorption the sorbent bears chloride ions (Cl 2*p* signal); this means that at least a significant fraction of Pd(II) is bound as chloro-anionic species. After reduction (and also after 30 cycles of use) the intensity of this signal is drastically reduced (almost disappearing). Figure 5-7 to Figure 5-10 report the HRES spectra for specific C 1*s*, O 1*s*, N 1*s*, Pd 3*d* and Cl 2*p*. Their assignments and their relative fraction for (a) identifying the binding mechanisms, (b) the effective reduction of Pd(II) into Pd(0), and (c) evaluating the stability of the catalyst after intensive use.

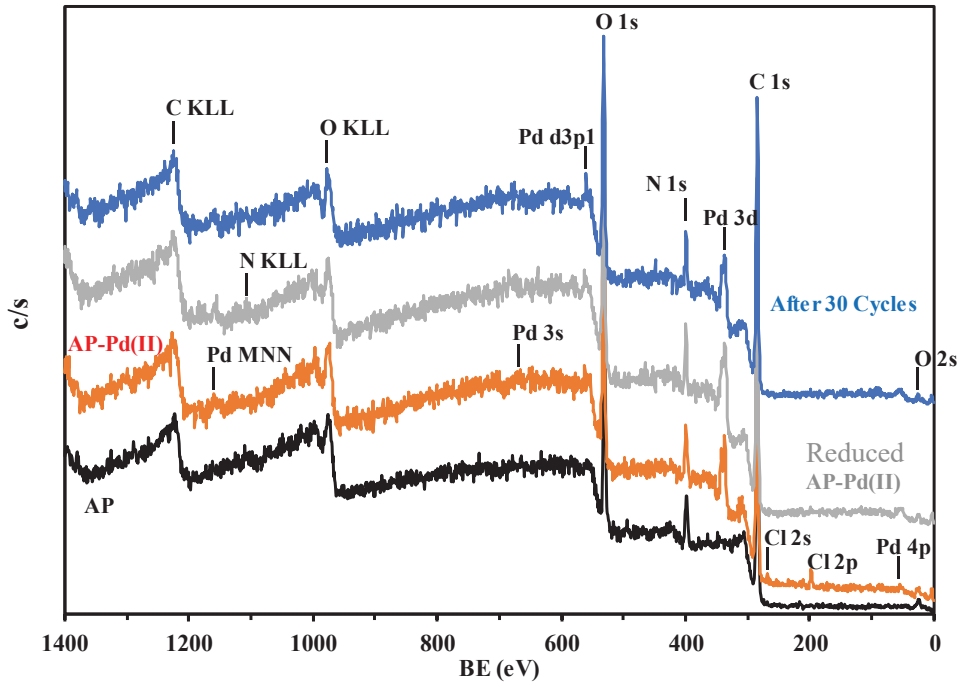

Figure 5-6 XPS survey analysis of AP, AP-Pd(II), AP-Pd(II) Reduced (catalyst) and catalyst after 30 Cycles.

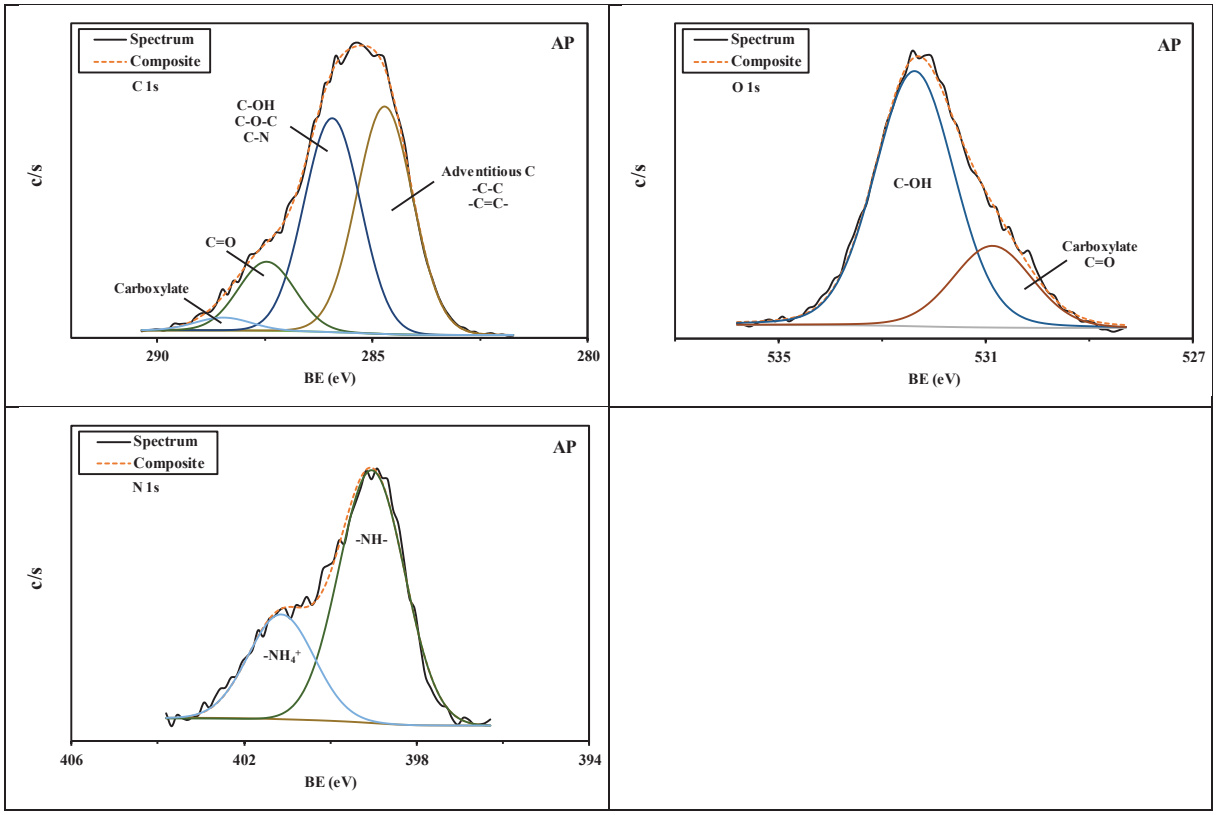

Figure 5-7 XPS analysis of AP sorbent.

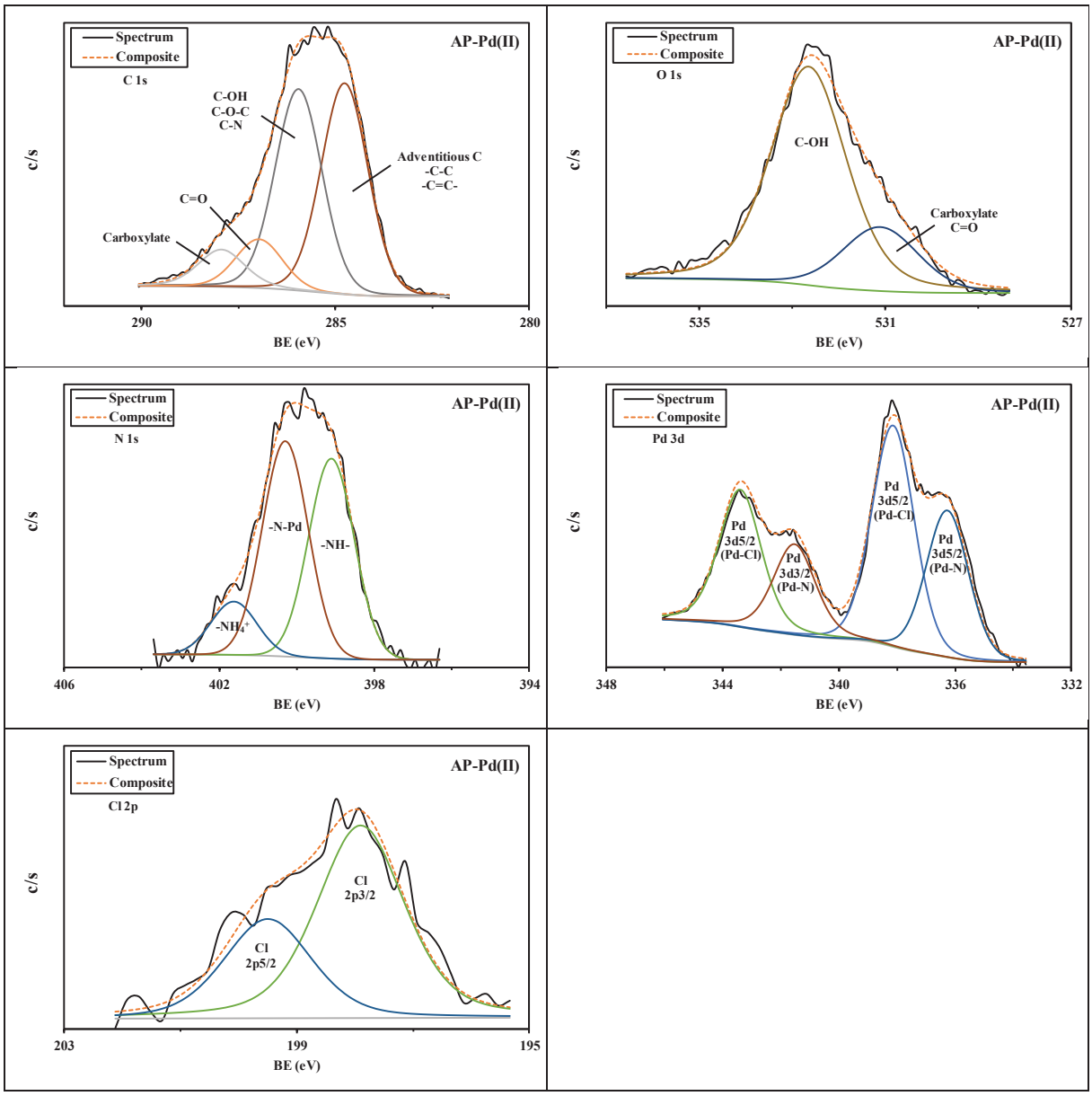

Figure 5-8 XPS analysis of AP-Pd(II).

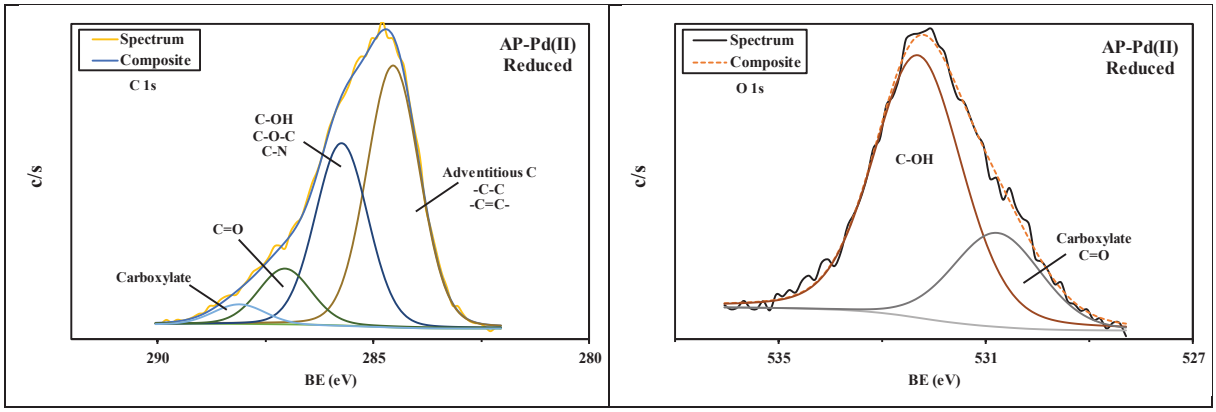

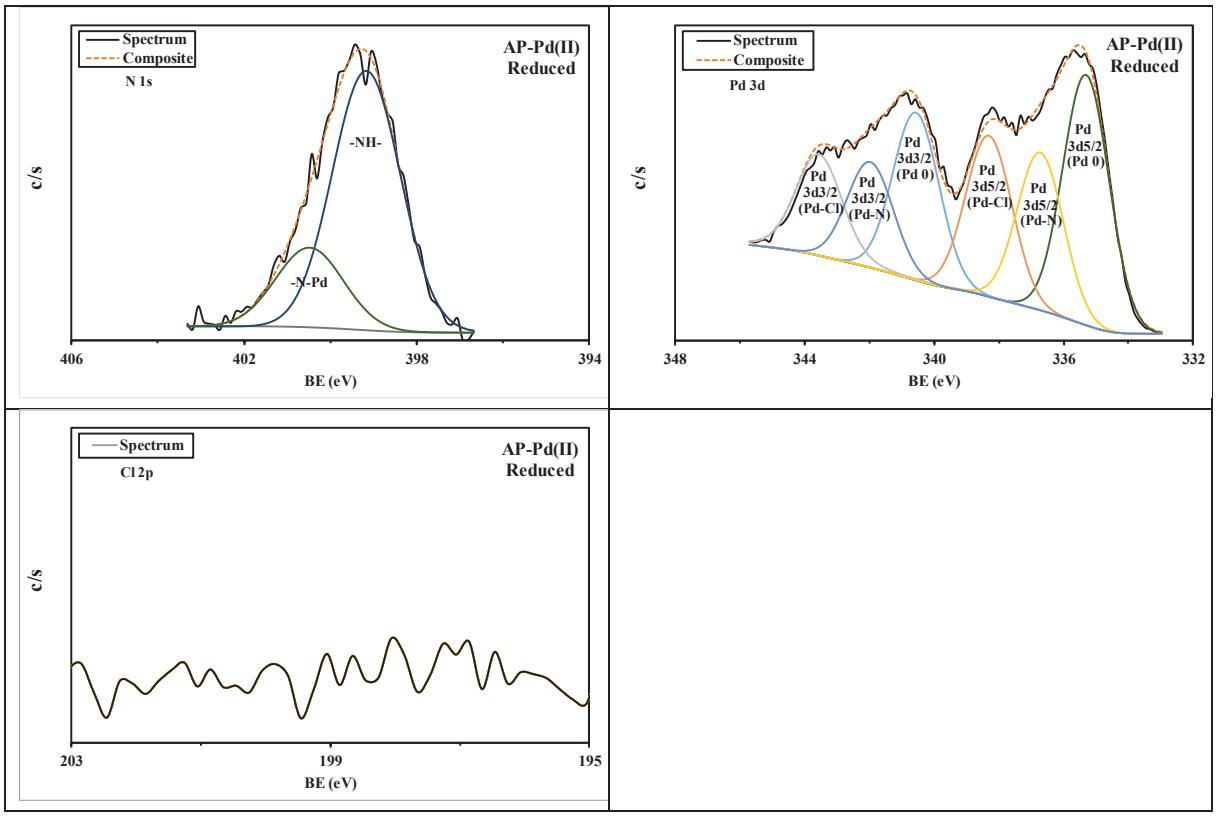

Figure 5-9 XPS analysis of AP-Pd(II) Reduced.

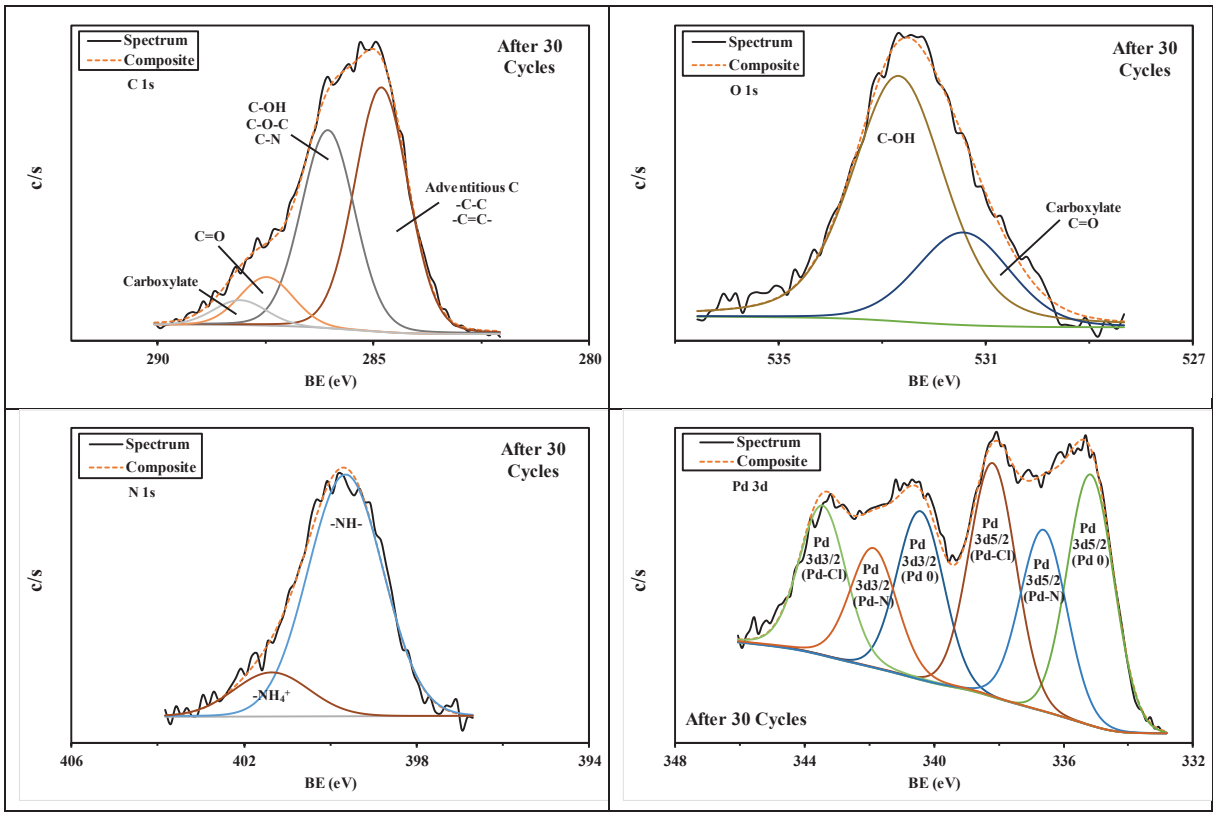

Figure 5-10 XPS analysis of catalyst after 30 Cycles.

The XPS analysis of AP sorbent confirms the presence of carboxylate groups (both on C 1*s* and O 1*s* signals) and amine and quaternary ammonium groups (399.1 eV (71%) and 401.1 eV (29 %), respectively). The protonation of amine groups and the quaternary ammonium sites are favorable for the sorption of anionic species (such as chloro-anionic species). After Pd(II) sorption the appearance of chlorine element confirms the binding of these chloro-anionic Pd species on the sorbent; a third band associated with N element appears as the bond between N and Pd. This is also confirmed by the coexistence of two pairs of deconvoluted bands (Pd $3d_{5/2}$ and Pd $3d_{3/2}$) for Pd *3d* signal corresponding to Pd-N (about 40 %), Pd-Cl (about 60 %) bonds. After Pd(II) reduction on the sorbent (synthesis of Pd(0) supported catalyst), the N 1*s* core level spectrum is very close to the spectrum for AP material (though the peak at high BE is now appearing as N-Pd species rather than the ammonium form). It is noteworthy that the C 1*s* signal loses its symmetry for the two highest bands, representative of adventitious C, C-C and –C=C- that increases comparatively to the second band representative of C-OH, C-O-C and C-N chemical groups. This probably means that the reduction conditions affected the chemical environment of these functional groups (including a reductive action on these groups). The intensity of Cl *2p* signal strongly decreased and it was not possible getting a clear identification of the bands: the reduction releases chloride by conversion of $PdCl_4^{2-}$ species into Pd(0). Obviously, the reduction is characterized by the appearance of a new band for Pd *3d*: the signal is deconvoluted on 3 pairs of bands corresponding to Pd-Cl (28 %), Pd-N (28 %) and Pd(0) (44 %) forms. This means that the reduction of Pd(II) is only partial. This may affect the catalytic activity of the membrane. The comparison of the XPS spectra for the different bands between AP-Pd(II) reduced and catalyst after 30 cycles shows that the profiles are roughly comparable: this is a clear demonstration of the stability of the support. The main differences are essentially identified in terms of relative fractions: distribution between –NH and N-Pd forms, and a little decrease in the proportion of Pd(0) (from 44 % to 37 %).

These results show some trends:

(a) metal binding occurs through electrostatic attraction/ion exchange between protonated amine groups (of PEI) and chloro-anionic Pd species

(b) a partial reduction of Pd(II) happens (limited to 44 %).

(c) there is a relative chemical stability of the AP-Pd(0) after 30 cycles of use.

5.4.2. Effect of Pd loading

Previous studies have suggested that the incorporation of PEI significantly improves the sorption capacity for Pd(II) from acidic solution owing to the abundant amine groups on this material. Thus, the alginate/PEI membrane is not only potentially a stabilizer for Pd nanoparticles, but also a potential sorbent for Pd(II) recovery. To test the sorption property of AP membranes for Pd(II) from acidic solution, the sorption isotherms were carried out by recirculating solutions containing different concentrations of Pd(II) through a fixed mass of AP membrane. It is noteworthy that, due to the amount of hydrochloric acid (1.1 M) in the stock solution, the predominant palladium species in those diluted working solutions is $PdCl_4^{2-}$. Figure 5-11 shows that the maximum sorption capacity reaches up to 223.6 mg Pd g^{-1}. The

partial protonation of amine groups makes the sorbent cationic at mild acid pH and then capable of binding chloro-anions. The eventual co-existence of free amine groups might also contribute to bind uncharged or free Pd(II) species; nevertheless, the strong predominance of chloro-anionic species limits the relevance of this mechanism. Table 5-2 reports Pd(II) sorption properties for a variety of materials. In general, phenolic hydroxyl groups-based materials such as tannin show the lowest sorption capacity among the listed materials. The sorption mechanism was reported as a combination of ligand substitution and redox reaction [40]. The raw algal biomass that contains a certain amount of amine and carboxyl groups shows comparable (slightly higher) sorption property compared to tannin. Amine group-based chitosan derivatives and aminated alginate and algal beads possess the highest sorption capacity; these materials can bind chloro-palladium complexes from acidic solution through electrostatic attraction [41] or coordinate to palladium(II) in neutral solution [42]. Owing to the abundant amine groups brought by PEI and the higher accessibility of the sorption sites on porous AP membranes, especially compared to the polymer beads, the membranes present much higher sorption capacity than other materials listed. This outstanding affinity of the membranes for Pd(II) is critical for improving the stability of Pd nanoparticles immobilized on this support. Indeed, a strong binding contributes to reduce metal leaching during the catalytic cycle; this is an especially important challenging for the development of efficient heterogeneous catalysts.

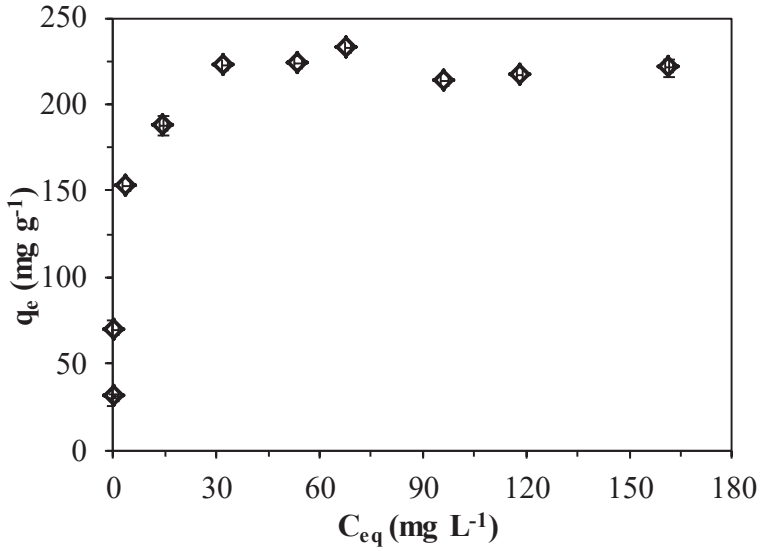

Figure 5-11 Pd(II) sorption isotherms using AP membranes (sorbent dosage = 0.25 g L^{-1}; pH: 1, adjusted by H_2SO_4 or NaOH; contact time = 48 h; T = 20 °C; flow rate = 30 mL min^{-1}).

Contrary to other nanoparticles, Pd nanoparticles immobilized on the membranes offer opportunities for application in fixed-bed column system in either recirculation mode or one-pass mode. Since Pd(II) is *in situ* reduced into Pd(0) on the membranes, the different conditions during loading process may lead to a change in distribution of Pd nanoparticles on the supports, and thus affect the catalytic performance. Therefore, the effect of Pd loading amount, flow rate

and membrane height during loading process was firstly studied in recirculation mode. The Pd loading amount is one of the most critical factors that markedly affect catalytic activity [43]. To study the effect of Pd loading amount, solutions with different initial Pd(II) concentrations (11, 16, 21, 28, and 52 mg L^{-1}) were recirculated through the membrane (weight: 255 ± 10 mg). The recovery efficiencies are 100, 99.8, 98.5, 97.1 and 71%, respectively and the corresponding sorption capacities are 43.8, 67.7, 84.0, 110.4 and 154.5 mg g^{-1}, respectively.

Table 5-2 Pd(II) sorption properties of a series of sorbents.

Sorbent	pH	q_m (mg g^{-1})	Ref.
Valonea tannin–formaldehyde resol resin	2	16.0	[44]
Tannin immobilized collagen fiber (BTICF) membrane	4	27.7	[45]
R. lanuginosum biomass	5	37.2	[46]
Montmorillonite modified alginate beads	4	99.0	[47]
Laponite modified alginate beads	4	146.9	[47]
L. digitata/PEI beads	1	90.5	[29]
C. crispus/PEI beads	1	142.6	[29]
Chitosan	6	90.9	[48]
Glutaraldehyde cross-linked chitosan resin	8	167.0	[48]
Ionic liquid impregnated chitosan	3	187.6	[49]
AP membrane	1	223.6	This work

After metal reduction, these as-prepared catalysts loaded with different Pd amounts were compared for 3-NP hydrogenation. A controlled experiment was performed with the raw membrane. As shown in Figure 5-12a, the concentration of 3-NP is not significantly reduced with the raw membrane, indicating that the hydrogenation of 3-NP is negligible in the absence of the active phase and that the sorption of the contaminant onto the membranes is also limited. Despite a slight decrease when applying membranes loaded with 11 mg or 16 mg Pd, their plots are almost overlapped with the kinetic profile obtained with the raw material. When the amount of Pd increases to 21 mg or higher, the concentration of 3-NP decreases significantly with increasing reaction time; however, the reason causes such a sharp improvement of hydrogenation efficiency remains unclear. The hydrogenation completely converts 3-NP into 3-AP within 10 min, showing the marked catalytic performance of AP/Pd catalyst. This reaction is well-known to follow the pseudo-first-order kinetics because an excess of HCOOH was used for the conversion process. To verify this hypothesis, $\ln(C_t/C_0)$ was plotted against reaction time (Figure 5-12b). The fine linear relationship confirms that this model is appropriate to describe the kinetics. To compare the catalytic efficiencies, the apparent rate constants (k, s^{-1}) and the

catalytic activity ($k_{Pd}=k/m_{Pd}$; s^{-1} g^{-1}) were calculated. Due to its lowest number of Pd sites, $AP/Pd_{21\ mg}$ has the slowest reaction with a k value of 6.52×10^{-3} s^{-1}. When the loading Pd amount grows by 6 mg, the reaction constant rate increases to 8.18×10^{-3} s^{-1}. Further increase in the Pd content from 27 mg to 37 mg does not change the rate constant value significantly. Similar result was reported by Jadbabaei et al. [50], who concluded that a higher Pd content does not necessarily result in higher catalytic activity, and the optimum Pd loading amount (i.e., the lowest Pd amount without sacrificing reactivity) is when the sorbed nitrophenol during the reaction is just non-detectable. Indeed, the k_{Pd} calculated for $AP/Pd_{37\ mg}$ (0.25 s^{-1} g^{-1}) is much lower than that of $AP/Pd_{27\ mg}$ (0.30 s^{-1} g^{-1}) and $AP/Pd_{21\ mg}$ (0.32 s^{-1} g^{-1}). The excessive loading of the support with catalytic metal (and further metal nanoparticles) may lead to agglomeration of particles with lower accessibility and less rationale use of the metal catalyst. Indeed, a previous study showed that an overloading Pd(II) on PEI particles resulted in large aggregates [36]. To maintain a high value for both k and k_{Pd}, $AP/Pd_{27\ mg}$ was chosen for further experiments.

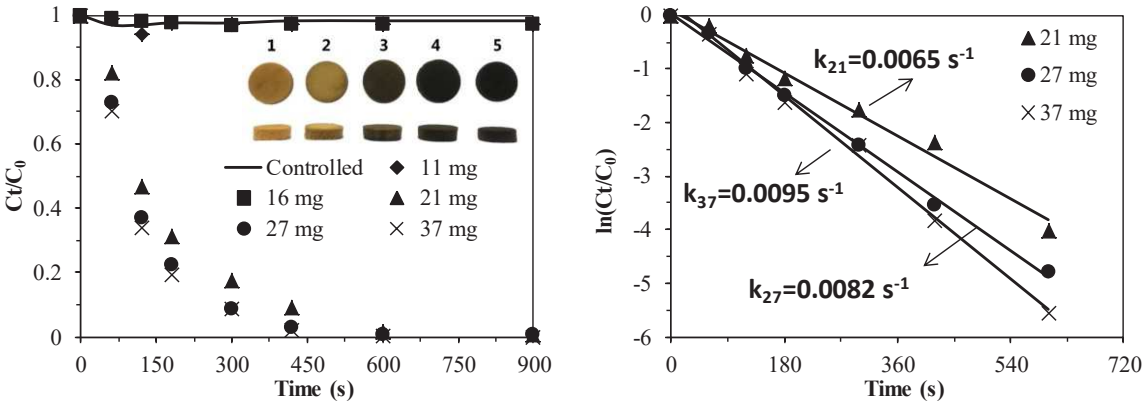

(a) (b)

Figure 5-12 Effect of Pd loading amount on the membranes on the hydrogenation of 3-NP (Pd(II) sorption process: Membrane mass = 255±10 mg; Flow rate = 30 mL min^{-1}; C_0 (Pd(II)) = 10-50 mg L^{-1}. 3-NP hydrogenation: C_0 (3-NP) = 50 mg L^{-1}; Volume = 0.1 L; pH (unadjusted) =2.861; Flow rate = 50 mL min^{-1}; $C_{(HCOOH)}$ = 0.2%): (a) C_t/C_0 versus reaction time; (b) $\ln(C_t/C_0)$ versus reaction time. The inset in (a) shows the photos of the catalysts loaded with different amount of Pd (increasing in the order from 1 to 5); the controlled experiment corresponds to the blank (membrane without Pd).

5.4.3. Effect of flow rate during Pd sorption on catalytic performance

The recirculation-mode system proposed for metal loading in this study requires a specific analysis of sorption kinetics regarding the necessity to force the solution to flow through the sorbent and to ensure the meal ions can be well dispersed on the membranes [51, 52]. A slow flow rate (FL) may easily lead to an accumulation of Pd(II) at the upper layer of the cylinder and to longitudinal metal gradient along the membrane packing. Figure 5-13a shows that a higher flow rate produces catalysts with higher catalytic performance. The value of k (shown in Figure 5-13b) increases significantly from 1.9×10^{-3} s^{-1} to 7.9×10^{-3} s^{-1} as the flow rate goes up from 5 mL min^{-1} to 30 mL min^{-1}. Further increasing the FL only leads to a slight

improvement on the apparent rate constant, the beneficial effect of increasing flow velocity tends to stabilize. Therefore, an even higher FL was not tested. The reason that causes this phenomenon should be that a higher FL leads to a more homogenous and less condensed distribution of Pd that allows more Pd sites to remain accessible as overloading due to heterogeneous dispersion may prevent sorption sites accessibility. The inset photo in Figure 5-13a shows the bottom of the cylinder. It is clear that at a low FL, the Pd loading is inhomogeneous with lower loading in the yellow (close to the raw color of the membranes) area. This inevitably leads to Pd overloading in other part and consequently to less accessible of Pd sites. Therefore, a FL of 50 mL min^{-1} was used for Pd(II) loading process in further experiments.

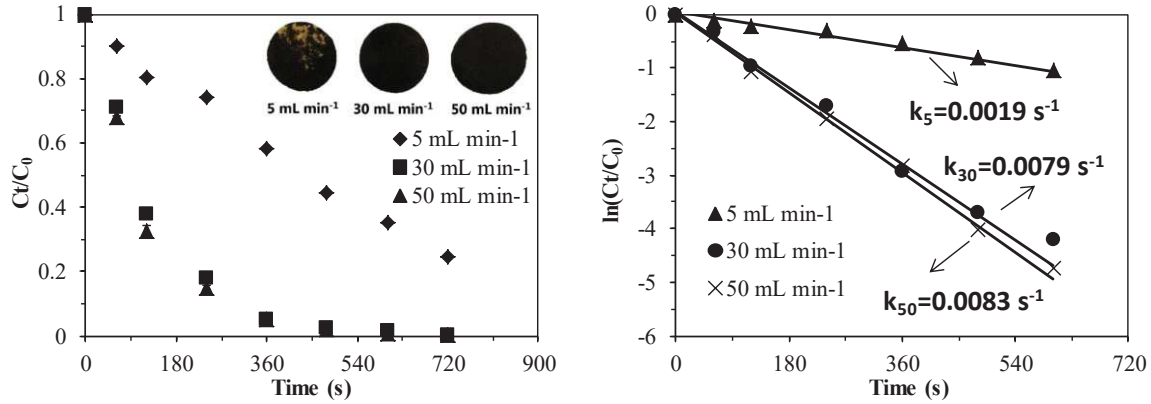

(a) (b)

Figure 5-13 Effect of flow rate applied for Pd(II) sorption on the hydrogenation of 3-NP (Pd(II) sorption process: Membrane mass = 255±10 mg; C_0 (Pd(II)) = 28 mg L^{-1}. 3-NP hydrogenation: Pd amount = 27 mg; Volume = 0.1 L; C_0 (3-NP) = 50 mg L^{-1}; pH (unadjusted) = 2.86; Flow rate = 50 mL min^{-1}; $C_{(HCOOH)}$ = 0.2%): (a) C_t/C_0 versus reaction time; (b) $\ln(C_t/C_0)$ versus reaction time. The inset in (a) shows the photos of the catalysts prepared by different flow rates.

5.4.4. Effect of membrane height during Pd sorption on catalytic performance

The effect of membrane height was studied using different masses of membranes with a same diameter. The masses of the membranes are 175, 255 and 313 mg and their corresponding thicknesses measured are 0.58, 0.85 and 1.06 cm, respectively. The values of Pd(II) loading amount on the membranes are very close, which are 26.1, 27.2 and 27.7 mg g^{-1}, respectively. Because the same amount of palladium (volume and concentration) has been circulated through the membranes of different heights, the density of Pd decreases with increasing membrane depth. Figure 5-14 shows that increasing the membrane thickness does not affect the hydrogenation efficiency; the recirculation mode may explain this result. However, the comparison of the apparent rate constants shows a higher relative catalytic activity for the thinner membrane (thickness: 0.85 cm). The less dense Pd distribution associated with the membrane thickness increase may thus result in fewer aggregates of the particles and thus increase the reduction performance. However, increasing the depth of the catalytic membrane

does not enhance catalytic performance. This result can be partially explained by a change in the effective flow velocity (permeate flux) in the catalyst module. The amount of water passing through these membranes with different thicknesses at a speed of 50 mL min^{-1} for 1 min was recorded for different depth of membrane. The volume passed through the membrane decreases from 49.8 ± 0.8 mL, to 47.8 ± 0.4 mL and to 41.1 ± 0.3 mL for depths increasing according 0.58 cm, 0.85 cm and 1.06 cm, respectively. Increasing the depth of the catalytic membrane modulates the admissible flow rate under selected experimental conditions.

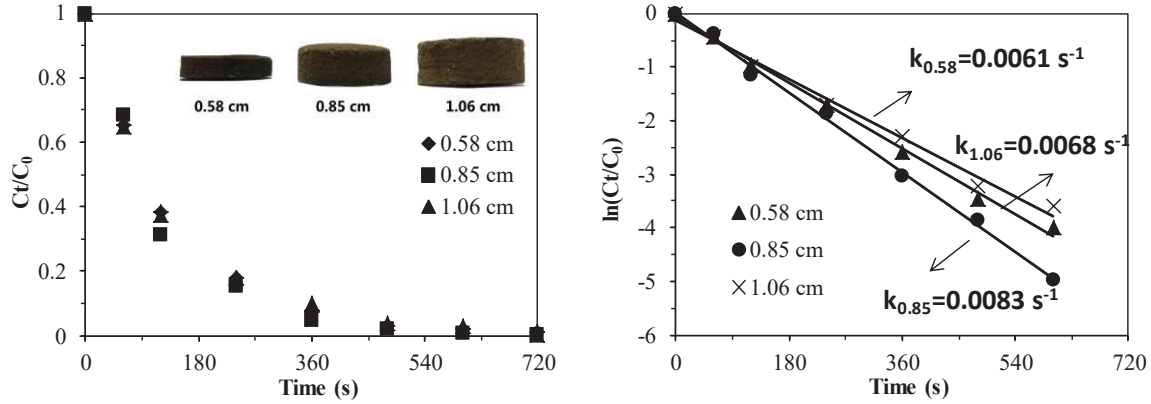

(a) (b)

Figure 5-14 Effect of membrane height on the hydrogenation of 3-NP (Pd(II) sorption process: Membrane mass: 175 mg, 255 mg and 313 mg (corresponding to the height of 0.58, 0.85 and 1.06 cm, respectively); C_0 (Pd(II)) = 28 mg L^{-1}. 3-NP hydrogenation: Pd amount, 26.1 mg, 27.2 mg and 27.7 mg (corresponding to the height of 0.58, 0.85 and 1.06 cm, respectively); C_0 (3-NP) = 50 mg L^{-1}; Volume = 0.1 L; pH (unadjusted) = 2.84; Flow rate, 50 mL min^{-1}; $C_{(HCOOH)}$ = 0.2%): (a) C_t/C_0 versus reaction time; (b) ln(C_t/C_0) versus reaction time. The inset in (a) shows the photos of the catalysts prepared using different mass of membranes.

5.4.5. Effect of solution pH and HCOOH concentration on catalytic performance

The solution pH may affect the catalytic reaction by changing the surface charge and the dissociation of the substrate and the hydrogen donor. The pK_a values of primary, secondary, and tertiary amine groups on PEI are 4.5, 6.7, and 11.6, respectively [53], while that of formic acid is 3.75 [54]. Figure 5-15a shows that degradation kinetics overlap when the initial pH is pH 3 or pH 4. Whereas when the initial pH decreases to pH 2 or increases to pH 5, the degradation rate decreases significantly. In addition, under these unfavorable conditions the residual concentration of 3-NP decreases but does not reach a plateau within selected contact time. The value of k calculated for pH 2 is 3.2×10^{-3} s^{-1} and 3.3×10^{-3} s^{-1} for pH 5, which are much lower than those of pH 3 and pH 4 (8.3×10^{-3} s^{-1} and 8.2×10^{-3} s^{-1}, respectively). One plausible explanation can be the pH dependence of the electrostatic interaction between formic acid/formate and the catalyst surface [34]. A higher solution pH makes the catalyst surface more negative and inhibits the access of formate ($HCOO^-$) anions; while at low pH, the competition

of competitor ions (brought by sulfuric acid for pH adjustment) may also decrease the binding of $HCOO^-$.

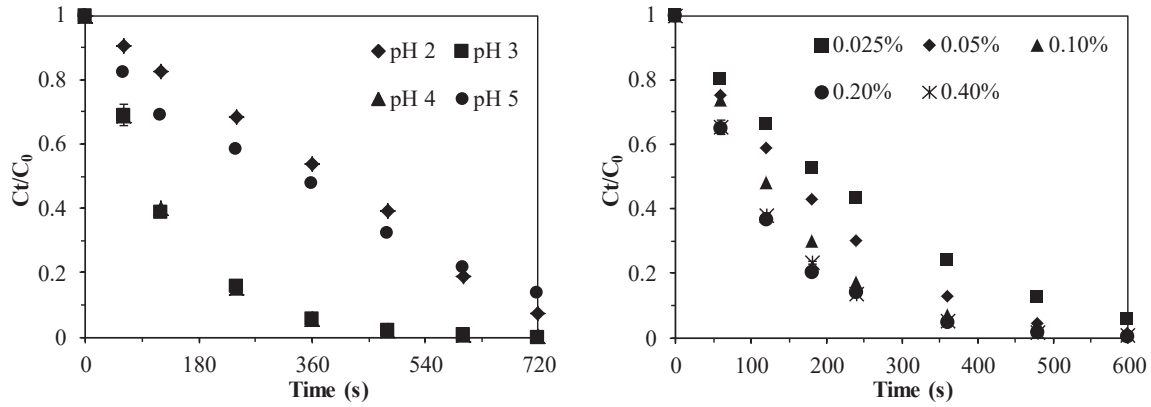

(a) (b)

Figure 5-15 (a) Effect of solution pH on the hydrogenation of 3-NP (Pd amount = 27 mg; C_0 (3-NP) = 50 mg L^{-1}; Flow rate = 50 mL min^{-1}; $C_{(HCOOH)}$ = 0.2%); (b) Effect of HCOOH concentration on the hydrogenation of 3-NP (Pd amount, 27 mg; C_0 (3-NP) = 50 mg L^{-1}; Flow rate = 50 mL min^{-1}).

The effect of the concentration of HCOOH was studied to select the optimal amount of HCOOH for 3-NP hydrogenation. The concentration of 3-NP was fixed at 50 mg L^{-1}, while that of HCOOH varied from 0.025 % w/w to 0.4 % w/w (corresponding to molar ratio of HCOOH/3-NP of 20 to 320) (Figure 5-15b). At low formic acid concentration (i.e., lower than 0.1 % w/w), the catalytic efficiency and the rate of 3-NP conversion are strongly decreased. Increasing the concentration of HCOOH above 0.2 % w/w does not significantly influence the catalytic activity. Thus, a HCOOH/3-NP molar ratio of 160 (0.2 % w/w of HCOOH for 3-NP concentration close to 50 mg L^{-1}) was chosen for further study. These conditions correspond to a strong excess of hydrogen donor and a negligible variation in its concentration during the catalytic reaction; this may explain that the kinetic profile can be modeled using the pseudo-first order rate equation.

5.4.6. Effect of flow rate during catalytic

The overall hydrogenation efficiencies are very similar at all flow rates (data not shown). However, the apparent rate constant, shown in Figure 5-16a, significantly increases with increasing flow rate. In the mode of recirculation, a slow flow rate reduces the amount of wastewater to be treated in a given time. In this case, a higher flow rate (i.e., a shorter contact time) may be generally preferred for a better catalytic performance. Therefore, in further studies, 60 mL min^{-1} was chosen as the optimum flow rate as the higher flow rate of 70 m Lmin^{-1} showed no significant difference.

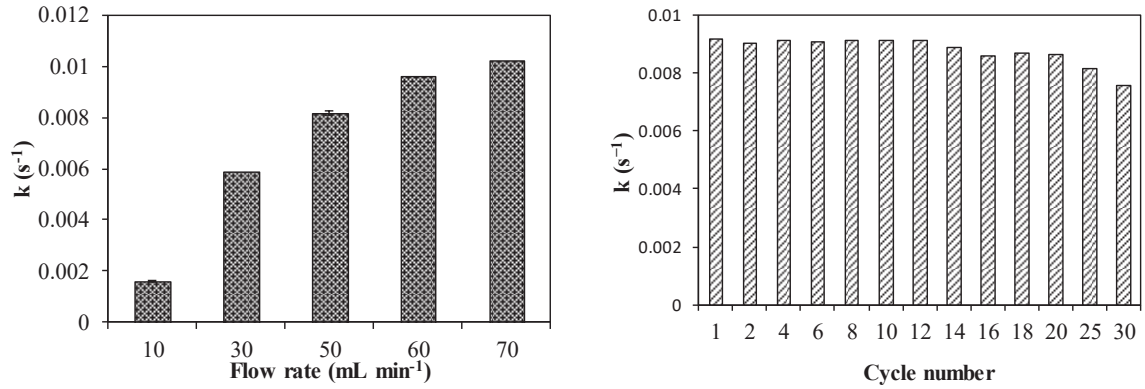

(a) (b)

Figure 5-16 (a) Effect of flow rate on the hydrogenation of 3-NP (Pd amount = 27 mg; C_0 (3-NP) = 50 mg L^{-1}; $C_{(HCOOH)}$ = 0.2%); (b) Reuse of the catalyst for 3-NP hydrogenation (Pd amount = 27.3 mg; C_0 (3-NP) = 50 mg L^{-1}; Flow rate = 60 mL min^{-1}; $C_{(HCOOH)}$ = 0.2%).

5.4.7. Turnover frequency (TOF) and recyclability of the catalyst

Besides the high catalytic activity and ease of recovery, a high catalytic stability is another highly required property for practical application. A reuse test was carried out over 30 cycles using AP/Pd catalyst. Owing to the specificity of the recirculation sorption system, separation process is not necessarily required; the membrane catalyst was washed using 100 mL of water and reused directly in the next round by replacing the treated solution with a freshly-prepared 3-NP solution. This should be advantageous in terms of easiness for practical applications. The results shown on Figure 5-16b indicate the catalytic activity of the Pd nanoparticles stabilized on AP membranes maintains unchanged for 14 successive cycles; significant decrease only appears after 20 cycles. This confirms that AP/Pd membranes are stable and reusable at least for 20 cycles. In most cases, the loss of catalytic activity is primarily due to metal leaching or support degradation. Indeed, the Pd loading amount of the catalysts determined by H_2SO_4-H_2O_2 digestion before and after 30 cycles is reduced by from 25.4 mg to 23.3 mg (8.3 % loss, shown in Table 5-3). The metal loss is partially caused by the support loss; mass loss of the catalyst before and after the 30 cycles is found to be 3.89%. Despite these facts, the catalytic activity of AP/Pd catalyst at 30-th cycle is still acceptable; actually, the loss on rate coefficient at the last cycle does not exceed 18 %. This can be explained by the well dispersion of Pd nanoparticles on AP membranes even after consecutive cycles; only a few aggregates of the nanoparticles are observed in the TEM image (shown on Figure 5-17, see SI) and the mean size measured is 8.00 ± 2.08 nm, which is close to the raw catalyst. The XPS analysis of recycled catalyst also confirmed minimal changes compared to original catalyst (Figure 5-9 and Figure 5-10). Another possible reason could be the partial decrease in the fraction of Pd effectively reduced on the catalyst (from 44 % to 37 %).

Table 5-3 Mass loss and Pd amount of AP/Pd membranes before and after 30 cycles.

Sample	Total mass (mg)	Pd concentration (mg g^{-1})	Pd amount (mg)
Raw AP/Pd	316.4	80.3 ± 1.2	25.4 ± 0.4
Reused AP/Pd	304.1	76.5 ± 1.7	23.3 ± 0.4

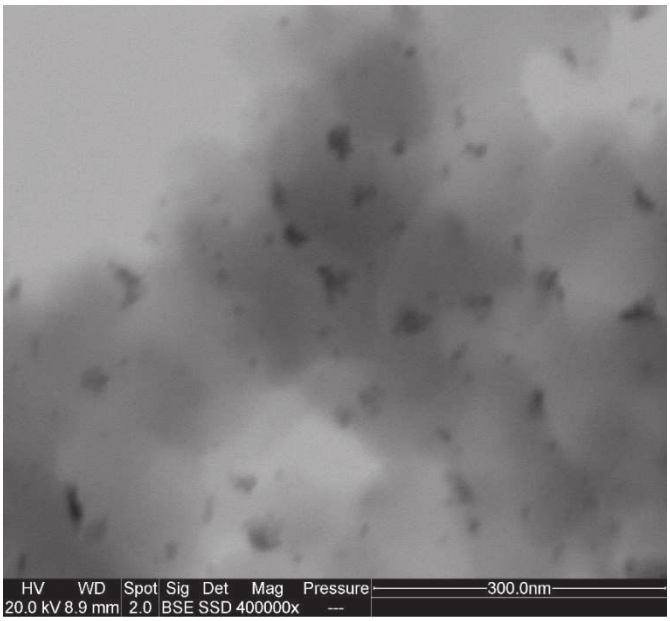

Figure 5-17 TEM image of reused AP/Pd catalyst.

Table 5-4 compares the catalytic performance of AP/Pd membranes with catalysts reported in the literature for the hydrogenation of nitrophenol compounds. When treating 100 mL of 50 mg L^{-1} 3-NP solution, the rate constant is slightly lower than Pd/silica [55], but very competitive compared to other catalysts [56-61]. The outstanding catalytic activity should be due to high amount of Pd loaded and well dispersion of Pd nanoparticles. Moreover, when compared to Pd nanoparticles supported on a similar material (algal biomass beads [36]), the rate constant improves significantly. This is owing to the much more porous structure of AP membranes and the unique treatment system (fixed-bed column system) that allow more effective mass transfer process. In order to further compare the catalytic activity of AP/Pd membranes with other catalysts reported previously, the turnover frequency (TOF, defined as the number of 3-NP molecules per metallic Pd per minute based on the total mass of metallic Pd, the unit is mmol $mmol^{-1}$ min^{-1}) of AP/Pd was evaluated from apparent rate constant (k). The value of TOF is 0.184 mmol $mmol^{-1}$ min^{-1} when the concentration of 3-NP is 700 mg L^{-1}, which is higher to those of Pd/Fe_3O_4 composites [62] and Pd-TNCs [63], but much lower than other catalysts [55, 64, 65]. However, it is noted that in this study, a much less poisonous agent (HCOOH), compared to $NaBH_4$ that was previously used in these literatures, was applied as hydrogen donor. In addition, all the catalyst composites listed are all nano-scale, which could lead to the difficulty of recovery or poor stability. For example, Xue et al. [58] observed a decrease on catalytic activity when reusing Pd/polypyrrole nanocapsules after the first hydrogenation.

Similarly, another study [66] showed that the catalytic activity of Pd/CuO nanoparticles decreased gradually during 6 cycles. Wang et al. [62] reported that the catalytic activity of Pd/Fe_3O_4 spheres decreased significantly in subsequent runs; the conversion decreased from 85% in the first cycle to 22% in the fifth cycle. These results indicate that the catalyst undergone gradual and relatively fast deactivation. They attributed this deactivation to the interaction between the aminophenol molecules and the Pd nanoparticles; the lone pair electrons on the N atom in aminophenol coordinate to the 4*d* orbitals of the palladium atoms, and as a result the catalytically active sites of the Pd nanoparticles are poisoned. The abundant amine groups on the membranes, a large size of the support and the uniqueness of the treatment system that requires no solid-separation process help the stability of AP/Pd catalyst for reusing in successive cycles. Therefore, compared to these nano-scale catalyst composites, the main advantages of AP/Pd membranes are: (1) no requirement of separation process after treatment, (2) high stability and (3) flexibility concerning the treatment system. Indeed, the membranes can be easily applied in fixed-bed system, using recirculation mode or one-pass mode.

Table 5-4 Comparison of the catalytic hydrogenation of nitrophenol compounds using various catalysts.

Composites	Type	$k \times 10^3$ (s^{-1}) [a]	$n_{nitrophenol}$ (mmol)	n_{Pd} (mmol)	TOF (min^{-1})	Ref.
HABA/PEI (Pd)	Millimeter-scale beads	0.022	–	–	–	[36]
Ni–Pt	Nanoparticles	1.93	–	–	–	[56]
PNIPA gels (Ag)	Core–Shell nanoparticles	3.50	–	–	–	[57]
Pd/polypyrrole	Nanocapsules	8.87	–	–	–	[58]
Pd/Fe_3O_4@SiO_2 @KCC-1	Nanocomposites	1.96	–	–	–	[59]
Pd/nano-silica	Nanocomposites	8.00	–	–	–	[60]
Pd/polyelectrolyte brushes	Nanocomposites	4.40	–	–	–	[61]
Pd/microgels	Nanocomposites	1.50	–	–	–	[61]
Pd/RGO [b]	Nanocomposites	–	1	1.2	6.38	[64]
$Pd_1(Co)_{15}$/RGO	Nanocomposites	–	1	0.5	396	[64]
Pd/silica	Nanocomposites	11.80	–	–	1.126	[55]
Concave Pd-TNCs	Nanoparticles	–	2×10^{-4}	1.5×10^{-4}	0.148	[63]
Flat Pd-TNCs	Nanoparticles	–	2×10^{-4}	1.5×10^{-4}	0.095	[63]
Solid Pd/Fe_3O_4	Nanocomposites	–	2.16	0.02	0.01	[62]
Hollow Pd/Fe_3O_4	Nanocomposites	–	2.16	0.02	0.015	[62]
Pd/graphene	Nanohybrids	2.35	2.9×10^{-4}	5×10^{-8}	13.63	[65]
AP/Pd	Foam	9.70	0.036	0.25	0.082	[c]
AP/Pd	Foam	1.53	0.50	0.25	0.184	[c]

[a] k: apparent rate constant. [b] RGO: reduced graphene oxide. [c]: this study.

5.4.8. Synthesis of AP/Pd and pathway of 3-NP hydrogenation

Figure 5-18 shows the mechanism of preparation of AP/Pd catalysts and suggests the reaction pathway for the 3-NP hydrogenation by HCOOH. The pK_a of carboxyl groups on alginate is approximately 4, while those of primary, secondary, and tertiary amine groups on PEI were reported as 4.5, 6.7, and 11.6, respectively [53]. Therefore, a simple pH adjusting makes the crosslinking between negatively charged carboxyl groups on alginate and positively charged amine groups on PEI possible. Besides, to improve the stability of the membranes, the free PEI on alginate was further crosslinked with GA as a post-treatment. In this case, alginate constitutes the support for PEI-GA; meanwhile, the PEI-GA crosslinking, in turn, improves the stability of the membranes. This double crosslinking avoids the collapse of the porous structure of the membranes. Unlike the conventional methods for preparing alginate-based membranes, AP membrane does not require strict drying conditions. An air drying process barely shrinks the porous material. The high percolating property allows palladium solution pass the material in a fixed-bed column system with a high flow rate, leading to good dispersion of Pd. After metal reduction, Pd nanoparticles can be firmly immobilized by the abundant amine groups on AP membranes, contributing to the high stability of the catalyst when reusing. This is consistent with the result from the "recyclability of the catalyst" section. To conclude, AP support plays an essential role in the determining the dispersion and stability of Pd nanoparticles:

(a) the surface of AP is positively charged due to the abundant amine groups on PEI, while Pd nanoparticles are generally negatively charged. Thus, Pd nanoparticles can be firmly immobilized through electrostatic interaction;

(b) the presence of alginate helps in distributing amine groups to the whole mass of AP membrane, preventing the aggregation of Pd nanoparticles trapped by amine groups;

(c) the unique structure (porous membrane) allows the application in fixed-bed column system. Thus, when loading metal ions, the high flow rate (such as 50 mL min^{-1}) can be applied and is beneficial to the good dispersion of Pd.

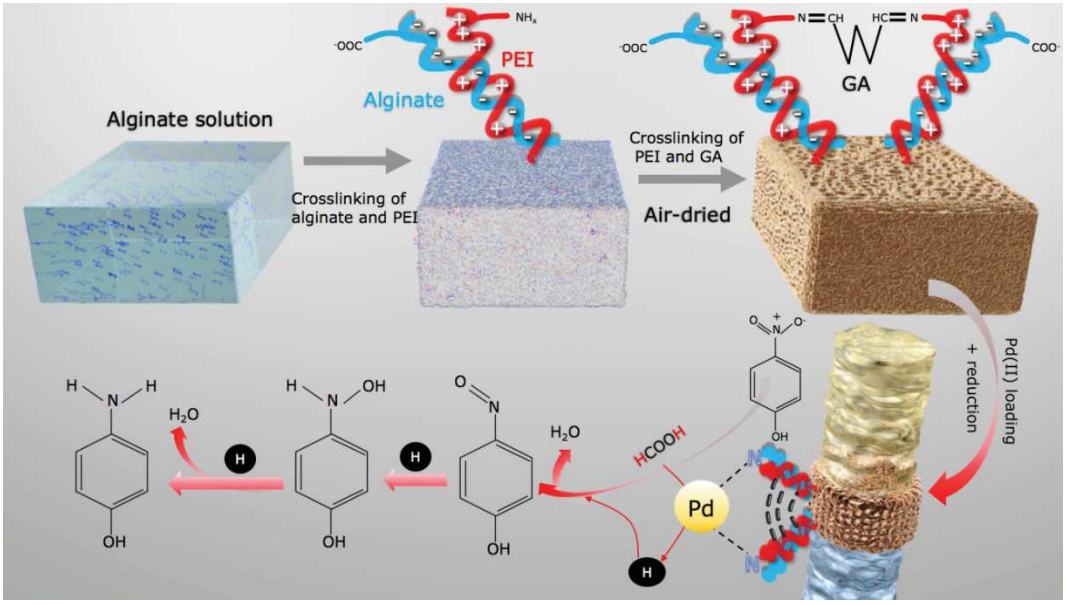

Figure 5-18 Mechanism of preparation of AP/Pd catalysts and proposed reaction pathway for the 3-NP hydrogenation by HCOOH

The decomposition of formic acid was reported to proceed through either the carboxyl (COOH) route or formate (HCOO) route [67]. The former process begins with the C-H bond dissociation and continues with the OH one, while the latter one starts with the O-H bond breaking, forming stable bidentate formate $HCOO_B$ intermediate. The presence of Pd nanoparticles induces the capture of hydrogen from HCOOH and thus assists the dissociation of HCOOH. Thereafter, the H· radical attacks the positively charged nitrogen of 3-NP, catalyzing the hydrogenation of 3-nitrophenol to the 3-aminophenol.

5.4.9. Tests in dynamic systems (one-pass mode)

To evaluate the catalytic performance of AP/Pd in the one-pass mode, the continuous reaction was carried out using the following experimental conditions: 100 mL of solutions with different initial 3-NP and HCOOH concentrations (molar ratio of HCCOH *vs.* 3-NP was maintained at 160) were fed through the catalytic membranes at different flow rates. The effluent was collected out of the reactor in fractions (4 mL for each). The outlet solutions look clear with generation of micro bubbles; this indicates the excess HCOOH is coming out along with 3-AP. As shown in Figure 5-19, when the flow rate is lower than 10 mL min^{-1}, the 3-NP concentration of the effluents is lower than 0.5 mg L^{-1}, regardless of the initial concentration. However, for an initial 3-NP concentration of 150 mg L^{-1} or 200 mg L^{-1}, as the flow rate increases to 20 mL min^{-1} or more, the reaction is not complete; the 3-NP concentration of effluents increases with increasing feed solution volume. An explanation may be the lack of enough Pd nanoparticles for treating the substrate for the selected residence time. This could be also explained by the progressive poisoning of AP/Pd catalysts by acidic species. Deng et al. [68] reported that supported Ru catalysts was poisoned when the concentration of formic acid or formate was higher than 10 mmol L^{-1}. The catalytic oxidation of formic acid produces poisoning species, which blocks the active sites of the Pd catalyst. As described above, formic acid decomposition

proceeds via either the formate (HCOO) or carboxyl (COOH) intermediate. Yoo et al. [69] observed that 60−82% of H_2 is produced via HCOO intermediate on Pd, indicating that the active sites were more likely blocked by COOH intermediate. Moreover, the carboxyl intermediate route produces CO, which could be another source of poisoning [69]. To regenerate the catalyst, a washing step was conducted to desorb the poisons by passing 40 mL of-water; thereafter, the 3-NP solution was continuously fed through the regenerated catalyst. Results shown on Figure 5-19d demonstrate that the catalytic performance of AP/Pd membranes can be easily recovered after washing with water, regardless of the feeding speed: poisoning species are weakly bound to AP/Pd membranes (easy elution).

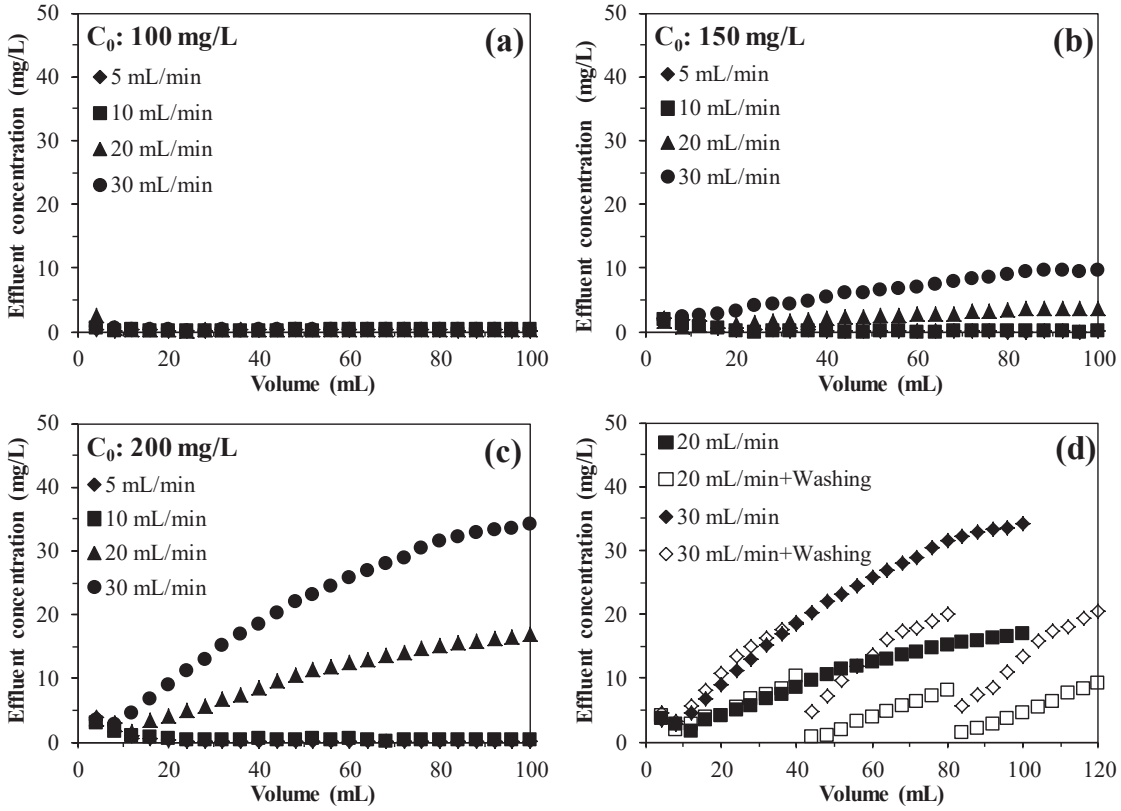

Figure 5-19 Hydrogenation of 3-NP in one-pass mode (Pd amount = 27.2 ± 0.3 mg; C_0 (3-NP) = 100-200 mg L^{-1}; Flow rate = 5-30 mL min^{-1}).

5.5. Principales conclusions

Les membranes Alginate/PEI synthétisées dans le cadre de cette thèse sont hautement macroporeuses, caractérisées par un porosité d'environ 70 %. Cela leur confère un haut pouvoir de percolation, avec des flux de l'ordre de 25 mL cm^{-2} min^{-1} (i.e., 15 m h^{-1} en drainage simple sous pression de la colonne d'eau de 0,006 bar). Elles sont par ailleurs mécaniquement stables : soumises pendant 3 jours à une agitation intense de 150 tr/min, la perte de masse de la membrane n'atteint pas 3 %.

Elles permettent une fixation importante du Pd(II), atteignant 224mg Pd g^{-1} à pH 1. L'analyse semi-quantitative des membranes (MEB-EDX) confirme qu'en mode optimisé (débit élevé : 50

mL min^{-1} ; vitesse supérieure à 6 m h^{-1}) l'adsorption s'effectue de manière homogène dans la membrane (surface et section). Le pH_{PZC} de la membrane proche de 6,3 permet de supposer que les groupements fonctionnels aminés protonés en milieu acide permettent la fixation du palladium sous forme d'anions métalliques ($PdCl_4^{2-}$). Cette hypothèse est confirmée par l'analyse XPS qui met en évidence la présence de chlore sur la membrane après adsorption du palladium, mais aussi d'interactions entre les groupes aminés et le Pd. Après réduction au moyen d'hydrate d'hydrazine, le palladium n'est que partiellement réduit : en surface le taux de réduction atteint 44 % (mesuré par XPS). L'analyse par XPS de la membrane ayant été utilisée pendant 30 batchs successifs révèle une excellente stabilité du matériau. L'observation en MET montre une dispersion homogène du palladium à la surface des feuillets de la membrane, avec des tailles de particules nanométriques de 7 à 8 nm (distribution centrée autour de 7,6 nm).

La comparaison des performances catalytiques (toutes conditions égales par ailleurs) de membranes ayant été chargées en Pd avec des flux croissants de la solution métallifère montrent qu'une vitesse limite est nécessaire afin de stabiliser la vitesse de conversion du 3-NP en 3-AP. En effet, pour un débit supérieur ou égal à 30 mL min^{-1} (i.e., vitesse superficielle : 3,7 m h^{-1}) la vitesse de conversion se stabilise : le coefficient apparent de vitesse cinétique de pseudo premier ordre approche k_1 = 0,008 s^{-1} (seulement 0,0019 s^{-1} pour un débit de 5 mL min^{-1}). Un débit élevé de la solution de palladium permet une distribution plus homogène du métal catalytique dans la membrane (tout en limitant la formation d'agrégats).

Cette formation d'amas de NPs de Pd peut également intervenir lorsque la membrane est excessivement chargée en Pd. L'efficacité d'un catalyseur est souvent améliorée en réduisant la taille des nanoparticules. Les tests réalisés sur des membranes chargés avec des quantités croissantes de Pd ont montré que l'activité catalytique se déclenche à partir d'une charge minimale de Pd (21 mg Pd/255 mg membrane) et augmente avec cette charge jusqu'à un taux de 27 mg Pd/255 mg membrane (k_1 = 0,0082 s^{-1}) ; au-delà, l'activité catalytique tend à se stabiliser (k_1 = 0,0095 s^{-1} pour une charge de 37 mg Pd/255 mg membrane). La vitesse optimale d'alimentation de la membrane dans la phase d'hydrogénation atteint un palier pour un flux de 60 mL min^{-1} (i.e., vitesse superficielle : 7,4 m h^{-1}) : ce résultat confirme l'importance d'assurer une conduite forcée de la solution au travers du réseau poreux (hétérogène en raison de la taille différente des pores et de la tortuosité du réseau poreux)

L'activité catalytique se maintient remarquablement stable pour 20 étapes successives de conversion du 3-NP en 3-AP, puis progressivement diminue (out en maintenant un niveau de conversion de 81 % de la conversion obtenue au premier cycle).

Dans le cas d'un traitement direct sans recirculation (mais à débit plus faible < 20 mL min^{-1} ≈ vitesse superficielle : 2,5 m h^{-1}) de très bonnes performances sont obtenues (conversion totale du 3-NP dans une solution de 100 mL à 200 mg L^{-1}, avec une membrane chargée à 27 mg Pd/255 mg membrane). Pour des débits plus élevés une perte d'efficacité est enregistrée. L'empoisonnement progressif des membranes peut être compensé par une cycle de nettoyage (eau bi-permutée) afin de régénérer la membrane catalytique.

5.6. References

[1] J. Gu, C.S. Hu, W.W. Zhang, A.B. Dichiara, Reagentless preparation of shape memory cellulose nanofibril aerogels decorated with Pd nanoparticles and their application in dye discoloration, Applied Catalysis B-Environmental, 237 (2018) 482-490.
[2] M. Islam, P. Mondal, A.S. Roy, K. Tuhina, Catalytic hydrogenation of various organic substrates using a reusable polymer-anchored palladium(II) complex, Journal of Materials Science, 45 (2010) 2484-2493.
[3] F. Cardenas-Lizana, M.A. Keane, The development of gold catalysts for use in hydrogenation reactions, Journal of Materials Science, 48 (2013) 543-564.
[4] H.G. Sogukomerogullari, Y. Karatas, M. Celebi, M. Gulcan, M. Sonmez, M. Zahmakiran, Palladium nanoparticles decorated on amine functionalized graphene nanosheets as excellent nanocatalyst for the hydrogenation of nitrophenols to aminophenol counterparts, Journal of Hazardous Materials, 369 (2019) 96-107.
[5] J. Xia, L. Zhang, Y. Fu, G. He, X. Sun, X. Wang, Nitrogen-doped carbon black supported $NiCo_2S_4$ catalyst for hydrogenation of nitrophenols under mild conditions, Journal of Materials Science, 53 (2018) 4467-4481.
[6] Y.M. Zhang, Y.H. Cao, D. Chen, P.L. Cui, J. Yang, Ionic liquid assisted synthesis of palladium nanoclusters for highly efficient formaldehyde oxidation, Electrochimica Acta, 269 (2018) 38-44.
[7] A. Wołowicz, Z. Hubicki, Adsorption characteristics of noble metals on the strongly basic anion exchanger Purolite A-400TL, Journal of Materials Science, 49 (2014) 6191-6202.
[8] Z. Zhang, G. Sebe, X.S. Wang, K.C. Tam, Gold nanoparticles stabilized by poly(4-vinylpyridine) grafted cellulose nanocrystals as efficient and recyclable catalysts, Carbohydrate Polymers, 182 (2018) 61-68.
[9] J. Li, X. Bai, Ultrasonic synthesis of supported palladium nanoparticles for room-temperature Suzuki–Miyaura coupling, Journal of Materials Science, 51 (2016) 9108-9122.
[10] C. Deng, Y. Li, W. Sun, F. Liu, Y. Zhang, H. Qian, Supported AuPd nanoparticles with high catalytic activity and excellent separability based on the magnetic polymer carriers, Journal of Materials Science, 54 (2019) 11435-11447.
[11] H. Wang, Y. Wan, Synthesis of ordered mesoporous Pd/carbon catalyst with bimodal pores and its application in water-mediated Ullmann coupling reaction of chlorobenzene, Journal of Materials Science, 44 (2009) 6553-6562.
[12] O.M. Wilson, M.R. Knecht, J.C. Garcia-Martinez, R.M. Crooks, Effect of Pd nanoparticle size on the catalytic hydrogenation of allyl alcohol, Journal of the American Chemical Society, 128 (2006) 4510-4511.
[13] A.B. Gawade, A.V. Nakhate, G.D. Yadav, Selective synthesis of 2,5-furandicarboxylic acid by oxidation of 5-hydroxymethylfurfural over $MnFe_2O_4$ catalyst, Catalysis Today, 309 (2018) 119-125.
[14] R. Das, V.S. Sypu, H.K. Paumo, M. Bhaumik, V. Maharaj, A. Maity, Silver decorated magnetic nanocomposite (Fe_3O_4@PPy-MAA/Ag) as highly active catalyst towards reduction of 4-nitrophenol and toxic organic dyes, Applied Catalysis B-Environmental, 244 (2019) 546-558.
[15] Y.Q. Zhao, Z.F. Wu, Y.Q. Wang, C. Yang, Y.X. Li, Facile fabrication of polystyrene microsphere supported gold-palladium alloy nanoparticles with superior catalytic performance for the reduction of 4-nitrophenol in water, Colloids and Surfaces a-Physicochemical and Engineering Aspects, 529 (2017) 417-424.
[16] S. Palchoudhury, J.R. Lead, A facile and cost-effective method for separation of oil-water mixtures using polymer-coated iron oxide nanoparticles, Environmental Science & Technology, 48 (2014) 14558-14563.

[17] J.G. Rosch, H. Winter, A.N. DuRoss, G. Sahay, C. Sun, Inverse-micelle synthesis of doxorubicin-loaded alginate/chitosan nanoparticles and in vitro assessment of breast cancer cytotoxicity, Colloid and Interface Science Communications, 28 (2019) 69-74.
[18] S. Ben Hammouda, N. Adhoum, L. Monser, Chemical oxidation of a malodorous compound, indole, using iron entrapped in calcium alginate beads, Journal of Hazardous Materials, 301 (2016) 350-361.
[19] B. An, H. Lee, S. Lee, S.H. Lee, J.W. Choi, Determining the selectivity of divalent metal cations for the carboxyl group of alginate hydrogel beads during competitive sorption, Journal of Hazardous Materials, 298 (2015) 11-18.
[20] A.G.D. Carvalho, M.T.D. Machado, H. Barros, C.B.B. Cazarin, M.R. Marostica, M.D. Hubinger, Anthocyanins from jussara (*Euterpe edulis Martius*) extract carried by calcium alginate beads pre-prepared using ionic gelation, Powder Technology, 345 (2019) 283-291.
[21] J. Zhao, Y.W. Zhu, G.W. He, R.S. Xing, F.S. Pan, Z.Y. Jiang, P. Zhang, X.Z. Cao, B.Y. Wang, Incorporating zwitterionic graphene oxides into sodium alginate membrane for efficient water/alcohol separation, ACS Applied Materials & Interfaces, 8 (2016) 2097-2103.
[22] Y.L. Ma, P.F. Qi, J.P. Ju, Q. Wang, L.Y. Hao, R. Wang, K.Y. Sui, Y.Q. Tan, Gelatin/alginate composite nanofiber membranes for effective and even adsorption of cationic dyes, Composites Part B-Engineering, 162 (2019) 671-677.
[23] W. Post, E. Jeoffroy, S.J. Garcia, S. van der Zwaag, Self-healing glass fiber reinforced polymer composites based on montmorillonite reinforced compartmented alginate fibers, Polymer Composites, 40 (2019) 471-480.
[24] L.E.E. Eibak, A.B. Hegge, K.E. Rasmussen, S. Pedersen-Bjergaard, A. Gjelstad, Alginate and chitosan foam combined with electromembrane extraction for dried blood spot analysis, Analytical Chemistry, 84 (2012) 8783-8789.
[25] S. Saha, A. Pal, S. Kundu, S. Basu, T. Pal, Photochemical green synthesis of calcium-alginate-stabilized Ag and Au nanoparticles and their catalytic application to 4-nitrophenol reduction, Langmuir, 26 (2010) 2885-2893.
[26] Y. Kuang, J.H. Du, R.B. Zhou, Z.L. Chen, M. Megharaj, R. Naidu, Calcium alginate encapsulated Ni/Fe nanoparticles beads for simultaneous removal of Cu(II) and monochlorobenzene, Journal of Colloid and Interface Science, 447 (2015) 85-91.
[27] M. Chtchigrovsky, Y. Lin, K. Ouchaou, M. Chaumontet, M. Robitzer, F. Quignard, F. Taran, Dramatic effect of the gelling cation on the catalytic performances of alginate-supported palladium nanoparticles for the Suzuki-Miyaura reaction, Chemistry of Materials, 24 (2012) 1505-1510.
[28] M. Kumar, G. Vijayakumar, R. Tamilarasan, Synthesis, characterization and experimental studies of nano Zn-Al-Fe_3O_4 blended alginate/Ca beads for the adsorption of rhodamin B, Journal of Polymers and the Environment, 27 (2019) 106-117.
[29] S. Wang, T. Vincent, C. Faur, E. Guibal, A comparison of palladium sorption using polyethylenimine impregnated alginate-based and carrageenan-based algal beads, Applied Sciences-Basel, 8 (2018).
[30] B. Loges, A. Boddien, H. Junge, M. Beller, Controlled generation of hydrogen from formic acid amine adducts at room temperature and application in H_2/O_2 fuel cells, Angewandte Chemie-International Edition, 47 (2008) 3962-3965.
[31] D.C. Gowda, S. Gowda, Formic acid with 10% palladium on carbon: A reagent for selective reduction of aromatic nitro compounds, Indian Journal of Chemistry Section B-Organic Chemistry Including Medicinal Chemistry, 39 (2000) 709-711.
[32] Y. Zhang, X. He, J. Ouyang, H. Yang, Palladium nanoparticles deposited on silanized halloysite nanotubes: synthesis, characterization and enhanced catalytic property, Scientific Reports, 3 (2013).

[33] T. Vincent, E. Guibal, Chitosan-supported palladium catalyst. 3. Influence of experimental parameters on nitrophenol degradation, Langmuir, 19 (2003) 8475-8483.
[34] R. Javaid, S.-i. Kawasaki, A. Suzuki, T.M. Suzuki, Simple and rapid hydrogenation of p-nitrophenol with aqueous formic acid in catalytic flow reactors, Beilstein Journal of Organic Chemistry, 9 (2013) 1156-1163.
[35] T. Vincent, P. Krys, C. Jouannin, A.-C. Gaumont, I. Dez, E. Guibal, Hybrid macroporous Pd catalytic discs for 4-nitroaniline hydrogenation: Contribution of the alginate-tetraalkylphosphonium ionic liquid support, Journal of Organometallic Chemistry, 723 (2013) 90-97.
[36] S. Wang, T. Vincent, C. Faur, E. Rodriguez-Castellon, E. Guibal, A new method for incorporating polyethyleneimine (PEI) in algal beads: High stability as sorbent for palladium recovery and supported catalyst for nitrophenol hydrogenation, Materials Chemistry and Physics, 221 (2019) 144-155.
[37] A.M. Perez-Coronado, L. Calvo, N. Alonso-Morales, F. Heras, J.J. Rodriguez, M.A. Gilarranz, Multiple approaches to control and assess the size of Pd nanoparticles synthesized via water-in-oil microemulsion, Colloids and Surfaces a-Physicochemical and Engineering Aspects, 497 (2016) 28-34.
[38] S.B. Simonsen, I. Chorkendorff, S. Dahl, M. Skoglundh, S. Helveg, Coarsening of Pd nanoparticles in an oxidizing atmosphere studied by in situ TEM, Surface Science, 648 (2016) 278-283.
[39] C. Zhang, Y. Leng, P. Jiang, J. Li, S. Du, Immobilizing palladium nanoparticles on nitrogen-doped carbon for promotion of formic acid dehydrogenation and alkene hydrogenation, ChemistrySelect, 2 (2017) 5469-5474.
[40] Y.-H. Kim, T. Ogata, Y. Nakano, Kinetic analysis of palladium(II) adsorption process on condensed-tannin gel based on redox reaction models, Water Research, 41 (2007) 3043-3050.
[41] S. Wang, T. Vincent, J.-C. Roux, C. Faur, E. Guibal, Pd(II) and Pt(IV) sorption using alginate and algal-based beads, Chemical Engineering Journal, 313 (2017) 567-579.
[42] K.J. Miller, T.T. Kitagawa, M.M. Abu-Omar, Kinetics and mechanisms of methyl vinyl ketone hydroalkoxylation catalyzed by palladium(II) complexes, Organometallics, 20 (2001) 4403-4412.
[43] T. Baran, I. Sargin, A. Mentes, M. Kaya, Exceptionally high turnover frequencies recorded for a new chitosan-based palladium(II) catalyst, Applied Catalysis a-General, 523 (2016) 12-20.
[44] M. Can, E. Bulut, A. Ornek, M. Ozacar, Synthesis and characterization of valonea tannin resin and its interaction with palladium (II), rhodium (III) chloro complexes, Chemical Engineering Journal, 221 (2013) 146-158.
[45] H.-W. Ma, X.-p. Liao, X. Liu, B. Shi, Recovery of platinum(IV) and palladium(II) by bayberry tannin immobilized collagen fiber membrane from water solution, Journal of Membrane Science, 278 (2006) 373-380.
[46] A. Sari, D. Mendil, M. Tuzen, M. Soylak, Biosorption of palladium(II) from aqueous solution by moss (*Racomitrium lanuginosum*) biomass: Equilibrium, kinetic and thermodynamic studies, Journal of Hazardous Materials, 162 (2009) 874-879.
[47] S. Cataldo, N. Muratore, S. Orecchio, A. Pettignano, Enhancement of adsorption ability of calcium alginate gel beads towards Pd(II) ion. A kinetic and equilibrium study on hybrid Laponite and Montmorillonite-alginate gel beads, Applied Clay Science, 118 (2015) 162-170.
[48] S. Nagireddi, V. Katiyar, R. Uppaluri, Pd(II) adsorption characteristics of glutaraldehyde cross-linked chitosan copolymer resin, International Journal of Biological Macromolecules, 94 (2017) 72-84.

[49] A.S.K. Kumar, S. Sharma, R.S. Reddy, M. Barathi, N. Rajesh, Comprehending the interaction between chitosan and ionic liquid for the adsorption of palladium, International Journal of Biological Macromolecules, 72 (2015) 633-639.
[50] N. Jadbabaei, R.J. Slobodjian, D. Shuai, H. Zhang, Catalytic reduction of 4-nitrophenol by palladium-resin composites, Applied Catalysis a-General, 543 (2017) 209-217.
[51] E. Guibal, S. Cambe, S. Bayle, J.-M. Taulemesse, T. Vincent, Silver/chitosan/cellulose fibers foam composites: From synthesis to antibacterial properties., Journal of Colloid and Interface Science, 393 (2013) 411-420.
[52] S. Wang, T. Vincent, C. Faur, E. Guibal, Algal foams applied in fixed-bed process for lead(II) removal using recirculation or one-pass modes, Marine Drugs, 15 (2017) Article N° 315.
[53] I. Willner, Y. Eichen, A.J. Frank, M.A. Fox, Photinduced electron-transfer processes using organized redeox-functionalized bipyridinium polyethyleneimine TiO_2 colloids and particulate assemblies, Journal of Physical Chemistry, 97 (1993) 7264-7271.
[54] J.M.A. Harmsen, L. Jelemensky, P.J.M. Van Andel-Scheffer, B.F.M. Kuster, G.B. Marin, Kinetic modeling for wet air oxidation of formic acid on a carbon supported platinum catalyst, Applied Catalysis a-General, 165 (1997) 499-509.
[55] J. Morere, M.J. Tenorio, M.J. Torralvo, C. Pando, J.A.R. Renuncio, A. Cabanas, Deposition of Pd into mesoporous silica SBA-15 using supercritical carbon dioxide, Journal of Supercritical Fluids, 56 (2011) 213-222.
[56] S.K. Ghosh, M. Mandal, S. Kundu, S. Nath, T. Pal, Bimetallic Pt-Ni nanoparticles can catalyze reduction of aromatic nitro compounds by sodium borohydride in aqueous solution, Applied Catalysis a-General, 268 (2004) 61-66.
[57] Y. Lu, Y. Mei, M. Drechsler, M. Ballauff, Thermosensitive core-shell particles as carriers for Ag nanoparticles: Modulating the catalytic activity by a phase transition in networks, Angewandte Chemie-International Edition, 45 (2006) 813-816.
[58] Y. Xue, X. Lu, X. Bian, J. Lei, C. Wang, Facile synthesis of highly dispersed palladium/polypyrrole nanocapsules for catalytic reduction of p-nitrophenol, Journal of Colloid and Interface Science, 379 (2012) 89-93.
[59] X. Le, Z. Dong, Y. Liu, Z. Jin, H. Thanh-Do, L. Minhdong, J. Ma, Palladium nanoparticles immobilized on core-shell magnetic fibers as a highly efficient and recyclable heterogeneous catalyst for the reduction of 4-nitrophenol and Suzuki coupling reactions, Journal of Materials Chemistry A, 2 (2014) 19696-19706.
[60] X. Le, Z. Dong, X. Li, W. Zhang, L. Minhdong, J. Ma, Fibrous nano-silica supported palladium nanoparticles: An efficient catalyst for the reduction of 4-nitrophenol and hydrodechlorination of 4-chlorophenol under mild conditions, Catalysis Communications, 59 (2015) 21-25.
[61] Y. Mei, Y. Lu, F. Polzer, M. Ballauff, M. Drechsler, Catalytic activity of palladium nanoparticles encapsulated in spherical polyelectrolyte brushes and core-shell microgels, Chemistry of Materials, 19 (2007) 1062-1069.
[62] H.-Q. Wang, X. Wei, K.-X. Wang, J.-S. Chen, Controlled synthesis of magnetic Pd/Fe_3O_4 spheres via an ethylenediamine-assisted route, Dalton Transactions, 41 (2012) 3204-3208.
[63] G. Fu, X. Jiang, L. Ding, L. Tao, Y. Chen, Y. Tang, Y. Zhou, S. Wei, J. Lin, T. Lu, Green synthesis and catalytic properties of polyallylamine functionalized tetrahedral palladium nanocrystals, Applied Catalysis B-Environmental, 138 (2013) 167-174.
[64] W. Dong, S. Cheng, C. Feng, N. Shang, S. Gao, C. Wang, Fabrication of highly dispersed Pd nanoparticles supported on reduced graphene oxide for catalytic reduction of 4-nitrophenol, Catalysis Communications, 90 (2017) 70-74.

[65] Z. Wang, C. Xu, G. Gao, X. Li, Facile synthesis of well-dispersed Pd-graphene nanohybrids and their catalytic properties in 4-nitrophenol reduction, RSC Advances, 4 (2014) 13644-13651.
[66] M. Nasrollahzadeh, S.M. Sajadi, A. Rostami-Vartooni, M. Bagherzadeh, Green synthesis of Pd/CuO nanoparticles by Theobroma cacao L. seeds extract and their catalytic performance for the reduction of 4-nitrophenol and phosphine-free Heck coupling reaction under aerobic conditions, Journal of Colloid and Interface Science, 448 (2015) 106-113.
[67] A.M. Ruppert, M. Jedrzejczyk, N. Potrzebowska, K. Kazmierczak, M. Brzezinska, O. Sneka-Platek, P. Sautet, N. Keller, C. Michel, J. Grams, Supported gold-nickel nano-alloy as a highly efficient catalyst in levulinic acid hydrogenation with formic acid as an internal hydrogen source, Catalysis Science & Technology, 8 (2018).
[68] L. Deng, Y. Zhao, J. Li, Y. Fu, B. Liao, Q.-X. Guo, Conversion of levulinic acid and formic acid into gamma-valerolactone over heterogeneous catalysts, Chemsuschem, 3 (2010) 1172-1175.
[69] J.S. Yoo, Z.-J. Zhao, J.K. Norskov, F. Studt, Effect of boron modifications of palladium catalysts for the production of hydrogen from formic acid, ACS Catalysis, 5 (2015) 6579-6586.

Chapter 6 Conclusions and perspectives

In conclusion, we summarize the main achievements obtained in this PhD thesis and describe next steps for further investigation perspectives.

6.1. Research conclusions

In this research work, highly percolating membranes were successfully synthesized with low energy drying procedures. These new membranes can be used for natural draining, free percolation without pumping. Since the objective of this thesis is to develop new alginate-based membranes for their applications as adsorbents and catalysts in water treatment, we conclude their performance in sorption and catalytic section in the following.

6.1.1. Sorption section

In the sorption part, the presence of carboxylic groups (alginate matrix) and amine (primary, secondary and tertiary amines from PEI) brings to the composite material multi-functionality and affinity for a broad range of metal ions.

(1) In the case of chromate (including Cr(VI) and TCr) sorption from acid solutions, the uptake kinetics are poorly affected by the flow rate but the time required for reaching equilibrium is quite long (about 3 days) though most of the sorption occurs within the first 24 h of contact. The pseudo-second order rate equation fits relatively well the kinetic profile, although the poor porosity at the surface probably controls the mass transfer (resistance to intraparticle diffusion). The sorption isotherms can be modeled using the Sips equation (for TCr profile) or the Langmuir equation (for Cr(VI) profile). The maximum sorption capacities reach values as high as 314 mg Cr(VI) g^{-1} and 331 mg TCr g^{-1} at pH 2.

The sorption properties are poorly affected by the presence of chloride and nitrate anions or calcium and copper cations (even in large excess: 800 mg L^{-1}); however, the presence of sulfate ions shows a much greater impact with substantial depreciation of sorption capacities. Tested on simulated electroplating wastewater, alginate/PEI membranes reveal sorption capacities comparable to the levels reached with pure synthetic solutions. Finally, despite the efficiency in desorption is weak, the process sounds promising for the polishing treatment of such industrial effluents.

(2) In the case of Se(VI) sorption by membranes, the optimum sorption is observed at pH 2 due to strong affinity of protonated (primary) amine groups for anionic species. The sorption isotherms are fitted by the Langmuir equation (better mathematical fit obtained with the 3-parameters equation of Sips): maximum sorption capacity reaches up to 83 mg g^{-1}. The flow rate (circulation mode) influences kinetic profiles at a superficial flow velocity below 2 m h^{-1}; above, the flow rate has a weak impact on the removal rate. The pseudo-first order rate equation fits well kinetic profiles, though the equilibrium sorption capacities calculated by the pseudo-second order rate equation are closer from experimental equilibrium values. Sulfate anions

(with chemical properties very close to SeO_4^{2-}) have a marked effect on selenate binding contrary to chloride and nitrate anions. Selenium can be easily desorbed from loaded sorbent using 0.01 M NaOH solutions (consistently with pH impact on Se(VI) sorption). The sorbent shows remarkable stability in the performances of both sorption and desorption, for at least four cycles.

(3) The sorption and competitive sorption of Hg(II) and Cu(II) in single and binary systems by the membranes was investigated. Results shows that the sorption capacity of Cu(II) can be negligible at low pH (below pH 2) and increased with increasing pH from 2 to 6, while the Hg(II) sorption capacity slightly changed from pH 1 (0.76 mmol g^{-1}) to pH 6 (0.84 mmol g^{-1}); this demonstrates that the membrane can efficiently bind Hg(II) in a wide pH range (1-6) and has an extraordinarily high selectivity of Hg over Cu especially in acidic condition. The kinetic studies find that under selected experimental conditions, Cu(II) sorption by membrane is faster than Hg(II) and the uptake kinetics of Hg(II) and Cu(II) are well fitted by the pseudo-second-order kinetic model based on the R^2 of 0.999. Langmuir, Freundlich and Sips are proposed for fitting the sorption equilibrium data in single system and best fit is obtained with the Sips equation. Simultaneously, the maximum sorption capacities for Hg(II) and Cu(II) reach to 1.60 mmol g^{-1} and 0.66 mmol g^{-1} respectively, which are higher than experimental values. Competitive Sips model can well predict the sorption data in binary system. The results show that the increase of Hg(II) concentration led to a dramatical fall in the sorption capacity of Cu(II), while there is no obvious decrease is found in Hg(II) sorption as the concentration of Cu(II) increased; this confirms that the membrane has a much higher affinity for Hg(II) than Cu(II). Thus, the membrane has promising performances for the removal of Hg(II) from aqueous solutions. Furthermore, the membrane is particularly useful for selective Hg(II) recovery from the Hg-Cu system, opening a new horizon in acidic wastewater treatment.

(4) The sorption of Cu(II) and Se(VI) by different crosslinking levels of PEI-GA resins was investigated, since the as-prepared membrane is operated using the proper reaction of alginate with amine groups of PEI, followed by a stabilizing crosslinking of primary amine groups (on PEI) using GA. Results show that the amount of GA for PEI crosslinking does not affect the adsorption for selenate, especially when the PEI-GA ratio is less than 2. Moreover, the adsorption efficiency for Se(VI) is hardly affected by storage conditions, while that for Cu(II) decreases significantly after 20-day storage compared to the freshly prepared ones. In addition, the adsorbents could selectively recover Se(VI) from Se(VI)-As(V) system and Cu(II) from Pb(II)-Cu(II) system. The results of this study should be useful for the synthesis and storage of various PEI-based or amine-rich adsorbents applied for the removal of aqueous contaminants including anions and cations.

6.1.2. Catalytic section

In the catalytic part, the study confirms that the prepared membrane which have a high affinity for Pd(II) (the maximum sorption capacity is 224 mg Pd g^{-1}), can be also used for manufacturing heterogeneous hydrogenation catalyst. The loaded Pd(II) can be partially reduced into Pd(0) nanoparticles using hydrazine hydrate ($N_2H_4 \cdot H_2O$) in alkaline solution (based on XPS analysis,

the yield of reduction is close to 44 %). The average size of Pd nanoparticles is close to 7-8 nm (measured by TEM). Pd-supported catalytic foam is successfully applied for 3-NP hydrogenation using HCOOH as hydrogen donor in a recirculation mode (batch mode). The best Pd(II) loading condition correspond, for a 255-mg amount of foam, to: an initial Pd(II) concentration of 28 mg L^{-1} at pH 1 (volume: 1 L), and flow rate of 50 mL min^{-1}. In the case of 3-NP hydrogenation, best operating conditions correspond to: (a) initial pH: 3-4; (b) flow rate: 60 mL min^{-1}; (c) HCOOH/3-NP molar ratio: 160.

Under selected experimental conditions, the kinetic profiles can be modeled using the pseudo-first order rate equation. The catalyst can be recycled: used for 30 successive cycles, it appears that the catalytic activity decreases after 20 cycles. In the one-pass mode (dynamic operating), the progressive poisoning of the catalyst decreases the hydrogenation efficiency; however, washing the catalyst with water allowed readily restoring catalytic activity.

6.2. Research perspectives

Based on this thesis, we have achieved to synthesize highly percolating membranes and investigated their applications in removal and recovery of metal ions from aqueous solution. Our results showed that the membranes have relatively high affinities for metallic anions and recover anions from the complex solutions, in particular at acidic conditions. However, we also found the membrane has no preference of metallic cations; this make more studies and modifications could be done on possible improving the sorption capacity of the membrane in cations.

Moreover, we have studied the application of membrane in Pd(II) recovery and as catalysts for 3-NP hydrogenation. This also offer very promising perspectives for developing membranes as stable catalytic supports based on their highly-percolating properties, confinement of catalytic nanoparticles, re-usable and easy to regenerate.

Furthermore, the obtained gelation membrane from the reaction between alginate and PEI shows special properties like water-holding, easy shaping and further functionalization, allowing for continuously development in their application. For example, taking gelation network as a solid template to fabricate superhydrophobic membrane for efficient oil-water separation would be an interesting research topic.

Résumé

L'alginate est un polymère hydrophile et biocompatible portant de nombreuses fonctions carboxyliques et de nombreux groupes hydroxyles. Ce travail a développé et optimisé le procédé de fabrication de membranes à haut pouvoir de percolation à base d'alginate. Ce procédé simple permet, par mélange de deux solutions d'alginate et de polyethyleneimine (PEI), d'obtenir un hydrogel structuré dont la stabilité est améliorée par réticulation (des fonctions aminées de la PEI par le glutaraldéhyde (GA)). Cette double interaction (PEI/alginate, PEI/GA) permet d'obtenir après séchage à l'air libre (donc peu énergivore et sans moyen sophistiqué contrairement aux procédés conventionnels) de produire des membranes macroporeuses autorisant la percolation par drainage simple de solutions. Ce matériau a été développé et utilisé pour deux types d'applications : (a) l'adsorption d'ions métalliques (cationiques et anioniques), et (b) l'hydrogénation de composés nitrophénoliques par catalyse hétérogène. Les membranes et leur interaction avec les ions métalliques ont été analysées par FTIR, MEB, et XPS. L'adsorbant est caractérisé par la présence de groupements carboxyliques et de fonctions aminées qui offre de nombreuses possibilités d'interaction avec les ions métalliques en jouant tant sur des propriétés de chélation (carboxylates, amines libres) que sur des propriétés d'échange ionique/attraction électrostatique (amines protonés) en fonction de la typologie du métal, de sa spéciation et du pH de la solution. Ces différentes possibilités ont été illustrées par une série d'expérimentations portant sur des ions métalliques tels que : Hg(II), Cu(II), Se(VI), Cr(VI), As(V). Ces différentes études ont permis d'illustrer : l'affinité particulière des membranes pour les anions métalliques (préférentiellement aux cations) en raison notamment de la plus grande disponibilité des fonctions aminées protonées. Par ailleurs, une étude complémentaire a été menée sur de la PEI réticulée par le GA (conditionnée sous forme de poudre) pour explorer l'effet de réticulation de la PEI sur la fixation des ions métalliques. L'étude a permis de démontrer que le taux de réticulation a un effet modéré sur l'adsorption des ions Se(VI). Enfin, après avoir brièvement étudié l'adsorption du Pd(II) sur les membranes, il a été procédé à une réduction du Pd(II) fixé sur le support (partiellement converti en Pd(0)) afin de synthétiser des membranes Pd/PEI/Alginate pour étudier une réaction simple d'hydrogénation du 3-NP en 3-AP. Ceci démontre la faisabilité d'application de ces supports pour une utilisation en catalyse hétérogène.

Mots clés : alginate; membrane macroporeuse; ion métallique; adsorbant; catalyse

Summary

Alginate is a hydrophilic and biocompatible polymer with abundant free carboxyl and hydroxyl groups. This work developed and optimized the process for the fabrication of highly-percolating membranes based on alginate. The simple process has been designed by mixing alginate and polyethyleneimine (PEI) to obtain a structured hydrogel and subsequently improved stability by crosslinking between glutaraldehyde (GA) and amine groups of PEI. This double interaction (PEI/alginate, PEI/GA) makes it possible to produce macroporous membranes, after air-drying (without energy-consuming and sophisticated drying procedure), allowing natural drainage. The prepared membranes have been used for two applications: (a) sorption of metal ions (cationic and anionic), and (b) hydrogenation of nitrophenolic compounds by heterogeneous catalysis. The membranes and their interactions with metal ions were analyzed by FTIR, SEM, and XPS. The adsorbent was characterized by the presence of carboxylic groups and amino functions, which offers numerous possibilities for interacting with metal ions by complexation (i.e., carboxylates, free amines) and ion exchange/electrostatic attraction (i.e., protonated amine groups) depending on the pH of solution and metal speciation. These different possibilities have been illustrated by a series of experiments on metal ions such as Hg(II), Cu(II), Se(VI), Cr(VI), As(V). These various studies illustrate the particular affinity of membranes for metal anions (preferentially to cations) due in particular to the greater availability of protonated amino functions. Furthermore, an additional study was conducted on PEI crosslinked with GA (as a powder) for exploring the effect of the crosslinking of PEI on the binding of metal ions. The study demonstrated that the crosslinking rate has a moderate effect on the sorption of Se(VI) ions. At last, after briefly studying the sorption of Pd(II) on the membranes, a reduction was made of Pd(II) loaded on the support (partially converted to Pd(0)) in order to synthesize catalysis for the hydrogenation of 3-NP to 3-AP. This demonstrates the feasibility of applying these supports for heterogeneous catalysis.

Key words: alginate; macroporous membrane; metal ions; adsorbent; catalysis.